



# Final Technical Report

## Numerical Modeling of Oil Containment by a Boom/Barrier System : Phase III

Submitted to :

U.S. Department of Transportation  
Attn : Rodney L. Cook  
Volpe National Transportation Systems Center  
55 Broadway, Cambridge, MA 02142-1093  
DOT Grant No. DTRS57-95-G-00065  
January 1997 to September 30th, 1999

Submitted by :

S.T. Grilli, T. Fake and M.L. Spaulding  
Department of Ocean Engineering  
University of Rhode Island Narragansett Bay Campus  
Narragansett, RI 02882

May 26, 2000

# Contents

<b>1</b>	<b>Introduction</b>	<b>1</b>
1.1	Problem overview . . . . .	7
1.2	Review of laboratory experiments . . . . .	12
1.2.1	OHMSETT experiments . . . . .	12
1.2.2	UNH experiments . . . . .	13
1.3	Principle of SlickMap models . . . . .	13
1.4	Principle of SlickMap's interactive user interface . . . . .	18
<b>2</b>	<b>Experiments at Ohmsett</b>	<b>19</b>
2.1	Introduction . . . . .	19
2.2	Experimental data and results . . . . .	20
2.2.1	Data Collection . . . . .	20
2.2.2	August 1997 experiments . . . . .	22
2.2.3	May 1998 experiments . . . . .	29
2.2.4	September 1998 experiments . . . . .	39
2.3	Analysis and inter-comparison of experimental results for straight booms of various drafts . . . . .	47
2.4	Analysis of interfacial friction for model calibration . . . . .	54
2.5	Conclusions . . . . .	58
<b>3</b>	<b>Analysis of UNH experiments</b>	<b>60</b>
3.1	Introduction . . . . .	60
3.2	May and July 1997 experiments . . . . .	62
3.2.1	Analysis of experimental results . . . . .	62
3.2.2	Computation of corresponding friction function . . . . .	69
3.3	August 1997 experiments . . . . .	74
3.4	August 1999 experiments . . . . .	76
3.5	Conclusions . . . . .	89
<b>4</b>	<b>Theoretical developments for SlickMap Model</b>	<b>93</b>
4.1	Static Initialization : Stage 1 Model . . . . .	93
4.1.1	Slick geometry and oil volume conservation . . . . .	94

4.1.2	Energy conservation . . . . .	95
4.1.3	Vertical and horizontal equilibrium equations . . . . .	96
4.1.4	Average friction coefficient . . . . .	99
4.1.5	Equivalence of mechanical work . . . . .	101
4.1.6	Solution of Stage 1 model equations . . . . .	103
4.2	Iterative Static Initialization : Stage 2 Model . . . . .	108
4.2.1	Pseudo-hydrostatic equilibrium equations . . . . .	109
4.2.2	External flow calculation . . . . .	110
4.2.3	Friction coefficient model equation . . . . .	112
4.2.4	Equivalence of mechanical work . . . . .	115
4.2.5	Iterative updating of slick geometry . . . . .	115
4.2.6	Smoothing of slick interface geometry and oil volume conservation	118
4.2.7	Results and discussion . . . . .	120
4.3	Time Updating of Oil Slick : Stage 3 Model . . . . .	124
4.3.1	Governing equations, boundary and initial conditions for the water flow . . . . .	126
4.3.2	Time stepping . . . . .	128
4.3.3	Analogy with Vortex Sheet method . . . . .	130
4.3.4	External flow calculation . . . . .	131
4.3.5	Pseudo-hydrostatic equilibrium in the slick . . . . .	131
4.3.6	Mechanical work and expression of pressure damping . . . . .	132
4.3.7	Expression of slick inertial damping . . . . .	135
4.3.8	Expression of friction coefficient function . . . . .	136
4.3.9	Time updating of slick geometry . . . . .	137
4.3.10	Smoothing and oil volume conservation . . . . .	139
4.3.11	Results and discussion . . . . .	142
4.4	Conclusions and future developments . . . . .	143
<b>5</b>	<b>SlickMap user manual</b>	<b>145</b>
5.1	Introduction . . . . .	145
5.2	Installation and setup . . . . .	147
5.3	Getting started . . . . .	148
5.3.1	Opening SlickMap . . . . .	148
5.3.2	SlickMap project philosophy . . . . .	148
5.4	Starting a new project . . . . .	149
5.5	Building a database . . . . .	149
5.5.1	Defining parameters of database and building tools window . . .	151
5.5.2	Working with the database building tools parameters . . . . .	154
5.5.3	Using the default Database values . . . . .	157
5.5.4	Controlled and dependent default database parameters . . . . .	159
5.5.5	Building a database with a velocity ramp . . . . .	161
5.6	Predesign toolbox . . . . .	161

5.6.1	User defined data . . . . .	162
5.6.2	Experimental data . . . . .	162
5.6.3	Catenary boom data . . . . .	163
5.7	Executing a project . . . . .	164
5.7.1	OilSlick graphics window . . . . .	166
5.7.2	Data window . . . . .	166
5.7.3	Project execution options . . . . .	166
5.8	Analysis options . . . . .	169
5.8.1	SlickMap plotting options . . . . .	170
5.8.2	Zooming in graphics window . . . . .	175
5.8.3	Measuring distances . . . . .	176
5.9	Project options . . . . .	176
5.9.1	Opening old projects . . . . .	177
5.9.2	Opening multiple projects . . . . .	178
5.9.3	Closing projects . . . . .	178
5.9.4	Use default database . . . . .	178
5.9.5	Edit existing database . . . . .	179
5.9.6	Editing default database . . . . .	179
5.9.7	Reasserting a project . . . . .	179
5.10	SlickMap accessories . . . . .	180
5.10.1	Printing . . . . .	180
5.10.2	Opening data files . . . . .	181
5.10.3	Editing options . . . . .	181
5.10.4	Exporting graphics . . . . .	181
5.10.5	Color options . . . . .	182
5.10.6	Getting help . . . . .	182
5.11	Data I/O structure . . . . .	182

**Bibliography**

**184**

## Abstract

The long term goal of these studies is to develop computer models that will help both gain fundamental insight into oil containment failure mechanisms and outline strategies and methods for limiting the occurrence and/or the intensity of these failures, in actual field situations.

This report presents results obtained at the University of Rhode Island, Department of Ocean Engineering, as part of a research project entitled : “Numerical Modeling of Oil Containment by a Boom/Barrier System : Phase III” (1/97-6/99). This project was supported by Grant No. DTRS57-95-G-00065 of the Department of Transportation, under funding from the Minerals Management Service (MMS). A 50% budget match was provided by the University of Rhode Island. The Phase III project is a third and fourth year continuation of Phase I project (8/94-12/95), entitled : “A hydrodynamic model of oil containment by a boom”, which was supported by DOT-USCG (US Coast Guards District No. 1), Grant No. DTRS57-94-G-00076 of the Department of Transportation FY 1994 Oil Pollution Research Grant Program, and Phase II project (7/95-12/97), entitled “Numerical Modeling of Oil Containment by a Boom/Barrier System”, which was also funded by the Coast Guards, as Grant No. DTRS57-95-G-00065 of the Department of Transportation. Both experimental and computational studies, carried out during Phase III of the project are presented in detail in this report. Results obtained during Phases I and II are only briefly summarized. Details can be found in final reports for Phases I and II [17, 22].

In Phase III, theoretical results obtained in Phases I and II as well as new theoretical developments and experimental results were used to develop a series of interactive model tools, referred to as *SlickMap*, for modeling oil slick containment by a boom and its possible failure. This report first gives details of experiments performed at OHMSETT (The National Oil Spill Response Test Facility), the by the University of Rhode Island, for both straight and catenary shaped booms, using Sundex or Hydrocal oil (Chapter 2). Laboratory experiments performed by the University of New Hampshire (UNH) are then analyzed in order to get functional shapes of friction parameters useful for the models (Chapter 3). Results of both of these sets of experiments are later used to calibrate SlickMap models. The report then provides the theoretical background for SlickMap’s numerical models of the vertical cross-sectional shape of an oil slick, contained by a straight boom, in a given uniform flow/tow velocity of water (Chapter 4). The boom shape is simplified to be represented by a vertical (skirt) plate of specified draft and thickness; the boom is assumed to be homogeneous and long in the direction perpendicular to the vertical plane of interest. Conversions are made in SlickMap from catenary shape booms to such straight booms. Finally, the report provides a detailed user’s manual for the interactive model tools developed under SlickMap (Chapter 5). These were developed in FORTRAN and implemented using *Visual Basic*<sup>TM</sup> for a PC Window interface system.

# Chapter 1

## Introduction

This report presents results obtained at the University of Rhode Island, Department of Ocean Engineering, as part of a research project entitled : “Numerical Modeling of Oil Containment by a Boom/Barrier System : Phase III” (1/97-6/99). This project was supported by Grant No. DTRS57-95-G-00065 of the Department of Transportation, under funding from the Minerals Management Service (MMS). A 50% budget match was provided by the University of Rhode Island. The Phase III project is a third and fourth year continuation of Phase I project (8/94-12/95), entitled : “A hydrodynamic model of oil containment by a boom”, which was supported by DOT-USCG (US Coast Guards District No. 1), Grant No. DTRS57-94-G-00076 of the Department of Transportation FY 1994 Oil Pollution Research Grant Program, and Phase II project (7/95-12/97), entitled “Numerical Modeling of Oil Containment by a Boom/Barrier System”, which was also funded by the Coast Guards, as Grant No. DTRS57-95-G-00065 of the Department of Transportation. The present report only covers developments, both experimental and computational, carried out during Phase III of the project. Results of earlier phases can be found in final reports for Phases I and II (Grilli *et al.* [17], 1996; Grilli *et al.* [19], 1997).

The Phase I project was aimed at developing a two-dimensional hydrodynamic model of *oil containment* by booms, to be used to investigate oil containment failure (Figs. 1.1 and 1.2). It was envisioned that this numerical model and its future improvements would help us both gain fundamental insight into oil containment failure mechanisms and outline strategies and methods for limiting the occurrence and/or the intensity of such failures, in actual field situations. Due to its more catastrophic nature, the failure mode referred to as *critical accumulation* was the main object of the study (Figs. 1.2 and 1.3).

Three main technical tasks were initially identified : (i) numerical model selection and design; (ii) model testing and validation; and (iii) application to oil containment failure. Extensive literature review and analysis of the physical, theoretical, and numerical problems relative to oil containment were conducted as part of task (i) (Grilli *et al.* [17], 1996). Based on this review, an initial simple modeling strategy,

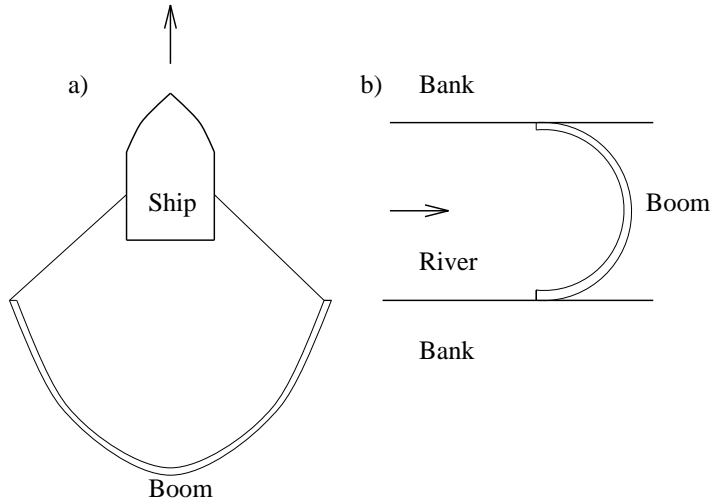


Figure 1.1: Planview of typical set-up for oil containment by : (a) a towed boom (ocean); or (b) a static boom (river). Arrows mark the direction and magnitude of the relative velocity  $U$  between boom and water.

using piecewise-constant Vortex Sheets (PCVS) to model the interfaces between fluids, was selected (hereafter referred to as the *Phase I model*). The Phase I model was implemented, validated, and used to predict oil containment failure, as part of tasks (ii) and (iii). In all cases, model results qualitatively showed the expected failure modes and the correct sensitivity to changes in physical parameters (e.g., Fig. 1.4). Details of the Phase I model development, implementation, and results can be found in Grilli *et al.* [17, 18].

The Phase II project involved various improvements of the Phase I model, hereafter referred to as the *Phase II models*, at both the level of the modeled physics (e.g., inclusion of friction effects at the oil-water interface) and the numerical methods used (e.g., higher-order Vortex Sheet discretization and time updating techniques). More specifically, model developments in Phase II studies focused on three major aspects :

- (i) improving the Piecewise Constant Vortex Sheet (PCVS) models, both periodic and non-periodic, developed during Phase I studies; for the non-periodic PCVS model, in particular, improvements were aimed at better addressing problems with complex boundary geometries (as needed to correctly include booms in VS models);
- (ii) developing and implementing a more accurate higher-order model, based on Continuous Vortex Sheets (CVS), which will ultimately provide a better representation of hydrodynamic instabilities in the oil containment problem (Grilli and Hu [21], 1997); and
- (iii) both implementing and validating a numerical method for calculating the quasi-

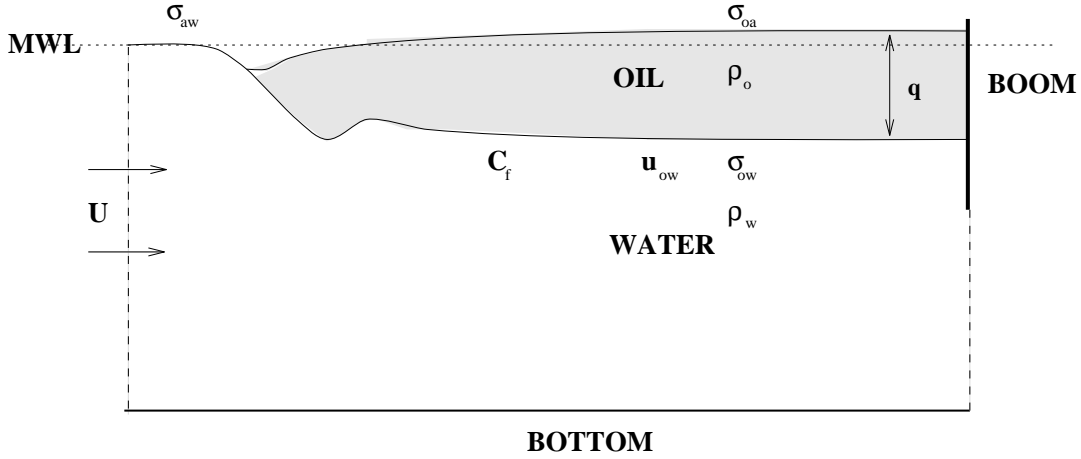


Figure 1.2: Sketch for initiation of oil containment failure by *critical accumulation*, with mention of important parameters :  $U$ , water-boom relative tow/flow velocity;  $\mathbf{u}_{ow}$ , oil-water relative velocity at the interface;  $\rho_o$ ,  $\rho_w$ , oil and water density, respectively;  $\sigma_{ow}$ ,  $\sigma_{oa}$ ,  $\sigma_{aw}$ , interfacial tension coefficients for oil-water, oil-air, and air-water, respectively;  $C_f$ , oil-water interfacial friction coefficient;  $q$ , oil slick depth; MWL, Mean Water Level.

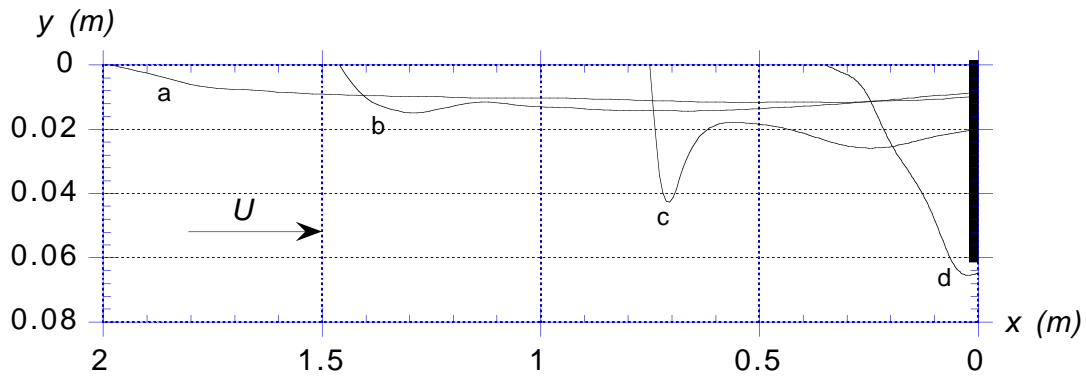
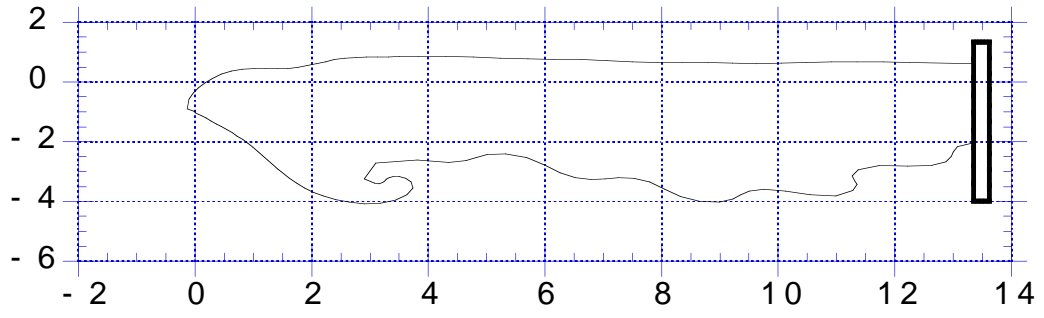
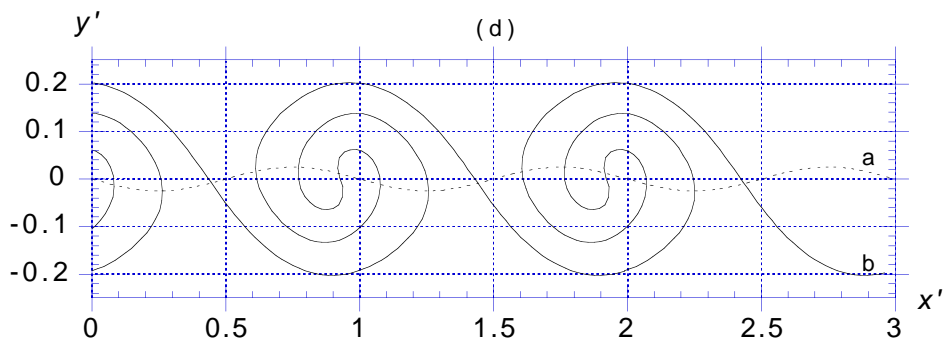
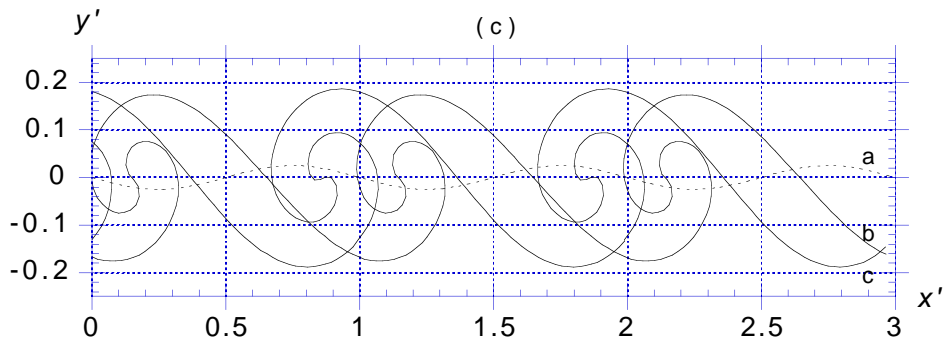
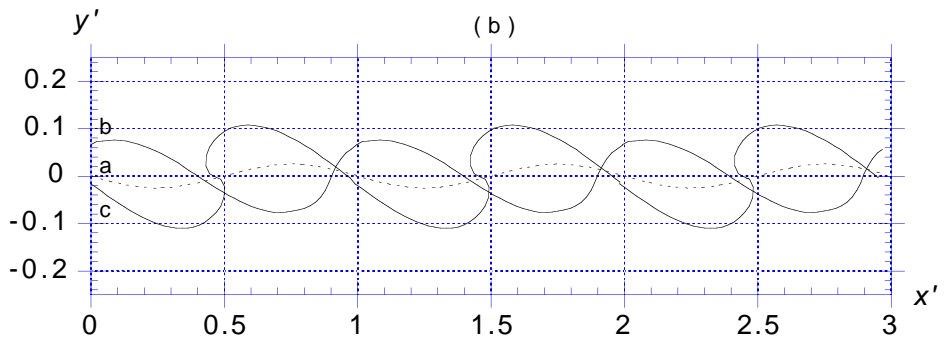
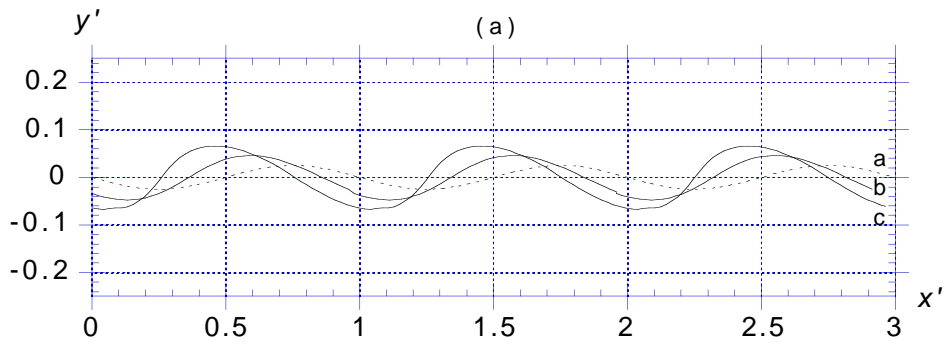


Figure 1.3: Experimental shapes of oil slicks measured in Delvigne's [9] (1989) experiments with Arabian light emulsion ( $\nu_o = 23 \text{ m}^2/\text{s}$ ) for relative water-boom velocity  $U = a : 0.065$ ;  $b : 0.095$ ;  $c : 0.128$ ; and  $d : 0.145 \text{ m/s}$ . The figure shows the increase in size of the headwave and the shortening of the slick as  $U$  increases from curve a to c and, finally, the failure by *critical accumulation* with the oil slick draining under the boom in curve d.





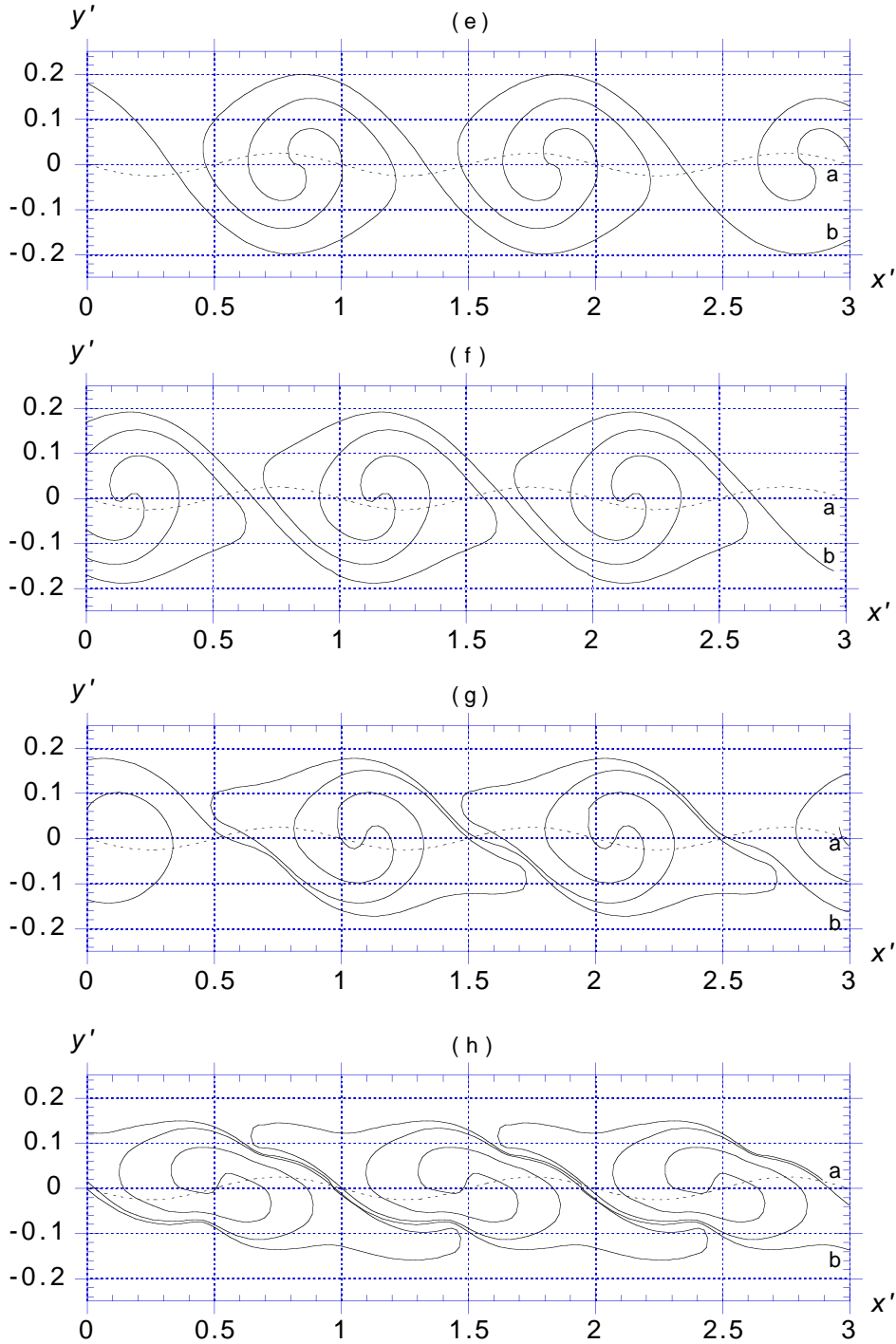


Figure 1.5: Results for periodic KH instability with wavelength  $\lambda = 0.1\text{m}$ ,  $|U| = 0.5$  m/s,  $\varphi = 1$ , and  $\sigma_{wo} = 0$ . curves show interfacial shape at time  $t$  (s) = (a) a : 0.0002, b : 0.060, c : 0.120; (b) a : 0.0002, b : 0.150, c : 0.240; (c) a : 0.0002, b : 0.330, c : 0.390; (d) a : 0.0002, b : 0.480; (e) a : 0.0002, b : 0.510; (f) a : 0.0002, b : 0.540; (g) a : 0.0002, b : 0.570; (h) a : 0.0002, b : 0.600. (---) represents the initial perturbation of the free surface

Despite their accuracy and relevance, the main drawbacks of the numerical models developed in Phases I and II, however, were that : (i) they did not really include a boom and a slick of finite length, but concentrated in the headwave region of the slick where Kelvin-Helmholtz (KH) instability waves were created; and (ii) except for the computation of the equilibrium quasi-steady shape of a slick, there had been no comparison (and thus calibration) of the time dependent models with experimental results. The development of a complete time dependent model of oil containment by a boom, and its experimental validation and calibration, were conducted as part of the Phase III studies described in this report. The new extended model, referred to as SlickMap, was implemented in a user-friendly interactive interface. Model results were compared with experimental data obtained in the University of New Hampshire (UNH) two-dimensional recirculating flume and three-dimensional data obtained at the OHMSETT (The National Oil Spill Response Test Facility) flume in New Jersey, which is operated by the Minerals Management Service (MMS). Dissipation mechanisms in the model (interfacial friction, slick circulation,...) were calibrated based on results of experiments.

In Chapter 2 of this report, we present results and discussions of experiments conducted at OHMSETT. In Chapter 3 of this report, we present results and discussions of experiments conducted at UNH. In Chapter 4, we present the theoretical development and validation of SlickMap model. And, in Chapter 5, we give a detailed user's manual for SlickMap.

In the following sections, we give a summary of key findings (from both the literature and this and earlier phases of this study), regarding oil containment failure, as well as a quick overview of laboratory experiments carried out at OHMSETT and UNH, and of SlickMap model.

## 1.1 Problem overview

Booms are one of the most commonly used techniques to collect and contain oil on the sea surface, or to protect specific areas against slick spreading by containment or diversion. In the collection mode, floating boom systems are deployed on the free surface, usually in U or V configurations, and towed towards the oil slick. In the diversion mode, they are used to direct oil to the shoreline or sheltered area.

The containment of oil by a boom is illustrated by the sketches in Fig. 1.1, which correspond to both an *ocean situation* in which a boom is towed by a boat at relative speed  $U$  over the water, and a *river situation* in which a fixed boom is placed across a river flow with current  $U$ . In both cases, oil accumulates inside the boom with the maximum accumulation occurring at the boom catenary's apex, where the maximum relative water velocity is observed. Considering the location of accumulation and the small curvature of the boom geometry around the apex point, it is often acceptable (as a first approximation) to simplify this essentially three-dimensional problem to a

*two-dimensional* one in the vertical plane intersecting the boom's apex (Fig. 1.2). We will see that this hypothesis is confirmed by experiments conducted at OHMSETT (Chapter 2). Assuming a large enough water depth, it is also reasonable to assume that, for both cases sketched in Fig. 1.1, the boom does not move and the water flows under the boom at a tow/flow velocity  $U$ , equal to the relative boom-water velocity.

In order to collect as much oil as possible in the shortest possible time, it is desirable to have a relative velocity which is as large as possible. For typical floating booms equipped with vertical skirts, however, various hydrodynamic instabilities at the oil-water interface, however, contribute to a fairly low practical limit for the relative velocity, on the order of 0.5 m/s or about 1 knot. In fact, for the idealized problem sketched in Fig. 1.2, laboratory observations show that interfacial waves start developing at the oil-water interface for relative current speeds,  $U \simeq 0.15$  m/s. For larger speeds, these waves become unstable and, in most cases, lead to substantial or even total loss of oil under the boom (Agrawal and Hale [1], Lau and Kirchifer [32], Wicks [44], Wilkinson [45, 46]).

In the literature, such instabilities are referred to as *boom containment failure modes* and three main types (or modes) of containment failures have thus far been identified. [Note that, in addition to these failure modes which occur in calm weather, the effectiveness of the boom in containing oil can be severely limited by the hydrodynamic behavior of both the boom and the slick under extreme weather conditions that may create high seas. Such factors have not been considered in the Phase I to III studies.] :

- *drainage failure*, where an increase in relative water-boom velocity  $U$  leads to an increase in interfacial friction stresses, causing both a shortening and a thickening of the slick beyond the barrier draft  $d$ , leading to containment failure;
- *entrainment failure*, where, for high relative oil-water velocities and low viscosity oils ( $\nu_o \leq 3,000$  cSt), large interfacial stresses occur and induce shear instabilities at the oil-water interface characterized by the formation of small fast-moving interfacial waves (ripples); for sufficiently large  $U$  (on the order of 0.25 m/s), these waves may grow unstable and break, leading to subsequent entrainment of oil droplets in the underlying flow;
- *critical accumulation*, where, for oils with larger viscosities ( $\nu_o \geq 3,000$  cSt or so) and velocity  $U$  usually lower than for the other two modes ( $U_{cr} \simeq 0.15$  m/s), the interface develops slow-moving larger scale oscillations (headwave) which eventually cause all of the oil to escape under the barrier, *independent* of barrier draft  $d$  (Fig. 1.3). This failure mode can also be seen in UNH experiments in Chapter 3 (e.g., Fig. 3.1).

Grilli *et al.* [17] conducted an exhaustive literature review of the oil containment problem and identified the key parameters and physical phenomena governing the

three failure modes listed above. They showed, in particular, that *critical accumulation* is the dominant failure mode for high viscosity oils that are found in many real slicks (Delvigne [9], Johnston *et al.* [27]). [In fact, due to weathering effects, oil slick viscosity increases rapidly with time for many oils.] They also clearly showed that interfacial waves occurring during entrainment and critical accumulation failure modes are both initiated and sustained by *shear instability* at the oil-water interface, usually referred to as a *Kelvin-Helmholtz (KH) instability* (Benjamin [5], Drazin [11], Jones [28], Rangel and Sirignano [38]). Based on these findings, Grilli *et al.* focused on numerical modeling of KH instability (in the context of oil containment by a boom) as the main objective for Phases I and II of this project.

KH instabilities at the oil-water interface result from the interplay of the following physical processes and parameters (Fig. 1.2),

- the relative *water-boom velocity*  $U$ , which controls the magnitude of interfacial friction forces and triggers and sustains KH instability (see Section 2.5.2 in Phase II report);
- the fluid *density difference*  $\Delta\rho_{ow} = \rho_w - \rho_o$ , which affects both slick thickness and spreading forces. [In applications, this parameter is often represented by the value of the oil/water density ration  $\varphi = \rho_o/\rho_w = 1 - \Delta\rho_{ow}/\rho_w$ .] (see Chapter 4 in Phase II report);
- $\Delta\rho_{ow}$  or  $\varphi$ , and the *surface tension* coefficient at the oil water interface,  $\sigma_{ow}$ , which both affect the growth of interfacial KH waves (see Section 2.5.2 in Phase II report);
- the interfacial *friction coefficient*  $C_f$ , which controls the magnitude of interfacial friction forces (and thus affects oil slick thickness) and is dependent on interfacial shape (including irregularities due to KH waves) (see Chapter 4 in Phase II report);
- *oil viscosity*  $\nu_o$ , which damps out short interfacial waves and limits the strength of internal circulation cells within the oil slick (hence justifying a quasi-hydrostatic assumption for highly viscous oil slicks).

Other parameters of lesser importance are  $\sigma_{aw}$  and  $\sigma_{oa}$ , the air-water and oil-air surface tension, respectively.

Many experimental and theoretical studies were pursued in the 1970's to understand the physics of oil containment by a boom and to identify the conditions leading to containment failure. More recently, there has been a renewed interest in studying this problem and attempts were made to use numerical modeling tools (Zalosh [47], Bai and Kim [2], Clavelle and Rowe [7], Ertekin and Sundararaghavan [13]). Among the existing models, however, only the work by Zalosh [47] included the key parameters, listed above, affecting interfacial instability, whereas the other models [2, 7, 13]

concentrated on representing fluid behavior in the bulk of the oil and water domains in front of and/or behind the boom, and totally ignored surface tension and KH waves on the oil–water interface.

In proposing the FY94 Phase I project, considering the high degree of complexity of physical mechanisms involved, it was anticipated that the developed model would only be a first step towards a more comprehensive model of oil containment that could eventually provide practically useful results. In Phase I, we thus identified three major phases in model development, corresponding to successive improvements of the level of physical phenomena modeled and, hence, also of modeling accuracy (see Grilli *et al.* [17]). The approach selected for the initial model, *the Phase I model*, was based on Zalosh’s model with both improved governing equations and numerical solution (see Grilli *et al.* [17]).

Development and implementation of the Phase II models took place as part of the FY95 project. It was shown that the Phase II models provided significant improvements of both the level of physics modeled and the numerical accuracy, compared to the Phase I model (see Grilli *et al.* [19]). In particular, quantitative results were given showing :

- effects of the key factors listed above, on the growth rate of interfacial KH instabilities;
- results of computations were given for the failure of a contained slick due to instabilities in the headwave;
- Finally, quantitative predictions for the equilibrium steady-state shape of a contained slick were given, which compared favorably with existing experiments.

As a summary, Fig. 1.6 gives an overall flowchart for the model development procedures followed during Phase II, with the model extensions and experimental validation/calibration tasks anticipated to be carried out in Phase III, at the end of Phase II studies. As indicated in the figure, the major progress in Phase II models, as compared to the Phase I model, were made in the development of new numerical algorithms for the periodic (KH instability) and non-periodic (oil-slick with a boom) Piecewise Constant Vortex Sheet (PCVS) models, and in the establishment and implementation of a higher-order model (CVS) of the same problems. Numerical/qualitative validation of the newly developed models were carried out at all stages of model developments, using both convergence tests and lower-order theoretical solutions (e.g., the linearized KH instability problem by Lamb [31]). As indicated, both the PCVS and the CVS models and related algorithms were alternately tested for the KH instability case, which contains infinite vortex sheets with periodic disturbances, and for an oil-boom containment setting, similar to that in Fig. 1.2, which consists of multiple discretized vortex sheets and several infinite sheets.

As shown in Fig. 1.6, Phase III studied involved :

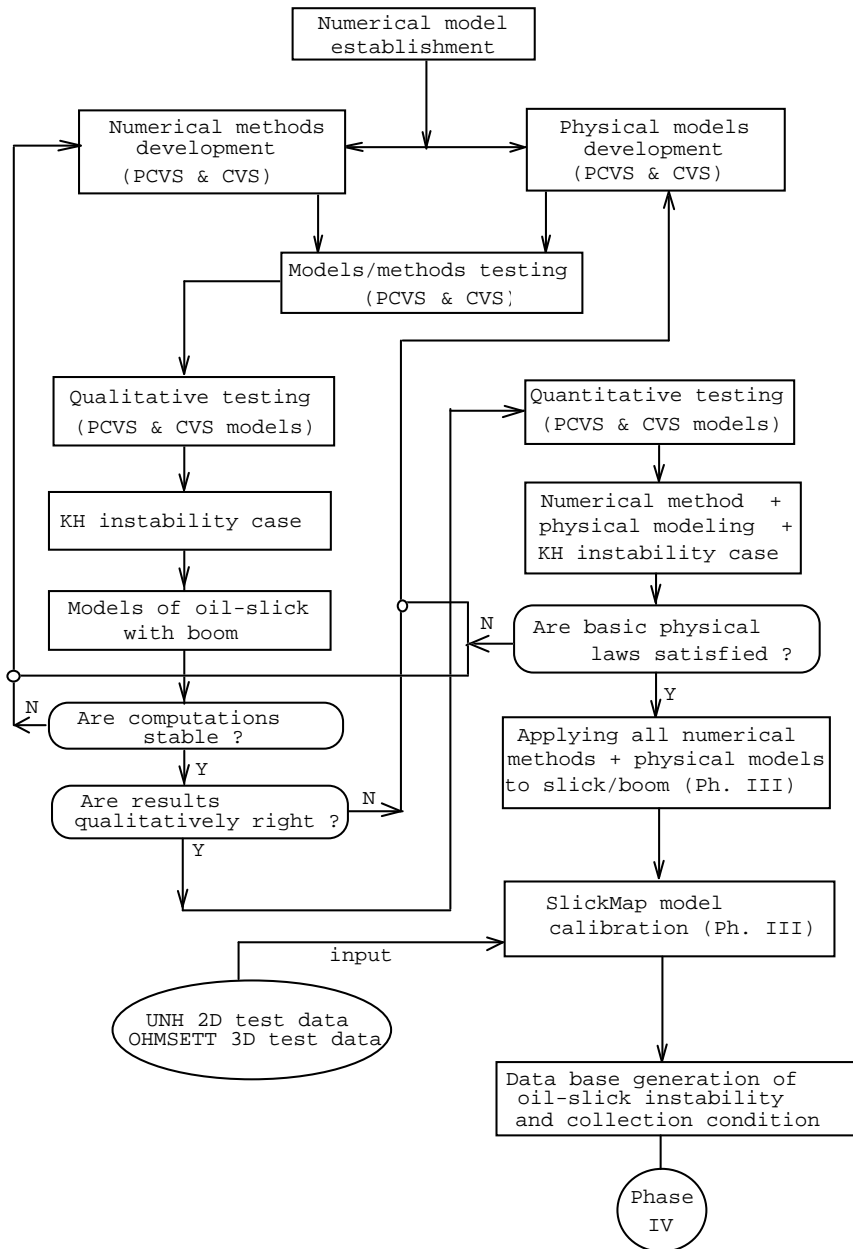


Figure 1.6: Flow chart of Phase II model development/validation procedure, with indication of Phase III development/validation/calibration tasks.

- carrying out and analyzing laboratory experiments of oil containment by booms (OHMSETT and UNH; Chapters 2 and 3);
- the development of a comprehensive efficient oil-slick boom model (referred to as SlickMap), implemented into a user-friendly interface (Chapters 4 and 5);
- Using the experimental data to calibrate/validate SlickMap model.

## 1.2 Review of laboratory experiments

### 1.2.1 OHMSETT experiments

Experiments were conducted at the MMS operated OHMSETT facility (National Oil Test Facility) in Sandy Hook New Jersey, during August 1997, May 1998, and September 1998. The purpose of these tests was four-fold :

- to better understand the physics of containment failure by *critical accumulation*;
- to provide experimental data for straight booms, that will allow the two-dimensional oil spill containment model SlickMap to be properly calibrated;
- to study the effect of *boom draft* on containment failure;
- to compare results obtained for a catenary shape boom (Figs. 1.1 and 2.10) to those obtained for a straight boom, and thus validate the use of SlickMap for actual three-dimensional towed booms;
- to compare OHMSETT large scale experiments to experimental results obtained, for smaller scales, at the University of New Hampshire (UNH), in well controlled laboratory conditions.

OHMSETT's facility is composed of a large scale open air tow tank filled with sea water (Fig. 2.1). Tests were performed that matched the type of boom geometry represented in the two-dimensional SlickMap model, i.e., straight booms with vertical plane skirts located below a float (e.g., Fig. 1.2). One of the booms was also tested in catenary shape, to compare results to those of straight booms (September 1988). For each boom, tow speed  $U$  was increased up to containment failure, for a number of oil slick volumes. Two types of oils were successively tested for each boom (Sundex 8600T and Hydrocal 300). The main data recorded in the tests was the slick length  $L$  measured along the tank axial direction, as a function of tow speed  $U$ .

A comparison of results obtained for each type of oil is made as a function of boom draft, and these results are used to estimate the average friction coefficients at the oil-water interval, which is used to initialize SlickMap Stage 1 model.

Full account of OHMSETT experiments and of their analysis is given in Chapter 2.

### 1.2.2 UNH experiments

From 1997 to 1999, the University of New Hampshire (UNH) conducted laboratory experiments of oil containment by booms, as part of a collaborative effort coordinated with URI's study.

URI analyzed UNH's experimental results, independently of UNH's own analyses of their results, reported in their reports for Phases II and III. The purpose of our analyses was two-fold :

- to learn more about the physics of oil containment failure by critical accumulation, in order to refine SlickMap numerical models;
- to calculate experimental values of friction coefficient variations along the water-oil interface, in order to define a functional variation of friction, to be used in SlickMap models for Stages 2 and 3.

UNH's experiments used Sundex oil, and took place in two flumes with a recirculating fresh water current, in a set-up similar to Delvigne's [9] (1989) experiments. For the latest set of experiments (August 1999), both the flume and the data acquisition system were upgraded. The barrier used to represent the boom consisted of a vertical plywood board with draft  $d = 0.038$  or  $0.064$  m (as in [9]). Rubberized horsehair was placed over a  $0.2$  m layer in front of the barrier, to inhibit corner vortices (e.g., Fig. 3.1). Oil was introduced in the flume while a low flow velocity  $U = 0.07$  m/s was maintained, in order for the oil to collect in front of the barrier. The flow speed was then increased by increments, up to containment failure. After each speed increase, measurements were taken after the slick reached a new equilibrium shape.

In June 1997, the URI team was provided with initial results of experiments conducted in May 1997 by UNH. Results were given in the form of digitized pictures of slick profiles taken through the tank transparent sidewalls, using a high resolution 35 mm video camera (see UNH's Phases II and III reports). In August and September 1997, similar results, but with a higher resolution, were provided. Finally, in August 1999, more results of the same type, obtained in the upgraded flume, were provided in the form of digitized water-oil interfaces.

Full account of UNH experiments and of their analysis is given in Chapter 3.

## 1.3 Principle of SlickMap models

SlickMap Models simulate the time evolution of an oil slick contained by a straight boom, with vertical skirt, in a vertical, two-dimensional, plane going through the boom middle (apex) section. The models were developed to work in three successive stages : (i) Stage 1 model : static initialization of slick shape (Fig. 1.7); (ii) Stage 2 model : iterative initialization of the static slick shape, to find a quasi-hydrostatic equilibrium for the initial current speed (Fig. 1.8); and (iii) Stage 3 model : dynamic

time-stepping of the quasi-hydrostatic slick shape, until equilibrium is achieved for the specified current or step change in current (Fig. 1.9), or containment failure occurs. Description of the models' input data and user interface are provided in a separate user's manual (Chapter 5).

In the models, only the global shape and behavior of the slick air-oil and water-oil interfaces are modeled. Hence, no attempt is made to resolve the small scale features of the slick geometry, although their effect is globally accounted for through using the experimentally validated interfacial friction coefficient function (FCF), and various other terms in the model.

The theoretical developments for SlickMap Model are detailed in Chapter 4. SlickMap models are based on assuming an ideal flow in the water (i.e., incompressible, inviscid, and irrotational) and a quasi-hydrostatic equilibrium in the oil slick. Various friction and dissipative effects are included at the oil-slick interface (head loss—energy dissipation, shear effects on the oil-water interface, approximate viscous circulation within the slick, effects of slick inertia). In Phases I and II models, the ideal flow approximation was expressed as a Vortex Sheet (VS) formalism, i.e., in a vorticity/circulation type flow representation. This led to using Biot-Savart boundary integral equations to describe the flow in the water (Batchelor [4]). Periodic interfacial instabilities were very accurately and efficiently modeled using a higher-order continuous VS model (Grilli and Hu [21]). In Phase III, however, it was determined that Biot-Savart equations expressed in a time dependent VS model, did not accurately satisfy no-flow conditions at solid boundaries, such as the boom. Hence, Stages 2 and 3 model formalisms were switched to using a velocity potential representation, instead of the circulation on the various interfaces, in which the normal flux naturally appears. Basically, however, the levels of approximation and the modeled physics are identical for Phases II and III (see Chapter 4 for details of the analogy of potential flow and VS method). The potential flow approach in SlickMap models is governed by continuity equation, expressed as a Boundary Integral Equation, using Green's 2nd identity. This equation is solved in Stage 2 and 3 models, using a higher-order Boundary Element Method (BEM).

Interfacial friction is calibrated in SlickMap models, using results of laboratory experiments (OHMSETT and UNH; see Chapters 2 and 3). For a given boom, the model solution is calculated for a specified oil slick volume per unit width of boom ( $V_o$ ; i.e., the linear volume), oil and water densities ( $\rho_o$  and  $\rho_w$ ), oil viscosity ( $\nu_o$ ), flow/tow speed ( $U$ ), average interfacial friction coefficient for an initial low speed  $U_o$  ( $C_{fm}$ ), and headwave length parameter ( $Y$ ). Model results include slick length ( $L$ ), maximum slick depth at the boom ( $D$ ), and oil slick geometry as a function of time and  $U$ .

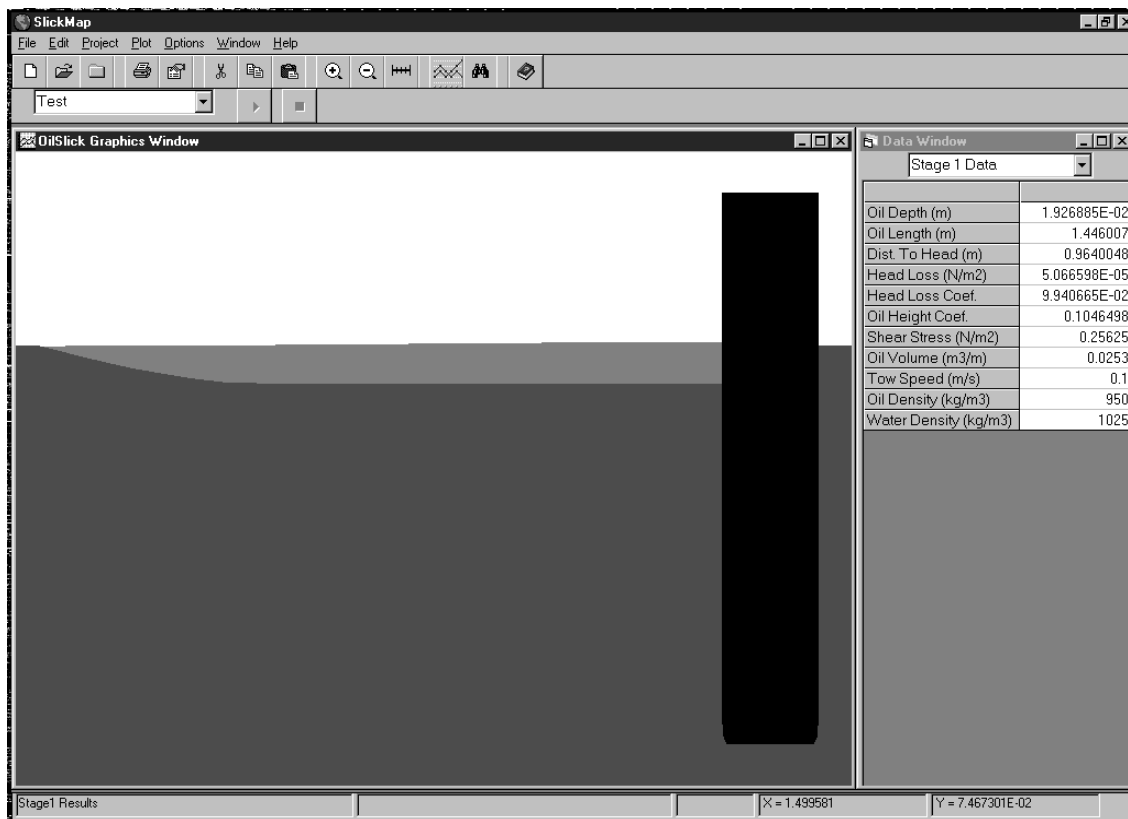


Figure 1.7: Typical SlickMap output screen for Stage 1 Model

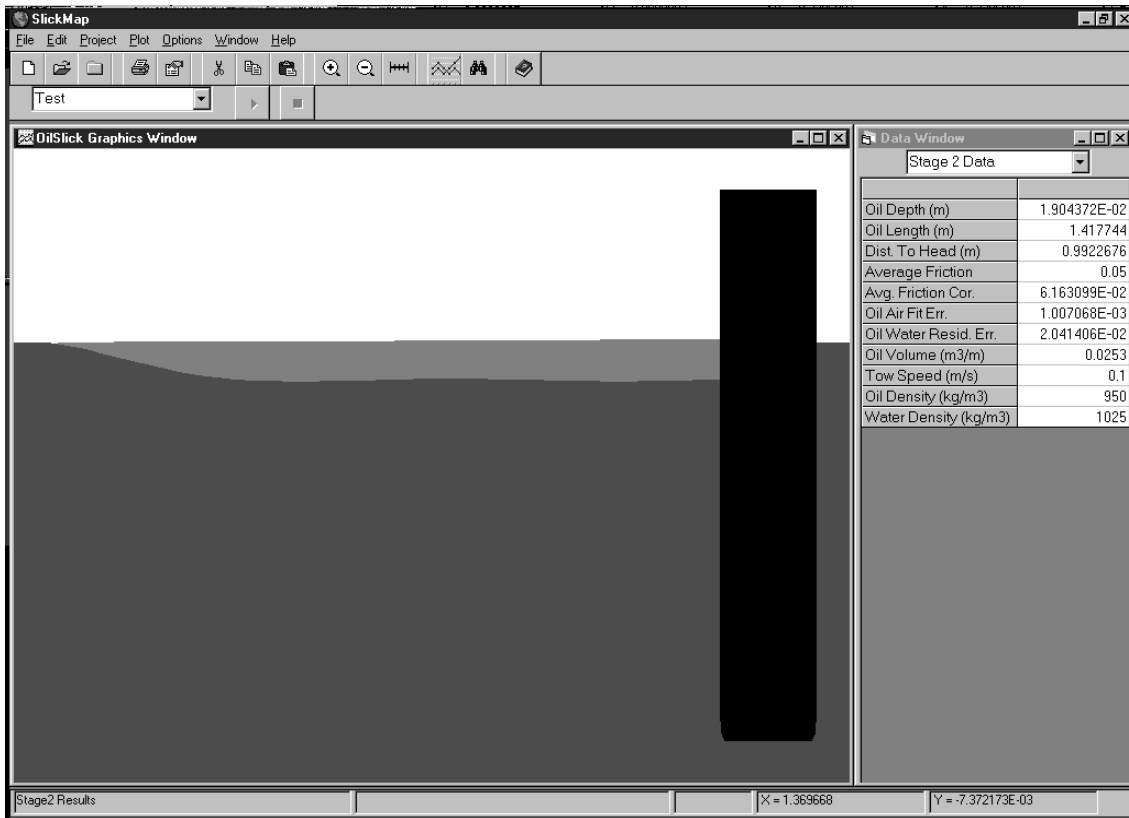


Figure 1.8: Typical SlickMap output screen for Stage 2 Model

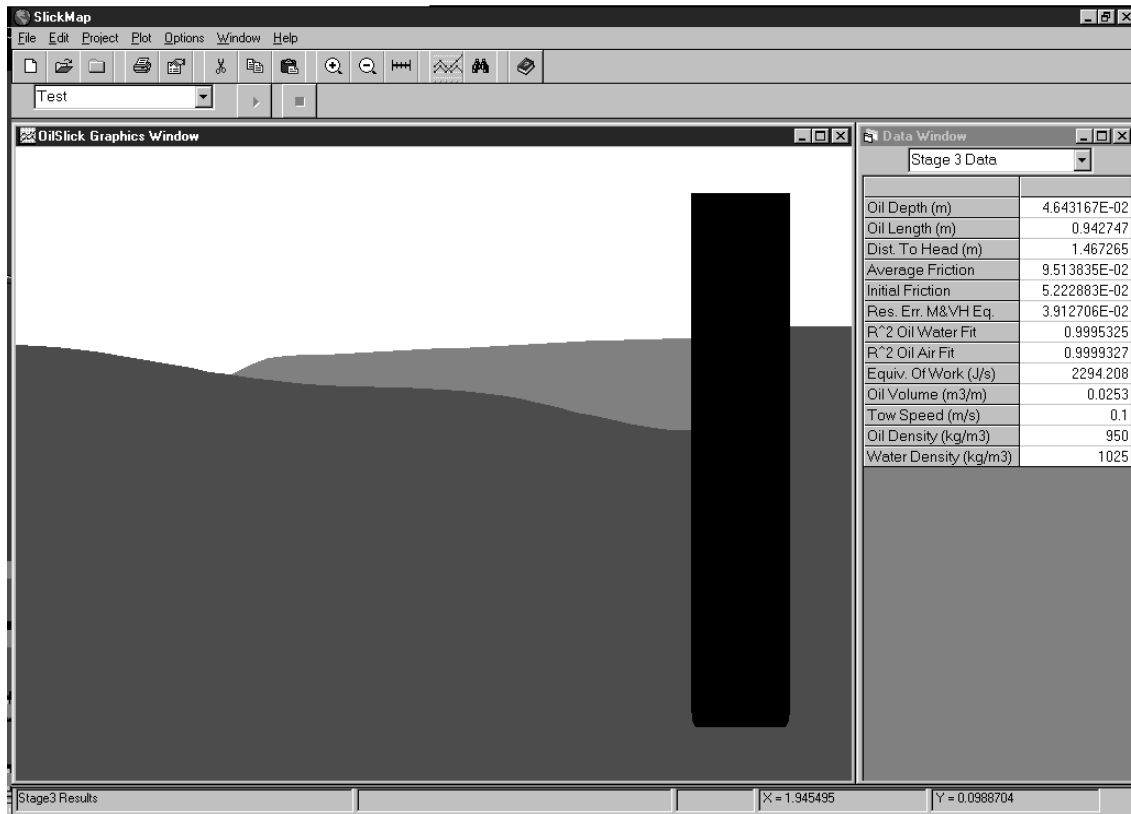


Figure 1.9: Typical SlickMap output screen for Stage 3 Model

## 1.4 Principle of SlickMap's interactive user interface

SlickMap models are programmed in FORTRAN. SlickMap's interface is implemented as an interactive user-friendly set of graphical tools, developed using the *Visual Basic*<sup>TM</sup> language, for a PC window environment. The interface allows for an educated user to easily set-up, run, and visualize results of the oil slick containment models implemented in SlickMap. These models, referred to as Stage 1, 2, and 3 models, as mentioned above, typically involve the input of geometric data (e.g., oil volume, boom draft and width,...), physical data (e.g., oil type, density, viscosity, interfacial tension, water current, ...), and numerical parameters (e.g., grids, discretization, number of iterations, maximum numerical errors,...). SlickMap's interface makes it easy to input the required data while offering standard default values whenever possible, automatically generating model grids, or allowing for accessing data bases of existing laboratory/experimental data. SlickMap lets the user interactively run the models, visualize the results as graphics (e.g., Figs. 1.7, 1.8, 1.9) or as list of numbers, and change the problem data. A detailed user's manual for SlickMap software is given in Chapter 5.

# Chapter 2

## Experiments at Ohmsett

### 2.1 Introduction

Experiments were conducted at the MMS operated OHMSETT facility (National Oil Test Facility) in Sandy Hook New Jersey, during August 1997, May 1998, and September 1998. The purpose of these tests was four-fold : (i) to better understand the physics of containment failure by *critical accumulation*; (ii) to provide experimental data for straight booms, that will allow the two-dimensional oil spill containment model SlickMap to be properly calibrated; (iii) to compare results obtained for a catenary shape boom (Fig. 2.10) to those obtained for a straight boom, and thus validate the use of SlickMap for actual three-dimensional towed booms; (iv) to compare OHMSETT large scale experiments to experimental results obtained, for smaller scales, at the University of New Hampshire (UNH), in well controlled laboratory conditions.

OHMSETT's facility is composed of a large scale open air tank (203.44 m long (667'),  $w = 19.812$  m wide (65') with a 2.4 m water depth (8')), filled with sea water from the nearby Sandy Hook Bay (with average salinity  $S \simeq 2.4\%$ ). The tank is equipped with a tow carriage, operated from a control tower located at one of the tank's extremities. The tow carriage is composed of a main bridge, directly attached to the tow cables, on which the crew and measuring equipment are located, and an auxiliary bridge, set at a fixed distance from the main bridge, to which the tested booms are attached. This bridge also has oil reservoirs (Figs. 2.1 and 2.2).

Tests were performed that matched the type of boom geometry represented in the two-dimensional SlickMap models, i.e., straight booms with vertical plane skirts located below a float (e.g., Fig. 4.1). Booms placed in catenary shape were also tested, to compare results to those of straight booms (September 1988). Oil containment was tested for three booms of different type and draft, at various tow speeds  $U \in [0, 1]$  knot, and for a number of slick volumes of oil  $v_o$  (in  $\text{m}^3$ ). In each case, tests were run by incremental speed steps, from low to high speed values, up to reaching containment failure. Two types of oils were successively tested for each boom (Sundex 8600T and Hydrocal 300). In addition to the standard environmental variables, such as air and



Figure 2.1: View of OHMSETT facility from the control tower, with both auxiliary (in the front) and main (in the back) bridges of the tow carriage.

water temperature, and wind speed, the main data recorded in the tests was the slick length  $L$  along the tank axial direction (see, e.g., Fig. 4.1) measured as a function of tow speed  $U$ . In all the tests, an underwater video camera was used to record the shape of the water-oil interface during the experiments.

## 2.2 Experimental data and results

### 2.2.1 Data Collection

The data obtained during each experiment included electronically and manually collected data.

The electronically collected data (water temperature, water level, wind speed and direction, tow carriage speed, etc. . .) was automatically measured by various sensors, and remotely recorded by computers located on the third floor of the OHMSETT Control Tower. [Note that the accuracy of tow carriage speed measurements is  $\pm 0.01$



Figure 2.2: View of auxiliary bridge and control tower at OHMSETT.

knot.] An underwater camera as well as a hand held camera were used to capture videos of the experiments from various positions. The underwater video camera was remotely operated by joysticks located on the main bridge of the tow carriage. The assigned operator used a control monitor to decide whether to zoom in or out and move the underwater camera. Some electronically collected data was monitored at locations other than the data collection computer, in order to control test conditions. The distribution pump rate and test fluid volume, for instance, were monitored on the main bridge, by operating technicians, as well as recorded on the data collection computer.

Manually collected data in these experiments, i.e., the slick length  $L$  from the boom to the leading edge for each level of tow speed  $U$ , was measured and recorded by an assigned technician located on the auxiliary bridge, using yardstick, measuring tape and grids installed for that purpose above the slick (see details below). Since the slick leading edge was not usually perfectly straight across the tank width, it was also the task of the technician to make the best visual reading of the average location of the slick leading edge (point O in Fig. 4.1). By comparing repetitions of identical experiments, we will see that such visual readings are fairly accurate.

Oil	$\mu$ (Kg/m.s)	$\varphi$	$\sigma_{wo}$ (N/m)	$\sigma_{oa}$ (N/m)	Solids and $H_2O$
Sundex	9.2	0.938	0.0344	0.0380	2.0%
Hydrocal	0.128	0.894	0.0259	0.0336	1.0%

Table 2.1: August 1997 tests. Nominal Oil Properties measured at OHMSETT at 25° C.

Oil and water property data were measured by the chemical technician, using fluid samples collected during the test period.

For each experiment, the test procedure was as follows :

- move the main and auxiliary bridges to the beginning of the tank (tower side);
- increase tow carriage speed to  $U = 0.2$  knot;
- release premeasured oil volume  $v_o$  in front of the boom;
- allow for the oil slick to stabilize in shape and make a record of its initial length  $L_o$ ;
- incrementally increase bridge speed by 0.05 knot;
- wait for the slick to stabilize and read the slick length  $L(U)$  for each incremental speed level;
- stop experiment at tank extremity or at containment failure.

## 2.2.2 August 1997 experiments

For these experiments, the auxiliary bridge was set 8.85 m (29') behind the main bridge axis. A straight fence-type boom (later referred to as Boom # 2), with skirt draft  $d = 0.305$  m (12"), manufactured by Applied Fabric Technology Inc., was used in these experiments. This boom was attached to vertical sliders, themselves located at each extremity of the tow carriage auxiliary bridge. Hence, the boom length was very close to the tank width  $w$ . The boom was made of a continuous skirt with 16 shallow draft floats located on both sides of the boom 1.219 m apart (Fig. 2.3). The water depth in the tank was 2.4 m. In this first series of tests, two calibration experiments were first run, with no data being recorded. Ten tests were then conducted, seven of which used Sundex 8600T oil (experiments 3 to 9) and three of which used Hydrocal 300 oil (experiments 10 to 12). The density of Sundex and Hydrocal oils for these experiments, measured afterwards on oil samples in OHMSETT's laboratory, was  $\rho_o = 955$  kg/m<sup>3</sup> and 897 kg/m<sup>3</sup>, respectively. Other corresponding physical data are

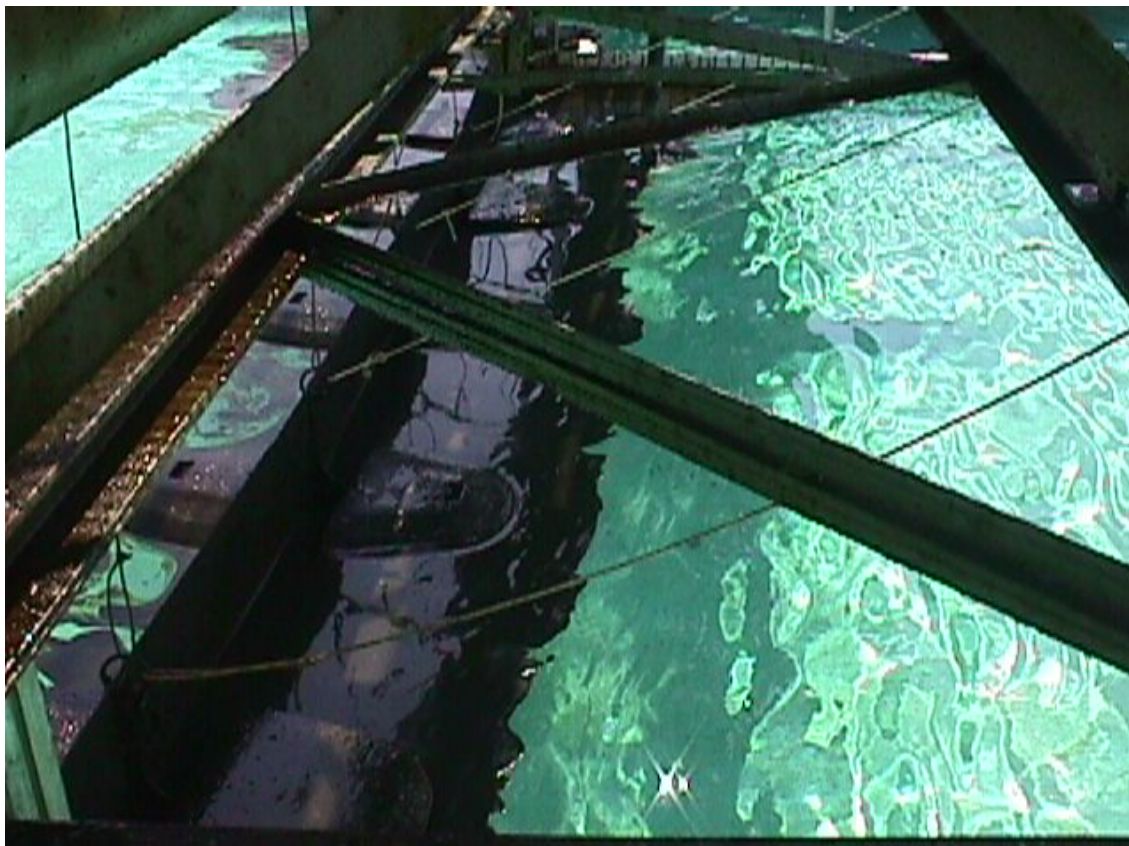


Figure 2.3: Boom used in August 1997 and May 1998 experiments. View of 12" draft Boom # 2 at containment failure with Sundex oil. Note, the vertical boom skirt and the buoyancy floats on both sides of the boom.

given in Table 2.1, i.e., dynamic viscosity  $\mu$ ,  $\varphi = \rho_o/\rho_w$ , interfacial tension water-oil  $\sigma_{wo}$  and surface tension oil-air,  $\sigma_{oa}$ , and solid and water part. The tank water density was  $\rho_w = 1,018 \text{ kg/m}^3$ . Experiments 3 to 5 used  $v_o = 0.627 \text{ m}^3$  (165 gal.) of Sundex oil (see below for an explanation of why this volume was selected), experiments 6 and 7 used  $v_o = 1.9 \text{ m}^3$  (500 gal.) of Sundex oil, and experiments 8 and 9 used  $v_o = 3.8 \text{ m}^3$  (1000 gal.) of Sundex oil. Experiments 10 to 12 used  $v_o = 1.9 \text{ m}^3$  (500 gal.) of Hydrocal oil.

In these experiments, a vertical plastic grid, with known mesh size (4" horiz. by 5/8" vert.), was installed in the tank, 13.564 m (i.e., 44.5' or 68.5% of the tank width) from the West sidewall. This was done in order to have an easy way of measuring slick length both above and under the water (as seen on video footages). The vertical grid was attached to the auxiliary bridge, 0.419 m in front of and perpendicular to the boom axis, and was taut in between two vertical cylindrical poles. The grid draft was 1.067 m and its emerged part was 0.76 m high. A 4' yardstick was attached both to the top part of the grid and to the boom axis, to accurately measure the small

slick lengths. In each experiment, oil was poured in front of the boom, in between the West wall and the grid.

Due to the grid, however, particularly for the more viscous Sundex oil and the smaller volume ( $v_o = 165$  gal.), it was observed that oil would stick to the grid and be partly prevented from flowing to the other side of the grid, hence, effectively increasing the measured slick length for each specified volume of oil. By carefully estimating the proportion of oil flowing to the other side of the grid, correction factors  $k_g$ , to be applied to each poured volume of oil  $v_o$  were developed and used to calculate the effective linear volume of oil  $V_o$  (see Tables 2.2 and 2.3) defined as,

$$V_o = \frac{v_o}{k_g w} \quad (2.1)$$

with  $k_b = 0.75, 0.95$ , and  $0.97$  for  $v_o = 165, 500$  and  $1,000$  gal. of oil, respectively. [Note, due to this unexpected problem with the grid, it was decided not to use the grid in later experiments carried out at OHMSETT as part of this study.]

Another factor affecting slick length, as compared to a simple straight barrier with plane skirt (such as used in SlickMap model and UNH experiments) is the presence of floats in front of the boom skirt. Detailed shapes for the floats were provided by the OHMSETT crew, and the horizontal area covered with floats on the slick side was calculated to be  $0.1108 \text{ m}^2$  per float or a total of  $1.772 \text{ m}^2$  for 16 floats. Over the width of the tank, this also corresponded to an average slick length increase of  $\Delta L = 0.0895 \text{ m}$ . Hence, the effective slick length was calculated (see Tables 2.2 and 2.3) as,

$$L = \tilde{L} - \Delta L \quad (2.2)$$

where  $\tilde{L}$  denotes the measured value.

The data measured for Sundex oil is given in Table 2.2 and plotted in Fig. 2.4, and the data measured for Hydrocal oil is given in Table 2.3 and plotted in Fig. 2.5. In each figure, an exponential curve fit has been applied to each data set obtained for the same volume of Sundex or Hydrocal oil,

$$L = A e^{-BU} \quad (2.3)$$

Curve fit coefficients  $A$  and  $B$  and corresponding  $R^2$  values are given in Table 2.4. Each curve fit is good, with  $R^2 \simeq 1$ . All the results for Sundex oil look quite similar in shape, i.e., with a similar rate of exponential decay in the relationship between slick length and tow speed (similar  $B$  coefficients in Table 2.4). Note that, in Fig. 2.5, the curve fit obtained for tests # 6 and 7 with 500 gal. of Sundex oil has been plotted for comparison with tests 10 to 12 which feature an identical volume of Hydrocal oil. We see that the slick obtained for Hydrocal oil is 2.5 m to 1.3 m longer than the slick obtained for Sundex oil, when speed is increased from  $U = 0.2$  to  $0.8$  kn. This could be due to the much smaller viscosity of the Hydrocal oil, as compared to the Sundex oil (about 27 times smaller in those tests).

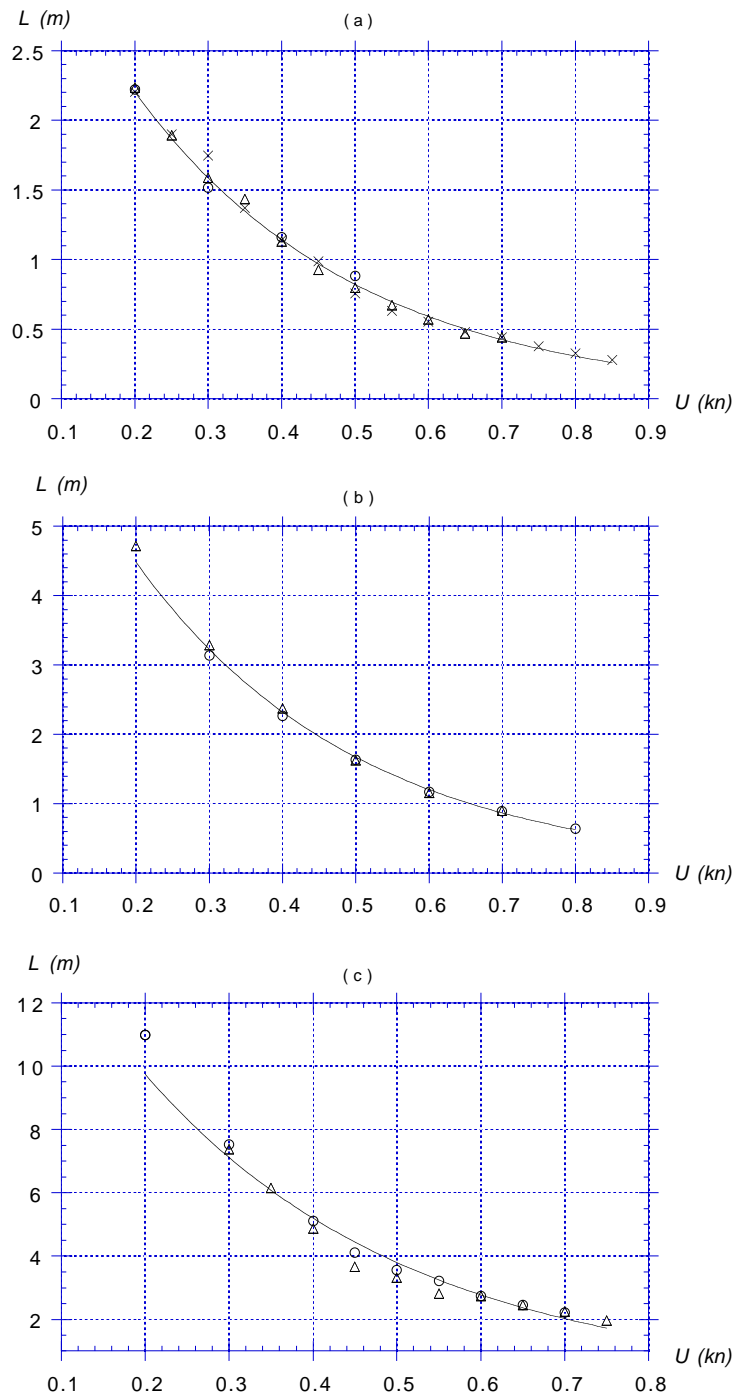


Figure 2.4: August 1997 experiments. Measured oil slick length  $L$  as a function of tow velocity  $U$  for Sundex oil and experiments : (a) ( $\circ$ ) 3, ( $\triangle$ ) 4, ( $\times$ ), 5 (165 gal.); (b) ( $\circ$ ) 6, ( $\triangle$ ) 7 (500 gal.); (c) ( $\circ$ ) 8, ( $\triangle$ ) 9 (1000 gal.). In each figure, (—) indicates an exponential curve fit to the data (see Eq. (2.3) and Table 2.4).

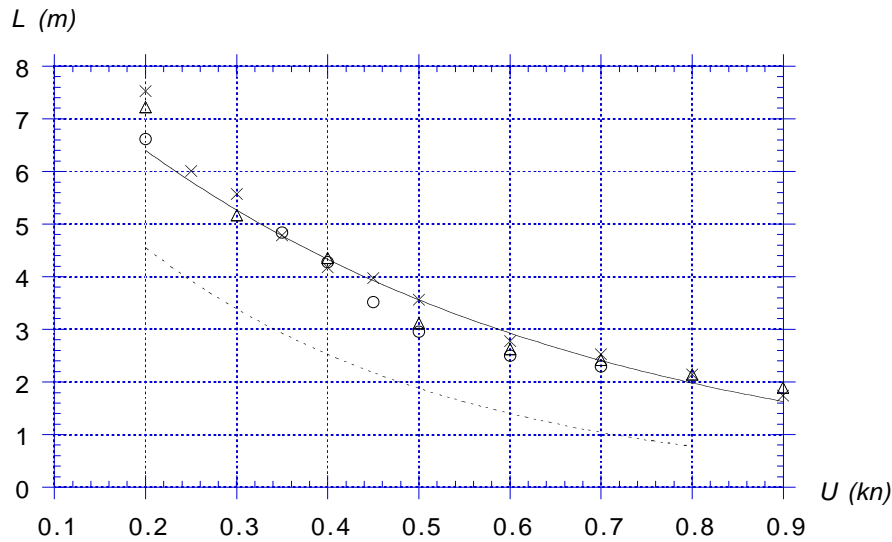


Figure 2.5: August 1997 experiments. (—) Measured oil slick length  $L$  (m) as a function of tow velocity  $U$  for Hydrocal oil and experiments : (○) 10, (△) 11, (×), 12 (500 gal.). (—) indicates an exponential curve fit to the data (see Eq. (2.3) and Table 2.4) and (- - -) is the fit to Sundex tests 6 and 7.

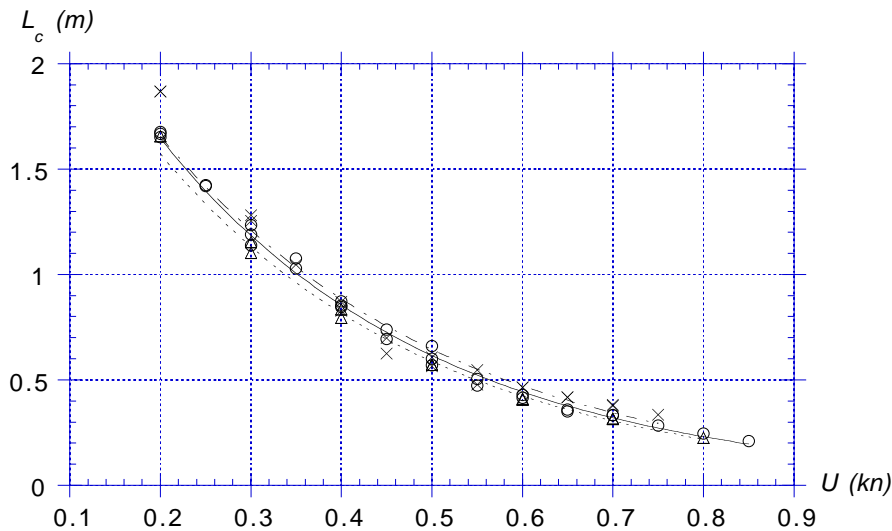


Figure 2.6: August 1997 experiments. Scaled oil slick length  $L_c$  to nominal volume  $V_o = 0.0316 \text{ m}^3/\text{m}$ , as a function of tow velocity  $U$  for Sundex oil experiments : (—○—) 3 to 5 (165 gal.), (- - -△- - -) 6,7 (500 gal.), and (- - × - -) 8,9 (1000 gal.). Lines indicate exponential curve fits to the scaled data for each set of experiments.

$V_o$ (m <sup>3</sup> /m) $U$ (kn)	0.0422 # 3	0.0422 # 4	0.0422 # 5	0.1010 # 6	0.1010 # 7	0.1977 # 8	0.1977 # 9
0.2	2.312	2.324	2.292		4.72	10.98	
0.25		1.981	1.988				
0.3	1.6072	1.676	1.836	3.607	3.289	7.531	7.378
0.35		1.524	1.46				6.519
0.4	1.252	1.219	1.228	2.266	2.375	5.118	4.864
0.45		1.016	1.076			4.102	3.669
0.5	0.972	0.889	0.848	1.631	1.626	3.568	3.314
0.55		0.762	0.721			3.213	2.806
0.6		0.66	0.644	1.174	1.156	2.73	2.73
0.65		0.588	0.568			2.451	2.451
0.7		0.533	0.532	0.894	0.902	2.222	1.968
0.75			0.468				
0.8			0.416	0.64			
0.85			0.368				

Table 2.2: August 1997 experiments. Effective oil slick length  $L$  measured as a function of tow velocity  $U$  for Sundex oil (experiments 3 to 9). Note,  $V_o$  is the corrected linear volume of contained oil.

For comparing with UNH May 1997 laboratory experiments (Chapter 3), which used 9.8 gal. of Sundex oil in a tank  $w' = 1.18$  m wide, i.e., for which the nominal linear oil volume was  $V_o = 0.0316$  m<sup>3</sup>/m, a volume of oil equal to  $9.8w/w' = 165$  gal. of Sundex oil was initially used in this first set of experiments. [It turned out that, due to the use of horsehair and other experimental factors at UNH, the actual linear volume measured on the data collected in UNH experiments (in the form of digitized images) was later found to be smaller, equal to  $V_o = 0.0253$  m<sup>3</sup>/m. Also, note that the boom draft used at UNH was also smaller, equal to  $d = 0.064$  m.] For sake of comparison between OHMSETT and UNH results, experiments 3 to 9 with Sundex oil were linearly scaled to the value of UNH's nominal linear volume,  $V_o = 0.0316$  m<sup>3</sup>/m, by multiplying the observed slick lengths by the ratio of corresponding linear volumes taken from Table 2.2. Results are plotted in Fig. 2.6 and we see that all the measured data for the three volumes of oil nicely collapse onto a single relationship. An exponential curve fit to all the scaled data for experiments 3 to 9 gives  $R^2 = 0.986$ ,  $A = 3.136$  and  $B = 3.242$ . The comparison of these scaled results with UNH results will be presented later in this Chapter.

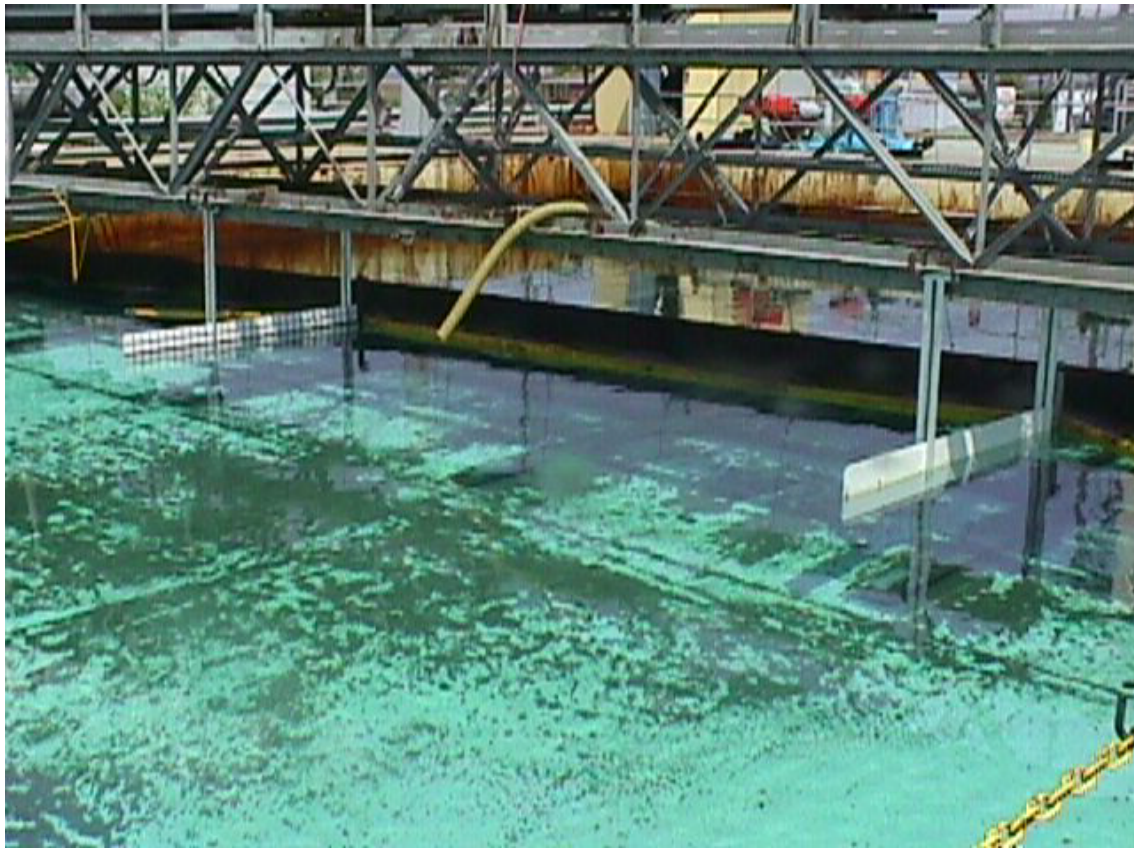


Figure 2.7: Test set-up for 6" shallow draft Boom # 1 used in May 1998 experiments.

$V_o$ (m <sup>3</sup> /m)	0.1010	0.1010	0.1010
$U$ (kn)	# 10	# 11	# 12
0.2	6.706	7.315	7.62
0.25			6.096
0.3		5.258	5.6642
0.35	4.928		4.877
0.4	4.369	4.445	4.267
0.45	3.607		4.064
0.5	3.048	3.20	3.658
0.6	2.591	2.718	2.870
0.7	2.388	2.5146	2.616
0.8		2.235	2.235
0.9		1.981	1.829

Table 2.3: August 1997 experiments. Effective oil slick length  $L$  measured as a function of tow velocity  $U$  for Hydrocal oil (experiments 10 to 12). Note,  $V_o$  is the corrected linear volume of contained oil.

Tests	$R^2$	A	B
# 3,4,5	0.995	4.254	3.286
# 6,7	0.996	8.642	3.282
# 8,9	0.979	18.259	3.141
# 10,11,12	0.961	9.472	1.956

Table 2.4: August 1997 experiments. Exponential curve fit coefficients for tests 3-12 (see Eq. (2.3)). Note,  $L$  is expressed in meters and  $U$  in knots.

### 2.2.3 May 1998 experiments

A total of fourteen tests were conducted at OHMSETT in May 1998, eight of which used Sundex 8600T oil (experiments 4 to 9, and 13,14) and six of which used Hydrocal 300 oil (experiments 1 to 3 and 10 to 12). The density of Sundex and Hydrocal oils for these experiments, measured afterwards on oil samples in OHMSETT's laboratory, was  $\rho_o = 946$  kg/m<sup>3</sup> and 911 kg/m<sup>3</sup>, respectively. The tank water temperature was 21° C and salinity  $S = 1.32\%$ . This led to a density  $\rho_w = 1,015$  kg/m<sup>3</sup>. Other corresponding physical data are given in Table 2.5.

A boom, manufactured by Slickbar Inc., with shallow skirt draft  $d = 0.153$  m (6") was used for the experiments 1 to 7 (Boom # 1; Fig. 2.7) and the same straight boom, with skirt draft  $d = 0.305$  m, as used in the August 1997 experiments, was used for tests 8 to 14 (Boom # 2; Fig. 2.3). Boom # 1 had a small cylindrical buoyancy float

Oil	$\mu$ (Kg/m.s)	$\varphi$	$\sigma_{wo}$ (N/m)	$\sigma_{oa}$ (N/m)	Solids and $H_2O$
Sundex	22.0	0.932	0.0288	0.0355	1.6%
Hydrocal	0.313	0.898	0.0234	0.0357	5.5%

Table 2.5: May 1998 tests. Nominal Oil Properties measured at OHMSETT at 25° C.

Boom	# 1	# 1	# 1	# 2	# 2	# 2
$U$ (kn)	# 1	# 2	# 3	# 10	# 11	# 12
0.3	1.676	1.626	1.676	1.575	1.485	
0.35		1.473	1.524	1.321	1.358	1.430
0.4	1.397	1.219	1.448	1.067	1.232	1.278
0.45		1.092	1.304	0.864	1.105	1.104
0.5	1.092	0.914	1.118	0.711	0.927	0.977
0.55		0.813	1.012	0.559	0.799	0.875
0.6	0.711	0.660	0.838	0.457	0.717	0.762
0.65		0.559	0.635	0.356	0.584	0.635
0.7	0.381	0.457	0.533	0.279	0.507	0.523
0.75		0.330	0.407	0.229	0.436	0.486
0.8	0.254	0.254	0.229	0.179	0.389	0.415
0.85			0.152	0.140	0.369	0.369
0.9					0.308	0.308

Table 2.6: May 1998 experiments. Effective oil slick length  $L$  measured for Booms # 1 and # 2, as a function of tow velocity  $U$  for Hydrocal oil (experiments 1 to 3, 10 to 12).

Boom	# 1	# 1	# 1	# 1	# 2	# 2	# 2	# 2
$U$ (kn)	# 4	# 5	# 6	# 7	# 8	# 9	# 13	# 14
0.2	1.659	1.549	1.499	1.473				
0.25	1.449	1.372	1.394	1.285				
0.3	1.221	1.143	1.093	1.164	1.180	1.231	1.307	1.053
0.35	1.043	0.909	0.889			1.002	1.125	0.977
0.4	0.839	0.698	0.656	0.808	0.824	0.824	0.901	0.875
0.45	0.713	0.561	0.554	0.605	0.723	0.647	0.748	0.672
0.5	0.581	0.455	0.452	0.478	0.573	0.494	0.647	0.570
0.55	0.433	0.328	0.382	0.362	0.451	0.392	0.530	0.469
0.6	0.281			0.206	0.332	0.290	0.443	0.367
0.65	0.154				0.250	0.189	0.367	0.316
0.7	0.052				0.182	0.138	0.316	0.249
0.75						0.090	0.240	0.229
0.8							0.177	0.158
0.85							0.113	0.127

Table 2.7: May 1998 experiments. Effective oil slick length  $L$  measured for Booms # 1 and # 2, as a function of tow velocity  $U$  for Sundex oil (experiments 4 to 9, 13, 14).

at the top (with diameter 0.216 m). Note that Boom # 2 was kept behind the shallow draft Boom # 1, to more easily recover lost oil after containment failure of the first boom.

For these experiments, the test region was limited to only a fraction of the tank width, of length  $w_o = 6.496$  m in between two 2.44 m long vertical plywood boards oriented along the tank main axis and fixed to the auxiliary bridge (Fig. 2.7). Wire gridding was mounted on the oil side region of both plywood boards and measuring tape was installed on the top of the leftward (West) board (Fig. 2.7). These measuring devices were installed to make it easy for an observer on the auxiliary bridge to measure the oil slick length. The source of oil was as usual from the auxiliary bridge oil distribution system. An oil pre-load hose was rigged at water level from the auxiliary bridge to provide the most unperturbed conditions as possible, for the oil slick to attain its initial steady-state shape at low tow speed (Fig. 2.7). A small platform was placed on the West side of the auxiliary bridge to allow an observer to monitor the experiments from a close proximity.

All of the experiments used  $v_o = 0.152$  m<sup>3</sup> (40 gal.) of Hydrocal or Sundex oil. The linear volume value was  $V_o = v_o/w_o = 0.0234$  m<sup>3</sup>/m for all of these experiments (which is close to UNH corrected linear volume; Chapter 3). Note that, for Boom # 2, the same correction in slick length as done for the August 1997 experiments (Eq. (2.2)) was applied to the measurements, to account for the effects of buoyancy floats.

The corrected slick lengths  $L$  measured as a function of tow speed  $U$  in the ex-

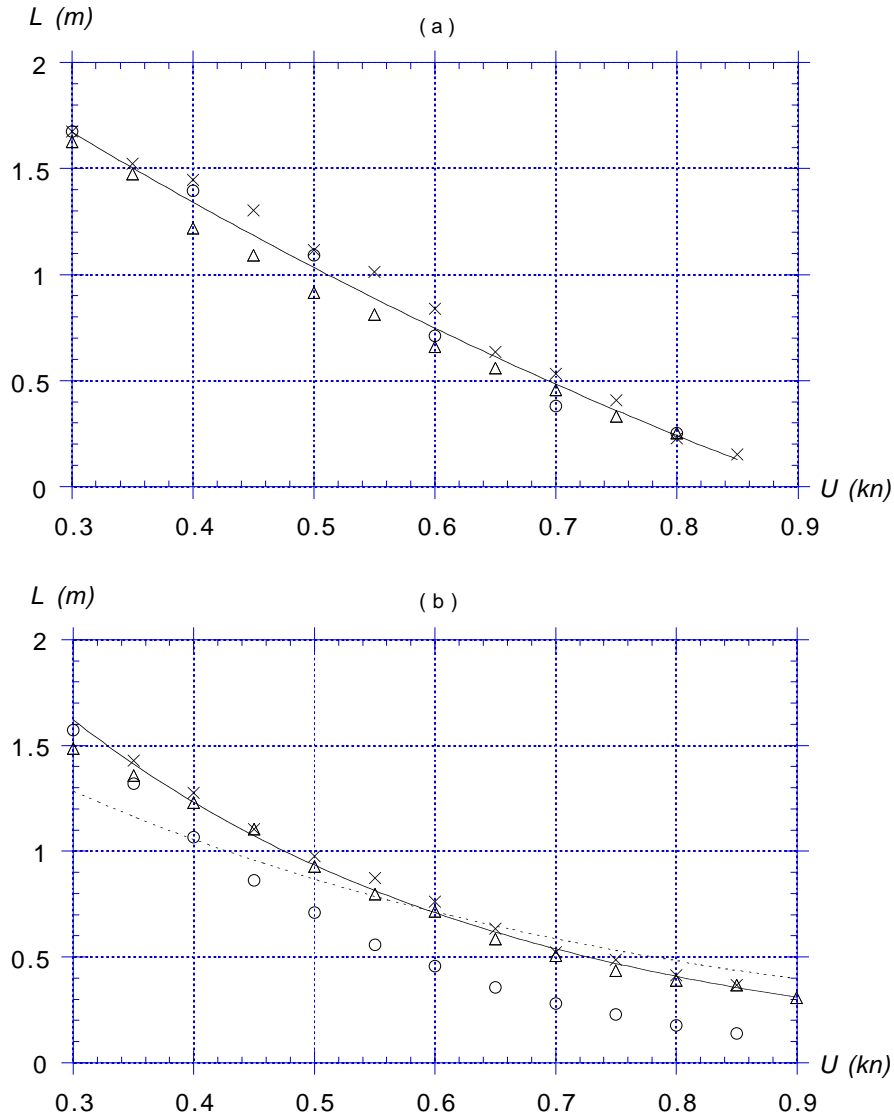


Figure 2.8: May 1998 experiments. Measured oil slick length  $L$  as a function of tow velocity  $U$  for Hydrocal oil ( $v_o = 40$  gal.;  $V_o = 0.0234$  m<sup>3</sup>/m) for : (a) Boom # 1 : (o) 1, ( $\Delta$ ) 2, ( $\times$ ) 3; (b) Boom # 2 : (o) 10, ( $\Delta$ ) 11, ( $\times$ ) 12. In each figure, (—) indicates a curve fit to the data and, in Fig. (b), (---) is the scaled curve fit for the August 1997 experiments with 500 gal. ( $V_o = 0.101$  m<sup>3</sup>/m) of Hydrocal oil for Boom # 2 (Fig. 2.5).

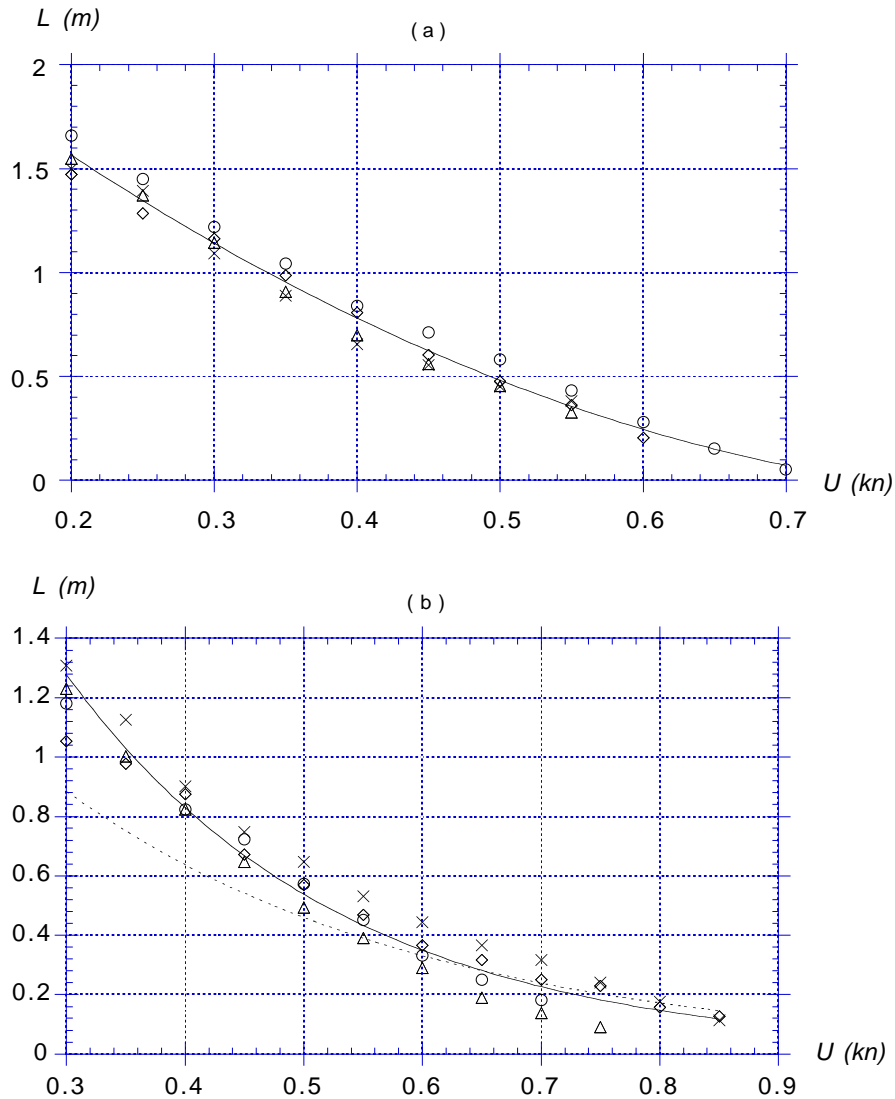


Figure 2.9: May 1998 experiments. Measured oil slick length  $L$  as a function of tow velocity  $U$  for Sundex oil ( $v_o = 40$  gal.;  $V_o = 0.0234$  m<sup>3</sup>/m) for : (a) Boom # 1 : (o) 4, ( $\Delta$ ) 5, ( $\times$ ) 6, ( $\diamond$ ) 7; (b) Boom # 2 : (o) 8, ( $\Delta$ ) 9, ( $\times$ ) 13, ( $\diamond$ ) 14. In each figure, (—) indicates a curve fit to the data and, in Fig. (b), (- - -) is the scaled curve fit for the August 1997 experiments with 165 gal. ( $V_o = 0.0422$  m<sup>3</sup>/m) of Sundex oil for Boom # 2 (Fig. 2.4a).

Tests	$R^2$	A	B	C
# 1,2,3	0.980	3.051	-6.000	3.629
# 4,5,6,7	0.986	2.600	-5.792	3.116

Table 2.8: May 1998 experiments. Quadratic curve fit coefficients for tests 1-7 for Boom # 1 (see Eq. (2.4)). Note,  $L$  is expressed in meters and  $U$  in knots.

Tests	$R^2$	A	B
# 11,12	0.989	3.709	-2.756
# 8,9,13,14	0.963	4.680	-4.325

Table 2.9: May 1998 experiments. Exponential curve fit coefficients for tests 11,12 and 8,9,13,14 for Boom # 2 (see Eq. (2.3)). Note,  $L$  is expressed in meters and  $U$  in knots.

periments for both booms, and using both oil types, are given in Tables 2.6 and 2.7. These results are also plotted in Figs. 2.8 and 2.9. In the experimental results for Boom # 1 (Figs. 2.8a and 2.9a), quadratic polynomial curve fits were applied to the data and plotted on the figures as (exponential fits did not provide as good  $R^2$  values),

$$L = A + BU + CU^2 \quad (2.4)$$

with the values of coefficients given in Table 2.8. In the experimental results for Boom # 2 (Figs. 2.8b and 2.9b), exponential curve fits similar to those applied to the August 1997 experiments (Eq. (2.3)) were applied to the data and plotted on the figures. Note that, in Fig. 2.8b, results for test # 10 lay quite below results for tests # 11 and 12. It turns out that test # 10 was performed at 9.30 am on the morning of the second day of experiments when, both the temperature was quite low and a strong wind was blowing in the tank axis towards the boom. Both of these effects led to a reduction of slick length (enhanced viscosity and wind stress). Test # 11 occurred at 10.15 am when both the temperature was higher and the wind had dropped to below 10 mph. We indeed see on the figure that results for tests # 11 and 12 (performed even later) agree well with each other. In view of these factors, test # 10 was considered an outlier and left out of further studies. In accordance, the corresponding curve fit only includes tests # 11 and 12.

The curve fit results for the August 1997 experiments using Boom # 2, scaled proportionally to their linear volume, have been plotted on Figs. 2.8b and 2.9b for comparison. We see that the agreement between the August 1997 and May 1998 experiments is quite good, for both types of oil, despite the difference in experimental set-up for Boom # 2.



Figure 2.10: September 1998 experiments. Test set-up for 19” draft boom with catenary shape.

Oil	$\mu$ (Kg/m.s)	$\varphi$	$\sigma_{wo}$ (N/m)	$\sigma_{oa}$ (N/m)	Solids and $H_2O$
Sundex	11.4	0.938	0.0345	0.0379	9.0%
Hydrocal	0.425	0.894	0.0270	0.0357	0.6%

Table 2.10: September 1998 experiments. Nominal Oil Properties measured at OHM-SETT at 25° C.

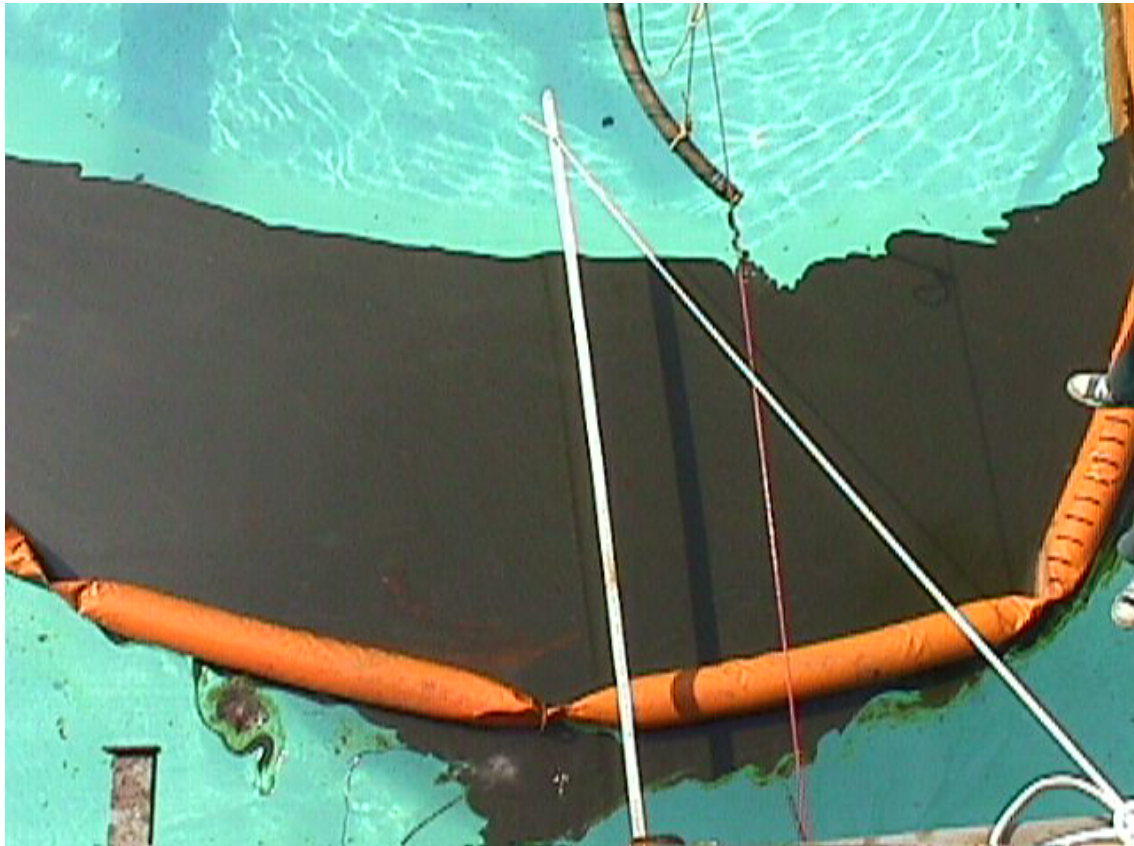


Figure 2.11: September 1998 experiments. Oil slick shape for 19" draft boom (Boom # 3) with catenary shape.



Figure 2.12: September 1998 experiments. Oil slick shape for 6" draft boom (Boom # 1) with catenary shape.

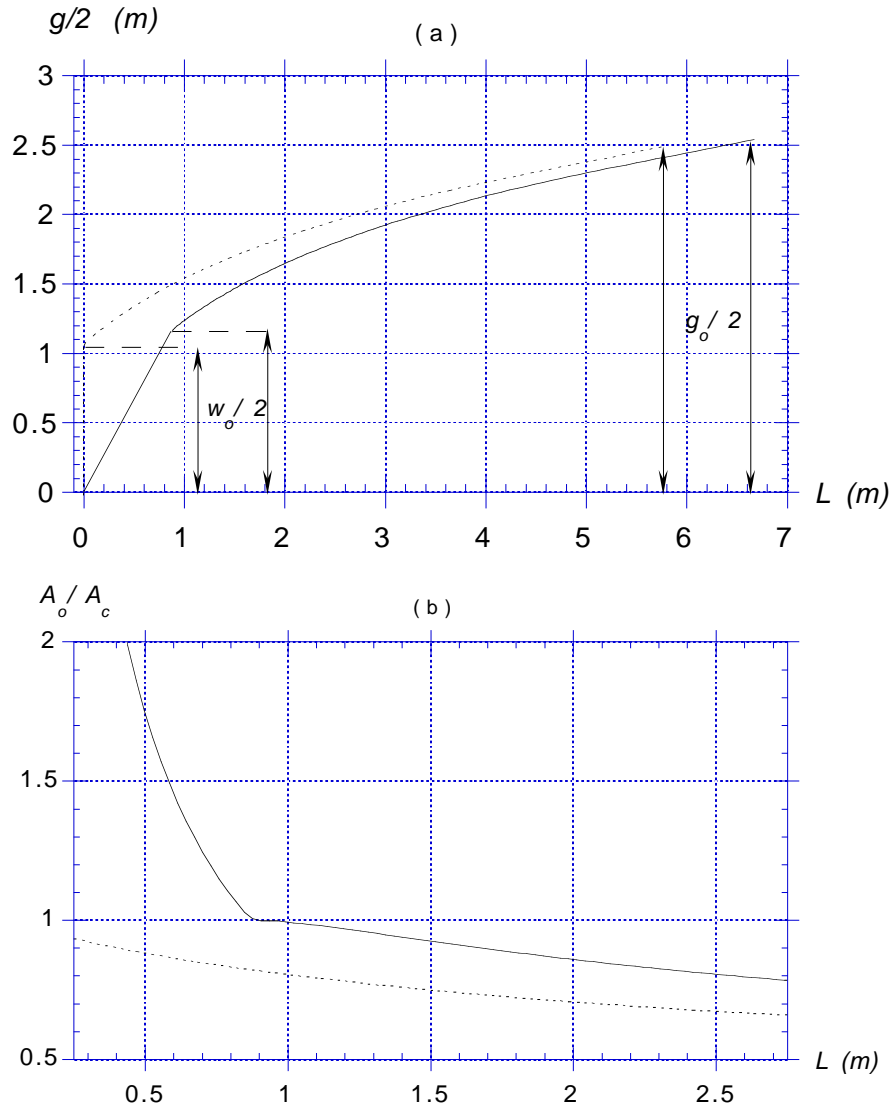


Figure 2.13: September 1998 experiments with : ( - - - - ) Boom # 1; ( — ) Boom # 3. (a) Theoretical catenary shape with correction for the first boom segment location according to experiments. (b) Fraction of oil volume  $V_o$  equivalent to a straight boom of length  $w_o$ .

Test #	1	2	3	4	5	6	7	8	9	10	11	12	13	14
Oil type	S	S	S	S	S	S	S	H	H	H	H	H	H	H
$v_o$ (gal.)	36	40	36	46	36	36	40	41	33	27	27	26	26	26

Table 2.11: September 1998 experiments. Oil type and volume data, with : (S) Sundex 8600T; (H) Hydrocal 300.

## 2.2.4 September 1998 experiments

These experiments were performed at OHMSETT using Sundex and Hydrocal oil, for two types of booms with catenary shape, in order to compare results with those obtained earlier for straight booms. The desired boom shape was specified by attaching ropes to the ends of the booms and to the main bridge, and adjusting the length of rope (Fig. 2.10).

A total of fourteen tests were conducted, seven of which with Sundex 8600T oil (experiments 1 to 7) and seven of which with Hydrocal 300 Oil (experiments 8 to 14). The density of Sundex and Hydrocal oils for these experiments, measured afterwards on oil samples in OHMSETT's laboratory, was  $\rho_o = 961 \text{ kg/m}^3$  and  $916 \text{ kg/m}^3$ , respectively. The density of water was  $\rho_w = 1,025 \text{ kg/m}^3$ . Other corresponding physical data are given in Table 2.10. A boom with draft  $d = 0.483 \text{ m}$  (19"; Boom # 3; Fig. 2.11) was used for tests 1 to 4 and 12 to 14, and the boom with draft  $d = 0.153 \text{ m}$  (6"; Boom # 1; Fig. 2.12), previously used in the May 1998 experiments, was used for tests 5 to 11. Boom # 1 consisted of 7 sections, each measuring 2.138 m (length  $\ell = 14.97 \text{ m}$ ), and Boom # 3 consisted of 10 sections, each measuring 1.524 m (length  $\ell = 15.24 \text{ m}$ ).

The oil volumes used for each test varied. Table 2.11 gives the volume of oil  $v_o$  used for each experiment, which varied between 26 and 46 gal. ( $0.0988$  and  $0.1748 \text{ m}^3$ ). Linear volumes  $V_o$  for equivalent straight booms were estimated to allow comparison with earlier experiments. Due to the catenary shape, this was done differently than for the straight booms used earlier; the catenary boom was thus assumed to locally behave as a straight boom for a boom section on both sides of the apex. The width of this region was estimated for each case, together with the volume of oil located inside and outside the region (see details below).

A graduated stick attached to the auxiliary bridge and suspended slightly above the boom was used to measure slick length (Fig. 2.10). Each measurement thus required two readings from the technician operating from the bridge side platform : (i) the boom's apex position, and (ii) the leading edge of the oil slick. The difference between these readings gives the actual oil slick length  $L$ .

Both booms were installed in the tank, with a catenary shape having a gap  $g_o$  to boom length  $\ell$  ratio of 1 to 3, which gives an opening in front of Boom # 1 of  $g_o = 4.99$

m, and Boom # 3 of  $g_o = 5.08$  m (Fig. 2.13). When conducting the experiments with Boom # 3, it was visually observed that one link on either side of the boom apex was always approximately normal to the direction of the flow; hence, it was assumed that a width  $w_o = 2.331$  m of the boom, centered at the apex, behaved as an equivalent straight boom (Fig. 2.11). For Boom # 1, it was observed that only one link, centered at the boom apex was always approximately normal to the direction of the flow; thus the equivalent straight boom had a width  $w_o = 2.138$  m (Fig. 2.12). The  $w_o$  values are found by solving the catenary equations given in the following.

We assume that the slick has an approximate catenary shape (Fig. 2.13a),

$$L = a \left\{ \cosh \left\{ \frac{g}{2a} \right\} - 1 \right\} - L_a \quad (2.5)$$

in which  $a$  is a coefficient representing the boom apex location,  $L_a$  is a slick length correction to account for the actual piecewise linear shape of the boom, and  $g$  is the boom gap corresponding to slick length  $L$ . For Boom # 3, we have  $L_a = 0$  and for Boom # 1,  $L_a = L_o = 0.734$  m (see below). Using Eq. (2.5), the boom theoretical length is calculated as,

$$\ell = 2a \sinh \left\{ \frac{g_o}{2a} \right\} \quad (2.6)$$

where  $g_o$  denotes the maximum boom gap. For given boom length  $\ell$  and maximum boom gap (here equal to  $g_o = \ell/3$ ), Eq. (2.6) can be solved for  $a$  and we find,  $a = 0.8949$  m and  $0.8790$  m for Boom # 3 and #1, respectively. Based on these equations, the slick area  $A$  for a given slick length  $L$  is calculated, for  $L > L_o - L_a$ , as,

$$A = g a \left\{ 1 + \frac{L + L_a}{a} \right\} - 2a^2 \sqrt{\left\{ 1 + \frac{L + L_a}{a} \right\}^2 - 1} + A_a \quad (2.7)$$

where, from Eq. (2.5),

$$g = 2a \operatorname{acosh} \left\{ 1 + \frac{L + L_a}{a} \right\} \quad (2.8)$$

and  $A_a$  is a correction area which accounts for the actual piecewise linear shape of the booms, given for Boom # 3 by,

$$A_a = w_o \frac{L + L_a}{2} - A(g = w_o, L = L_o - L_a) \quad (2.9)$$

and for Boom # 1 by,

$$A_a = -A(g = w_o, L = L_o - L_a) \quad (2.10)$$

In these equations,  $L_o = 0.872$  or  $0.734$  m is the height for the location of the first boom segment on the theoretical catenary, leading to a width  $g = w_o = 2.331$  or  $2.138$  m (given by solving Eqs. (2.5) and (2.6) for a boom length equal to  $\ell/5$  or for  $g = w_o$ ), for Boom # 3 or # 1, respectively. For  $L \leq L_o - L_a$ , we simply have  $A = A_o$ , with  $A_o$

the slick area for the equivalent straight boom. For Boom # 3, taking into account the piecewise linear geometry of the boom, we have for  $L > L_o - L_a$ ,

$$A_o = w_o \left( L + L_a - \frac{L_o}{2} \right) \quad (2.11)$$

and for  $L \leq L_o$ , we have,

$$A_o = w_o \frac{(L + L_a)^2}{2 L_o} \quad (2.12)$$

with the equivalent boom width reduced to  $w_o L/L_o$ . For Boom # 1, for  $L > L_o$ , we have,

$$A_o = w_o (L + L_a - L_o) \quad (2.13)$$

For  $L \leq L_o - L_a$ , we set  $A_o = A$ .

The linear slick volume corresponding to the equivalent straight boom of width  $w_o$  is finally calculated as,

$$V_o \simeq \frac{A_o}{A_c} \frac{v_o}{w_o} \quad (2.14)$$

with  $A_o$  defined as above and  $A_c = A$  for  $L > L_o - L_a$  and  $A_c = AL/L_o$  or  $A$ , for Boom # 3 or 1, respectively when  $L \leq L_o - L_a$ . Fig. 2.13b gives  $A_o/A_c$  calculated as a function of  $L$  with Eqs. (2.7) to (2.13), for both boom types.

Tables 2.12 and 2.13 give measured slick lengths as a function of tow speed, for both boom and oil types. Figs. 2.14 and 2.15 show results of experiments for Sundex and Hydrocal oil, using Boom # 3 (tests 1 to 4, 12 to 14). Figs. 2.14a and 2.15a show these results, linearly scaled for an identical slick volume  $v_o = 40$  gal; exponential curve fits to the data are also shown (coefficients are given in Table 2.14). Figs. 2.14b and 2.15b show the same results for an equivalent straight boom of linear volume  $V_o = 0.0316$  m<sup>3</sup>/m, obtained by applying Eq. (2.14). An exponential curve fit to the results is also shown (coefficients are given in Table 2.15), and compared to the exponential fits obtained for August 1997 experiments 3 to 9 and 10, 11, with Boom # 2, scaled for the same linear volume (Figs. 2.5 and 2.6). Boom # 2 only had a 12" draft and, expectedly, led to somewhat shorter slick lengths and earlier boom failure than Boom # 3 (see next Section for more details on boom intercomparisons).

Figs. 2.16 and 2.17 show results of experiments for Sundex and Hydrocal oil, using Boom # 1 (tests 5 to 7, 8 to 11). Figs. 2.16a and 2.17a show these results, linearly scaled for an identical slick volume  $v_o = 40$  gal; exponential curve fits to the data are also shown (coefficients are given in Table 2.14). Figs. 2.16b and 2.17b show the same results for an equivalent straight boom of linear volume  $V_o = 0.0316$  m<sup>3</sup>/m, obtained by applying Eq. (2.14). An exponential curve fit to the results is also shown (coefficients are given in Table 2.15), and compared to the exponential fits obtained for May 1998 experiments 4 to 7 and 10, 11, with Boom # 1, scaled for the same linear volume (Figs. 2.8a and 2.9a). Although Boom # 1 was straight in the May 1998 experiments and had a catenary shape in the September 1998 experiments, after

Boom	#3	#3	#3	#3	#1	#1	#1
$U$ (kn)	#1	#2	#3	#4	#5	#6	#7
0.25						1.976	1.854
0.3		2.083	1.981	2.489	1.750	1.778	1.702
0.35						1.326	1.397
0.4	1.397	1.524	1.499	1.880	1.242	1.016	1.067
0.45						0.847	0.864
0.5	1.118	1.194	1.143	1.753	0.960	0.706	0.762
0.55			1.118		0.762	0.649	0.660
0.6	0.940	1.143	0.914	1.600	0.677	0.536	0.559
0.65			0.864		0.508	0.395	0.457
0.7	0.864	0.864	0.762	1.219	0.452	0.339	0.406
0.75			0.635		0.367	0.310	0.305
0.8	0.711	0.787	0.660	0.940	0.197		
0.9		0.711	0.508	0.864			
1.0		0.686					

Table 2.12: September 1998 experiments with Sundex oil. Oil slick length  $L$  measured at the apex for both boom types, as a function of tow velocity  $U$  (experiments 1 to 7).

Boom	#1	#1	#1	#1	#3	#3	#3
$U$ (kn)	#8	#9	#10	#11	#12	#13	#14
0.3			3.086	3.048	2.1590	2.1336	2.1590
0.4	2.057	2.186	2.145	2.296	1.829	1.829	1.829
0.5	1.660	1.817	1.882	1.957	1.600	1.524	1.600
0.55	1.611						
0.6	1.462	1.509	1.580	1.580	1.346	1.321	1.270
0.65	1.388						
0.7	1.165	1.108	1.129	1.204	0.972	1.143	1.041
0.75	1.041						
0.8	0.867	0.862	0.865	0.828	0.907	0.838	0.940
0.85	0.743						
0.9	0.620	0.677	0.640	0.640	0.648	0.762	0.838

Table 2.13: September 1998 experiments with Hydrocal oil. Oil slick length  $L$  measured at the apex for both boom types, as a function of tow velocity  $U$  (experiments 8 to 14).

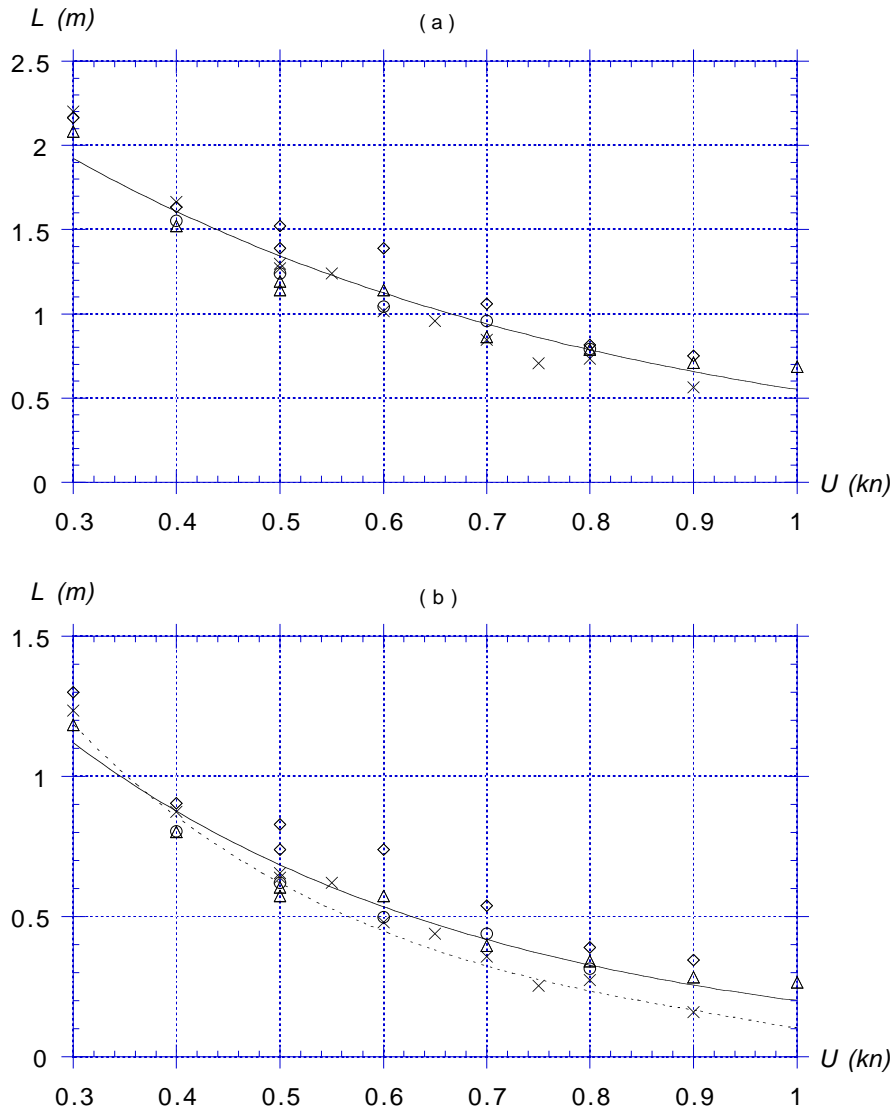


Figure 2.14: September 1998 experiments. Boom # 3 and Sundex oil, exper. # : ( $\circ$ ) 1, ( $\triangle$ ) 2, ( $\times$ ) 3, ( $\diamond$ ) 4. (a) Slick length measured as a function of tow speed scaled for  $v_o = 40$  gal., with (—) an exponential fit to the data. (b) Equivalent straight boom slick length calculated from Fig. (a), scaled for  $V_o = 0.0316$   $m^3/m$ , with (—) an exponential fit to the data, and (- - - -) an exponential fit to August 1997 experiments 3 to 9 with Boom # 2, scaled for the same linear volume (Fig. 2.6).

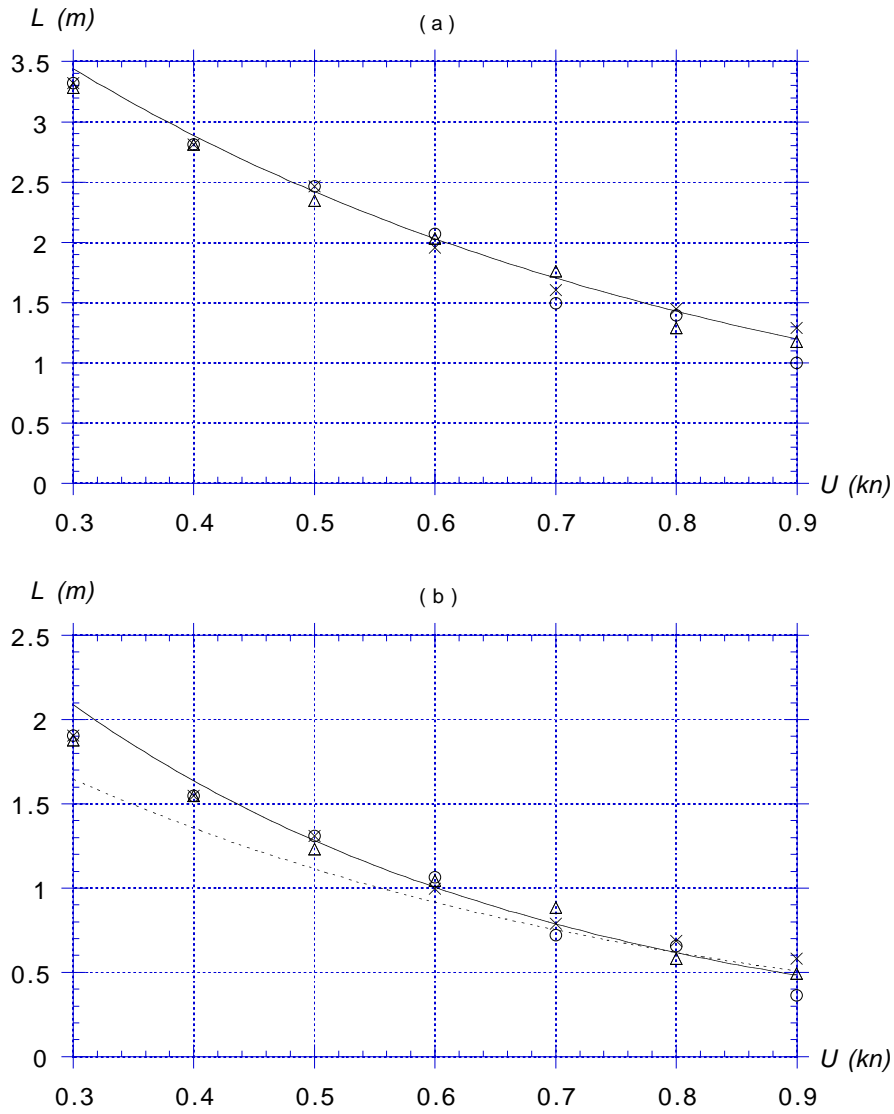


Figure 2.15: September 1998 experiments. Boom # 3 and Hydrocal oil, exper. # : (o) 12, ( $\Delta$ ) 13, ( $\times$ ) 14. (a) Slick length measured as a function of tow speed scaled for  $v_o = 40$  gal., with (—) an exponential fit to the data. (b) Equivalent straight boom slick length calculated from Fig. (a), scaled for  $V_o = 0.0316$  m<sup>3</sup>/m, with (—) an exponential fit to the data, and (- - - -) an exponential fit to August 1997 experiments 10 and 11 with Boom # 2, scaled for the same linear volume (Fig. 2.5).

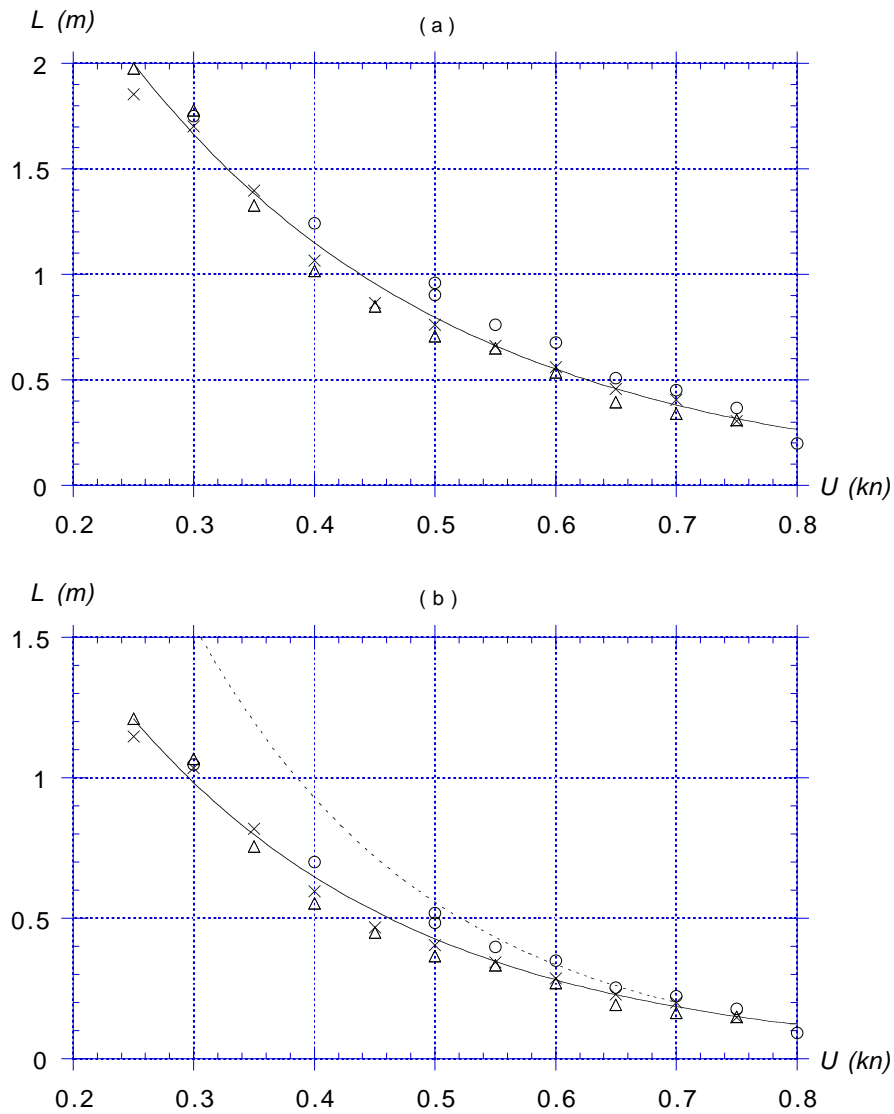


Figure 2.16: September 1998 experiments. Boom # 1 and Sundex oil, exper. # : (o) 5, ( $\Delta$ ) 6, ( $\times$ ) 7. (a) Slick length measured as a function of tow speed scaled for  $v_o = 40$  gal., with (—) an exponential fit to the data. (b) Equivalent straight boom slick length calculated from Fig. (a), scaled for  $V_o = 0.0316$  m<sup>3</sup>/m, with (—) an exponential fit to the data, and (- - - -) an exponential fit to May 1998 experiments 4 to 7 with Boom # 1, scaled for the same linear volume (Fig. 2.9a).

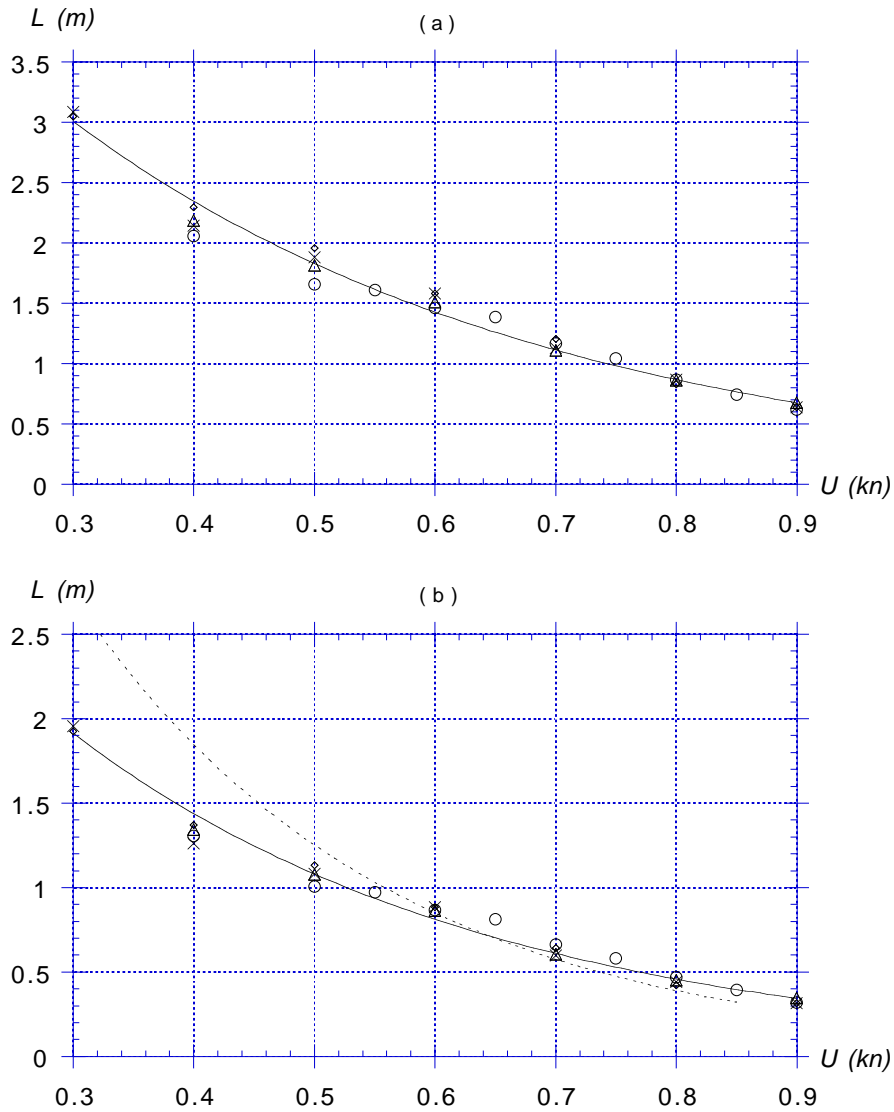


Figure 2.17: September 1998 experiments. Boom # 1 and Hydrocal oil, exper. # : (o) 8, ( $\Delta$ ) 9, ( $\times$ ) 10, ( $\diamond$ ) 11. (a) Slick length measured as a function of tow speed scaled for  $v_o = 40$  gal., with (—) an exponential fit to the data. (b) Equivalent straight boom slick length calculated from Fig. (a), scaled for  $V_o = 0.0316$  m<sup>3</sup>/m, with (—) an exponential fit to the data, and (- - - -) an exponential fit to May 1998 experiments 1 to 3 with Boom # 1, scaled for the same linear volume (Fig. 2.8a).

Tests	$R^2$	A	B
# 1 to 4	0.925	3.290	-1.789
# 5 to 7	0.976	5.026	-3.685
# 8 to 11	0.978	6.341	-2.486
# 12 to 14	0.969	5.832	-1.759

Table 2.14: September 1998 experiments. Exponential curve fit coefficients for un-scaled tests # 1 to 14 for Booms # 3 and 1 (see Tables 2.12, 2.13, and Eq. (2.3)). Note,  $L$  is expressed in meters and  $U$  in knots.

Tests	$R^2$	A	B
# 1 to 4	0.920	2.344	-2.462
# 5 to 7	0.978	3.436	-4.172
# 8 to 11	0.982	4.509	-2.857
# 12 to 14	0.963	4.3375	-2.437

Table 2.15: September 1998 experiments. Exponential curve fit coefficients for scaled tests # 1 to 14 for Booms # 3 and 1 (see Figs. 2.14 to 2.17, and Eq. (2.3)). Note,  $L$  is expressed in meters and  $U$  in knots.

scaling is done, we see that results (particularly for the larger speeds :  $U > 0.5$  kn) are fairly identical and that the critical speed of containment failure for the catenary shaped boom is well estimated in experiments using a straight boom, provided the appropriate volume corrections have been made (see next Section for more details on boom/experiments intercomparisons).

## 2.3 Analysis and inter-comparison of experimental results for straight booms of various drafts

A few comparisons between results of various experiments performed for the same oil and scaled for the same linear volume were already made in earlier Sections. Thus, August 1997 and May 1998 experiments for Boom # 2 used as a straight boom, were compared in Figs. 2.8b and 2.9b, for Hydrocal and Sundex oil, respectively. September 1998 experiments for Boom # 3 used in catenary shape, were compared to August 1997 experiments for Boom # 2 used as a straight boom, in Figs. 2.14b and 2.15b, for Sundex and Hydrocal oil, respectively. Finally, September 1998 experiments for Boom # 1 used in catenary shape, were compared to May 1998 experiments for Boom

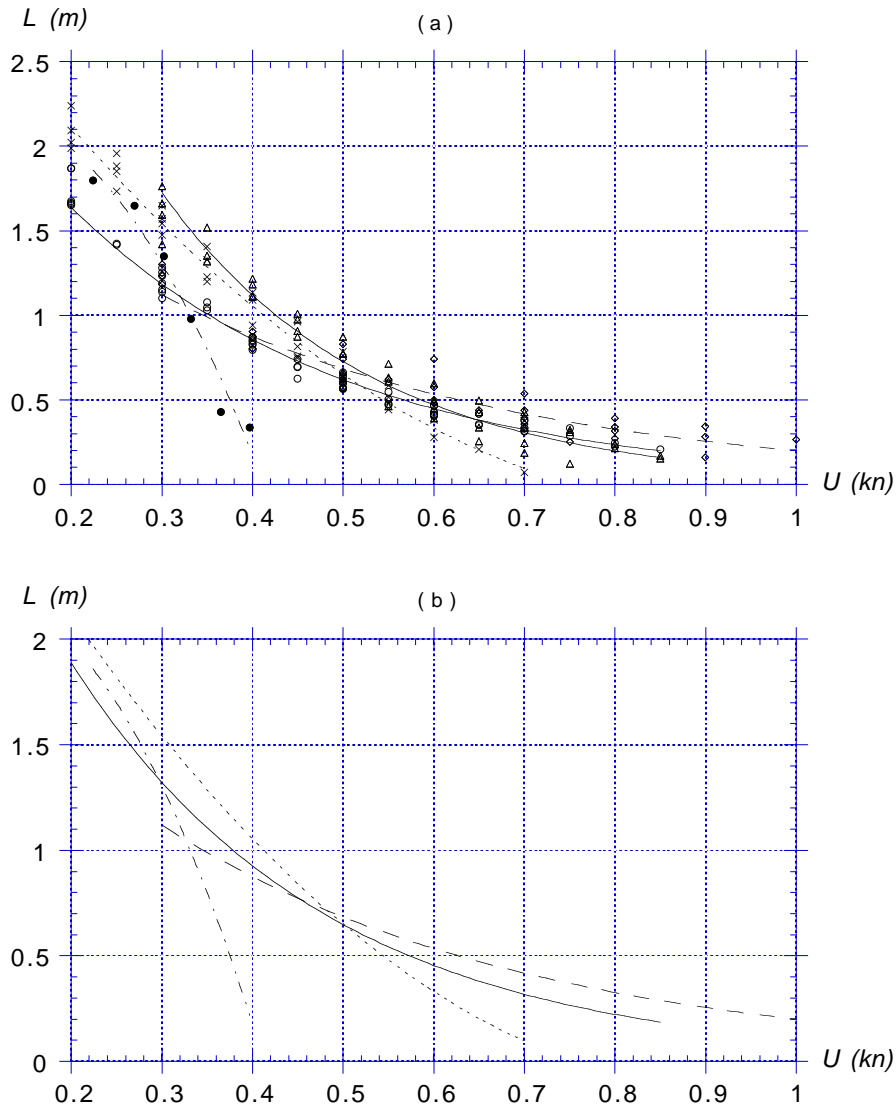


Figure 2.18: OHMSETT and UNH experiments with Sundex oil, scaled for  $V_o = 0.0316 \text{ m}^3/\text{m}$ . Exponential or quadratic curve fits of slick length measured as a function of flow speed (Table 2.17), for Boom # : (-----) 1, (——) (97 and 98) 2, (—) 3, (— —) 4. In Fig. (a), symbols indicate experimental results for Boom # : ( $\times$ ) 1, ( $\circ$ ) 2 (97), ( $\triangle$ ) 2 (98), ( $\diamond$ ) 3, ( $\bullet$ ) 4. In Fig. (b), only the curve fits are shown and both results for Boom # 2 have been grouped together.

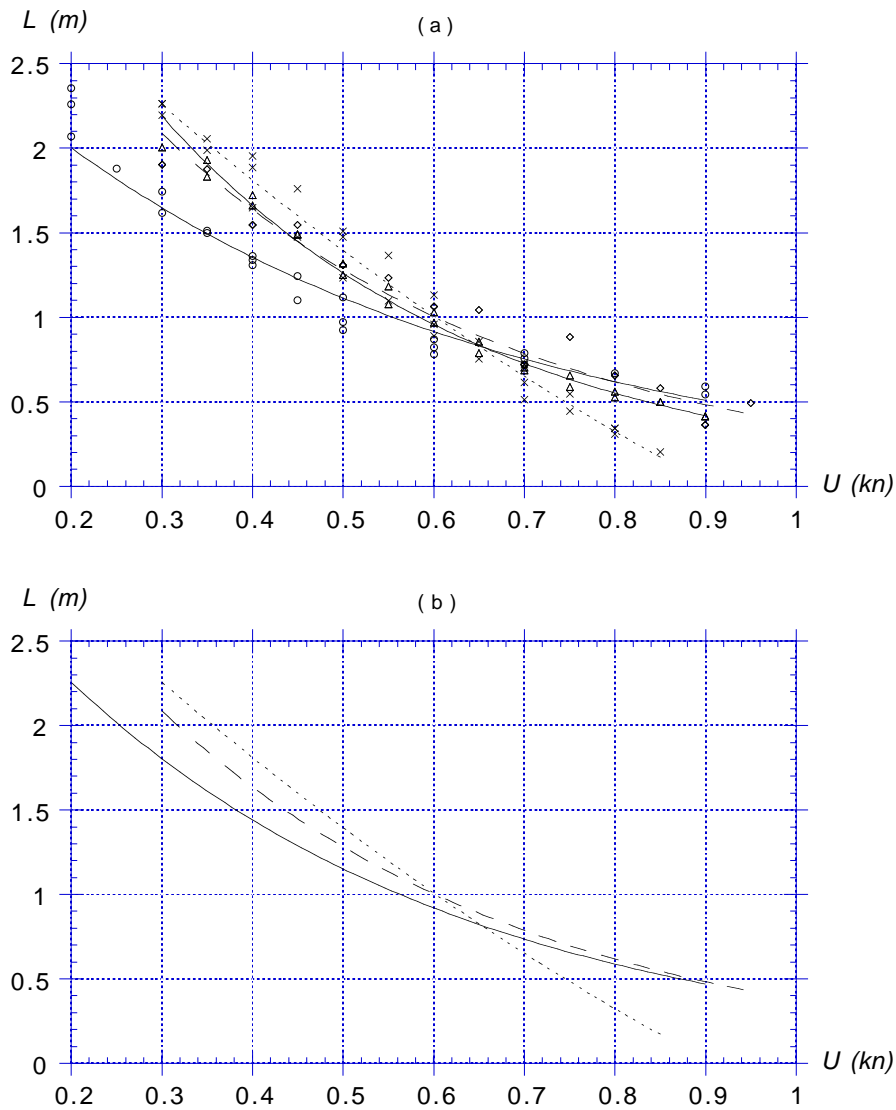


Figure 2.19: OHMSETT experiments with Hydrocal oil, scaled for  $V_o = 0.0316 \text{ m}^3/\text{m}$ . Exponential or quadratic curve fits of slick length measured as a function of flow speed (Table 2.18), for Boom # : ( - - - - ) 1, ( — ) (97 and 98) 2, ( — — ) 3. In Fig. (a), symbols indicate experimental results for Boom # : ( $\times$ ) 1, ( $\circ$ ) 2 (97), ( $\Delta$ ) 2 (98), ( $\diamond$ ) 3. In Fig. (b), only the curve fits are shown and both results for Boom # 2 have been grouped together.

Boom	$d$ (in)	$d$ (m)	Type
# 1	6	0.153	Cyl./skirt
# 2	12	0.305	Fence
# 3	19	0.483	Cyl./skirt
# 4	2.5	0.064	Horseh./fence

Table 2.16: Summary of characteristics of booms used in August 1997, May 1998 and September 1998 experiments at OHMSETT (Booms # 1 to 3) and for UNH laboratory experiments (Boom # 4).

Boom	Type	$R^2$	A	B	C
# 1	quadr.	0.982	3.511	-7.822	4.208
# 2	exp.	0.916	3.851	-3.561	
# 3	exp.	0.920	2.344	-2.462	
# 4	quadr.	0.964	1.965	4.606	-22.67

Table 2.17: Curve fit coefficients (exp. : exponential, eq. (2.3); quadr. : quadratic, Eq. (2.4)) for scaled tests for Booms # 1 to 4 with Sundex oil (straight booms with  $V_o = 0.0316 \text{ m}^3/\text{m}$ ; Fig. 2.18). Note, coefficients are for  $L$  expressed in meters and  $U$  in knots.

# 1 used as a straight boom, in Figs. 2.16b and 2.17b, for Sundex and Hydrocal oil, respectively. Boom characteristics are summarized in Table 2.16.

Here, a systematic comparison is made for both oil types, between results obtained for various straight booms, scaled for an identical linear volume  $V_o = 0.0316 \text{ m}^3/\text{m}$ , corresponding to a slick volume  $v_o = 0.627 \text{ m}^3$  (165 gal.) of oil in OHMSETT, spread out over the width of the tank ( $w = 19.812 \text{ m}$ ). September 1998 experiments showed that, when properly scaled, results obtained for a boom used in catenary shape are nearly identical to those obtained for the same boom used as a straight barrier, particularly for  $U \geq 0.5 \text{ kn}$ . Thus, all the results measured in terms of slick length  $L$  as a function of tow speed  $U$ , for the same boom and oil, but for different volumes of oil and boom geometry, can nearly collapse onto the same functional relationship, when proper scaling is applied. This relationship is usually quite well approximated by a negative exponential or by a quadratic law (Eqs. (2.3) and (2.4)). Now, in order to show the effect of boom draft  $d$ , i.e., boom type, on slick containment failure, an inter-comparison is made between such results scaled for the same straight boom.

In addition to the three booms successively used at OHMSETT (Booms # 1 to 3), a fourth boom (Boom # 4) is introduced, which represents the fixed horsehair barrier of draft  $d = 0.064 \text{ m}$  (2.5") used in UNH's laboratory experiments, performed using

Boom	Type	$R^2$	A	B	C
# 1	quadr.	0.979	3.773	-5.500	1.482
# 2	exp.	0.937	3.534	-2.242	
# 3	exp.	0.963	4.338	-2.437	

Table 2.18: Curve fit coefficients (exp. : exponential, eq. (2.3); quadr. : quadratic, Eq. (2.4)) for scaled tests for Booms # 1 to 3 with Hydrocal oil (straight booms with  $V_o = 0.0316 \text{ m}^3/\text{m}$ ; Fig. 2.19). Note, coefficients are for  $L$  expressed in meters and  $U$  in knots.

Sundex oil only (see Chapter 3), in a flume of width  $w' = 1.18 \text{ m}$  and depth  $h = 0.762 \text{ m}$ . Note that these experiments were run using fresh water. Measured slick profiles were provided by UNH in the form of digitized images, for 6 current velocities :  $U = 0.119, 0.135, 0.151, 0.168, 0.184$  and  $0.200 \text{ m/s}$  ( $0.224$  to  $0.397 \text{ kn}$ ). Slick length  $L$  was calculated from these results. A volume of oil  $v_o = 0.0372 \text{ m}^3$  (9.8 gal.) was used in these experiments, corresponding to a theoretical linear volume  $V_o = v_o/w' = 0.0316 \text{ m}^3/\text{m}$  (which is the reference linear volume used in the above scalings). Due to the  $0.2 \text{ m}$  thick horsehair used in the boom barrier, however, and to various other effects in the laboratory flume, such as a slightly non-uniform slick across the flume width, the linear volume was estimated from the slick profiles to be smaller at  $V'_o = 0.0253 \text{ m}^3/\text{m}$ . Hence, UNH results presented here have been scaled by a factor  $V_o/V'_o = 1.25$ .

Figs. 2.18 and 2.19 show scaled experimental results obtained for Sundex and Hydrocal oils, respectively, assuming straight booms and a linear volume  $V_o = 0.0316 \text{ m}^3/\text{m}$ . In Figs. 2.18a and 2.19a, symbols indicate individual experimental points as described in the previous Section. Lines indicate curve fits. Note that there were two sets of experiments for Boom # 2 (August 1997 and May 1998). In Figs. 2.18b and 2.19b, only the curve fits are shown and both sets of results for Boom # 2 are grouped together (curve fit coefficients and types are given in Tables 2.17 and 2.18). Slick lengths for different booms are fairly identical for low speeds ( $U \leq 0.3 \text{ kn}$ ). For higher speeds, however, slick length reduces faster, the smaller the boom draft, leading to containment failure at a smaller (critical) speed, the smaller the boom draft. For both types of oil, the difference between results for Boom # 2 and 3, however, becomes marginal at height speed, indicating that the effect of increasing boom draft on critical velocity is gradually decreasing, the larger the draft.

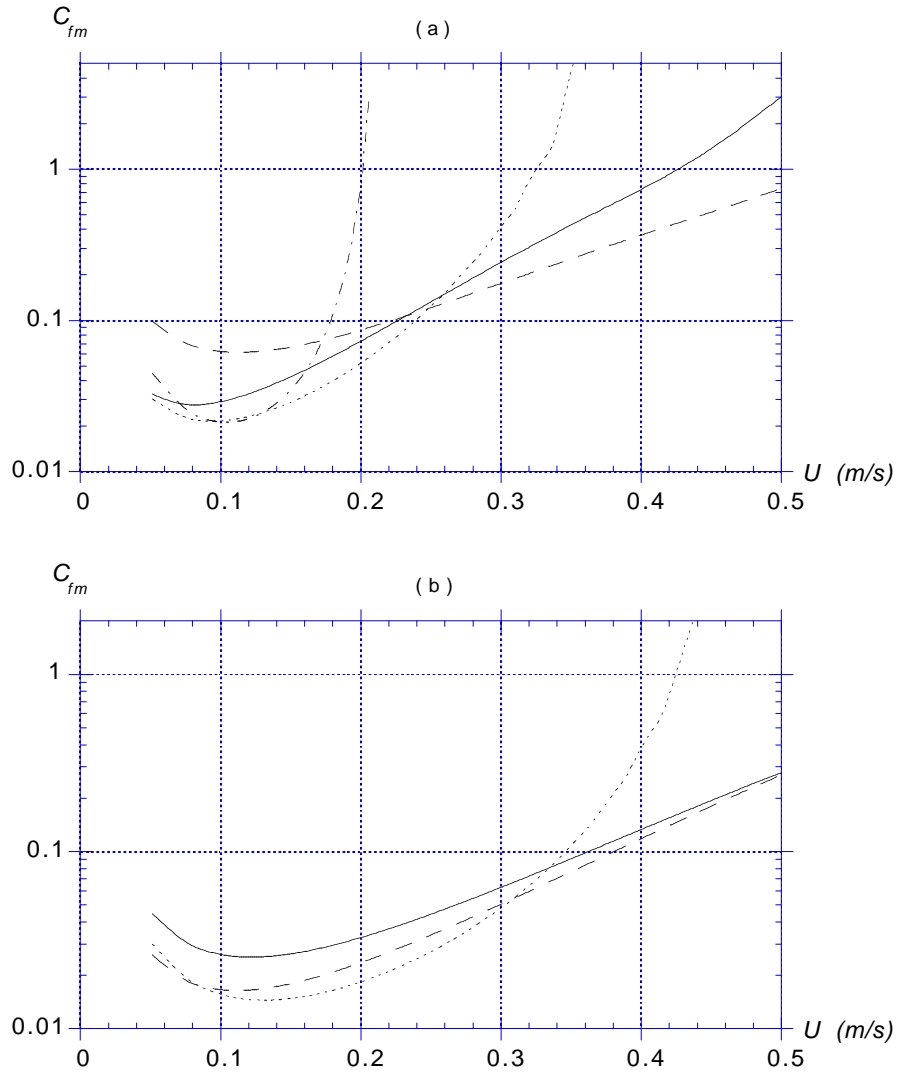


Figure 2.20: Average interfacial friction coefficient calculated with SlickMap Stage 1 static model, as a function of tow/flow velocity, for OHMSETT and UNH experiments with : (a) Sundex oil; (b) Hydrocal oil, scaled for  $V_o = 0.0316$  m<sup>3</sup>/m (Figs. 2.18 and 2.19). Curves correspond to Boom # : (- - - -) 1, (—) 2, (— —) 3, (— - —) 4, as defined in Table 2.16.

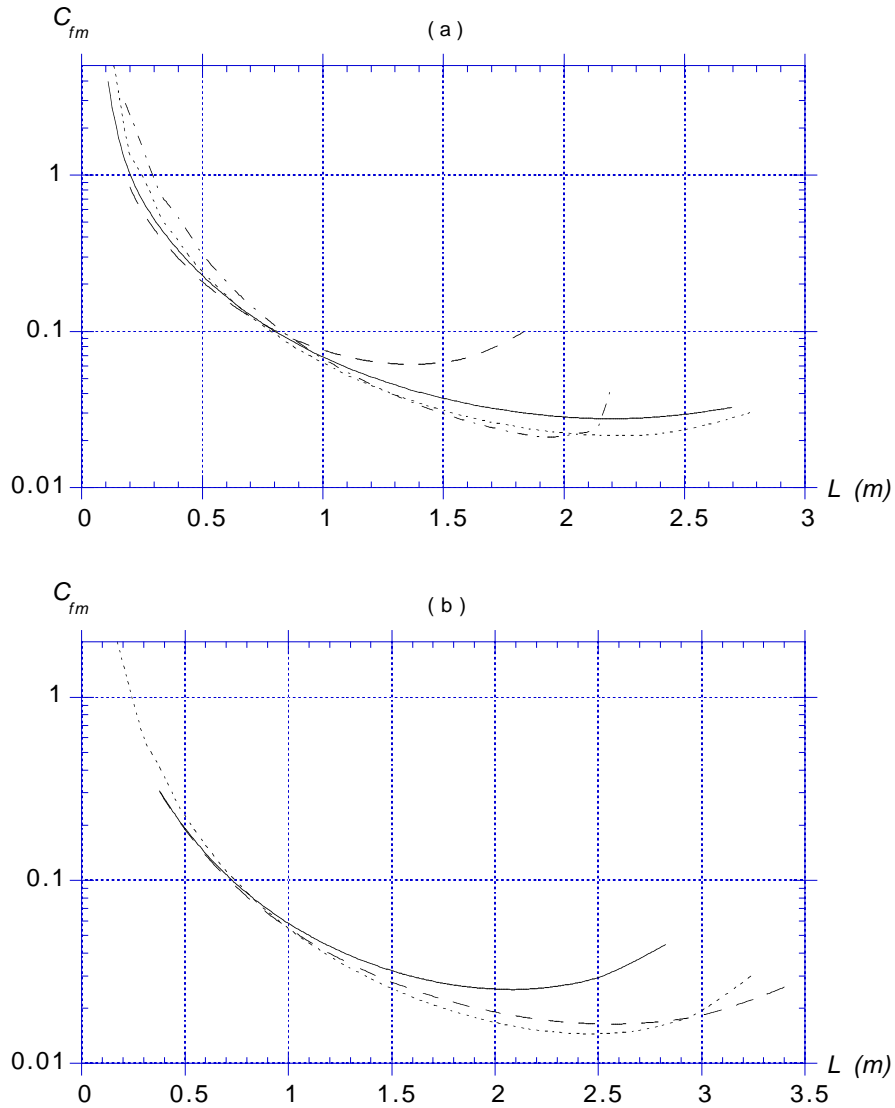


Figure 2.21: Average interfacial friction coefficient calculated with SlickMap Stage 1 static model, as a function of slick length, for OHMSETT and UNH experiments with : (a) Sundex oil; (b) Hydrocal oil, scaled for  $V_o = 0.0316 \text{ m}^3/\text{m}$  (Figs. 2.18 and 2.19). Curves correspond to Boom # : (-----) 1, (—) 2, (— —) 3, (— — —) 4, as defined in Table 2.16.

## 2.4 Analysis of interfacial friction for model calibration

One of the crucial factors in calibrating SlickMap models for Stages 2 and 3 to simulate experimental results, is the value of friction along the oil-water interface (Chapter 4). To do so, a functional form for the friction coefficient function  $C_f$  was derived from detailed measurements of oil-water interface shapes made at UNH (Chapter 3), and used in SlickMap models for Stages 2 and 3 (Eq. (4.63)). This function, however, has several parameters which both govern its shape and magnitude (Eqs. (4.64) to (4.66)). The parameters governing the magnitude of  $C_f$  can be related to the average value of the friction coefficient along the interface,  $C_{fm}$  (Eq. (4.67)).

In SlickMap Stage 1 model, a simple static initialization of slick shape is performed (Fig. 4.1), in which no detailed variation of interfacial friction is required, but just a global  $C_{fm}$  value. In the absence of experiments, it is up to the user to provide SlickMap with a realistic  $C_{fm}$  value, based on which slick shape can be initialized, assuming all of the other physical parameters are known (water density,  $\rho_w$ , oil density  $\rho_o$ , tow/flow velocity  $U$ , linear volume  $V_o$ ). When experiments are available, these can be used to calculate  $C_{fm}$  for a low initial value of  $U$ .

In this Section, scaled slick lengths  $L$ , measured at OHMSETT and UNH as a function of tow/flow velocity  $U$ , for the four (equivalent) straight booms listed in Table 2.16, and for both types of oil, Sundex and Hydrocal (Figs. 2.18 and 2.19), are used together with Stage 1 model Eqs. (4.47) to (4.49), to calculate the corresponding values of the average interfacial friction coefficient  $C_{fm}$ . These values will constitute a data base of experimental results that SlickMap users will be able to access when running Stage 1 model, to obtain realistic initial friction values, and hence slick shapes, for their problems. The measured experimental variations  $L(U)$ , scaled for  $V_o = 0.0316 \text{ m}^3/\text{m}$ , were curve fitted to exponential or polynomial functions, for each type of oil (Tables 2.17 and 2.18). These curve fits are used here, *in lieu* of the raw experimental data, in order to obtain more continuous  $C_{fm}$  variations, as a function of  $U$  and  $L$ . Since all the data for each type of oil was scaled together, average values of the experimental oil densities were used to calculate  $C_{fm}$ , i.e.,  $\rho_o = 954$  and  $908 \text{ kg/m}^3$  for Sundex and Hydrocal oils, respectively. For the salt water at OHMSETT (i.e., Booms #1, 2, and 3), an average  $\rho_w = 1,019 \text{ kg/m}^3$  was used, and  $\rho_w = 1,000 \text{ kg/m}^3$  was used for the fresh water used at UNH (Boom # 4). Results of computations for  $C_{fm}$  are given in Figs. 2.20 and 2.21, as a function of  $U$  and  $L$ , respectively.

Figs. 2.22 and 2.23 show corresponding variations of the effective flow coefficient  $S_h$  (i.e., one minus the head loss coefficient; Eq. (4.12)), the relative oil height above mean water level at the boom,  $\chi$ , in proportion of slick depth, and slick depth  $D$  at the boom, calculated as a function of tow/flow velocity  $U$ , using Stage 1 model, for Sundex and Hydrocal oils, respectively (Fig. 4.1). Considering the experimental range of tested velocities, it should be stressed that the applicability of Stage 1 model equations (i.e., to a low, static, tow/flow velocity) implies that these results (for both

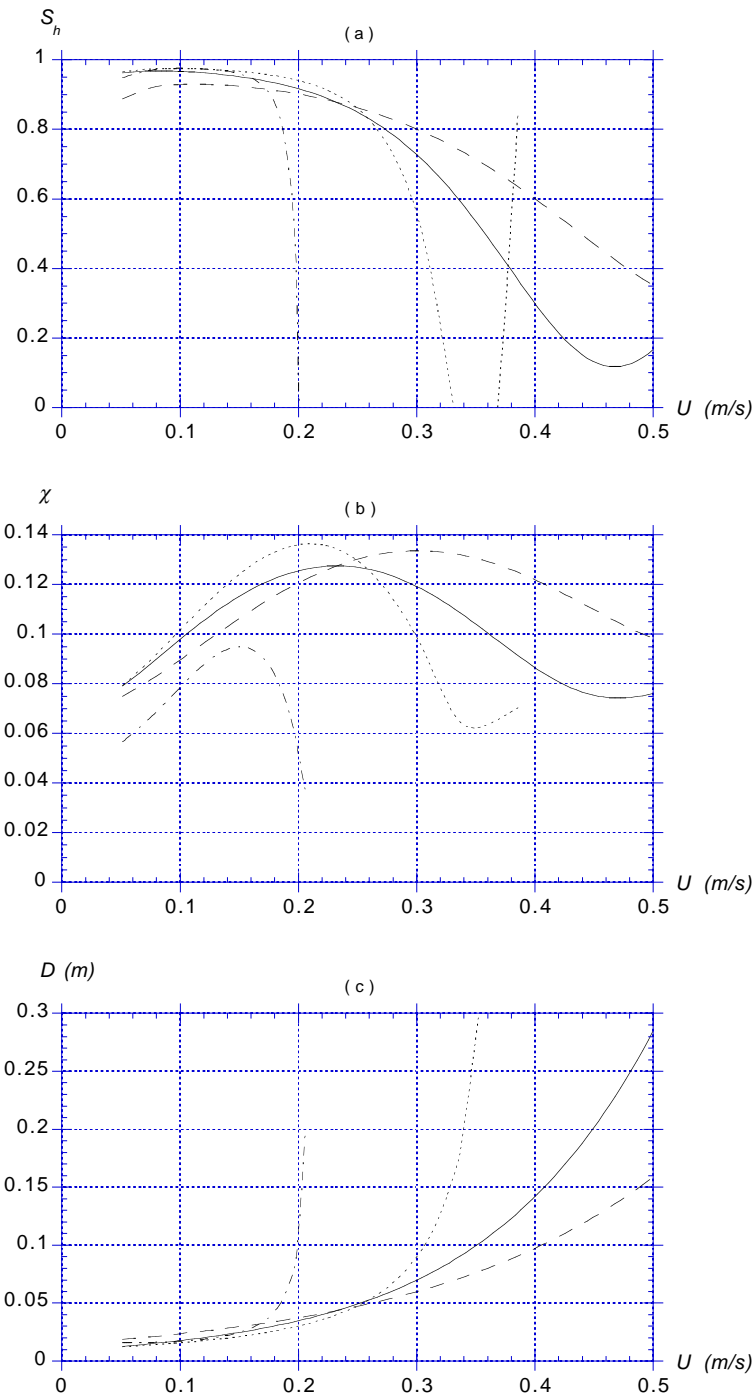


Figure 2.22: Values of SlickMap Stage 1 model parameters, as a function of tow/flow velocity, for OHMSETT and UNH experiments with Sundex oil, scaled for  $V_o = 0.0316 \text{ m}^3/\text{m}$  (Fig. 2.18). Curves correspond to Boom # : (-----) 1, (—) 2, (— —) 3, (— - —) 4, as defined in Table 2.16.

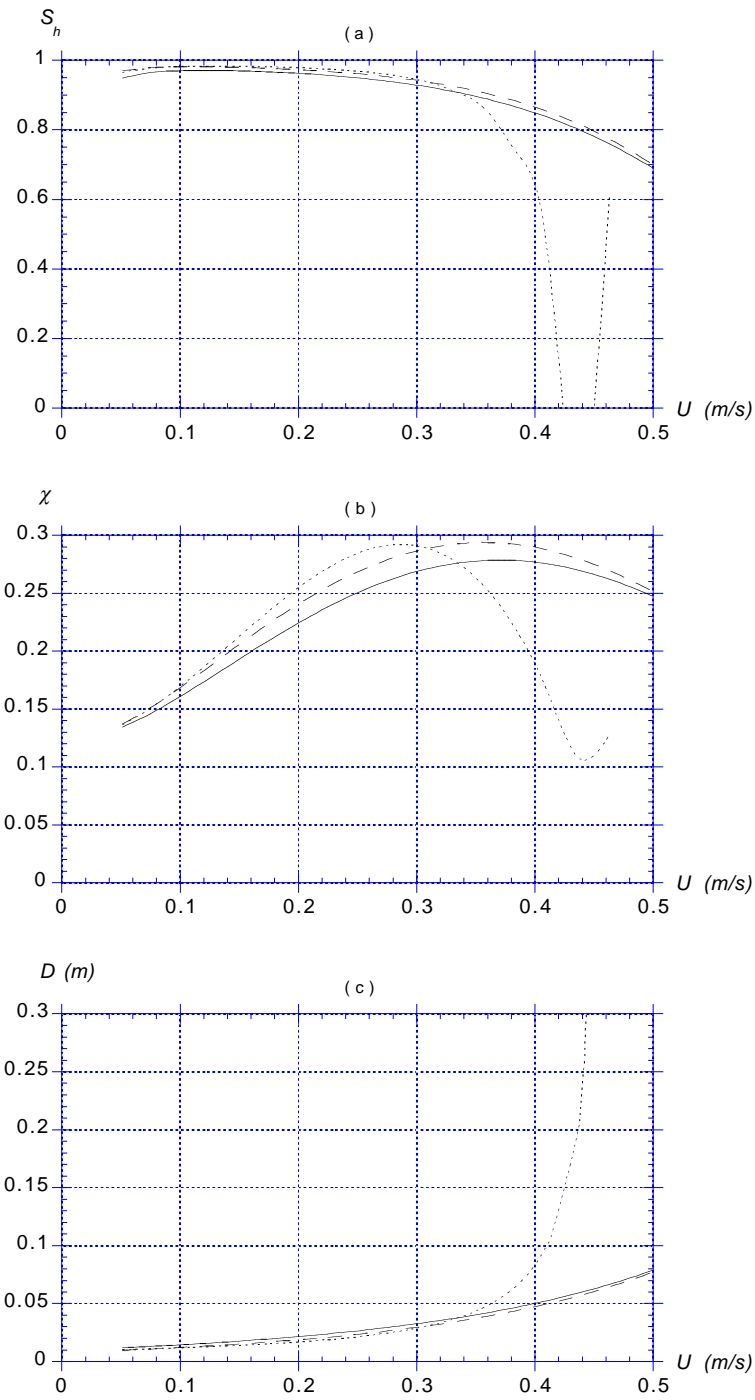


Figure 2.23: Values of SlickMap Stage 1 model parameters, as a function of tow/flow velocity, for OHMSETT experiments with Hydrocal oil, scaled for  $V_o = 0.0316 \text{ m}^3/\text{m}$  (Fig. 2.19). Curves correspond to Boom # : ( - - - - ) 1, ( — ) 2, ( — · — ) 3, as defined in Table 2.16.



Figure 2.24: August 1997 experiments. Underwater oil-water interface shape for 12” draft boom (Boom # 2), for test # 2 with  $U = 0.51$  kn.

the average friction coefficient and the other model parameters) should only be used, for Booms # 1, 2, and 3, roughly, in between  $U = 0.05$  and  $0.25$  m/s and for Boom # 4, in between  $U = 0.05$  and  $0.15$  m/s. In this velocity range, all the variations of model parameters calculated for Booms # 1, 2, and 3, tested at OHMSETT, for  $C_{fm}$ ,  $S_h$ ,  $\chi$  and  $D$  are found to be quite close to each other. This results from the small differences in measured scaled slick length  $L$  (Figs. 2.18 and 2.19) and indicates that boom draft  $d$  only has a minor influence on slick parameters for velocities significantly lower than the critical velocity of oil containment failure. Such low velocities also correspond to large slick lengths  $L$ , and thus to small slick depths  $D$ , much smaller than boom draft.

For larger flow velocities, Figs. 2.20 to 2.23 show that Stage 1 model equations account for the decrease in measured slick lengths by providing a very large increase in the average friction coefficient and, hence, a resulting large decrease in the effective flow coefficient. Such large increases in interfacial friction, in fact, correspond to a dynamically enhanced interfacial roughness, through the development of Kelvin-Helmholtz shear instability waves (see, e.g., Fig 3.1), beyond a certain velocity threshold. Underwater video footages recorded in all of the experiments at OHMSETT showed a gradual build up and downstream propagation of Kelvin-Helmholtz waves on the oil-water interface, as tow velocity is increased. Fig. 2.24 shows an example of one frame extracted from underwater video camera footages taken at OHMSETT, during August 1997 experiments (set-up test # 2 for  $U = 0.51$  kn). The front part of the slick in the picture denotes the headwave region where KH waves are being continuously created through shear instability. These waves propagate downstream on the

interface and are gradually dissipated, as long as the tow velocity stays significantly below the critical velocity of containment failure.

In Stage 3 model, an additional parameterization of  $C_f$  is introduced to model Kelvin-Helmholtz wave effects on interfacial friction (Eq. (4.143)).

For other values of boom draft specified by SlickMap users, than those in Table 2.16, curves  $L(U)$  are first interpolated in between the experimental curve fits, and then  $C_{fm}$  is calculated for the specified initial  $U$  value.

## 2.5 Conclusions

The following conclusions can be drawn from the analysis of results of experiments conducted at OHMSETT, as part of URI studies :

- Despite the very simple measuring devices used in each experimental campaign (August 1997, May 1998, September 1998), a good repeatability of slick length measurements as a function of tow speed is observed for each individual test (Figs. 2.4, 2.5, 2.8, 2.9, 2.14, 2.15, 2.16, 2.17).
- After linear scaling of the linear oil volumes, all the tests performed for the same boom and oil type, during an experimental campaign, nearly collapse onto a single relationship (e.g., Fig. 2.6).

This is due to the same rate of exponential decay in the  $L(U)$  relationships measured for different oil volumes (e.g., Table 2.4, tests 3-12), which indicates that the headwave dynamics is nearly identical and that the change in oil volume only leads to a proportional change in length of the back of the slick.

- For identical sets of experimental parameters, slick lengths obtained for Hydrocal oil are larger than those obtained for Sundex oil (e.g., Fig. 2.5). This is likely due to the much lower viscosity of the Hydrocal oil.
- Tests performed for the same boom and oil in two different experimental campaigns, i.e., for different experimental set-ups and environmental conditions, also lead to good agreement of the measured  $L(U)$  relationships, after linear scaling of the linear oil volumes is done. This is particularly true for the larger tow speeds, i.e., closer to containment failure (Figs. 2.8b and 2.9b for Boom # 2).

This confirms both the relevance and the accuracy of the experimental procedures used in OHMSETT experiments.

- Experiments performed with booms towed in catenary shape (September 1998) closely simulate the actual operation of booms used for oil slick containment.

Results of such experiments show that, when proper scaling of the oil volume is done (purely based on boom geometry), the measured  $L(U)$  variations obtained

for a catenary shape boom are quite close to those measured for the same boom put in a straight position transverse to the tank, particularly for the larger tow speeds ( $U > 0.5$  kn), i.e., closer to containment failure (Figs. 2.16b and 2.17b for Boom # 1).

This indicates that the critical velocity of containment failure of a catenary shape boom can be accurately predicted by the critical velocity of an equivalent straight boom. This justifies the use of SlickMap models, which predict the oil containment behavior of straight booms (Chapters 4 and 5), to make reasonable predictions of the oil containment performance of catenary shape booms of identical characteristics and same equivalent linear volume of oil  $V_o$ .

- The intercomparison of scaled experimental results obtained for straight booms of various drafts (both at OHMSETT and at UNH) shows a fairly similar behavior of the  $L(U)$  relationships for low tow/flow speeds ( $U < 0.3$  kn; Figs. 2.18 and 2.19). For larger speeds, slick length decreases quicker, and a given slick length is achieved for a lower speed, the smaller the boom draft.

The critical velocity of oil containment failure decreases with boom draft. For sufficiently large draft, however, the marginal gain in critical velocity value becomes negligible when draft is increased.

- The scaled experimental results  $L(U)$  measured for 4 boom types/drafts and 2 oil types were used as input to the static SlickMap Stage 1 model and average interfacial friction coefficient values  $C_{fm}$  were calculated. These will be used to initialize slick shape in SlickMap model, for a low initial tow/flow velocity  $U = 0.2$  to  $0.3$  kn.

Computations for the larger flow velocities show that, in order to account for the experimentally measured slick lengths, the static model predicts a very large increase in interfacial friction. Such an increase can only be obtained through the occurrence of Kelvin-Helmholtz interfacial waves. The underwater video camera used in all of the experiments at OHMSETT indeed showed a gradual build up and downstream propagation of Kelvin-Helmholtz waves on the oil-water interface, as tow velocity is increased (e.g., Fig. 2.24).

Kelvin-Helmholtz interfacial wave effects are included in SlickMap Stage 3 model through an adequate parameterization of interfacial friction, as a function of the calculated interfacial dynamics (Eq. (4.143)).

# Chapter 3

## Analysis of UNH experiments

### 3.1 Introduction

From 1997 to 1999, the University of New Hampshire (UNH) conducted laboratory experiments of oil containment by booms, as part of a collaborative effort coordinated with URI's study, in a set-up similar to Delvigne's [9] (1989) experiments. UNH's experiments used Sundex oil, and took place in a flume with a recirculating fresh water current (i.e.,  $\rho_w = 1,000 \text{ kg/m}^3$ ). The flume width was  $w' = 1.18 \text{ m}$  and the water depth was  $h = 0.762 \text{ m}$ . The barrier used to represent the boom consisted in a vertical plywood board with draft  $d = 0.064 \text{ m}$  (as in [9]), and a  $0.013 \text{ m}$  thickness (see, e.g., Fig. 4.1). Rubberized horsehair was placed over a  $0.2 \text{ m}$  layer in front of the barrier, to inhibit corner vortices (Fig. 3.1). Hence, the total barrier width was  $0.213 \text{ m}$ . Oil was introduced in the flume while a low flow velocity  $U = 0.07 \text{ m/s}$  was maintained, in order for the oil to collect in front of the barrier. The flow speed was then increased by  $0.0163 \text{ m/s}$  increments, up to a maximum speed of  $0.2 \text{ m/s}$  (about  $0.4 \text{ kn}$ ). After each speed increase, measurements were taken after the slick reached a new equilibrium shape. Due to sidewall effects, leading to increased friction, the slick shape was slightly non-uniform over the width of the tank, with a larger slick length  $L$  in the middle of the tank than on the sidewalls.

In June 1997, the URI team was provided with initial results of experiments conducted in May 1997 by UNH. Results were given in the form of digitized pictures of slick profiles taken through the tank transparent sidewalls, using a high resolution  $35 \text{ mm}$  video camera. In August and September 1997, similar results, but with a higher resolution, were provided (Fig. 3.1). Finally, in August 1999, more results of the same type were provided in the form of digitized water-oil interfaces (for details, see UNH's Phases II and III reports).

The digitized pictures consisted in matrices of gray color values given on a  $0$  to  $255$  scale. The geometric scales of the pixels in the experimental pictures, in the vertical and horizontal directions, were found using pictures of a  $0.1$  by  $0.01 \text{ m}$  line and of a  $0.05 \text{ m}$  diameter circle (Fig. 3.1). In each digitized picture, the locations of the water-

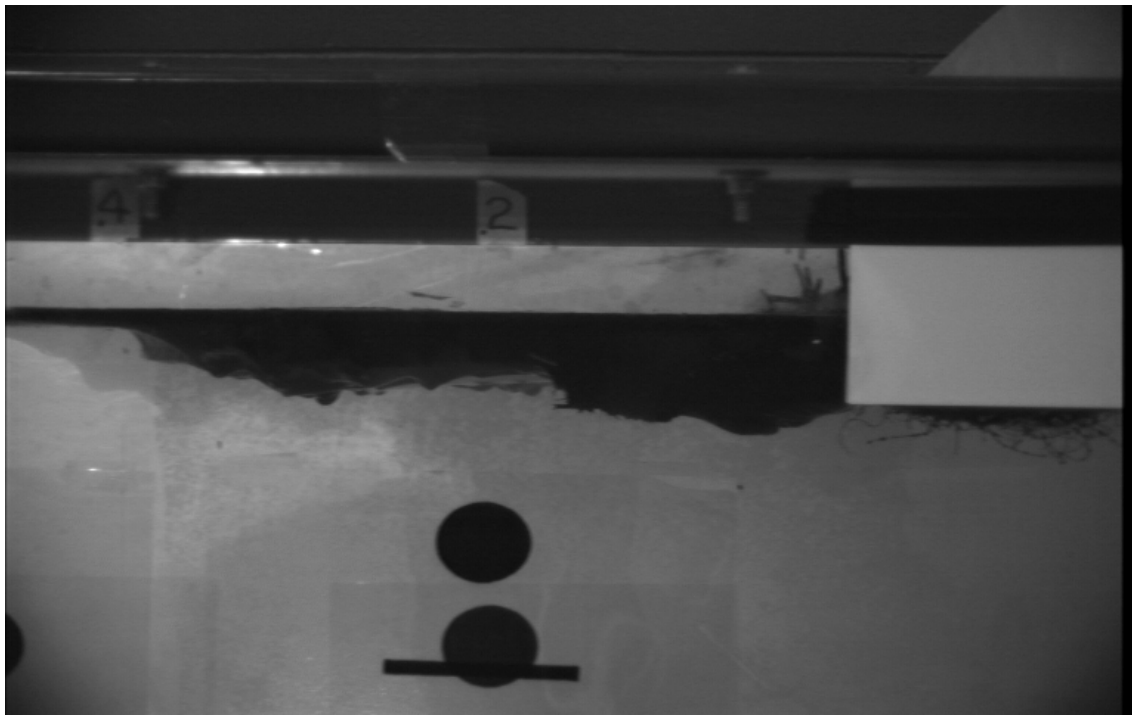


Figure 3.1: UNH August 1997 experiments with Sundex oil. Sideview of oil slick profile close to containment failure, in the recirculating flume. The plywood boom is to the right of the picture, with the horsehair in front of it hidden by a white rectangle. Note the line and circle at the bottom of the picture, used for setting scales.

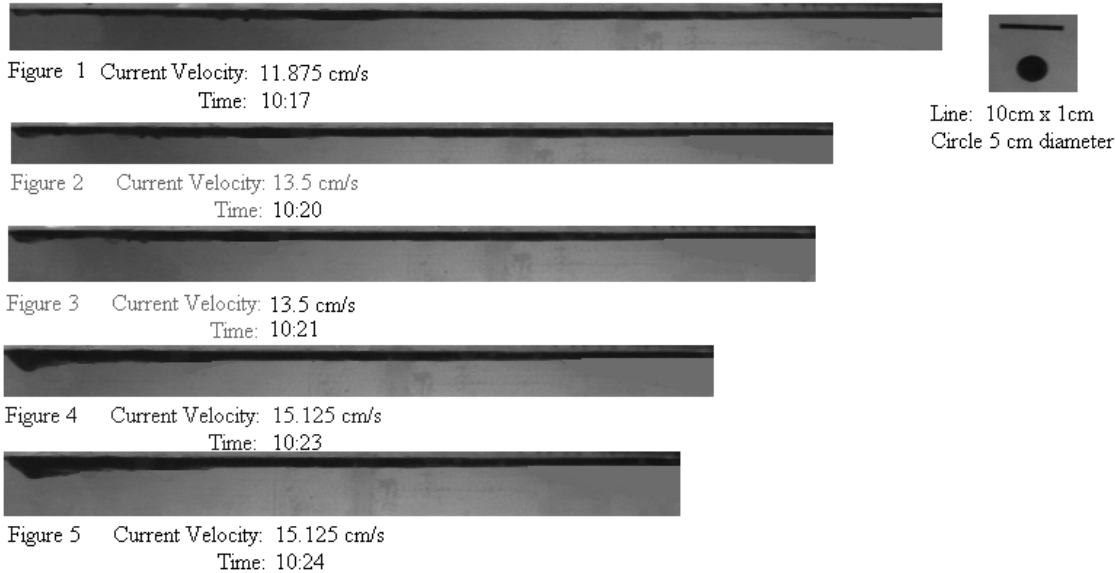


Figure 3.2: UNH May 1997 experiments with Sundex oil. Digitized pictures 1 to 5.

oil and oil-air interfaces were determined, for each column of pixels, by identifying the pixels for which there was a large jump in gray scale value, when moving from the bottom to the top of the picture.

The following describes URI's analysis of UNH's experimental results. These analyses were performed independently of UNH's own analyses of their results, reported in their reports for Phases II and III. The purpose of our analyses was two-fold : (i) to learn more about the physics of oil containment failure by critical accumulation, in order to refine SlickMap numerical models; (ii) to calculate experimental values of friction coefficient variations along the water-oil interface, in order to define a functional variation to be used in SlickMap models for Stages 2 and 3.

## 3.2 May and July 1997 experiments

### 3.2.1 Analysis of experimental results

UNH's first set of laboratory experiments, in May 1997, used a volume  $v_o = 0.0372$  m<sup>3</sup> (9.8 gal.) of Sundex oil, i.e., the nominal linear oil volume in the flume was  $V_o = v_o/w' = 0.0316$  m<sup>3</sup>/m. The oil density in these experiments was  $\rho_o = 960$  kg/m<sup>3</sup> and the kinematic viscosity was  $\nu_o = 0.02$  m<sup>2</sup>/s; hence  $\mu_o = \rho_o \nu_o = 19.2$  kg/ms (at 20° Celsius).

Fourteen digitized pictures were provided by UNH in June 1997, for these experiments, corresponding to 1 to 3 pictures for each of 6 flow velocities (Figs. 3.2 and

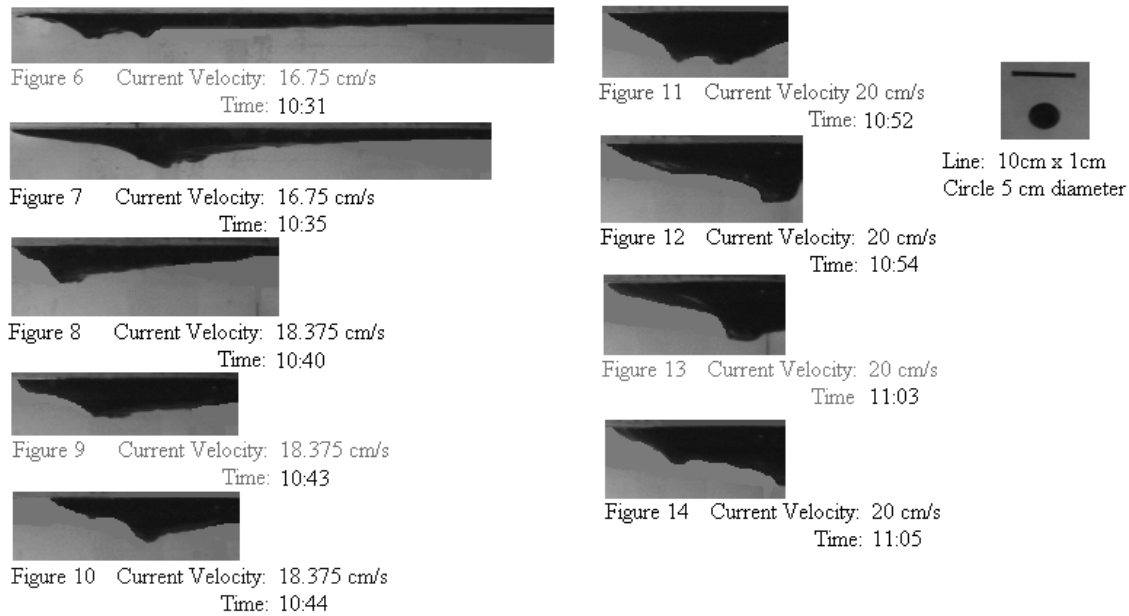


Figure 3.3: UNH May 1997 experiments with Sundex oil. Digitized pictures 6 to 14.

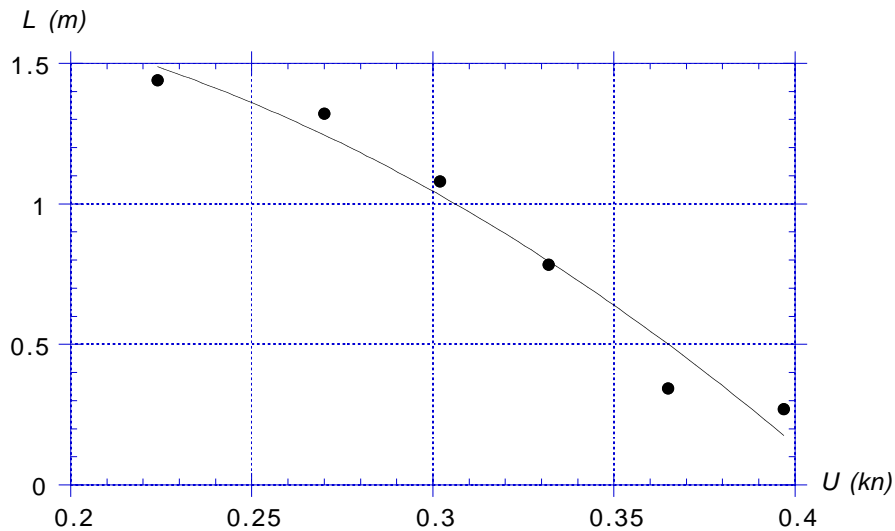


Figure 3.4: UNH May 1997 experiments with Sundex oil. (●) Slick length  $L$  measured as a function of flow velocity  $U$  in the initial experiments. (—) indicates a quadratic curve fit to the data.

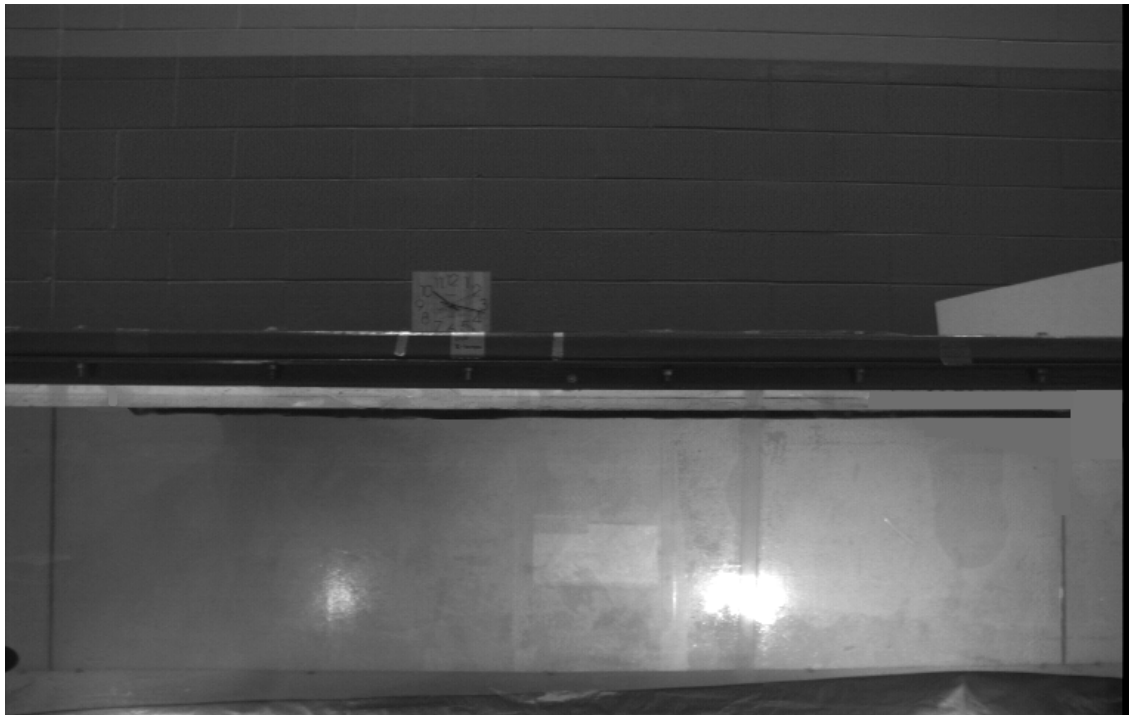


Figure 3.5: UNH July 1997 experiments with Sundex oil. Digitized picture No. 10 for case (a) with  $U = 0.119$  m/s.

3.3) :  $U = 0.119, 0.135, 0.151, 0.168, 0.184$  and  $0.200$  m/s ( $0.224$  to  $0.397$  kn). These pictures had a resolution of 757 by 484 pixels in the horizontal and vertical directions, respectively. This corresponded to about 4.4 pixels/cm horizontally, and 3.8 pixels/cm vertically. Since the slick thickness was on the order of a few centimeters, this only represented a resolution of 8-15 pixels in the vertical direction for the oil slick. From these pictures, the stabilized length of the slick  $L$  was measured for each speed (Fig. 3.4). After proper scaling, these results were used for comparison with OHMSETT's experiments (see Fig. 2.18, Chapter 2).

In these experiments, the oil-air interface shape was not recorded with great accuracy and, in the pictures, in the words of one of the experimentators (Chris Doane), "the oil-air shape, to the resolution of the measurements, is effectively a straight line." Hence, in the following, it is assumed that the measured value of  $m$  is unreliable and is just used as a reference for calculating  $\eta$ . Also the low vertical resolution of the slick shape led to a fairly irregular digitized water-oil interface shape. Hence, for a more accurate analysis of slick profiles, a larger set of digitized pictures was requested by URI. UNH run a second set of similar experiments in July 1997 and, in August 1997, URI was provided with 10 pictures taken at 10 sec intervals, for each of three

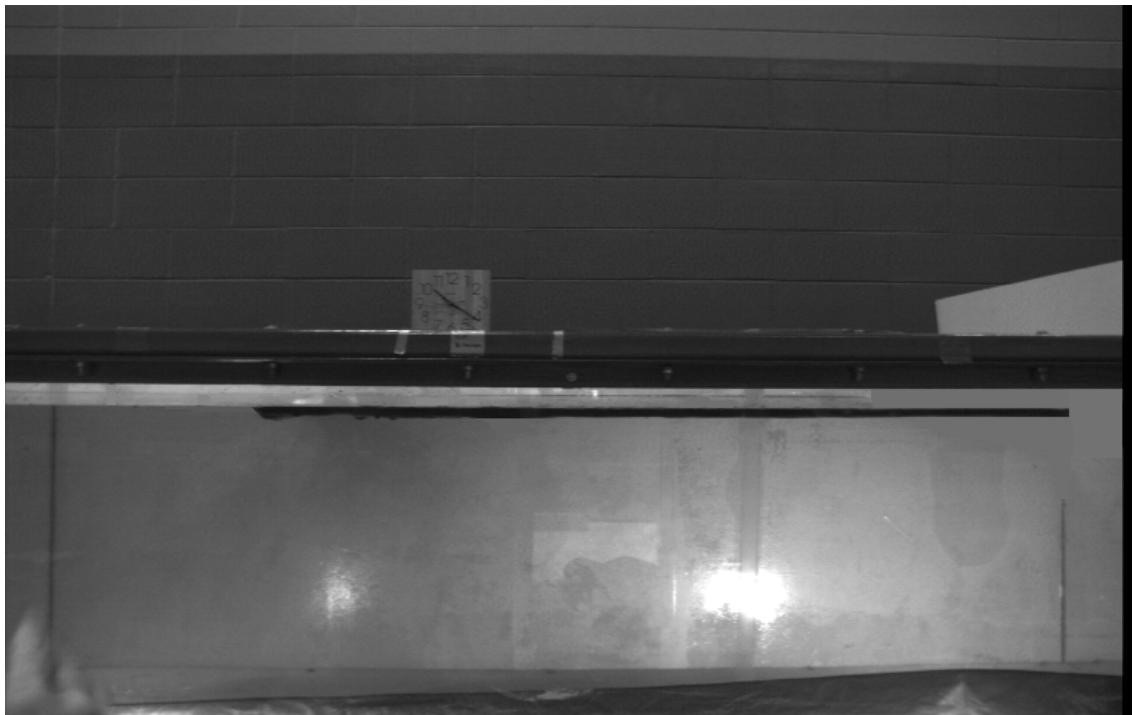


Figure 3.6: UNH July 1997 experiments with Sundex oil. Digitized picture No. 10 for case (b) with  $U = 0.135$  m/s.



Figure 3.7: UNH July 1997 experiments with Sundex oil. Digitized picture No. 10 for case (c) with  $U = 0.151$  m/s.

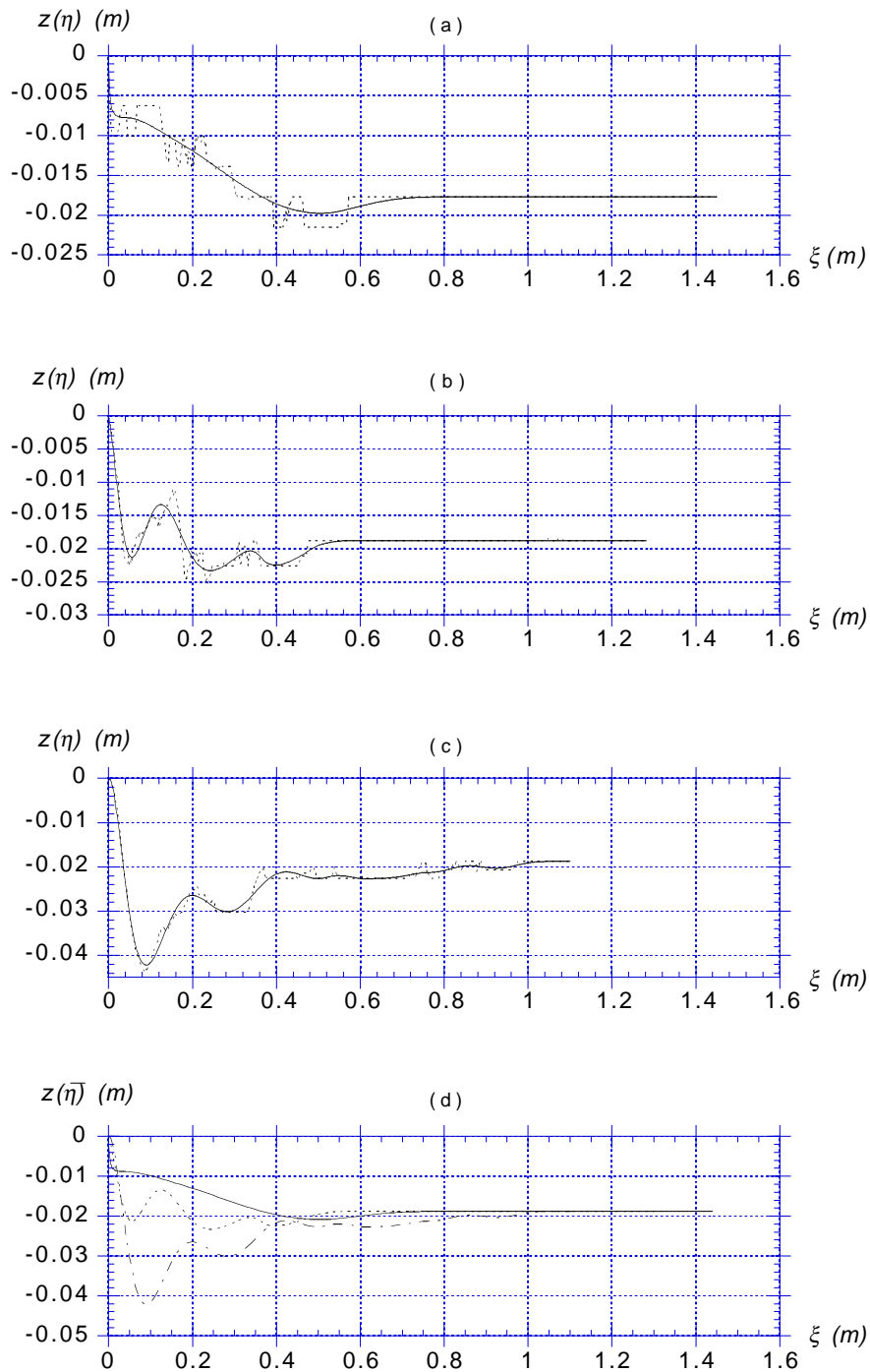


Figure 3.8: UNH July 1997 experiments with Sundex oil. Water-oil interface shape measured for  $U =$  (a) 0.119, (b) 0.135, (c) 0.151 m/s, with (---) the average  $\bar{\eta}$  calculated for 10 pictures taken at 10 sec intervals, and (—) the curve fits to this data. Fig. (d) shows the three average slick profiles superimposed at the same scale for :  $U =$  (—) 0.119, (---) 0.135, (- - -) 0.151 m/s.

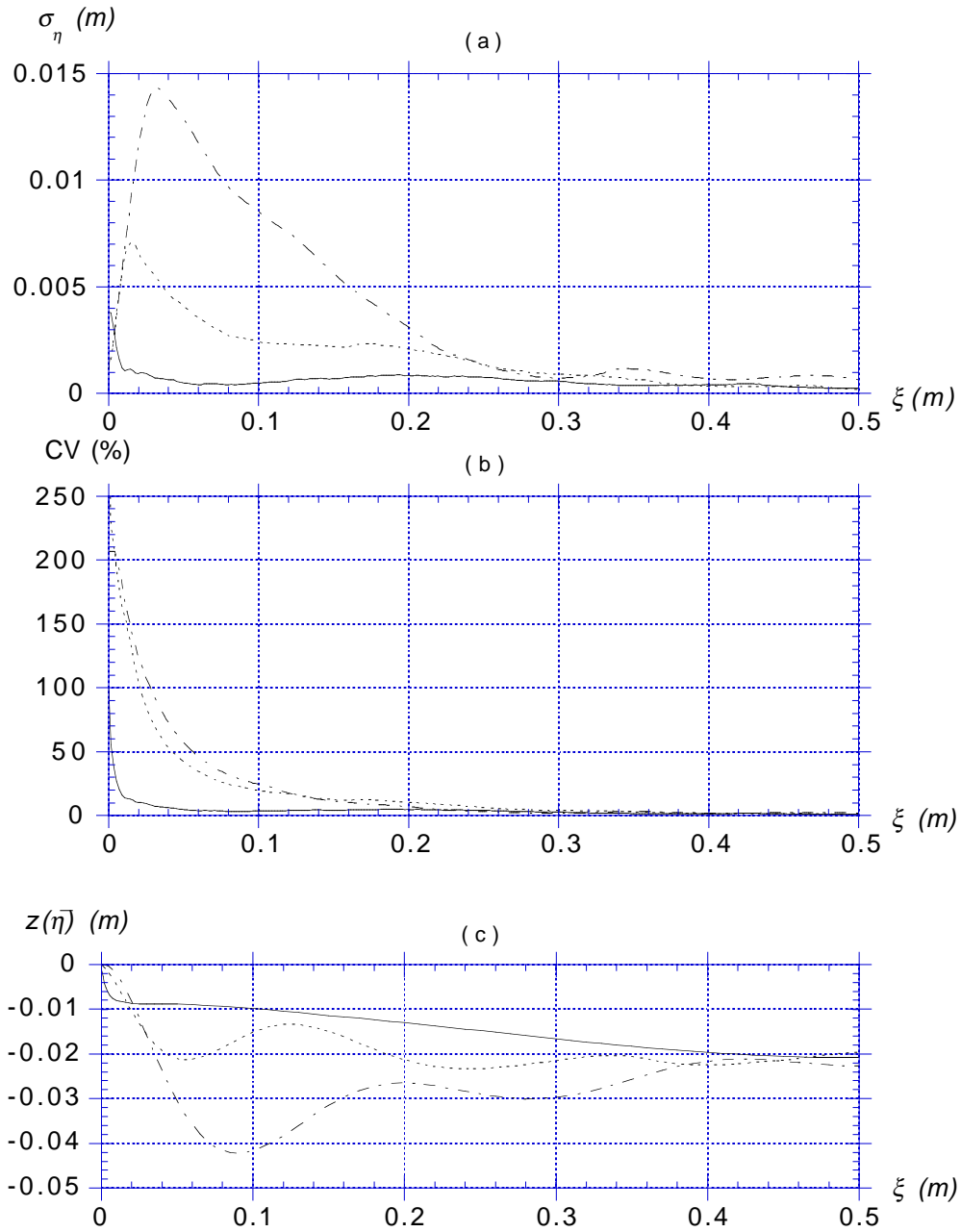


Figure 3.9: UNH July 1997 experiments with Sundex oil, for  $U =$  (—) 0.119, (----) 0.135, (- - -) 0.151 m/s. (a) Standard deviation calculated for 10 pictures taken at 10 sec intervals. (b) Coefficient of variation,  $CV = \sigma_\eta / \bar{\eta}$ . (c) Average slick profile  $\bar{\eta}$ , for  $\xi \leq 0.5$  m.

flow velocities :  $U = 0.119, 0.135, 0.151$  m/s. Figs. 3.5, 3.6, and 3.7 show examples of such pictures. The water-oil interface location was averaged as  $\bar{\eta}(\xi)$ , for each set of 10 pictures, and its standard deviation  $\sigma_{\eta}(\xi)$  was also calculated. The latter gives a measure of the intensity of fluctuations in shape of the oil-water interface, e.g., due to Kelvin-Helmholtz instabilities. High order polynomial curve fits were applied to the average water-oil interface shapes. Fig. 3.8 shows both the measured average shapes and the curve fits for each of the three sets of data. The development of a head-wave and of a more wavy interface is apparent as flow velocity is increased. Fig. 3.9 shows standard deviations and coefficients of variation  $CV = \sigma_{\eta}/\bar{\eta}$ . Large fluctuations in interface shape only occur in the headwave region, roughly for  $\xi < 0.3$  m, for the two larger flow velocities; and increasingly so, the larger the velocity. This indicates the occurrence of Kelvin-Helmholtz interfacial waves for the larger flow velocities. This was also observed in the underwater video records taken during OHMSETT's experiments.

The surface integration of the curve fitted slick profiles in Fig. 3.8, gives similar linear volumes of :  $V_o = 0.0253, 0.0251$  and  $0.0256$  m<sup>3</sup>/m for cases (a), (b) and (c), respectively, or an average of  $0.0253$  m<sup>3</sup>/m (which is the value used for the comparisons with OHMSETT's results). This represents only 80 % of the nominal linear volume or the equivalent of 7.85 gal. of oil in the flume. As mentioned above, however, the slick was observed to be non-uniform over the width of the tank. One picture overlooking the flume, in UNH's report, shows a slick length at the sidewalls only about 90 % of the slick length in the middle of the flume. Hence, the true average slick length would be about 5% larger than measured on the sidewalls. Since the slick depth at the horsehair is about  $D = 0.0176, 0.0189, 0.0188$  m for cases (a), (b) and (c), respectively, this effect of non-uniformity leads to an average linear volume loss of  $0.00118$  m<sup>3</sup>/m, or 3.7% of the nominal value. The remaining 16.3 % difference can be explained by assuming that oil is present within the horsehair, and fills about 40% of its 0.2 by 0.064 m cross-section; a realistic value for horsehair porosity (see, e.g. Fig. 3.1).

### 3.2.2 Computation of corresponding friction function

The three average interface shapes obtained from UNH's July 1997 experiments (Fig. 3.8) were used as input for SlickMap Stage 2 model of the slick quasi-steady shape (Chapter 4) to calculate both the tangential velocity distribution  $u_s(\xi)$  and the corresponding friction coefficient function  $C_f(\xi)$ , for an actual water-oil interface shape. In Stage 2 model, the slick water-oil interface is assumed to be stable and represents a streamline for the underlying water flow (Section 2.2).

The tangential velocity was obtained by specifying the measured slick, water depth, and boom geometries in the model and using the flow velocity  $U$ , as upstream and downstream boundary conditions (Fig. 4.10). The friction function was obtained, following a procedure similar to that used by Milgram and Van Houten's (1978) [34], by solving quasi-hydrostatic equilibrium equations (4.52)-(4.58) within the slick, for

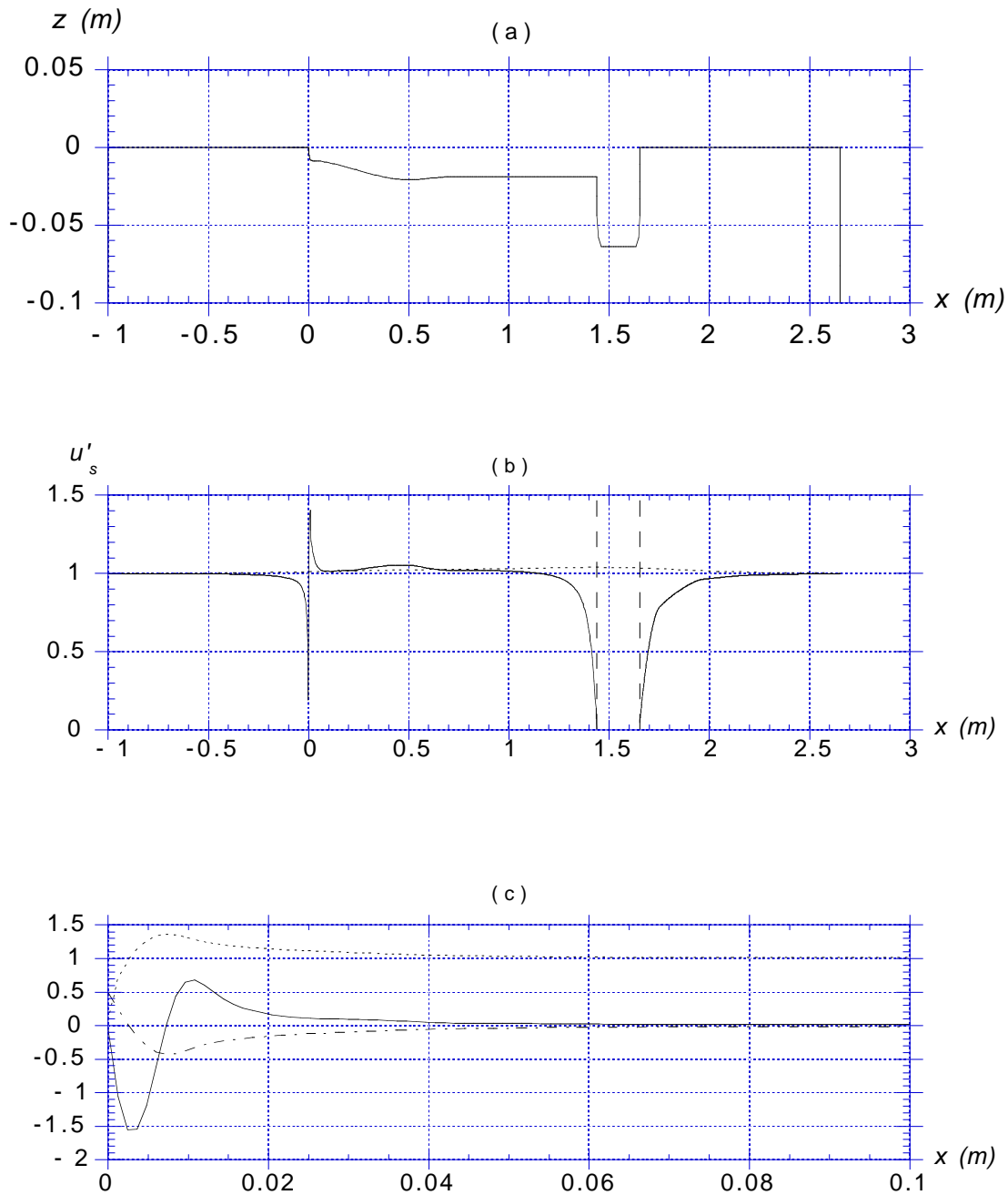


Figure 3.10: UNH July 1997 experiment with Sundex oil, for case (a) Fig. 3.8 with  $U = 0.119$  m/s. Computations in SlickMap Stage 2 model. (a) Shape of slick and boom geometry in BEM model. (b) Calculated tangential velocity on : (—) water-air and water-oil interfaces; (---) flume bottom. (c) Calculated : (—)  $C'_f$ ; (---)  $u'_s$ ; (---)  $p'_D$ ; on water-oil interface.

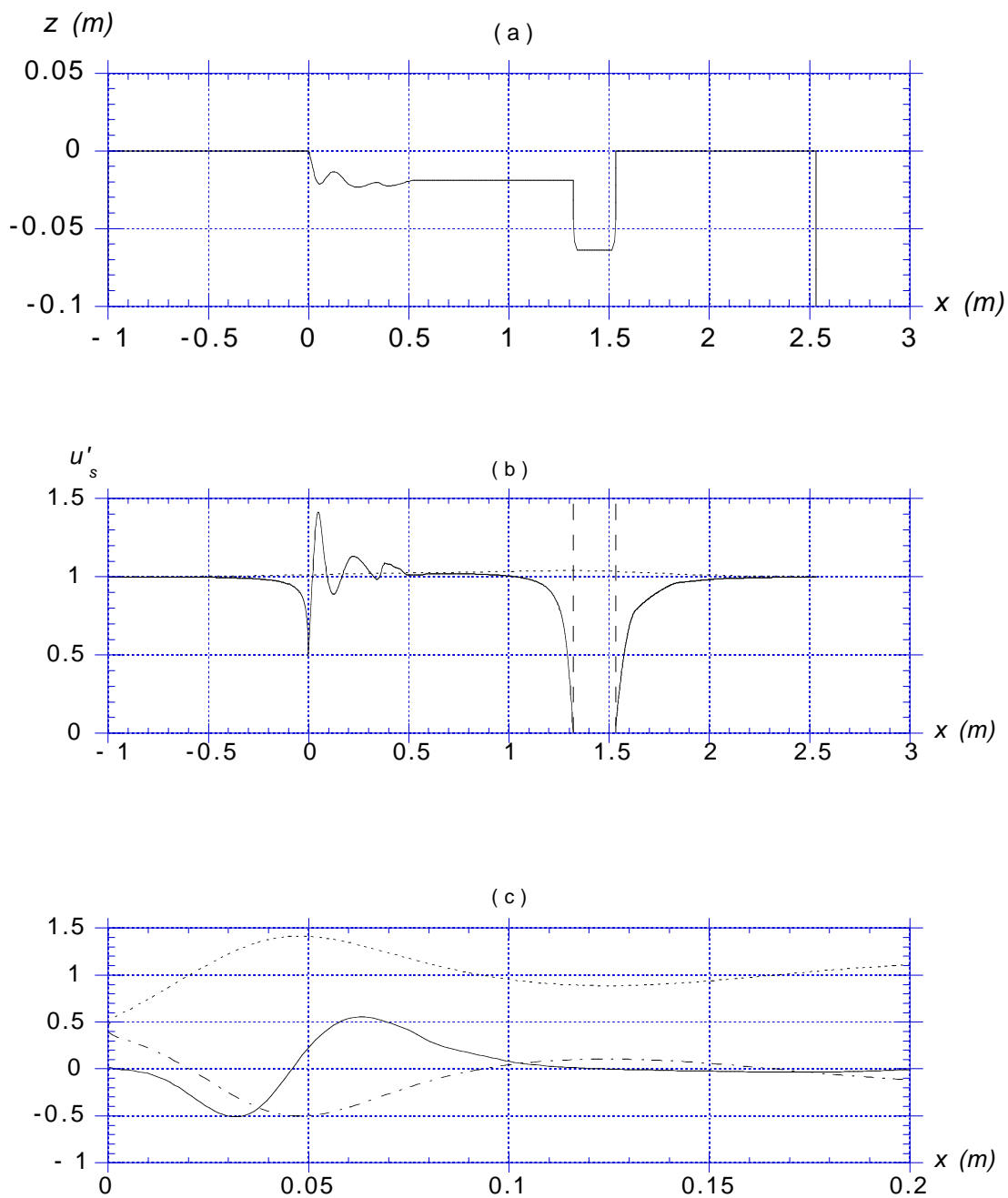


Figure 3.11: UNH July 1997 experiment with Sundex oil, for case (b) Fig. 3.8 with  $U = 0.135$  m/s. Computations in SlickMap Stage 2 model. (a) Shape of slick and boom geometry in BEM model. (b) Calculated tangential velocity on : (—) water-air and water-oil interfaces; (- - - -) flume bottom. (c) Calculated : (—)  $C'_f$ ; (- - -)  $u'_s$ ; (- - -)  $p'_D$ ; on water-oil interface.

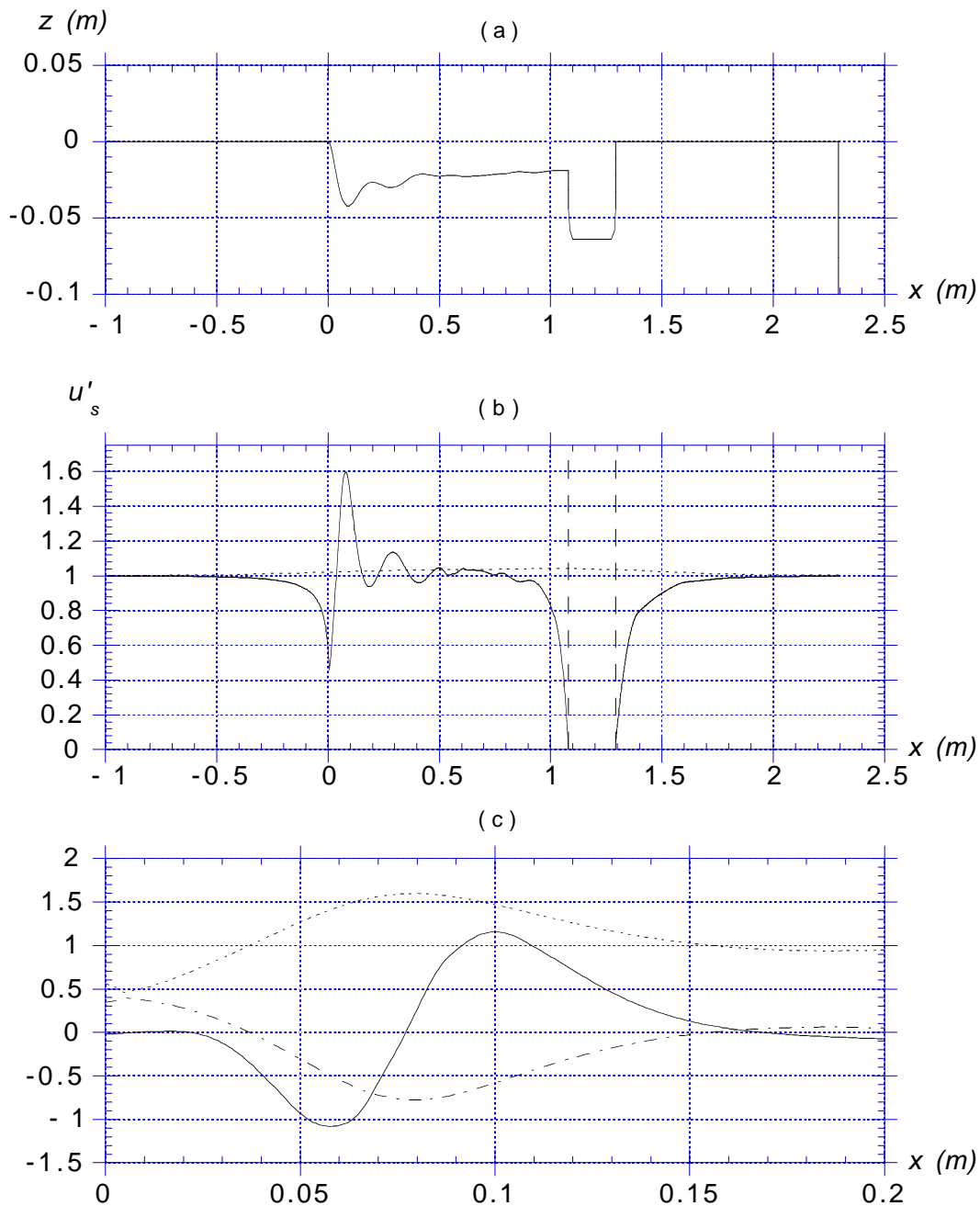


Figure 3.12: UNH July 1997 experiment with Sundex oil, for case (c) Fig. 3.8 with  $U = 0.151$  m/s. Computations in SlickMap Stage 2 model. (a) Shape of slick and boom geometry in BEM model. (b) Calculated tangential velocity on : (—) water-air and water-oil interfaces; (- - - -) flume bottom. (c) Calculated : (—)  $C'_f$ ; (- - -)  $u'_s$ ; (- - -)  $p'_D$ ; on water-oil interface.

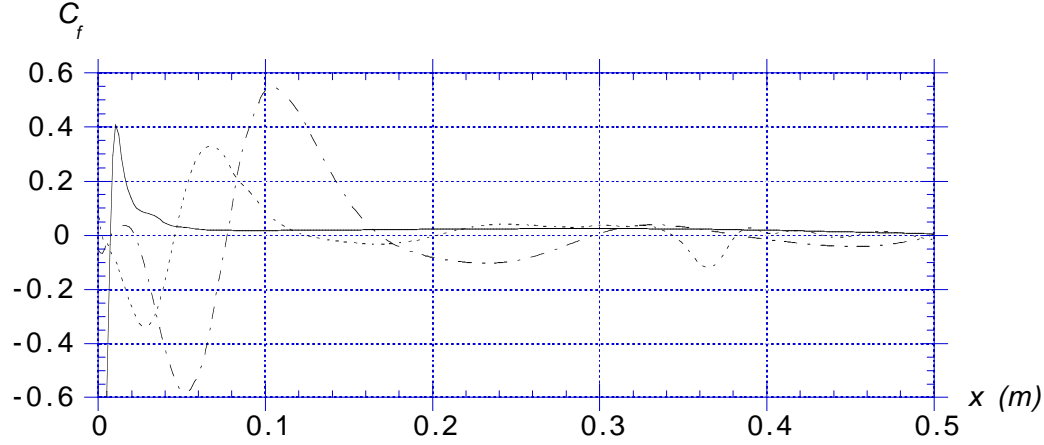


Figure 3.13: UNH July 1997 experiment with Sundex oil, for three cases in Fig. 3.8 with  $U =$  (—) 0.119; (- - - -) 0.135, (- - —) 0.151 m/s. Computations with SlickMap Stage 2 model of friction function  $C_f$ .

specified values of  $u_s$ ,  $\eta$ ,  $d\eta/d\xi = -\tan\beta$ , and  $du_s/d\xi$  (in which  $u_s$ 's derivative was also obtained from SlickMap's solution). Combining the quasi-hydrostatic equations, assuming  $C_h = 0$  (no head loss), we find, in non-dimensional form,

$$C_f' = -\frac{1}{\varphi} \{1 - u_s'^2 + 2\eta'\} \left\{ \tan\beta(1 - \varphi) + u_s' \frac{du_s'}{d\xi'} \right\} \quad (3.1)$$

with  $C_f = C_f'/u_s'^2$  and  $u_s = -\partial\psi/\partial n$  (Eq. (4.60)).

Figs. 3.10, 3.11 and 3.12 show computational results for the three cases selected from July 1997 experiments. Parts (a) of the figures give the slick and boom geometry, obtained from Fig. 3.8, as discretized in the BEM model. Parts (b) of the figures show results for the tangential velocity  $u_s'$ , calculated on both the water-air and water-oil interfaces and on the bottom. On the latter, the non-dimensional tangential velocity is very close to 1 (i.e.,  $U$ ), and only slightly increases below the boom. This could be expected as the ratio of boom draft to water depth is quite large,  $d/h = 8.25$ . In front of the slick, the non-dimensional tangential velocity gradually drops from a value of 1, for the free stream, to a lower value (0.2 to 0.5) at the leading edge of the slick. Tangential velocity then quickly increases to a value 1.4-1.6 in the headwave, then drops back to 1, while oscillating, out of phase with the water-oil interface geometry oscillations. Closer to the boom, the tangential velocity starts gradually dropping to zero, to satisfy the no-flow condition at the boom. The same occurs downstream of the boom, where the tangential velocity increase from zero to 1. Parts (c) of the figures show variations of  $C_f'$ ,  $u_s'$  and  $p_D'$  in the slick headwave. In each case, the friction function is first negative close to the leading edge, due to the rapid increase in flow velocity and related drop in dynamic pressure. This indicates a reversal of the shear stress. The friction function then increases up to a maximum value and then drops

to almost zero beyond the first few oscillations in the water-oil interface geometry corresponding to the slick headwave. Milgram and Van Houten (1978) observed a similar behavior for  $C'_f$  and  $p'_D$ .

Finally, Fig. 3.13 shows the variation of  $C_f$  in the slick headwave for the 3 cases. These are similar to the variations discussed for  $C'_f$ . Such results, together with Milgram and Van Houten initial calculations, were used to develop functional expressions for  $C_f$  as a function of various shape parameters, which are used in SlickMap Stage 2 and 3 models (Eqs. (4.63) and (4.143)).

### 3.3 August 1997 experiments

A third set of plane barrier experiments was run at UNH in early August 1997, using Sundex oil, in a set-up similar to the earlier experiments. Results were provided to the URI team in September 1997, in the form of two time series of digitized pictures, taken 2 sec apart, for flow velocities  $U = 0.114$  and  $0.157$  m/s. To get a better resolution in the digitized slick pictures, the camera was moved closer to the flume transparent sidewall than in earlier experiments. Each picture still had 768 by 484 pixels in the horizontal and vertical directions, respectively but, due to the change in position of the camera, the resolution of the slick itself was increased to 11 pixels per cm, which is more than twice better than in the May and July 1997 experiments.

A volume  $v_o = 0.0304$  m<sup>3</sup> (8 gal.) of Sundex oil was used, i.e., the nominal linear oil volume in the flume was  $V_o = v_o/w' = 0.0258$  m<sup>3</sup>/m. The oil density in these experiments was  $\rho_o = 960$  kg/m<sup>3</sup> and the kinematic viscosity was  $\nu_o = 0.015$  m<sup>2</sup>/s; hence  $\mu_o = \rho_o \nu_o = 14.4$  kg/m s (at 20° Celsius).

In the first set of results, for a low flow speed  $U = 0.114$  m/s, the slick was fairly long and the total slick length was covered in three overlapping parts, by successively moving the camera to the headwave region, to the middle region, and then close to the boom. Labeled markers were positioned every 0.2 m on the flume top rail, to keep track of longitudinal position. This first set consisted in a time series of images, taken 2 sec apart : (i) 62 images over the markers 0.8 to 1.2 m; (ii) 62 images over the markers 0.4 to 0.8 m; and (iii) 76 images over the markers 0 to 0.4 m. For such a low flow speed, fluctuations in slick shape were observed to be quite small (see, e.g. Fig. 3.9) and it was possible to reconstitute views of the whole slick profile from 3 pictures taken at sequential times. Fig. 3.14 for instance gives an example of such a reconstituted slick profile. The average slick shape and its standard deviation were calculated for the three sets of images, (i)-(iii), using 62 reconstituted pictures. Results are plotted in Fig. 3.15 for  $x < 1$  m, and compared to those obtained for  $U = 0.119$  m/s in July 1997 experiments (Fig. 3.8a, Fig. 3.9). In part (a), we see that, despite the smaller linear volume of oil, the average slick shape in the headwave is very close to that found in July 1997 experiments for almost the same speed. Due to the smaller volume, the total slick length is  $L = 1.25$  m, i.e., about 0.20 m smaller

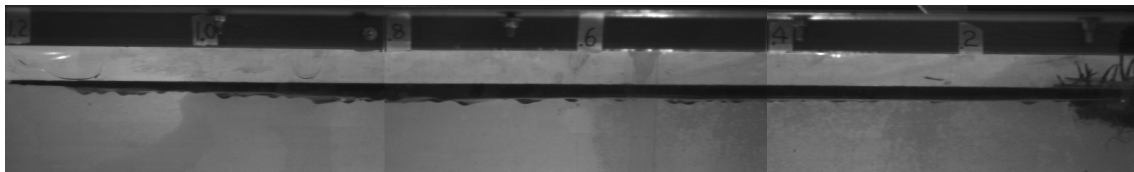


Figure 3.14: UNH August 1997 experiments with Sundex oil. Sideview of oil slick profile for  $U = 0.114$  m/s, reconstituted from three overlapping partial views taken at different times by the digital camera.

than for July 1997 experiment case (a) which is proportional to the difference in slick volume. In parts (b) and (c), both the standard deviation and coefficient of variation of  $\bar{\eta}$  follow the same trends as in July 1997 experiment case (a), but are about twice as large. This is likely due to the increased resolution (about twice better) in the August 1997 experiments, which leads to a better quantification of fluctuations and, hence to larger values of  $\sigma_{\eta}$  and CV.

In the second set of results, for  $U = 0.157$  m/s, the slick is close to containment failure and its length is sufficiently reduced to be recorded in one view by the camera, when moved close to the boom. This second set consists in a time series of 270 images, taken 2 sec apart, recorded starting 662 sec after the flume flow speed was brought up to  $U = 0.157$  m/s. Figs. 3.16 to 3.21 show a sequence of such pictures, taken every 100 sec and Fig. 3.22 shows the corresponding smoothed water-oil interface profiles. We see, the slick interface is constantly changing and fluctuating, while keeping a nearly constant length, as Kelvin-Helmholtz waves are being created at the headwave and propagate down the slick interface, eventually leading to some loss of oil under the boom. Also, it is clear from the pictures that cross flume variations, i.e., three-dimensional effects are becoming significant. Finally, the slick length, about 0.45 m, is quite smaller than that measured in the May 1997 experiments, for almost the same speed (about 0.75 m), which is due to the smaller slick volume. Here, however, the reduction in slick length, is more than proportional to the reduction in slick volume, probably because the flow velocity is close to the critical velocity and fluctuations (Kelvin-Helmholtz waves) in the interface shape lead to enhanced friction and slick reduction for the part of the slick which is close to the boom.

### 3.4 August 1999 experiments

These experiments were conducted in the recently upgraded recirculating flume at UNH (12.2 m long,  $w = 1.22$  m wide and 1.22 m high), with a reduced ambient turbulence and a higher achievable flow velocity. The main purpose of these experiments was to confirm earlier results obtained by UNH (and provided to URI) using the previous, less performant, flume and data acquisition system.

A plane panel with constant draft was positioned vertically across the tank (at  $x = 0$  in Fig. 3.24). Slick profiles were recorded using a single digital computer system connected to 3 high resolution video cameras. Each camera viewfield was set to cover an overlapping section of the initial slick length. Simultaneous data acquisition was accomplished using coded camera signals.

Results discussed below correspond to UNH experiments 1 and 2 (those without waves), which used a panel of draft  $d = 0.038$  and  $0.064$  m (as in the earlier experiments with Boom # 4), respectively. As before, horsehair was set in the 0.2 m in front of the barrier. Water depth was  $h = 0.75$  m. The oil volume was  $v_o = 0.0218$  m<sup>3</sup> (5.74 gal.), hence the linear volume was  $V_o = v_o = 0.0179$  m<sup>3</sup>/m. Fresh water was

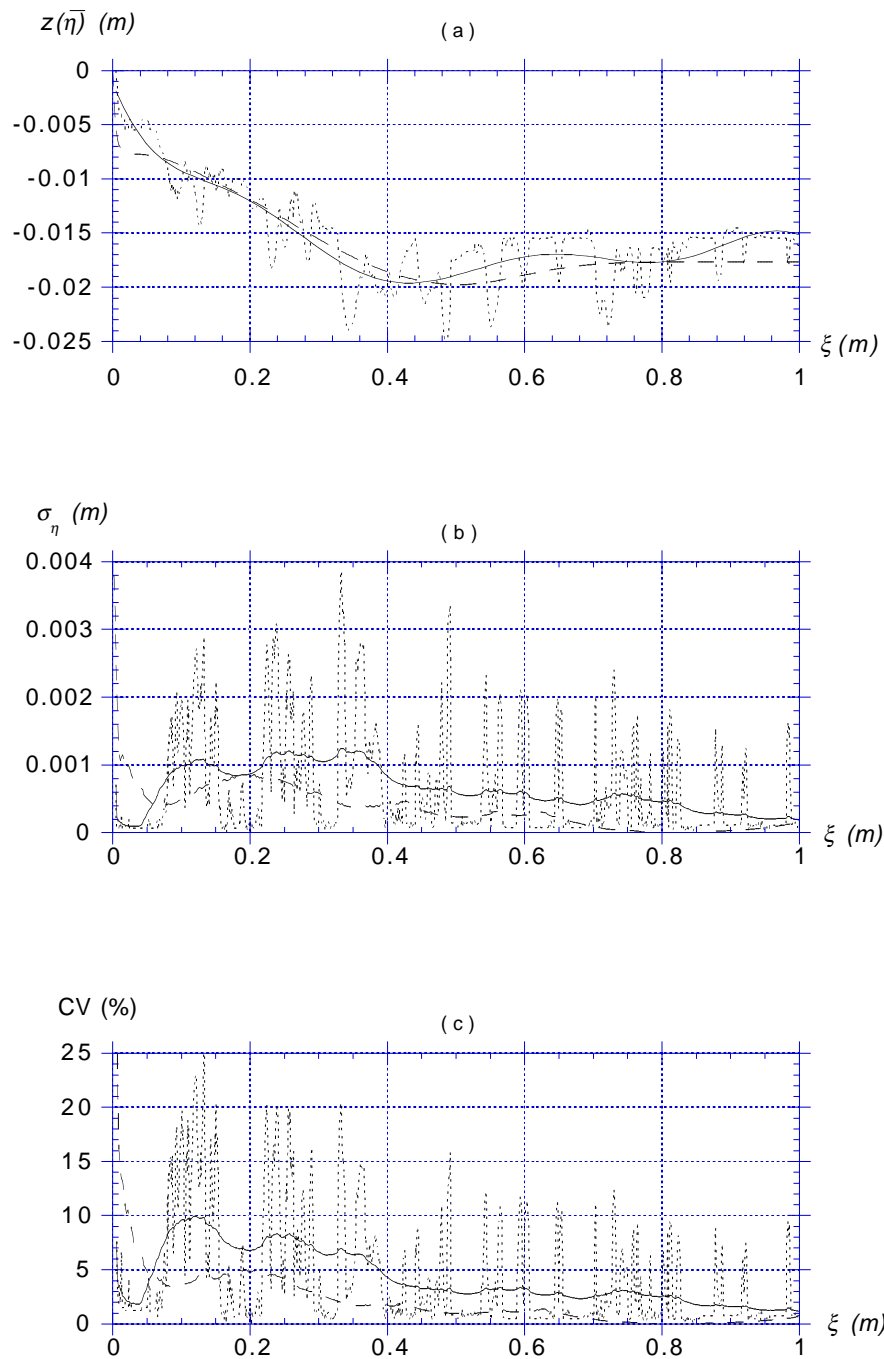


Figure 3.15: UNH August 1997 experiments with Sundex oil, for  $U = 0.114$  m/s, using 62 pictures, 2 sec apart for three overlapping views : (---) data; (—) curve fit; (- - -) July 1997 data, for  $U = 0.119$  m/s (cases (a)). (a) Average slick profile  $\bar{\eta}$ , for  $\xi \leq 1$  m. (b) Standard deviation of slick profile. (c) Coefficient of variation,  $CV = \sigma_{\eta} / \bar{\eta}$ .

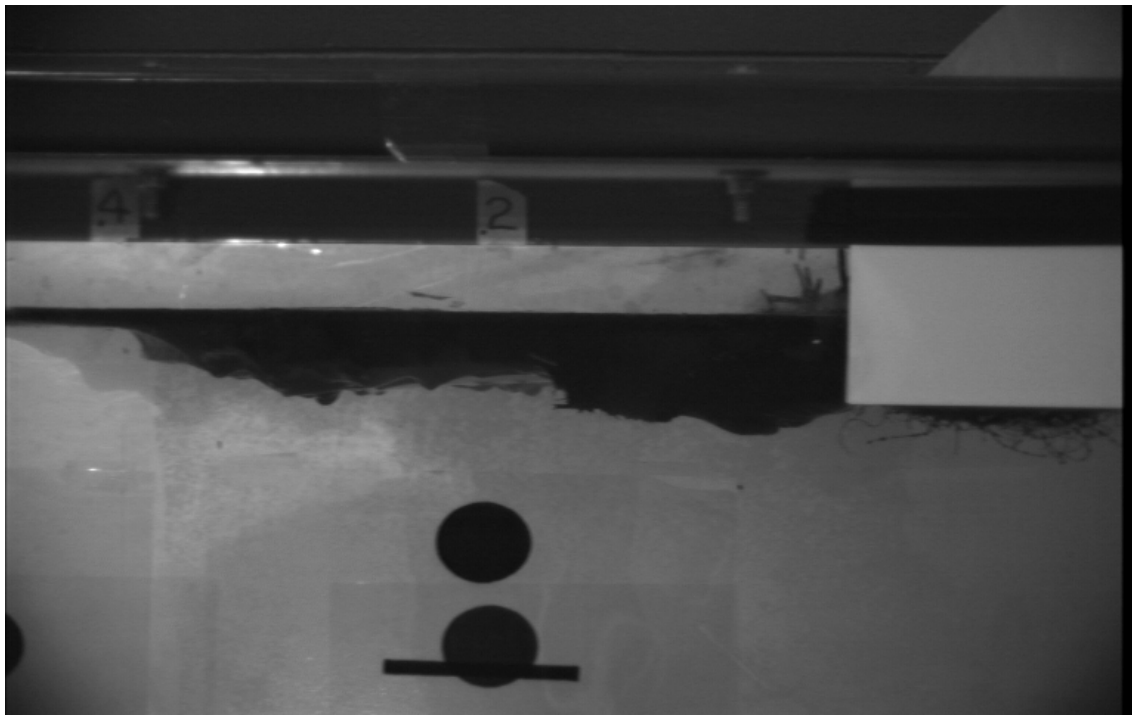


Figure 3.16: UNH August 1997 experiments with Sundex oil for  $U = 0.157$  m/s. View of oil slick profile at  $t = 662$  sec after speed has been specified.

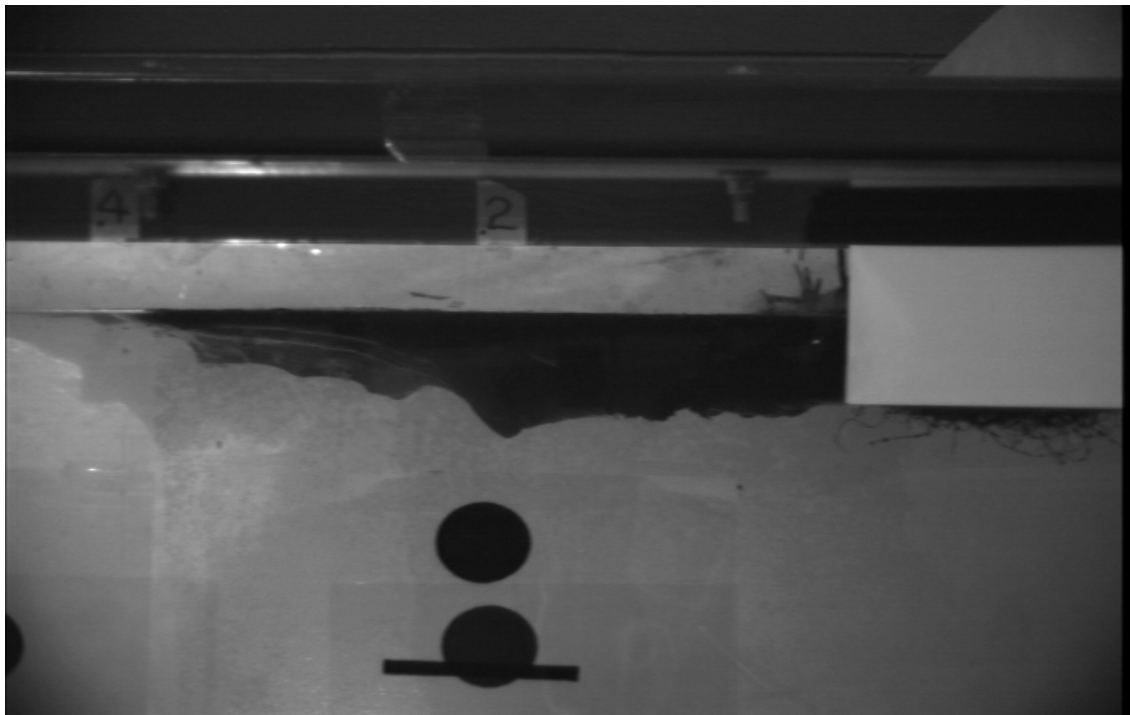


Figure 3.17: UNH August 1997 experiments with Sundex oil for  $U = 0.157$  m/s. View of oil slick profile at  $t = 762$  sec after speed has been specified.

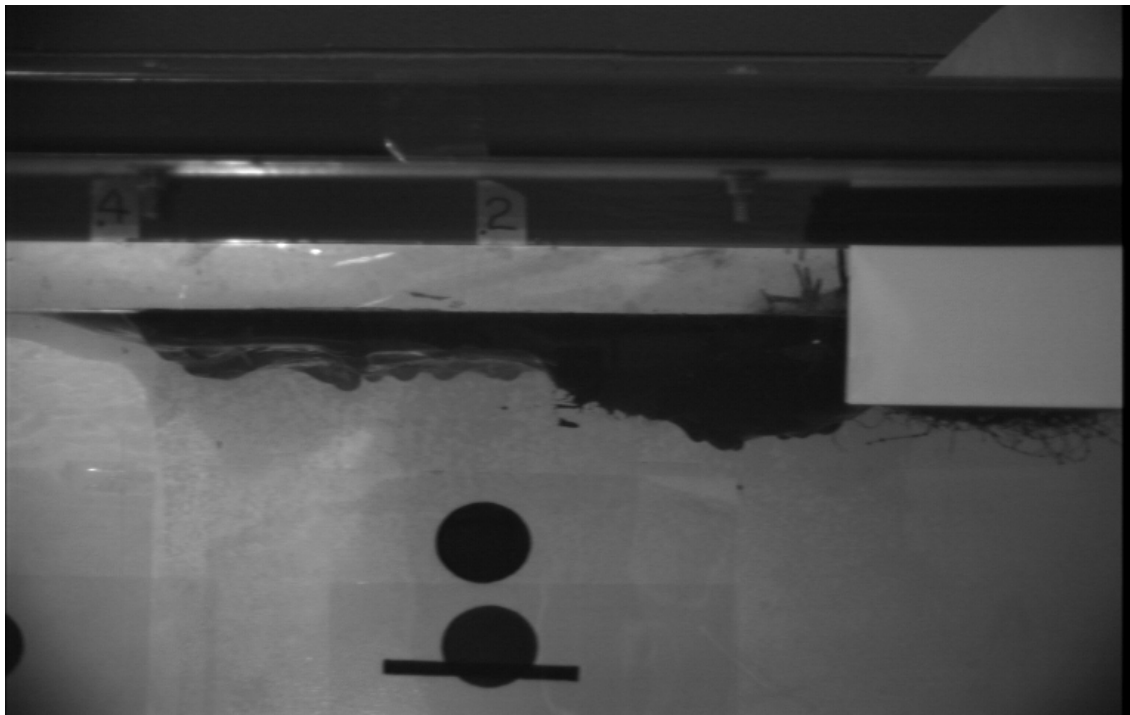


Figure 3.18: UNH August 1997 experiments with Sundex oil for  $U = 0.157$  m/s. View of oil slick profile at  $t = 862$  sec after speed has been specified.

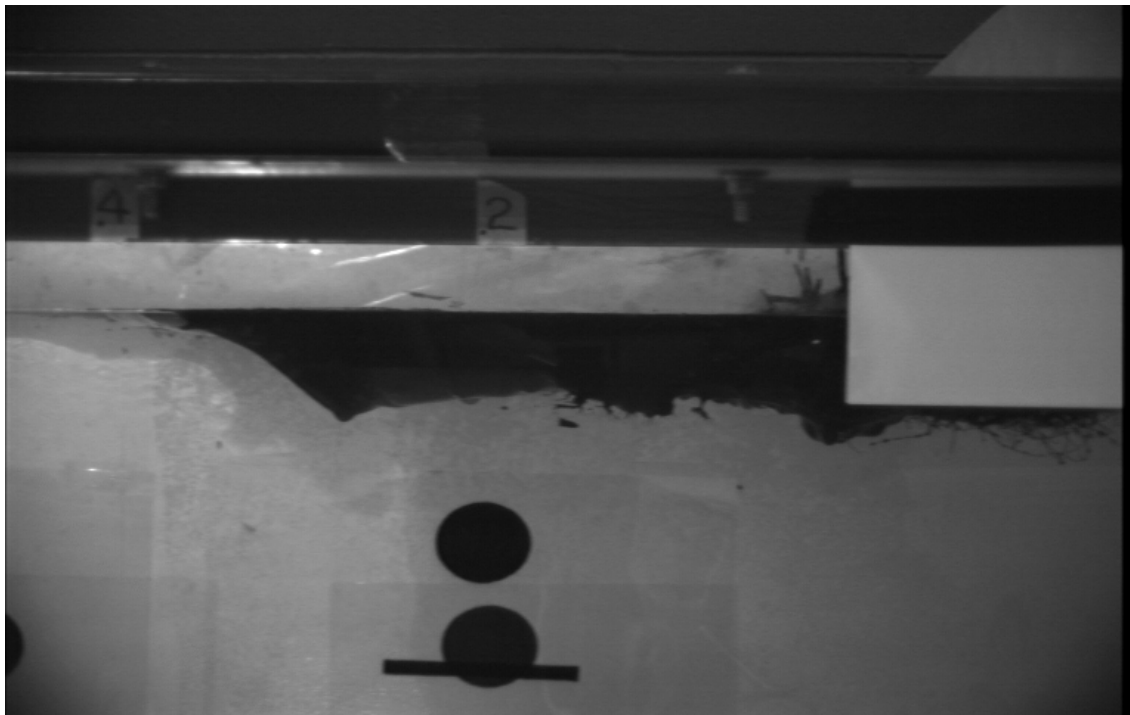


Figure 3.19: UNH August 1997 experiments with Sundex oil for  $U = 0.157$  m/s. View of oil slick profile at  $t = 962$  sec after speed has been specified.

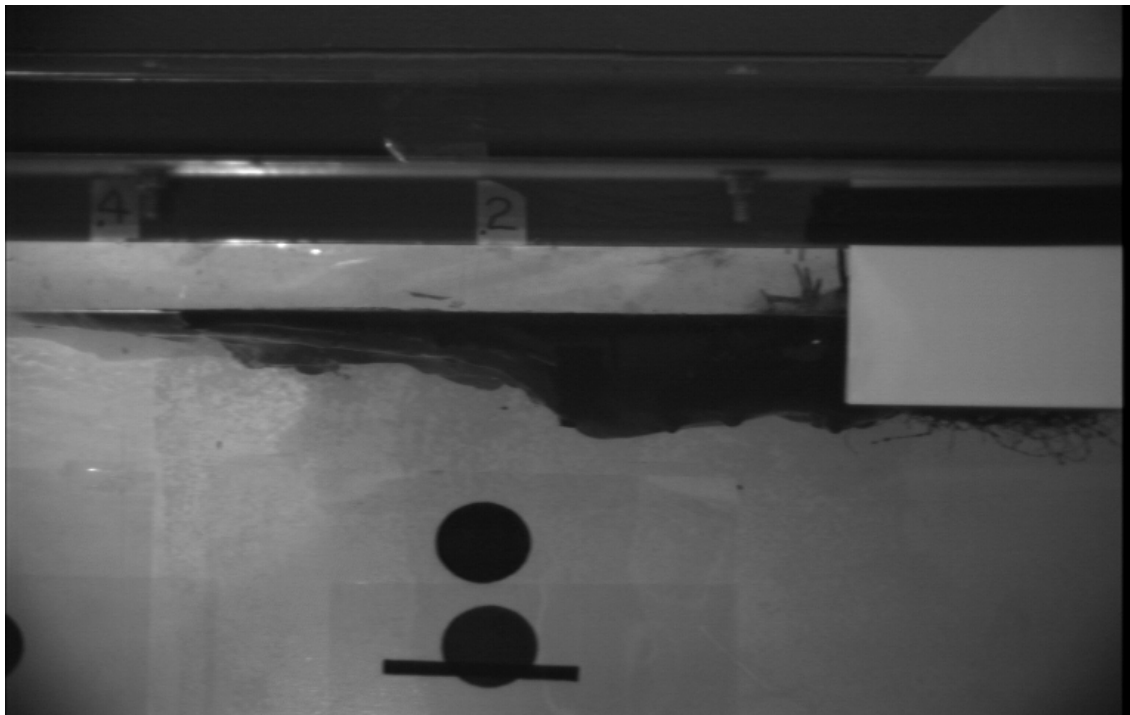


Figure 3.20: UNH August 1997 experiments with Sundex oil for  $U = 0.157$  m/s. View of oil slick profile at  $t = 1,062$  sec after speed has been specified.

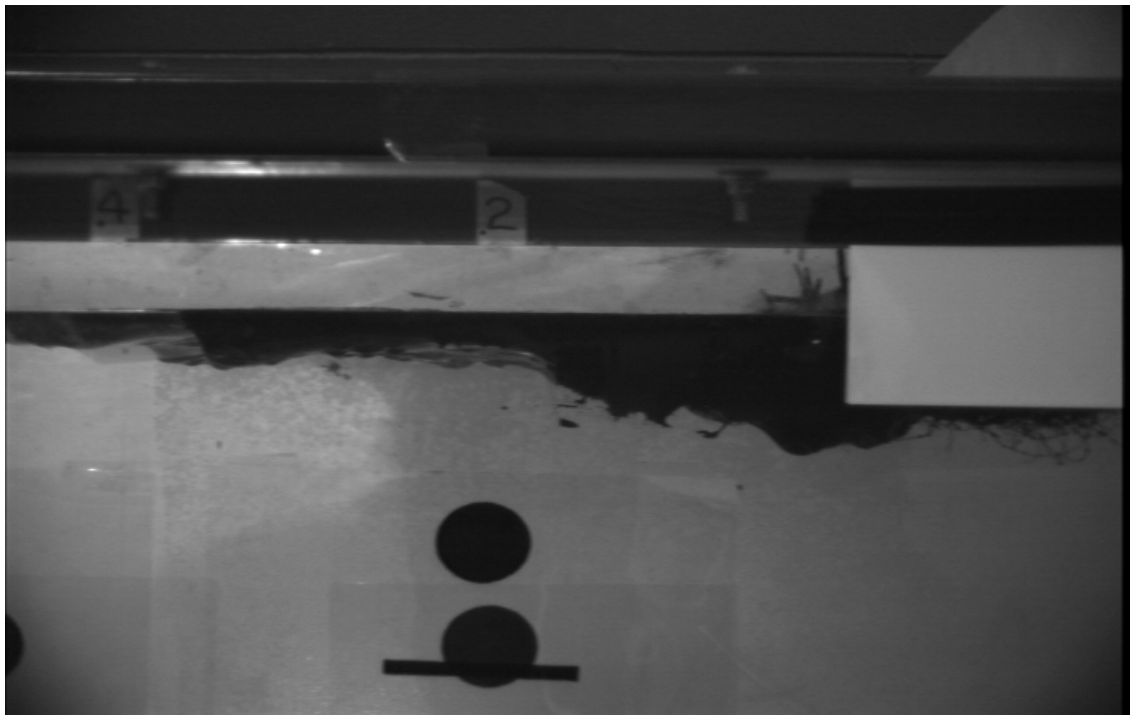


Figure 3.21: UNH August 1997 experiments with Sundex oil for  $U = 0.157$  m/s. View of oil slick profile at  $t = 1,162$  sec after speed has been specified.

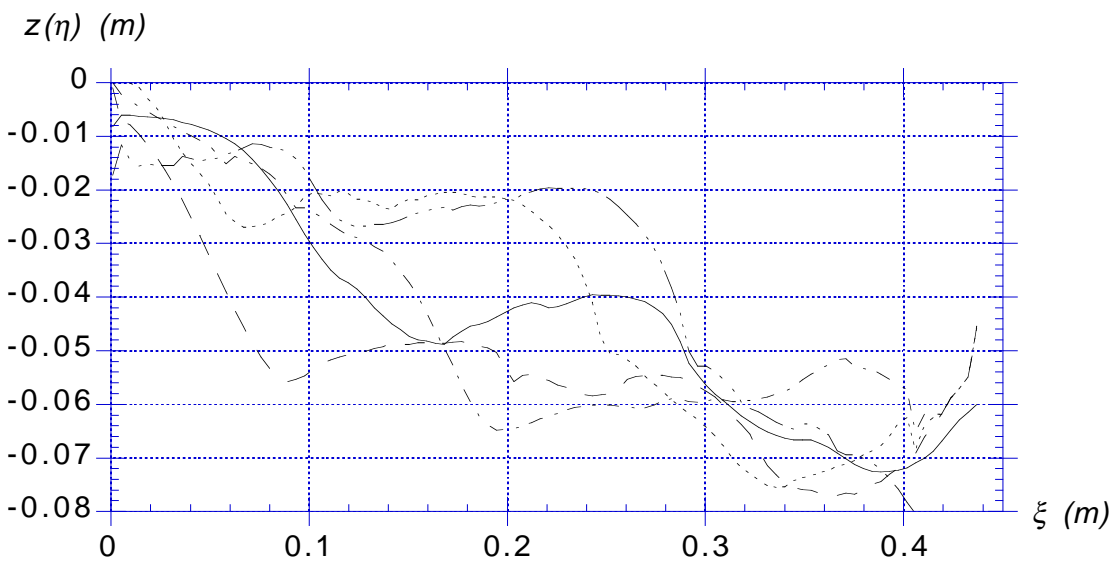


Figure 3.22: UNH August 1997 experiments with Sundex oil for  $U = 0.157$  m/s. Smoothed oil slick water-oil interface profiles at  $t =$  (—) 662; (- - - -) 762; (- - -) 862; (— —) 962; (— -) 1,062; and (— - -) 1,162 sec, after flow speed has been specified.

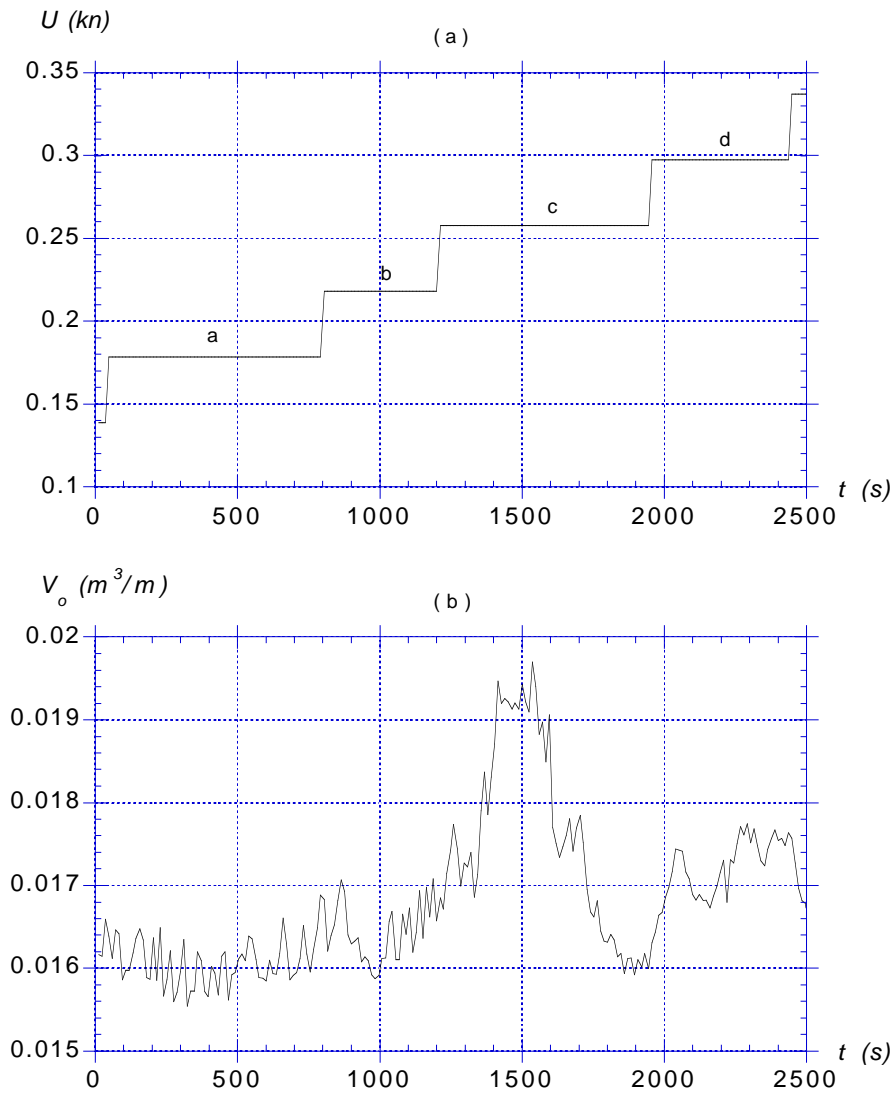


Figure 3.23: UNH August 1999 experiments 1, with Sundex oil and  $d = 0.038$  m. (a) Flow velocity specified as a function of time. (b) Linear volume as a function of time.

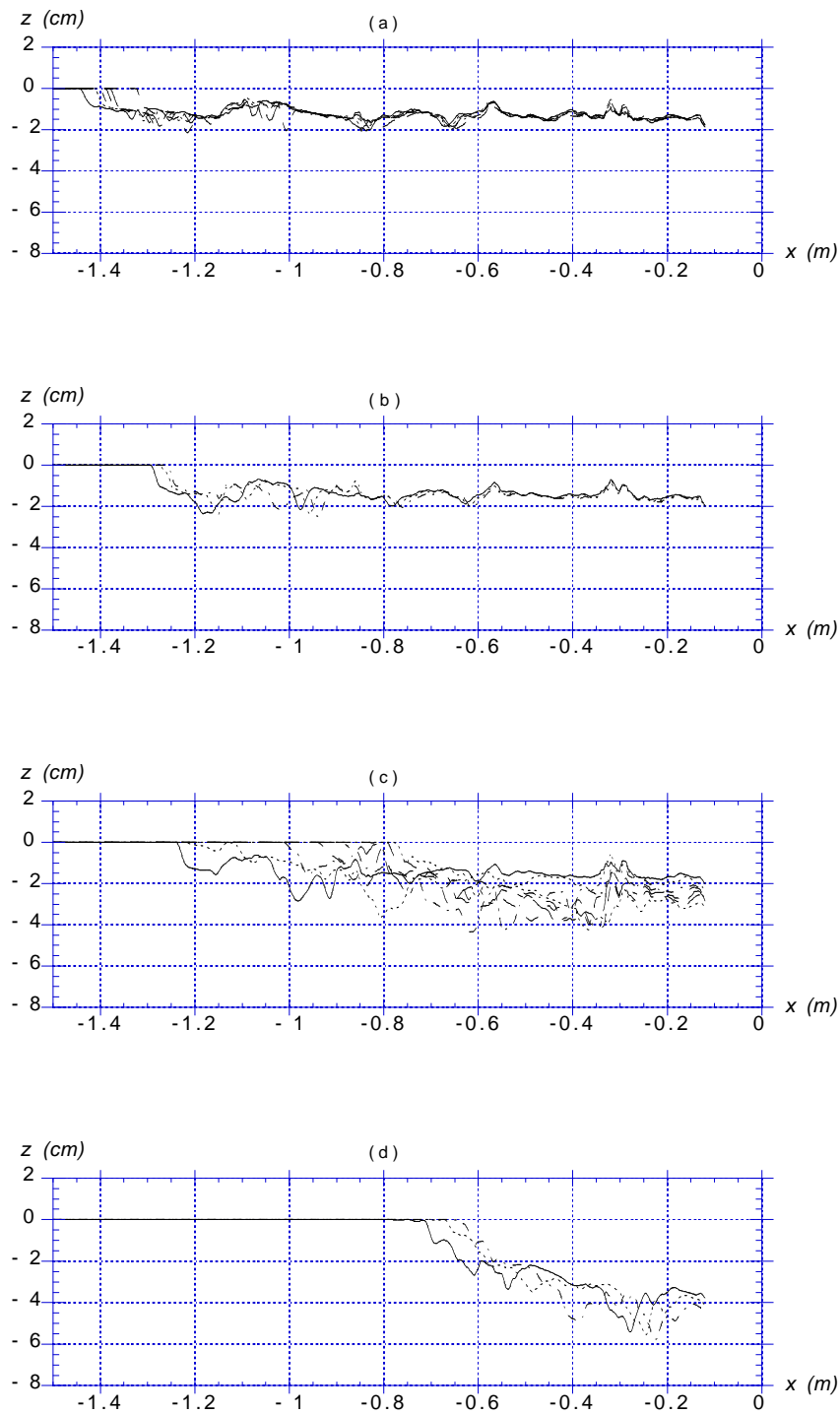


Figure 3.24: UNH August 1999 experiments 1, with Sundex oil and  $d = 0.038$  m. (a) to (d) : Every 10 recorded slick profiles for 4 flow speeds a-d shown in Fig.3.23a.

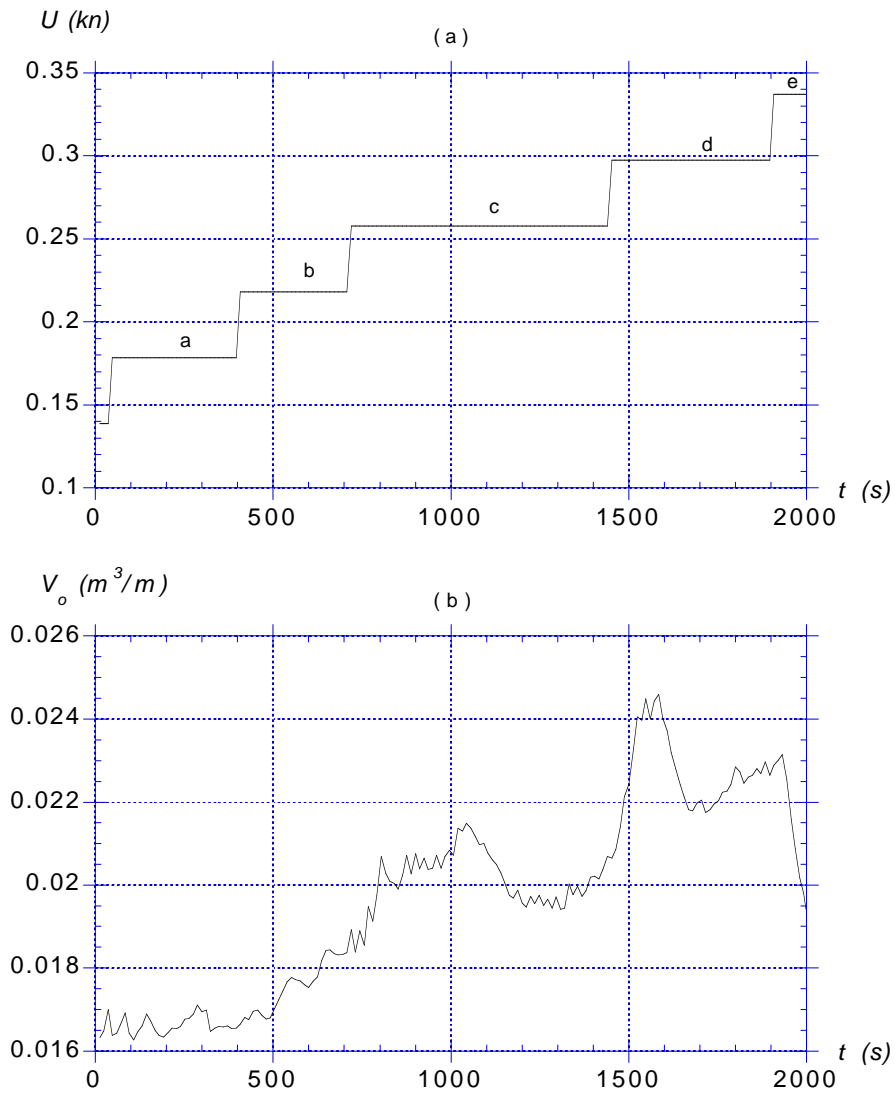


Figure 3.25: UNH August 1999 experiments 2, with Sundex oil and  $d = 0.064$  m. (a) Flow velocity specified as a function of time. (b) Linear volume as a function of time.

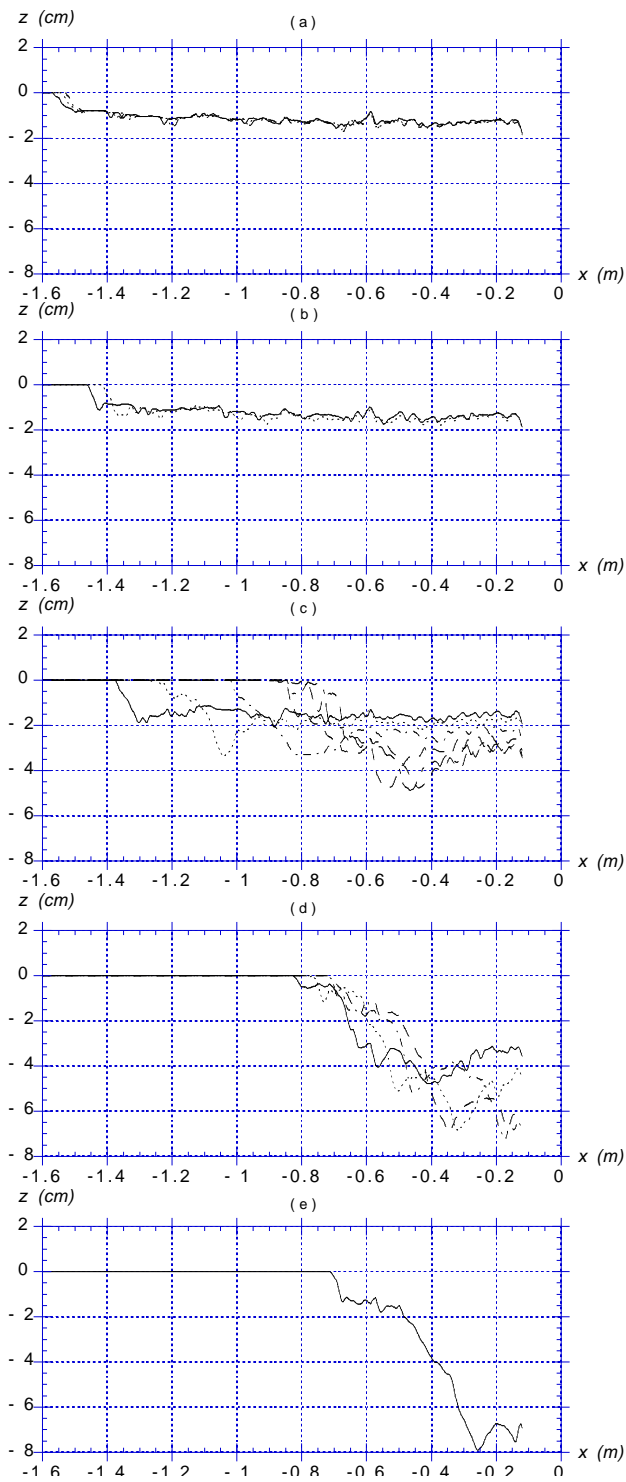


Figure 3.26: UNH August 1999 experiments 2, with Sundex oil and  $d = 0.064$  m. (a) to (d) : Every 10 recorded slick profiles for 5 flow speeds a-e shown in Fig.3.25a.

used with  $\rho_w = 1,000 \text{ kg/m}^3$  and Sundex oil was used in the slick, with  $\rho_o = 960 \text{ kg/m}^3$  (hence,  $\varphi = 0.96$ ) and  $\nu_o = 0.018 \text{ m}^2/\text{s}$ . Flow speed was set to  $U = 0.07 \text{ m/s}$  while deploying the oil, then increased to  $0.09 \text{ m/s}$  ( $0.18 \text{ kn}$ ; e.g., Fig. 3.23a). Flow speed was then increased by  $0.02 \text{ m/s}$  steps.

In these experiments, UNH carried out the data analysis of the digitized pictures and provided URI, in August 1999, with 220 and 181 slick profiles  $\eta(x)$  recorded for experiments 1 and 2, respectively (1678 and 1676 values for each profile, respectively). UNH's data processing procedure was essentially similar to that developed by URI, as explained above, for UNH's earlier experimental results, which were provided as digitized images.

Fig. 3.23a shows flow speed  $U$  as a function of time for experiment 1, and Fig. 3.25a shows the same for experiment 2. Fig. 3.23b shows the linear volume  $V_o$  calculated as a function of time for experiment 1, by integrating the measured slick profiles. Fig. 3.25b shows the same results for experiment 2. The calculated linear volumes are slightly smaller, by about 8%, than the theoretical value  $0.0179 \text{ m}^3/\text{m}$ , during the first 1,000 and 500 sec of each experiments, respectively. This is consistent with earlier UNH's experiments where we observed a reduction of linear volume, due to sidewall effects and to some oil leaking into the horsehair. During this phase, slick shape only varies slowly and mostly in the headwave region (Figs. 3.24a and b for  $x < -0.8 \text{ m}$ , and 3.26a and b for  $x < -1 \text{ m}$ ). More significant variations in linear volume can be seen later in the experiments, indicating that some cross-flume three-dimensional effects occur. During this phase, the two-dimensional slick profiles show an intensified dynamics (Figs. 3.24c and d and 3.26c to e).

Figs. 3.24 and 3.26 show sets of recorded profiles, 10 frames apart for each of 4 or 5 flow speed values, set in the experiments (Figs. 3.23a and 3.25a). The last figures in each series correspond to containment failure, with some loss of oil below the boom. Failure occurs slightly later for the larger draft.

Finally, Fig. 3.27 shows a comparison of slick length  $L$  measured in experiment 2 (from leading edge to horsehair), as a function of flow speed  $U$ , with results of UNH May 1997 experiments for the same boom draft (Fig. 3.4). Exponential curve fits are shown, to both the raw results and the same results linearly scaled for  $V_o = 0.0253 \text{ m}^3/\text{m}$  (the reference linear volume for the earlier experiments). The agreement between the scaled curve fit and the May 1997 results is quite good, confirming the good reproducibility of experimental results in the new UNH flume.

### 3.5 Conclusions

The following conclusions can be drawn from the analysis of results of experiments conducted at the University of New Hampshire, in coordination with URI studies :

- May 1997 experiments provided 6 values of slick length  $L$  as a function of flow speed  $U$  (Fig. 3.4) for a vertical straight boom/barrier of draft  $D = 0.064$

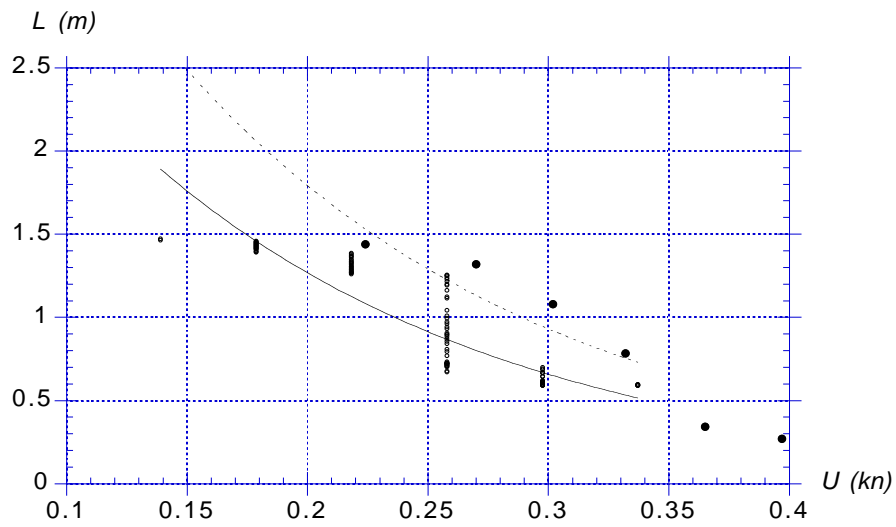


Figure 3.27: UNH August 1999 experiments 2, with Sundex oil and  $d = 0.064$  m. (o) Measured slick length  $L$  as a function of flow speed and (—) exponential curve fit to the data. (- - -) Exponential curve fit to the same data linearly scaled to a linear volume  $V_o = 0.0253$  m<sup>3</sup>/m. (●) UNH May 1997 experiments.

m. These results are used together with OHMSETT's experimental results, for estimating boom draft effect on slick length (Chapter 2).

- July 1997 experiments confirmed slick length values and profiles measured in May 1997 experiments and provided detailed water-oil interface shapes for three flow velocities (Fig. 3.8). Standard deviation or coefficient of variation for time series of interface shapes (Fig. 3.9) can be used as measures of small scale geometric fluctuations in the interface, which are indicative of the occurrence of small scale Kelvin-Helmholtz waves, known to be a precursor to larger scale containment failure.
- Using SlickMap Stage 2 model, the July 1997 measurements were used to calculate friction coefficient variations  $C_f(\xi)$  along the interface for the three specified flow velocities (Fig. 3.13). These results were helpful to derive functional expressions of friction in SlickMap Stage 2 and 3 models.
- Higher-resolution August 1997 experiments confirmed the earlier results for slick water-oil interface shape, for the lower flow velocity (Fig. 3.15). August 1997 results for the higher-velocity showed a very active dynamics in the water-oil interface when the flow velocity is close to the critical speed leading to containment failure (Fig. 3.22). These results indicate the need for a dynamic model of containment failure in which interfacial (Kelvin-Helmholtz) waves are taken into account.

The August 1999 experiments conducted in the new UNH flume using a more accurate recording system, essentially confirmed the earlier results, showing fluctuations only in the headwave region, for low flow speeds, then a very active slick dynamics and gradual shortening for intermediate speeds, with the build-up and propagation of interfacial waves. For critical speeds, the slick does not shorten further but thickens, as the headwave propagates downstream, until oil is lost under the boom.

- The detailed measurements of water-oil interface shapes made in UNH experiments clearly show the increasing occurrence of small scale geometric features, particularly in the headwave region, as flow velocity is increased. These features have been identified in earlier Phases of this study (see Phase I and II reports) as Kelvin-Helmholtz shear instability waves. Such waves increase interfacial friction, leading to slick shortening and, eventually, to the unstable slick shortening at constant flow speed referred to as *critical accumulation* (e.g., Figs. 3.16 to 3.21). This is consistent with observations made by Delvigne [9].

As much as Kelvin-Helmholtz waves are key to the understanding and modeling of containment failure, UNH experimental results also show that these waves occur at a scale much smaller than the global oscillations defining the water-oil interface shape (e.g., fitted or smoothed profiles in Figs. 3.8, 3.15 or 3.22).

Hence, such small waves can likely not be accurately and individually resolved in a realistic numerical model of containment failure, but their effect, particularly on interfacial friction must be included in the model, in a way that is flow velocity dependent. This is the modeling approach followed in SlickMap Stage 3 model (Chapter 4).

# Chapter 4

## Theoretical developments for SlickMap Model

### 4.1 Static Initialization : Stage 1 Model

The purpose of the *Stage 1 model* is to estimate an *approximate initial slick shape*, on which actual computations will be performed using the Stage 2 and 3 models. This is done using static equilibrium and energy conservation equations, assuming a pseudo-hydrostatic force balance within the slick (Section 4.1.3). A global head loss coefficient  $C_h$  is introduced to model energy dissipation along the water-oil interface (Section 4.1.2). This coefficient is estimated from the shear stress average work along the interface (Section 4.1.5). The slick is assumed to take a realistic, albeit, theoretical shape, including a headwave, and to act as a solid wall, as far as the underlying water flow (Fig. 4.1; Section 4.1.1).

For each slick case, in addition to the boom geometry and water depth, a series of physical parameters is initially specified :

- $V_o$  : linear volume of oil per unit width of boom ( $\text{m}^3/\text{m}$ ) (i.e., linear volume) [Note, SlickMap has a tool transforming total slick volume  $v_o$  ( $\text{m}^3$ ) contained by a catenary shape boom into the linear volume.];
- $U$  : free water flow velocity (i.e., relative current speed;  $\text{m}/\text{s}$ );
- $\rho_w$  : specific mass of water ( $\text{kg}/\text{m}^3$ );
- $\rho_o$  : specific mass of oil ( $\text{kg}/\text{m}^3$ ), or density ratio  $\varphi = \rho_o/\rho_w$ ;
- $Y$  : approximate fraction of slick length initially covered by the headwave (typically one-third);

The following parameters are estimated by Stage 1 model :

- $L$  : oil slick length ( $\text{m}$ );

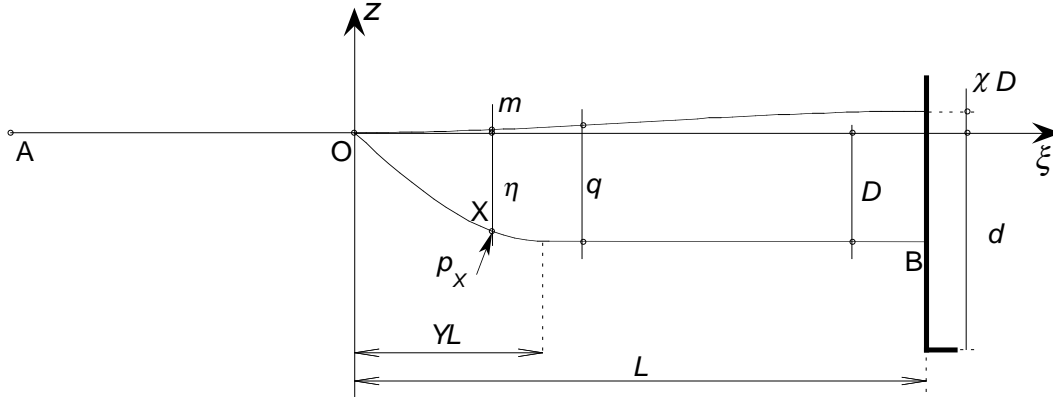


Figure 4.1: Sketch of slick shape and parameters for the Stage 1 model, with indication of the important parameters.

- $D$  : oil slick depth at boom skirt ( $\xi = L$ ) (m);
- $C_h$  : friction head loss coefficient;
- $\chi$  : fraction of  $D$  representing the oil slick height above MWL at the boom;
- $C'_{fm}$  : average friction coefficient for water-oil interface;

Before accessing the Stage 1 model, SlickMap goes through a pre-design tool in which the user is asked :

- either to provide the average friction coefficient on the oil/water interface as input;
- or to specify the slick length, from which average friction can be calculated. In both cases, when available, an existing data base of experimental results (UNH, OHMSETT; see Chapters 2 and 3) can also be used to supply values of  $C'_{fm}$  or  $L$ , as a function of specified physical parameters. In this case, no additional information has to be provided by the user.
- In case the boom has a catenary shape, the user can provide the volume of oil  $v_o$  and SlickMap pre-design tools calculates the equivalent  $V_o$ .

#### 4.1.1 Slick geometry and oil volume conservation

In Stage 1, the air-oil interface geometry,  $m(\xi)$ , is assumed to take a third-order shape above the mean water level (MWL), as a function of,  $\xi = x - x_h$  (with  $x_h$ , the abscissa of the slick leading edge O), with a zero slope at both extremities, for  $\xi = 0$  and  $L$  (Fig. 4.1). Thus,

$$m(0) = \frac{dm}{d\xi}(0) = \frac{dm}{d\xi}(L) = 0 \quad \text{and} \quad m(L) = \chi D$$

and we find,

$$m(\xi) = \chi D \frac{\xi^2}{L^2} \left( 3 - \frac{2\xi}{L} \right) \quad (4.1)$$

Following Zalosh (1974), we assume that the shape of the water-oil interface of the slick (i.e., underwater oil thickness measured from MWL),  $\eta(\xi)$ , is made of a headwave region with sinusoidal thickness variation, for  $\xi \leq \xi_o = YL$ , and a back region with constant thickness  $D$ , for  $\xi > \xi_o$ , i.e.,

$$\begin{aligned} \eta(\xi) &= D \sin \left( \frac{\pi \xi}{2\xi_o} \right) & ; \xi \leq \xi_o \\ \eta(\xi) &= D & ; \xi > \xi_o \end{aligned} \quad (4.2)$$

In all cases, the oil volume per unit width of boom,  $V_o$ , is specified and, hence, one must impose in the model that this volume is conserved. For the static slick geometry thus defined, oil volume conservation can be expressed as,

$$\begin{aligned} V_o &= \int_0^{YL} \eta(\xi) d\xi + DL(1 - Y) + \int_0^L m(\xi) d\xi \\ &= DL \left\{ Y \left( \frac{2}{\pi} - 1 \right) + 1 + \frac{\chi}{2} \right\} \end{aligned}$$

or,

$$V_o = DL \left\{ \varepsilon_1 + \frac{\chi}{2} \right\} \quad (4.3)$$

with the specified coefficient,

$$\varepsilon_1 = Y \left( \frac{2}{\pi} - 1 \right) + 1 \quad (4.4)$$

### 4.1.2 Energy conservation

Energy conservation for the water flow around the slick—considered as a solid body—can be expressed in the form of a Bernoulli equation. Assuming the flow is uniform to  $|\mathbf{u}_A| = U$ , far upstream of the slick leading edge, e.g. at A (Fig. 4.1), we have, for any point X along the slick water-oil interface,

$$p_A + \frac{1}{2} \rho_w U^2 + \rho_w g z_A = p_X + \frac{1}{2} \rho_w |\mathbf{u}_X|^2 - \rho_w g \eta + \Delta p_X \quad (4.5)$$

in which  $p_A = 0$  is the atmospheric pressure,  $\eta = -z$ , and  $p_X$  and  $\Delta p_X$ , are the total pressure and pressure (head) loss at X, respectively.

The last term in Eq. (4.5) represents a pressure drop due to frictional loss of energy along the slick interface in between O and X. Assuming, as a first approximation, that there is no loss between A and O, the slick leading edge, and that all of the

loss gradually occurs within the headwave region, for  $\xi < \xi_o$ , proportionally to oil underwater thickness, we further have,

$$\Delta p_X = \Delta p \frac{\eta}{D} \quad (4.6)$$

in which  $\Delta p$  is the total head loss occurring along the slick interface, between O and B, defined as,

$$\Delta p = \frac{1}{2} \rho_w C_h U^2 \quad (4.7)$$

with  $C_h$ , a nondimensional head loss coefficient. Combining Eqs. (4.5) to (4.7), we get,

$$p_X = \rho_w g \eta + \frac{1}{2} \rho_w U^2 \left\{ 1 - \frac{|\mathbf{u}_X|^2}{U^2} - \eta \frac{C_h}{D} \right\} \quad (4.8)$$

We also have, by definition of a pressure,

$$p_X = p_H + p_D \quad \text{and,} \quad p_H = \rho_w g \eta \quad (4.9)$$

with  $p_H$  and  $p_D$  the hydrostatic and hydrodynamic pressures at X, respectively. Hence, from Eqs. (4.8) and (4.9), we finally have,

$$p_D = \frac{1}{2} \rho_w U^2 \left\{ 1 - \frac{|\mathbf{u}_X|^2}{U^2} - \eta \frac{C_h}{D} \right\} \quad (4.10)$$

Physically, Eq. (4.8) indicates that the pressure continuously increases from 0 at the slick leading edge to,

$$p_B = \rho_w g D + \frac{1}{2} \rho_w U^2 \{1 - C_h\} \quad (4.11)$$

at the boom skirt, where there is a flow stagnation point and  $|\mathbf{u}_B| = 0$ , where the pressure is composed of the hydrostatic part, augmented by the drop in kinetic energy of the flow, mitigated by the frictional energy loss. Note, in the following, for clarity we will sometimes use the effective flow coefficient  $S_h$  defined as,

$$S_h = 1 - C_h \quad (4.12)$$

### 4.1.3 Vertical and horizontal equilibrium equations

As in Milgram and Van Houten (1978), we assume that the oil slick is in pseudo-hydrostatic equilibrium on top of the underlying water flow. Thus, horizontal and vertical equilibrium equations are derived for the oil slick, by considering a free-body diagram such as in Fig. 4.2.

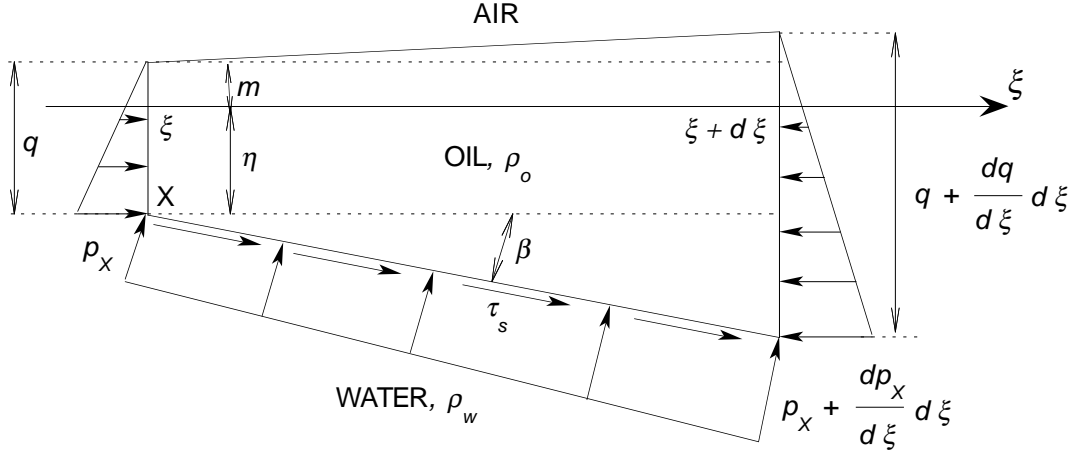


Figure 4.2: Free-body diagram for pseudo-hydrostatic equilibrium in oil slick

We find, at any point X of the water-oil interface, for the vertical (pressure) equilibrium equation,

$$p_X = \rho_o g q - \frac{\sigma_{wo}}{R} \quad (4.13)$$

where  $\sigma_{wo}$  denotes the interfacial tension for water-oil interface and  $1/R = \partial\beta/\partial s = \beta_s$  is the curvature of the interface. [Note, interfacial tension is assumed to be zero at Stage 1, due to the smooth interface.]

Combining Eqs. (4.9) and (4.13), we find,

$$p_D = \rho_w g (\varphi q - \eta) - \sigma_{wo} \beta_s \quad (4.14)$$

or, for  $\sigma_{wo} = 0$ ,

$$q = \frac{1}{\varphi} \left\{ \frac{p_D}{\rho_w g} + \eta \right\} \quad (4.15)$$

Applying this equation on the boom skirt at B, where the total slick thickness is defined as  $q = (1 + \chi) D$  (Fig. 4.1), and using Eqs. (4.11) and (4.12), we find,

$$\chi = \frac{1}{\varphi} \left\{ \frac{U^2}{2gD} S_h + 1 \right\} - 1 \quad (4.16)$$

or,

$$\chi = \varepsilon_3 \frac{S_h}{D} + \varepsilon_2 \quad (4.17)$$

with the specified coefficients,

$$\varepsilon_2 = \frac{1}{\varphi} - 1 \quad \text{and,} \quad \varepsilon_3 = \frac{U^2}{2g\varphi} \quad (4.18)$$

[Note,  $\varepsilon_3$  has the dimension of a length.]

For the horizontal (shear) equilibrium equation, we find, neglecting interfacial tension's horizontal projection,

$$\frac{1}{2} \rho_o g q^2 - \frac{1}{2} \rho_o g \left( q + \frac{dq}{d\xi} \right)^2 + \tau_s \cos \beta d\xi + \frac{1}{2} \left( 2p_X + \frac{dp_X}{d\xi} \right) \sin \beta d\xi = 0$$

where  $\tau_s$  denotes the frictional shear stress along the interface. Neglecting second-order terms with respect to first-order contributions, and using,

$$\frac{d\eta}{d\xi} = -\tan \beta \quad (4.19)$$

we finally get, for  $\beta \ll 1$ ,

$$\tau_s + p_X \frac{d\eta}{d\xi} = \rho_o g q \frac{dq}{d\xi} \quad (4.20)$$

Shear stress along the water-oil interface appears as a result of interfacial friction, which is essentially driven by the water flow —since we assumed there is no flow within the slick—. Hence, shear stress in Eq. (4.20) can classically be defined as,

$$\tau_s = \frac{1}{2} \rho_w C_f u_s^2 \quad (4.21)$$

in which  $u_s = (\mathbf{u}_X \cdot \mathbf{s})$  is the flow velocity along the interface in the tangential direction  $\mathbf{s}$ ,  $C_f$  is the interfacial friction coefficient, which varies along the interface as a function of small scale interfacial geometric features (e.g., KH waves) and of small scale features of the water flow induced by those (e.g., eddies, ...). Since the slick is assumed for Stage 1 model to behave as a solid wall, there is no normal velocity along the interface and, simply,  $u_s = |\mathbf{u}_X|$ .

An alternative definition of shear stress will also be used, by introducing the equivalent friction coefficient,

$$C'_f = \frac{u_s^2}{U^2} C_f \quad (4.22)$$

Combining Eqs. (4.21) and (4.22), we have,

$$\tau_s = \frac{1}{2} \rho_w C'_f U^2 \quad (4.23)$$

which is now defined as a function of the free flow velocity  $U$ .

Combining Eqs. (4.13), (4.20), (4.18) and (4.22), we find,

$$C'_f = \frac{1}{\varepsilon_3} q \left\{ \frac{dq}{d\xi} - \frac{d\eta}{d\xi} \right\} \quad (4.24)$$

or, with the geometric definitions in Fig. 4.1,

$$C'_f = \frac{1}{\varepsilon_3} (m + \eta) \frac{dm}{d\xi} \quad \text{with} \quad q = m + \eta \quad (4.25)$$

For Stage 1 model, the right-hand-side of Eq. (4.25) is defined from both the input parameters and the assumed slick geometry. It should be noted that, when  $\xi > \xi_o$  and  $\eta = D$  i.e.  $q = D + m$ , we have  $dm/d\xi = dq/d\xi$ ; this will lead to some simplifications in the expression for the average friction coefficient derived below.

#### 4.1.4 Average friction coefficient

In the Stage 1 model, the slick geometry is defined by Eqs. (4.1) and (4.2). Hence, Eq. (4.25) can be applied to express the variation of the equivalent friction coefficient  $C'_f$ . To also express the variation of friction coefficient  $C_f$ , using Eq. (4.22), simple hypotheses for the variation of the tangential velocity  $u_s$  are introduced, as,

$$\begin{aligned} u_s &= \frac{U}{\cos \beta} & \text{for } \xi \leq \xi_o \\ u_s &= U & \text{for } \xi > \xi_o \end{aligned} \quad (4.26)$$

Finally, equations can be averaged over the slick length to provide the values of average friction coefficients  $C'_{fm}$  and  $C_{fm}$ . The latter being a user or experimentally supplied parameter in the problem.

Combining Eqs. (4.1) and (4.25), we find,

$$C'_f = \frac{6D}{\varepsilon_3 L^2} \chi \left\{ \eta(\xi) + \frac{\chi D}{L^2} \xi^2 \left( 3 - \frac{2\xi}{L} \right) \right\} \xi \left( 1 - \frac{\xi}{L} \right) \quad (4.27)$$

with  $\eta(\xi)$  given by Eq. (4.2). Using the velocity definition (4.26), we see that  $C'_f = C_f$  for  $\xi > \xi_o$ . Hence, average friction coefficients can be calculated as,

$$\begin{aligned} (C'_{fm}, C_{fm}) &= \frac{1}{L} \int_0^{YL} C'_f(\xi) (1, \cos^2 \beta) d\xi + \frac{1}{L} \int_{YL}^L C'_f(\xi) d\xi \\ &= (I_{11}, I_{12}) + I_2 \end{aligned} \quad (4.28)$$

Integrating Eq. (4.27) for  $\eta(\xi) = D$ , we find,

$$I_2 = \frac{D^2}{L \varepsilon_3} \chi \left\{ (1 - 3Y^2 + 2Y^3) + \frac{\chi}{2} (1 - (9 - 12Y - 4Y^2)Y^4) \right\} \quad (4.29)$$

and we also have, formally,

$$(I_{11}, I_{22}) = \frac{D^2}{L \varepsilon_3} \chi \left\{ \frac{24}{\pi^2} Y^2 f_{1,2} + \chi 6 Y^4 g_{1,2} \right\} \quad (4.30)$$

with, for  $C'_{fm}$ ,

$$\begin{aligned} f_1 &= 1 - 2 \left( 1 - \frac{2}{\pi} \right) Y \\ g_1 &= \frac{3}{4} - Y + \frac{1}{3} Y^2 \end{aligned} \quad (4.31)$$

both known from the input data. For  $C_{fm}$ , using Eq. (4.2), we first define,

$$\cos^2 \beta = \{1 + \varepsilon_4^2 \cos^2(\varepsilon_4 (\xi/D))\}^{-1} \quad \text{with} \quad \varepsilon_4 = \frac{\pi}{2Y} \frac{D}{L} \quad (4.32)$$

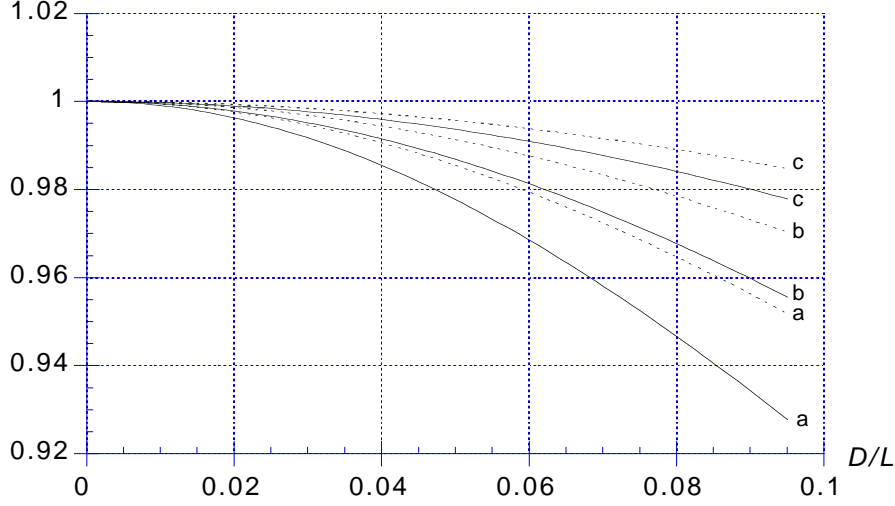


Figure 4.3: Functions  $f_2/f_1$  (—) and  $g_2/g_1$  (- - -) from Eq. (4.35), as a function of  $Y = a: 1/4$ ,  $b: 1/3$ ,  $c: 1/2$ , and  $D/L$ .

and, from Eqs. (4.27), (4.28) and (4.32), we define,

$$\begin{aligned}
 f_2 &= \int_0^{\pi/2} \frac{u(1 - \frac{2Y}{\pi}u) \sin u}{1 + \varepsilon_4^2 \cos^2 u} du \\
 g_2 &= \frac{16}{\pi^4} \int_0^{\pi/2} \frac{u^3(3 - \frac{10Y}{\pi}u + \frac{8Y^2}{\pi^2}u^2)}{1 + \varepsilon_4^2 \cos^2 u} du
 \end{aligned} \tag{4.33}$$

with  $u = \pi\xi/(2YL)$ . Integrals in Eq. (4.33) cannot be expressed in closed form and must be numerically calculated as a function of input parameter  $Y$  and variable  $D/L$  (with  $\varepsilon_4(Y, D/L)$  given by Eq. (4.32)). For  $Y = 1/3$ , for instance, Eq. (4.31) gives  $f_1 = 0.7577$  and  $g_1 = 0.4537$  whereas, for  $D/L = 0.05$ , Eq. (4.33) gives  $f_2 = 0.7478$  and  $g_2 = 0.4498$ , which are close but not quite equal to  $f_1$  and  $g_1$ . Furthermore, we easily verify that to the limit for  $D/L \rightarrow 0$ ,  $f_2$  and  $g_2$  tend to  $f_1$  and  $g_1$ , respectively. Figure 4.3 gives the variation of  $f_2/f_1$  and  $g_2/g_1$  as a function of  $Y$  and  $D/L$  values.

Finally, combining Eqs. (4.28) to (4.33), we find for the average friction coefficients,

$$(C'_{fm}, C_{fm}) = \frac{D^2}{L \varepsilon_3} \chi \{F_{1,2} + \chi G_{1,2}\} \tag{4.34}$$

with,

$$\begin{aligned}
 F_{1,2} &= 1 + Y^2 \left( \frac{24}{\pi^2} f_{1,2} - 3 \right) + 2Y^3 \\
 G_{1,2} &= \frac{1}{2} + Y^4 \left( 6g_{1,2} - \frac{9}{2} \right) + 2Y^5(3 - Y)
 \end{aligned} \tag{4.35}$$

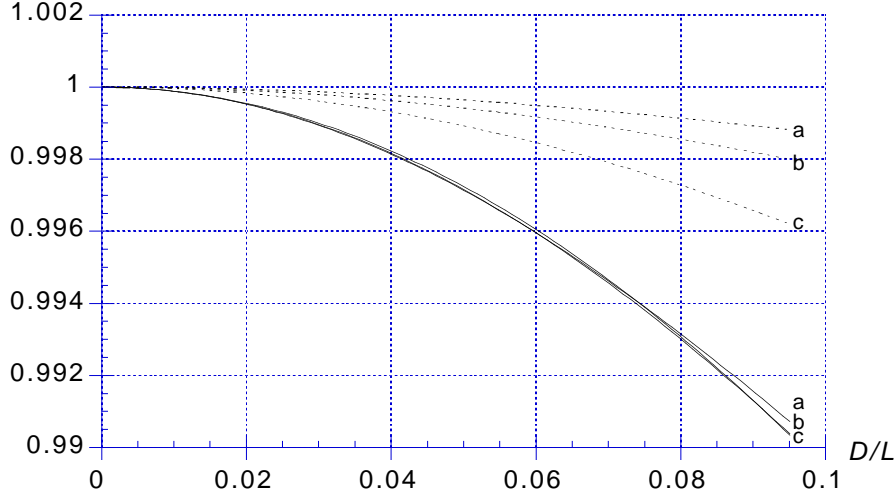


Figure 4.4: Functions  $F_2/F_1$  (—) and  $G_2/G_1$  (- - - -) from Eqs. (4.31) and (4.33), as a function of  $Y = a: 1/4$ ,  $b: 1/3$ ,  $c: 1/2$ , and  $D/L$ .

For  $Y = 1/3$ , for instance, Eq. (4.35) gives  $F_1 = 0.9455$  and  $G_1 = 0.5000$  whereas, for  $D/L = 0.05$ , Eq. (4.33) gives  $F_2 = 0.9428$  and  $G_2 = 0.4997$ , which are close but not quite equal to  $F_1$  and  $G_1$ . Figure 4.4 gives the variations of  $F_2/F_1$  and  $G_2/G_1$  as a function of  $Y$  and  $D/L$  values.

#### 4.1.5 Equivalence of mechanical work

Head loss coefficients  $C_h$  or  $S_h$  are estimated in the Stage 1 model by expressing that the work of the shear stress along the water-oil interface, denoted as boundary  $\Gamma_{sl}$  (between O and B on Fig. 4.1), is equivalent to the work of the pressure (head) energy loss  $\Delta p_X$ , defined by Eqs. (4.6) and (4.7), along the interface.

First, the power dissipated by  $\tau_s$  for the flow occurring in the tangential direction to the interface is expressed as,

$$\mathcal{P}_\tau = \int_{\Gamma_{sl}} \tau_s u_s ds \quad (4.36)$$

or, with the definition (4.23),

$$\mathcal{P}_\tau = \frac{1}{2} \rho_w U^2 \int_{\Gamma_{sl}} C'_f u_s ds = \frac{1}{2} \rho_w U^3 L \tilde{C}'_f \quad (4.37)$$

with the definition,

$$\tilde{C}'_f = \frac{1}{UL} \int_{\Gamma_{sl}} C'_f u_s ds \quad (4.38)$$

The travel time of a water particle along the interface boundary  $\Gamma_{sl}$  can be estimated as,

$$T_t = \int_{\Gamma_{sl}} \frac{ds}{u_s} \simeq \frac{L}{U} \quad \text{for } t = 0 \quad (4.39)$$

Hence, with Eqs. (4.37) and (4.39), the work of the shear stress between O and B can be estimated as,

$$\mathcal{W}_\tau = T_t \mathcal{P}_\tau \simeq \frac{1}{2} \rho_w U^2 L^2 \tilde{C}'_f \quad (4.40)$$

Now,  $\Delta p$  represents a total energy loss per unit volume of fluid at the boom skirt. This pressure drop, however, occurs progressively along the slick and produces a work acting against the flow velocity  $u_s$ , whose power can be expressed as,

$$\mathcal{P}_p = \int_{\Gamma_{sl}} \Delta p_X u_s ds = \frac{1}{2} \rho_w \frac{U^3 L}{D} C_h \tilde{\eta} \quad (4.41)$$

with  $\Delta p_X$  given by Eqs. (4.6), (4.7), and the definition,

$$\tilde{\eta} = \frac{1}{UL} \int_{\Gamma_{sl}} \eta u_s ds \quad (4.42)$$

Similarly, the work of  $\Delta p_X$  is,

$$\mathcal{W}_p = T_t \mathcal{P}_p \simeq \frac{1}{2} \rho_w U^2 L^2 C_h \frac{\tilde{\eta}}{D} \quad (4.43)$$

Hence, using the definition of the slick geometry Eq. (4.2), and the hypothesis made for the velocity variation in the slick headwave, Eq. (4.26), we find, from Eq. (4.38), using Eq. (4.32) and  $d\xi = \cos\beta ds$ ,

$$\tilde{C}'_f = \frac{1}{L} \left\{ \int_0^L C'_f d\xi + \varepsilon_4^2 \int_0^{YL} C'_f \cos^2(\varepsilon_4(\xi/D)) d\xi \right\} \quad (4.44)$$

It can be shown, using Eq. (4.27), that the second integral in Eq. (4.44) can be neglected for the Stage 1 model, and we simply find  $\tilde{C}'_f = C'_{f_m} \simeq C_{f_m}$  (the latter assumption will be discussed below). For Eq. (4.42), by analogy with similar transformations made before, we have,

$$\begin{aligned} \tilde{\eta} &= \frac{D}{L} \left\{ L(1-Y) + \frac{2YL}{\pi} \int_0^{\pi/2} (1 + \varepsilon_4^2 \cos^2 u) \sin u du \right\} \\ &= D \left\{ \varepsilon_1 + \frac{1}{6Y} \left( \frac{D}{L} \right)^2 \right\} \end{aligned} \quad (4.45)$$

It is now assumed that pressure and shear stress works are equivalent or,  $\mathcal{W}_p = \mathcal{W}_\tau$  and, from Eqs. (4.39) to (4.45), we find,

$$C_h \simeq \frac{(C'_{f_m}, C_{f_m})}{\varepsilon_1 + \frac{1}{6Y} \left( \frac{D}{L} \right)^2} \quad (4.46)$$

Using Eq. (4.12), we similarly get  $S_h$ .

### 4.1.6 Solution of Stage 1 model equations

Equations developed above for the Stage 1 model, are now combined to find all the parameters of an initial static slick, assuming that  $V_o, U, \varphi, Y$  and  $C'_{fm}$  or  $C_{fm}$  are specified as input.

Thus, from the volume conservation Eq. (4.3), we have,

$$L = \frac{V_o}{D(\varepsilon_1 + \frac{\chi}{2})} \quad (4.47)$$

with definition (4.4) for  $\varepsilon_1$ . From the energy conservation and vertical equilibrium Eq. (4.17) and from the equivalent work Eq. (4.46), with definitions (4.12) and (4.18) of  $S_h, \varepsilon_2$  and  $\varepsilon_3$ , we have,

$$\begin{aligned} \chi &= \frac{\varepsilon_3}{D} S_h + \varepsilon_2 \\ S_h &= 1 - \frac{(C'_{fm}, C_{fm})}{\varepsilon_1 + \frac{1}{6Y} \left( \frac{D}{L} \right)^2} \end{aligned} \quad (4.48)$$

From the average friction Eq. (4.34), with definitions (4.31), (4.33) and (4.35), we have, using Eq. (4.47),

$$D = \left\{ \frac{\varepsilon_3 V_o (C'_{fm}, C_{fm})}{\chi (F_{1,2} + \chi G_{1,2}) (\varepsilon_1 + \frac{\chi}{2})} \right\}^{\frac{1}{3}} \quad (4.49)$$

In SlickMap, at the pre-design Stage, prior to running the Stage 1 model, two cases are possible depending on whether : (i) the average friction  $C_{fm}$  or  $C'_{fm}$ ; (ii) or the initial slick length  $L$  are specified, both for a low initial current/flow velocity. Thus, for specified values of the other input parameters,  $L$  (i) or  $(C_{fm}, C'_{fm})$  (ii),  $D$ , and  $\chi$  are found by iterating Eqs. (4.47) to (4.49) until convergence is reached. This is done using two nested iteration loops. The first loop uses  $(C_{fm}, C'_{fm})$  (i) or  $S_h$  (ii) as an iteration parameter, starting from an initial value of 0.1 or 1, respectively, in the first Eq. (4.48). The second (inner) loop uses  $D$  as the iteration parameter, starting from an initial value of  $D = \varepsilon_3$ . After convergence of the iterations is reached, the initial slick shape is expressed by Eqs. (4.1) and (4.2).

Note that, as discussed before, when  $C'_{fm}$  is used as a parameter, functions  $F_1$  and  $G_1$  take constant values for a given  $Y$ , whereas when  $C_{fm}$  is used, functions  $F_2$  and  $G_2$  also (weakly) depend on  $D/L$ , through the effect of  $\varepsilon_4$  in integrals for  $f_2$  and  $g_2$  in Eq. (4.33) (see Figs. 4.3 and 4.4). In the latter case, the iterative solution is thus made slightly more complicated.

Figure 4.5 illustrates the solution performed with the Stage 1 model, but in a slightly different manner in which friction is unknown and the slick aspect ratio  $D/L$  is specified. Variations of average friction coefficients  $C_{fm}$  and  $C'_{fm}$  are calculated

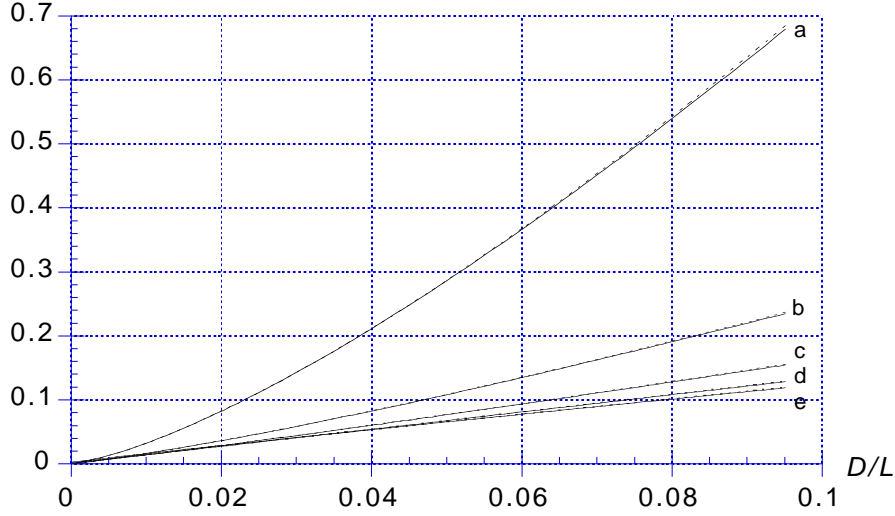


Figure 4.5: Functions  $C_{fm}$  (—) and  $C'_{fm}$  (- - - -) from Eqs. (4.47) to (4.49), as a function of  $U =$  a: 0.1, b: 0.2, c: 0.3, d: 0.4, e: 0.5 (m/s), and  $D/L$ , for  $Y = 1/3$ ,  $\varphi = 0.927$ , and  $V_o = 0.0235 \text{ m}^3/\text{m}$ .

for various values of current speed  $U = 0.1$  to  $0.5$  m/s, and  $D/L$ , assuming  $Y = 1/3$ ,  $\varphi = 0.927$ , and  $V_o = 0.0235 \text{ m}^3/\text{m}$  (which corresponds to some of the experiments described in Chapters 2 and 3). As could be expected from Figs. 4.3 and 4.4, the difference between both expressions of the average friction coefficient,  $C_{fm}$  or  $C'_{fm}$ , is minor in Stage 1 (which *a posteriori* justifies some of the approximations made earlier). Also we see that, as expected, as  $U$  decreases, for a given slick aspect ratio, the average friction coefficient increases. Figs. 4.6 and 4.7 give variations of  $L, D, \chi$  and  $S_h$  calculated for the same cases as in Fig. 4.5.

Figure 4.8 shows the solution obtained with the Stage 1 model, in the case  $C_{fm}$  is specified (in between 0.025 and 0.2 in the figures) and the slick parameters are calculated as a function of current speed  $U$ , still assuming  $Y = 1/3$ ,  $\varphi = 0.927$ , and  $V_o = 0.0235 \text{ m}^3/\text{m}$ , as in Figs. 4.5 to 4.7. Finally, Fig. 4.9 shows slick shapes  $m(\xi)$  and  $\eta(\xi)$ , calculated at Stage 1 for a few selected cases in Fig. 4.8, with  $C_{fm} = 0.1$  and  $U = 0.1$  to  $0.4$  m/s. We see in these figures that, as expected, the slick shortens and thickens as the current speed increases, while keeping the theoretical shape shown in Fig. 4.1.

Shapes and slick parameters estimated with the Stage 1 model are iteratively refined using the Stage 2 model, by using a more accurate tangential velocity variation, calculated over the slick water-oil interface by a Boundary Element Method.

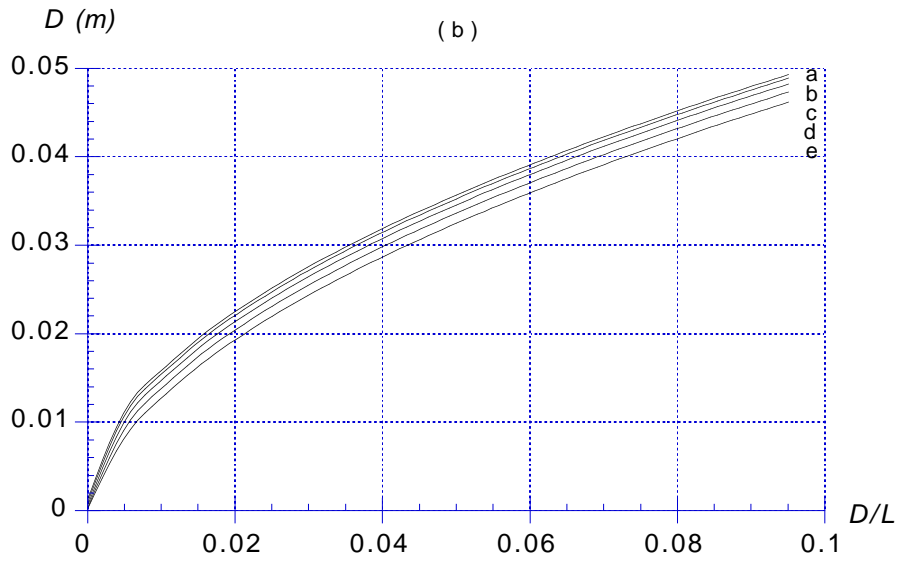
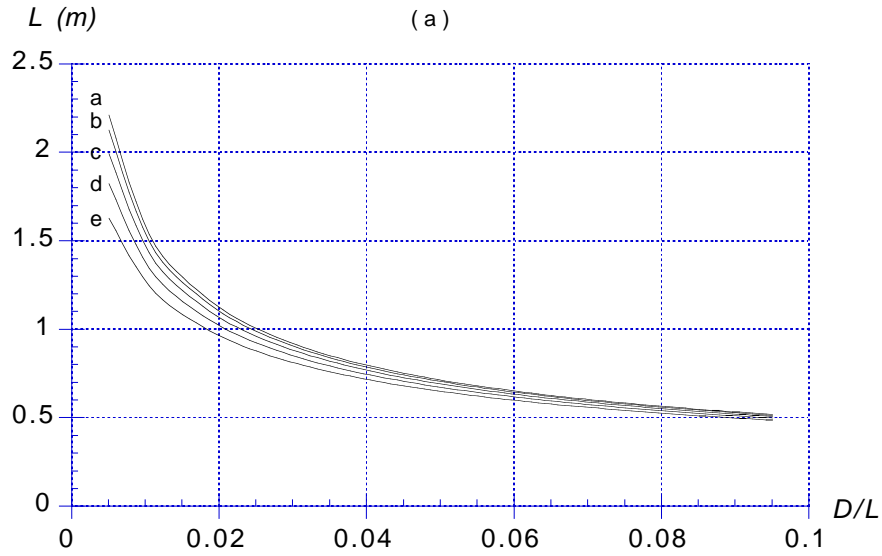


Figure 4.6: Variations of : (a)  $L$  and (b)  $D$ , calculated for the same cases as in Fig. 4.5 ( $C_{fm}$  case), as a function of  $U =$  a: 0.1, b: 0.2, c: 0.3, d: 0.4, e: 0.5 (m/s), and  $D/L$ , for  $Y = 1/3$ ,  $\varphi = 0.927$ , and  $V_o = 0.0235 \text{ m}^3/\text{m}$ .

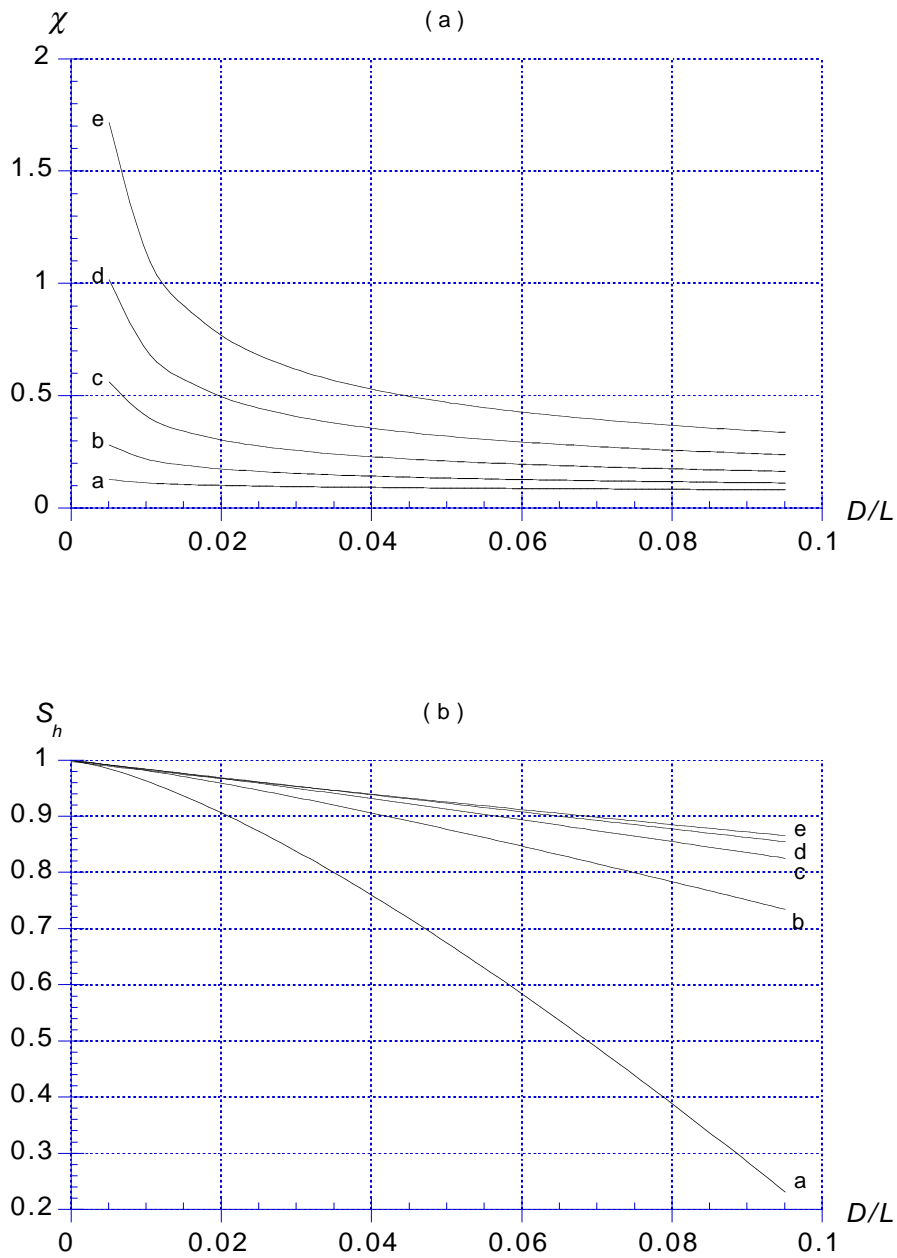


Figure 4.7: Variations of : (a)  $\chi$  and (b)  $S_h$ , calculated for the same cases as in Fig. 4.5 ( $C_{fm}$  case), as a function of  $U =$  a: 0.1, b: 0.2, c: 0.3, d: 0.4, e: 0.5 (m/s), and  $D/L$ , for  $Y = 1/3$ ,  $\varphi = 0.927$ , and  $V_o = 0.0235 \text{ m}^3/\text{m}$ .

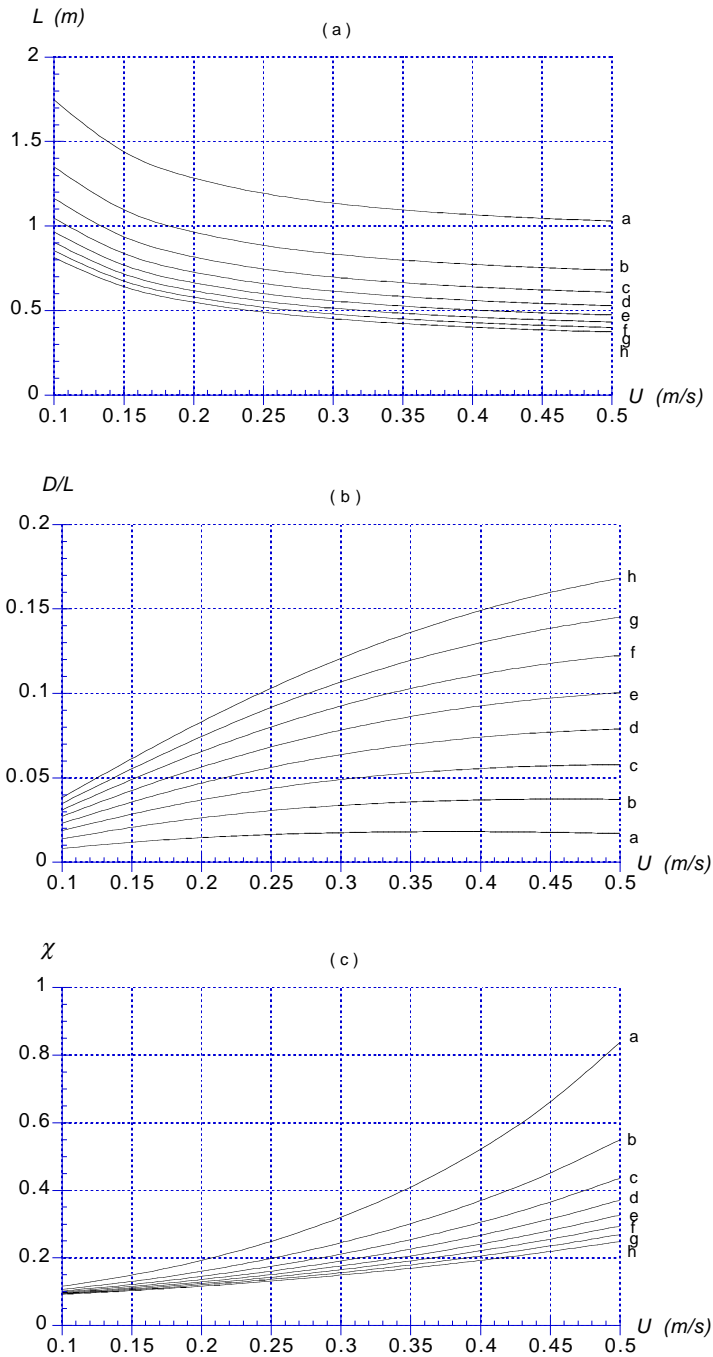


Figure 4.8: Variations of : (a)  $L$ , (b)  $D/L$ , and (c)  $\chi$  calculated as a function of  $U$  for  $C_{fm} =$  a: 0.025, b: 0.05, c: 0.075, d: 0.10, e: 0.125, f: 0.15, g: 0.175, h: 0.20, for  $Y = 1/3$ ,  $\varphi = 0.927$ , and  $V_o = 0.0235 \text{ m}^3/\text{m}$ .

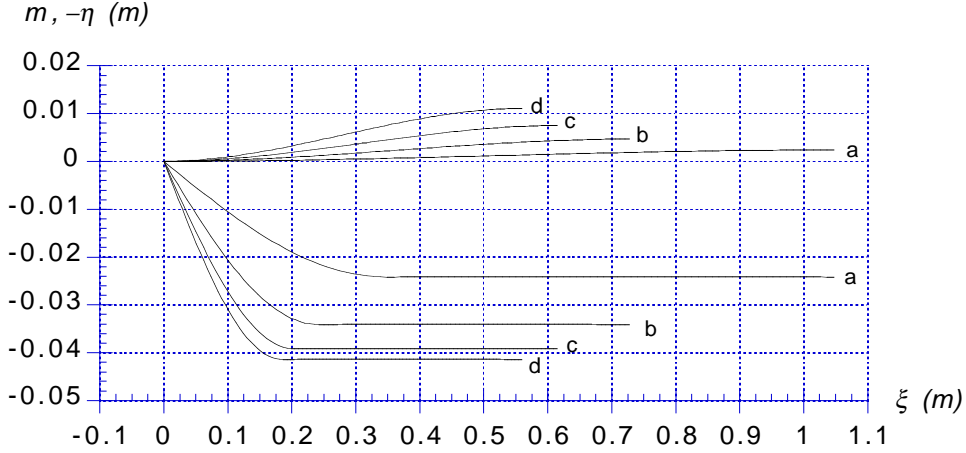


Figure 4.9: Shape of oil slick at Stage 1 for selected cases of Fig. 4.8, with  $Y = 1/3$ ,  $\varphi = 0.927$ ,  $V_o = 0.0235 \text{ m}^3/\text{m}$ ,  $C_{fm} = 0.1$  and  $U =$ : a: 0.1, b: 0.2, c: 0.3, d: 0.4 m/s.

## 4.2 Iterative Static Initialization : Stage 2 Model

In the Stage 2 model, the initial static slick shape, estimated with the Stage 1 model, is refined by calculating the external (ideal) flow in the water and iteratively refining slick shape through applying pseudo-hydrostatic equilibrium equations, including a head loss, similar to those used in Stage 1 (Section 4.2.1). The head loss coefficient is again found by applying the principle of equivalent work (Section 4.2.4).

In this static calculation, the air-water free surfaces upstream and downstream of the slick, and the slick water-oil interface, are still assumed to act as solid walls as far as the underlying water flow; hence, there is no normal flow velocity and interfaces are represented by no-flow boundary conditions. The ideal (irrotational) flow calculation is performed by a Boundary Element Method (BEM), using a discretization of the whole boundary of the water domain, made of nodes and higher-order elements to interpolate between the nodes (Section 4.2.2).

Interfacial friction, represented by the friction coefficient function (FCF)  $C_f(\xi)$ , is the key mechanism governing variations of oil slick thickness  $q(\xi)$ . In SlickMap, it is assumed that the average friction coefficient  $C_{fm}$  is specified by the user, or obtained from a data base of experiments. Assuming identical average friction values, the shape selected for the FCF will affect the formation of the slick headwave and, ultimately, slick stability and containment failure. In the Stage 2 model, a canonical equation, function of several parameters, is introduced to model the FCF and its average value is iteratively adjusted to match the user-specified average friction coefficient along the slick (Section 4.2.3).

Based on flow calculations, the two interfaces, air-oil and water-oil, of the oil slick are individually updated, node by node, such as to satisfy the equilibrium equations; their shape is then smoothed out by a high degree polynomial, to eliminate small ir-

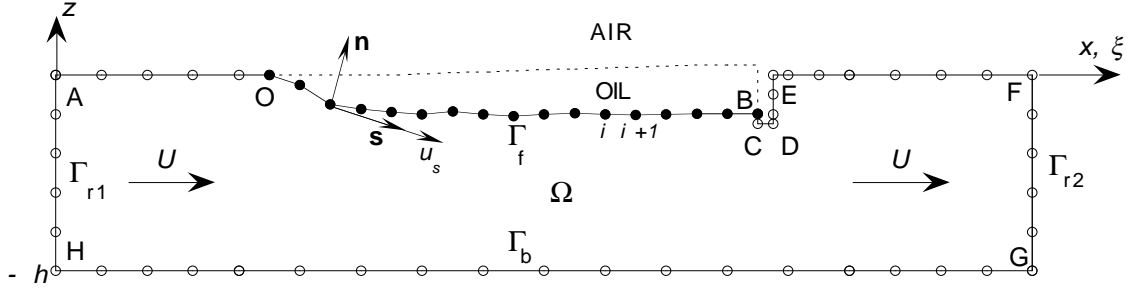


Figure 4.10: Sketch of computational domain  $\Omega$  and boundaries  $\Gamma_f$ ,  $\Gamma_{r1}$ ,  $\Gamma_{r2}$  and  $\Gamma_b$  for the external water flow computation using streamfunction theory and the BEM model. Boundaries  $\Gamma_f$  and  $\Gamma_b$  are rigid no-flow boundaries and a uniform flow  $U$  is specified on boundaries  $\Gamma_{r1}$  and  $\Gamma_{r2}$ . Discretization nodes ( $\circ$ ) and ( $\bullet$ ) are used in the BEM solution of the water flow and locations of nodes ( $\bullet$ ) on the slick water-oil interface are iteratively calculated to satisfy equilibrium equations. Nodes marked as  $i, i + 1$ , illustrate the iterative method of interfacial updating.

regularities generated during the iterative solution. After smoothing has been applied to the interfaces, the slick length is adjusted by moving the boom in order to specify oil volume conservation (Section 4.2.5).

#### 4.2.1 Pseudo-hydrostatic equilibrium equations

Equations used within the slick in the Stage 2 model are the same equations as used in the Stage 1 model, to express : (i) energy conservation including a head loss, Eq. (4.9); (ii) pseudo-hydrostatic equilibrium (vertical Eq. (4.15) and horizontal Eq. (4.25)); and (iii) mechanical work equivalence Eq. (4.41). We also note that, due to the no-flow condition at the water-oil interface, we have :  $|\mathbf{u}_X| = \mathbf{u} \cdot \mathbf{s} = u_s$  (Fig. 4.10).

In Stage 2, the following non-dimensional (primed) variables are introduced, to simplify the algebraic developments, based on a length scale  $\propto U^2/g$ , a velocity scale  $\propto U$ , and a stress scale  $\propto \rho_w U^2$ ,

$$\xi' = \frac{g\xi}{U^2} \quad ; \quad q' = \frac{gq}{U^2} \quad ; \quad \eta' = \frac{g\eta}{U^2} \quad ; \quad u'_s = \frac{u_s}{U} \quad (4.50)$$

$$p'_D = \frac{pD}{\rho_w U^2} \quad ; \quad \tau'_s = \frac{\tau_s}{\frac{1}{2}\rho_w U^2} = C'_f \quad ; \quad C'_f = C_f u'^2_s \quad (4.51)$$

Using definitions (4.50) and (4.51), Eqs. (4.9), (4.15), and (4.25) with (4.18) transform into,

$$p'_D = \frac{1}{2}(1 - u'^2_s - C'_h \eta') \quad (4.52)$$

with,

$$C'_h = C_h \frac{U^2}{gD} = \frac{C_h}{D'} \quad (4.53)$$

$$q' = \frac{1}{\varphi} \{p'_D + \eta'\} \quad \text{with,} \quad q' = m' + \eta' \quad (4.54)$$

and

$$\frac{dm'}{d\xi'} = \frac{C'_f}{2\varphi q'} \quad (4.55)$$

Combining Eqs. (4.52) to (4.55), we further have,

$$\frac{dm'}{d\xi'} = \frac{C'_f}{2(p'_D + \eta')} = \frac{C'_f}{1 - u_s'^2 + (2 - C'_h)\eta'} \equiv f_m(\xi') \quad (4.56)$$

Differentiating Eq. (4.54) with respect to  $\xi'$  and using (4.19), we also have,

$$\frac{dq'}{d\xi'} = -\frac{1}{\varphi} \left\{ \tan \beta \left(1 - \frac{C'_h}{2}\right) + u_s' \frac{du_s'}{d\xi'} \right\} \equiv f_q(\xi') \quad (4.57)$$

and, using Eqs. (4.56) and (4.57),

$$\frac{d\eta'}{d\xi'} = f_q(\xi') - f_m(\xi') \quad (4.58)$$

## 4.2.2 External flow calculation

In the slick pseudo-hydrostatic equilibrium equations presented above, the effect of the underlying water flow is transmitted through both the dynamic pressure and the shear stress at the interface. Both of these, essentially, depend on the water flow velocity at the water-oil interface  $\Gamma_f$ , represented by the tangential velocity  $u_s$ , and on the interface geometry (Fig. 4.10).

At Stage 2, the slick is assumed not to move, i.e., to be in static equilibrium for each successive iteration. Hence, the water flow is considered as an external flow past an obstacle having a geometry defined by the slick and boom. The free surface upstream of the slick and downstream the boom, together with the water/slick interface and the boom, are assumed to be rigid walls, as well as the bottom, i.e., A-F and G-H are *streamlines*. Due to the slenderness of the slick geometry, an ideal flow approximation, implying no flow separation, is made for the water flow under the slick. Note, flow separation will occur downstream of the boom but should not significantly influence the flow in the vicinity of the slick, particularly in the headwave region.

Using a streamfunction representation of the ideal flow in the water domain  $\Omega$ , continuity equation reads (Fig. 4.10),

$$\nabla^2 \psi = 0 \quad ; \text{ in } \Omega \quad (4.59)$$

where  $\psi$  is the streamfunction defined such that,

$$u = -\frac{\partial\psi}{\partial z} \quad ; \quad w = \frac{\partial\psi}{\partial x} \quad ; \quad u_s = \mathbf{u} \cdot \mathbf{s} = -\frac{\partial\psi}{\partial n} \quad (4.60)$$

where  $(u, w)$  are horizontal and vertical velocity components in the water and  $\mathbf{n}$  and  $\mathbf{s}$  denote the normal and tangential directions along the slick interface, respectively. Eq. (4.59) is solved using a Boundary Integral Equation representation (BIE),

$$\alpha(\mathbf{x}_l) \psi(\mathbf{x}_l) = \int_{\Gamma(\mathbf{x})} \left\{ \frac{\partial\psi}{\partial n} G(\mathbf{x}, \mathbf{x}_l) - \psi \frac{\partial G(\mathbf{x}, \mathbf{x}_l)}{\partial n} \right\} d\Gamma(\mathbf{x}) \quad (4.61)$$

in which,

$$G(\mathbf{x}, \mathbf{x}_l) = -\frac{1}{2\pi} \log |\mathbf{x} - \mathbf{x}_l| \quad (4.62)$$

is the free space Green's function,  $\mathbf{x} = (x, z)$  and  $\mathbf{x}_l = (x_l, z_l)$  represent position vectors for points on the boundary  $\Gamma$ , and  $\alpha(\mathbf{x}_l)$  is a geometric coefficient.

The BIE (4.61) is solved using a higher-order Boundary Element Method (BEM) (Grilli and Subramanya [22, 24]), together with boundary conditions expressing no-flow on the bottom boundary  $\Gamma_b$  and on the free surface, slick interface and boom  $\Gamma_f$ ; and uniform incoming and outgoing flows on lateral boundaries  $\Gamma_{r_1}$  and  $\Gamma_{r_2}$ . Note that the present method was developed for (and thus requires) domains with boundaries located at finite distance. Hence, a bottom and lateral boundaries are always needed to make sure  $\Gamma$  is a closed boundary. If one wishes to solve for the flow under a slick in very deep water, one just has to locate the bottom boundary far enough below the slick for this boundary not to influence the flow close to the slick interface. In practical computations, we found that, when the bottom boundary was located at least ten times deeper than the boom draft, no significant influence of the bottom boundary could be found on the tangential velocity at the slick interface. Lateral boundaries should be located far enough ahead and behind the slick for the horizontal flow velocity to be very close to  $U$ . Using SlickMap for the Stage 2 model, the user can easily define parameters for the BEM discretization, i.e., the size of the BEM domain upstream and downstream of the boom, and node and element densities on each boundary segment of the BEM domain (Fig. 4.10). Default values for the BEM parameters are first proposed that the user is then free to modify at will (see details in Chapter 5).

In a streamfunction representation, no-flow boundary conditions correspond to specifying streamlines with  $\overline{\psi} = \text{constant}$ . In the present case, we set  $\overline{\psi} = 0$  on  $\Gamma_b$  and  $\overline{\psi} = hU$  on  $\Gamma_f$  (i.e., A to F). Horizontal flow conditions are specified as  $\overline{\psi}_n = 0$  on  $\Gamma_{r_1}$  and  $\Gamma_{r_2}$ , where indices  $n$  indicate partial  $n$ -derivative. Note that the latter boundary condition does not impose  $u = U$  but only  $w = 0$  on lateral boundaries. The solution will produce  $u = U$  provided lateral boundaries are located far enough from the slick and boom. In this case, a linearly varying streamfunction should be obtained in the vertical direction, as the solution of Eq. (4.61), on  $\Gamma_{r_1}$  and  $\Gamma_{r_2}$ , i.e.,  $\psi = |z| U$ .

The solution on  $\Gamma_f$  directly provides,  $u_s = -\partial\psi/\partial n = -\psi_n$ , along the slick interface, to be used in the slick equilibrium equations. Hence, the ideal flow solution allows one to calculate the dynamic pressure and the shear stress along the slick (provided  $C_f$ 's variation is known), for any assumed slick shape.

The numerical solution of Eqs. (4.61) and (4.62), with relevant boundary conditions, is performed using a higher-order BEM method in which discretization nodes are specified on boundary  $\Gamma = \Gamma_b + \Gamma_f + \Gamma_{r1} + \Gamma_{r2}$  and quadratic isoparametric elements are used to interpolate in between discretization nodes on the lateral and bottom boundaries, and cubic elements with continuity of the slope on the various interfaces and free surfaces. Both regular and singular integrals in Eq. (4.61) are performed numerically, using Gauss quadrature methods for the regular integrals, and a similar method, well-suited to logarithmic singularities, for the singular integral. An algebraic system of equations is thus assembled and solved for the unknowns at the discretization nodes, i.e.,  $\psi$  or  $\psi_n$ , whichever is not set by boundary conditions. Details of the BEM method and numerical integrations can be found in Grilli *et al.* [22, 24, 25]. Finally, quasi-singular integrals occurring when a node, not on the boundary, is close to the boundary are handled by adaptive integration (Grilli and Subramanya [23])

Additional difficulties arise in the numerical solution of the present problem in relation to the proper representation of BIE's for corners located at the intersections between boundaries having different types of boundary conditions and normal directions (points A, F, G, and H in Fig. 4.10). To address corner problems in the BEM algorithm, double-node representations and corner compatibility equations are used (Grilli and Svendsen [25]). Within boundary  $\Gamma_f$ , there are also points with discontinuities in the tangential direction. These are the corners points B to E for the BEM boundary along the boom. To eliminate this problem at the boom corners C and D, the sharp corner is replaced by small quarter circles of radius  $b/10$ , where  $b$  denotes the boom width. For B and E, due to the two normal directions, double-nodes are also used; physically, however, the velocity must be zero and this is also specified in the numerical solution.

### 4.2.3 Friction coefficient model equation

Milgram and Van Houten (1978) [34] estimated the variation of the FCF  $C_f(\xi)$  along experimentally measured oil slicks contained by a boom, using pseudo-hydrostatic equilibrium equations similar to Eqs. (4.52) to (4.55) (with  $C_h = 0$ ; no head loss) and back-calculating the friction coefficient variation corresponding to a measured slick shape. In Phase III/1 of this project, we performed similar analyses, using detailed laboratory experiments carried out at the University of New Hampshire (see Chapter 3). Using results of new field experiments at OHMSETT (see Chapter 2), performed during Phase III, and static analyses similar to those described in Stage 1, we also estimated values of average friction coefficients for measured slick lengths at given tow speeds (see Chapter 2). In the Phase II report, we proposed preliminary theoretical

considerations related to boundary layer theory, to qualitatively define the shape of the FCF. These were further refined during Phases III/1 and 2.

From these experimental and theoretical analyses, it appears that  $C_f$  shows a sharp increase in front of the headwave, followed by a gradual decrease in the back of the headwave. Therefore, as also concluded in [34], dynamic pressure plays an important role in determining slick shape in the headwave region. As will be shown in the computational results, both  $\eta'$  and  $u'_s$  exhibit significant variations in the headwave region and, hence, so does  $p'_D$ , through Eq. (4.52).

In Stage 2 model, a semi-empirical representation of  $C_f(\xi)$  is introduced along the slick, based on a few coefficients which will be estimated based on both physics and experiments. The variation  $C_f \propto \xi^{-1/2}$  obtained from simple laminar boundary layer theory for a smooth plate (Batchelor, 1967), indicates that  $C_f$  should decrease from a large initial value, as  $\xi$  increases, and asymptotically tend to zero. One should expect, however, for a rough boundary,  $C_f$  to eventually reach a small but non-zero value, say  $C_{fo}$ , at the back of the slick. At the front of the slick, experiments show that  $C_f$  values are bounded and drop to zero at the slick leading edge. Combining these observations, the following equation is used for representing the variation of  $C_f$  along the slick,

$$C_f = C_{fo} \left\{ 1 - e^{-\mu\xi'} + \alpha \chi e^{-\beta\chi} \right\} \quad \text{with,} \quad \chi = \left( \frac{\xi'}{\xi'_p} \right)^\gamma \quad (4.63)$$

where  $\mu$ ,  $\alpha$ ,  $\beta$ , and  $\gamma$ , are nondimensional coefficients and  $C_{fo}$  and  $\xi'_p$  are partly estimated based on experiments.

The FCF modeled by Eq. (4.63) is zero for  $\xi' = 0$ , at the slick leading edge, and tends to  $C_{fo}$  for a large  $\xi' \simeq L' = Lg/U^2 \gg 1$ , at the boom skirt. We now further assume that : (i) the maximum friction is,  $C_f(\xi'_p) = \lambda C_{fo}$ , and occurs at the peak location  $\xi'_p = \delta \xi'_o$ , representing a fraction  $\delta$  of the headwave length  $\xi'_o = YL'$ ; and (ii) at the back of the headwave, for  $\xi' = \xi'_o$ , friction is down to,  $C_f(\xi'_o) = (1 - \epsilon/2) C_{fo}$ , with  $\epsilon \ll 1$ . We find, from condition (i),

$$\alpha = \frac{\mu \kappa \delta \xi'_o}{\gamma (\beta - 1) e^{-\beta}} \quad \text{with,} \quad \kappa = e^{-\mu' \delta \xi'_o} \quad (4.64)$$

and,

$$\beta = 1 + \frac{\mu \kappa \delta \xi'_o}{\gamma (\lambda - 1 + \kappa)} \quad (4.65)$$

and from condition (ii),

$$\mu = -\frac{1}{\xi'_o} \log \frac{\epsilon}{2} \quad (4.66)$$

Hence, assuming  $\epsilon$  is set to a small value, e.g., 1%, and using Eqs. (4.64) to (4.66), only three independent shape parameters must be specified to define the FCF Eq. (4.63) :  $\delta \in [0, 1]$ ,  $\lambda \geq 1$  and  $\gamma \geq 1$ , which specify the location, elevation, and peakedness, respectively, of the maximum friction within the headwave region. Figure

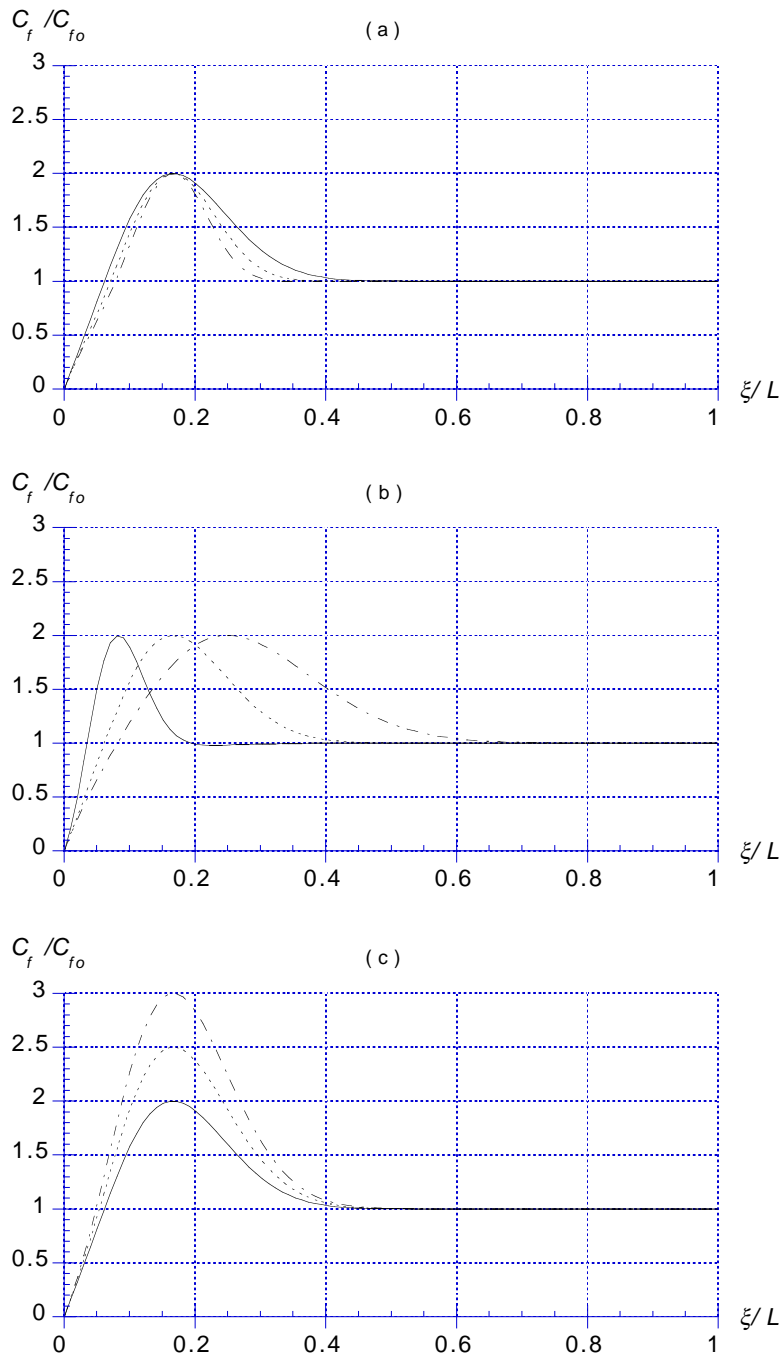


Figure 4.11: Scaled Friction Coefficient Function  $C_f/C_{f0}$  as a function of dimensionless slick abscissa  $\xi/L$ , for  $\epsilon = 0.01$ ,  $Y = 1/3$ , and : (a)  $\delta = 0.5$ ,  $\lambda = 2$ ,  $\gamma = 2$  (—), 2.5 (---), 3 (— —); (b)  $\gamma = 2$ ,  $\lambda = 2$ ,  $\delta = 0.25$  (—), 0.5 (-----), 0.75 (— —); (c)  $\gamma = 2$ ,  $\delta = 0.5$ ,  $\lambda = 2$  (—), 2.5 (-----), 3 (— —).

4.11 illustrates the sensitivity of  $C_f/C_{fo}$  to variations of  $\gamma$ ,  $\delta$ , and  $\lambda$ , for  $\epsilon = 0.01$  and  $Y=1/3$ . Clearly, both  $\gamma = 2$  in Fig. 4.11a and  $\delta = 0.5$  in Fig. 4.11b, provide a better distribution of the friction variation over the headwave region (for  $\xi/L = 0$  to  $Y = 1/3$ ); hence, these values are used in calculations with SlickMap.

The value of friction in the back of the slick,  $C_{fo}$ , is obtained from the specified average friction coefficient as,

$$C_{fo} = \frac{L'(C_{fm}, C'_{fm})}{\int_0^{L'} (1, u_s'^2) \{1 - e^{-\mu\xi'} + \alpha \chi e^{-\beta\chi}\} d\xi'} \quad (4.67)$$

Figure 4.12 shows the sensitivity of  $C_{fm}/C_{fo}$  to variations of  $\lambda$ ,  $\gamma$ , and  $Y$ , for  $\epsilon = 0.01$  and  $\delta = 0.5$ . The figure shows that  $\lambda$ , i.e., the relative peak friction value is the parameter providing the largest variation of the average friction, whereas changes in  $Y$  and  $\gamma$  produce less variation of average friction. Hence, the values  $Y = 1/3$  and  $\gamma = 2$  will be used in calculations with SlickMap, whereas both  $C_{fo}$  and (to a lesser extent)  $\lambda$ , will be made problem dependent.

#### 4.2.4 Equivalence of mechanical work

Head loss coefficients  $C_h$  or  $S_h$  are re-calculated at Stage 2 for each iterative refinement of the slick shape  $\eta(\xi)$  and underlying flow tangential velocity  $u_s(\xi)$ . As in Stage 1, this is done by expressing that the work of the shear stress along the water-oil interface, denoted as boundary  $\Gamma_{sl}$  (between O and B on Fig. 4.10), is equivalent to the work of the pressure (head) loss  $\Delta p_X$ , defined by Eqs. (4.6) and (4.7), along the interface.

Equations therefore are the same as those used in Stage 1 but integrals defining  $\tilde{C}'_f$ ,  $T'_i$ , and  $\tilde{\eta}$  have to be performed numerically, using the calculated values of  $\eta(\xi)$  and  $u_s(\xi)$ , as well as the friction function  $C_f(\xi)$  defined by Eq. (4.63). Thus, using Eqs. (4.39) to (4.43), and (4.50) to (4.53), we have, assuming that  $\mathcal{W}_p = \mathcal{W}_\tau$ ,

$$C_h = \frac{\tilde{C}'_f D'}{\tilde{\eta}'} \quad \text{or,} \quad C'_h = \frac{\tilde{C}'_f}{\tilde{\eta}'} \quad (4.68)$$

[Using Eq. (4.12), we similarly get  $S_h$ .] with,

$$\tilde{C}'_f = \frac{1}{L'} \int_{\Gamma_{sl}} C_f u_s'^3 ds' \quad (4.69)$$

and,

$$\tilde{\eta}' = \frac{1}{L'} \int_{\Gamma_{sl}} \eta' u_s' ds' \quad (4.70)$$

#### 4.2.5 Iterative updating of slick geometry

Starting from the approximate slick shape calculated in Stage 1 :  $\eta^o(\xi)$ , and  $m^o(\xi)$ , a BEM discretization is defined for the water domain, such as sketched in Fig. 4.10 and

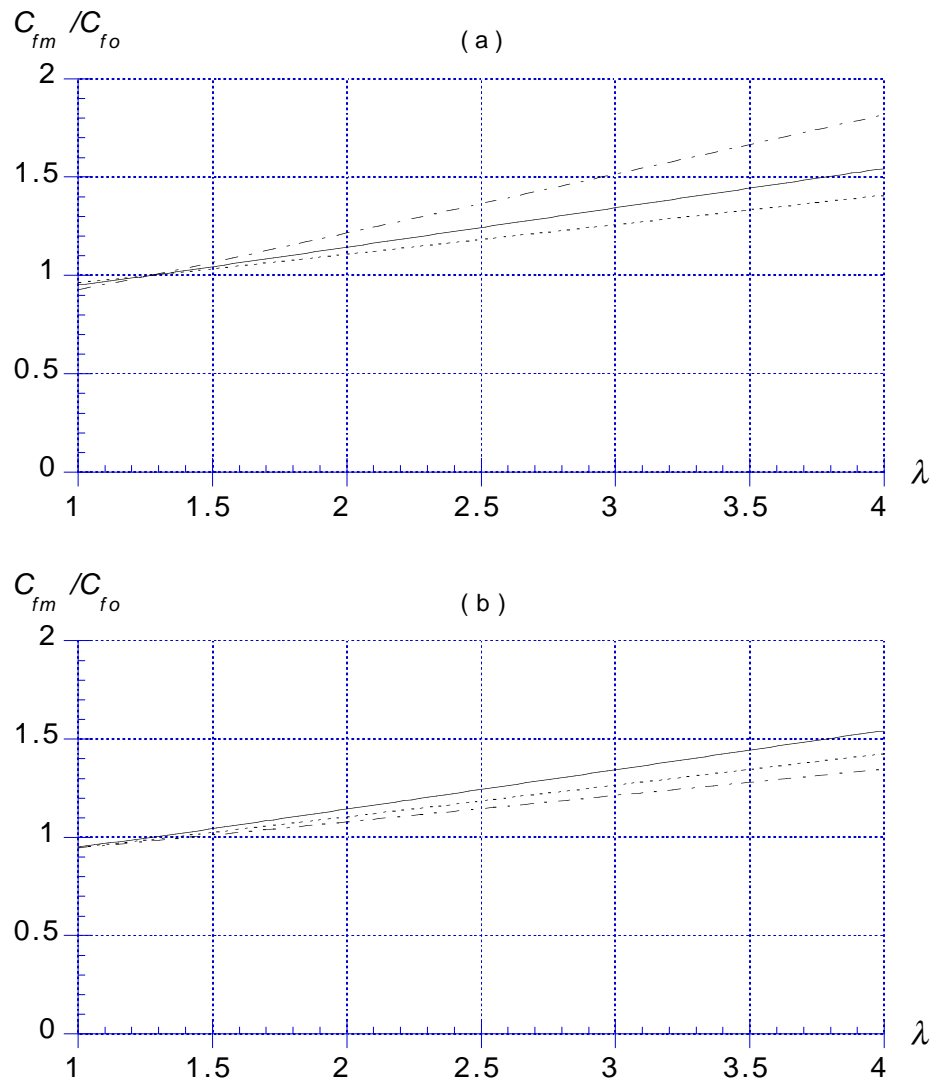


Figure 4.12: Scaled average friction coefficient  $C_{fm}/C_{fo}$  as a function of parameter  $\lambda$ , for  $\epsilon = 0.01$ ,  $\delta = 0.5$  and : (a)  $\gamma = 2$ ,  $Y = 1/4$  (· · · · ·),  $1/3$  (—),  $1/2$  (— — —); (b)  $Y = 1/3$ ,  $\gamma = 2$  (—),  $2.5$  (· · · · ·),  $3$  (— — —).

the underlying water tangential flow velocity  $u_s^o = -\psi_n$  is calculated along the water-oil interface boundary  $\Gamma_{sl}$  (O-B on the figure), which is a subsection of  $\Gamma_f$  (where the superscript o denotes the first iteration in the process).

Pseudo-hydrostatic Eqs. (4.52)-(4.58) are integrated node by node along  $\Gamma_{sl}$ , with respect to  $\xi'$ , to calculate an updated slick geometry, for the next iteration, and so on until convergence is reached within some error margin. At each iteration, the geometry is smoothed and conservation of oil volume is specified.

More specifically, referring to Eqs. (4.56) and (4.58), we define, for iteration  $k$  and for points  $i = 1, \dots, N_{sl} - 1$ ,

$$\Delta m'_{i+1}^k = \int_i^{i+1} f_m^k(\xi') \cos \beta ds' \quad (4.71)$$

$$\Delta \eta'_{i+1}^k = \int_i^{i+1} \{f_q^k(\xi') - f_m^k(\xi')\} \cos \beta ds' \quad (4.72)$$

with, in the definition of  $f_m^k$  and  $f_q^k$ , using Eqs. (4.68) to (4.70),

$$C'_h{}^k = \frac{\tilde{C}'_f{}^k}{\tilde{\eta}'^k} \quad (4.73)$$

in which  $d\xi' = \cos \beta ds'$ , with  $s'$  the nondimensional curvilinear abscissa along the water-oil interface  $\Gamma_{sl}$ , discretized by  $N_{sl}$  points. Note, these integrals are calculated by numerical integration (Gauss quadrature) within each BEM element of  $\Gamma_{sl}$ .

Based on Eq. (4.55), we define the following residual function,

$$\mathcal{R} = \frac{1}{2} C'_f - \varphi q' \frac{dm'}{d\xi'} \quad (4.74)$$

or, using Eqs. (4.19) and (4.57),

$$\mathcal{R} = \frac{1}{2} C'_f + q' \left\{ u'_s \frac{du'_s}{d\xi'} - (\varphi - 1 + \frac{1}{2} C'_h) \tan \beta \right\} \quad (4.75)$$

which tends to zero when pseudo-hydrostatic equilibrium equations are fully satisfied in the slick.

For a given iteration  $k$ , the slick updating to iteration  $(k + 1)$  is performed as follows, for  $i = 2, \dots, N_{sl} - 1$ ,

$$\begin{aligned} \tilde{m}'_{i+1} &= m_i^k + \Delta m'_{i+1}^k \\ m'^{k+1}_{i+1} &= m'^k_{i+1} + \rho (\tilde{m}'_{i+1} - m'^k_{i+1}) \end{aligned} \quad (4.76)$$

for the oil-air interface, and,

$$\begin{aligned} \tilde{\eta}'_{i+1} &= \eta_i^k + \Delta \eta'_{i+1}^k + (\xi'_{i+1} - \xi'_i) \frac{\mathcal{R}_{i+1}^k}{\varphi q'^k_{i+1}} \\ \eta'^{k+1}_{i+1} &= \eta'^k_{i+1} + \rho (\tilde{\eta}'_{i+1} - \eta'^k_{i+1}) \end{aligned} \quad (4.77)$$

for the water-oil interface. In these equations,  $\rho$  indicates a relaxation coefficient (selected to 0.35 in SlickMap), and the third term in the first Eq. (4.77) right-hand-side is a correction of residual errors at iteration  $k$ , obtained by integrating Eq. (4.56) by finite differences.

At each iteration, a residual root-mean-square error is calculated for the equilibrium equations applied along the slick interface as,

$$\text{RMS}_e = \left\{ \frac{1}{N_{sl}} \sum_{i=1}^{N_{sl}} (\mathcal{R}_i^k)^2 \right\}^{1/2} \quad (4.78)$$

Iterations are stopped when either a maximum pre-set number of those is reached or  $\text{RMS}_e$  becomes smaller than a pre-set value (e.g., 5%).

## 4.2.6 Smoothing of slick interface geometry and oil volume conservation

Polynomials of degree  $N_P$  are defined to model the slick interface geometry, as a function of  $\xi$  such as,

$$P(\xi) = \sum_{n=1}^{N_P} p_n \xi^n \quad (4.79)$$

which automatically satisfies  $P(0) = 0$ . Such polynomials are curve fitted to both  $\eta$  and  $m$  after each iteration (degrees  $N_{P_m}$  and  $N_{P_\eta}$ ). In addition, for both interfaces, the end slope at the boom skirt is specified to be zero, due to the no-flow condition, i.e.,

$$\frac{dP(\xi)}{d\xi}(L) = \sum_{n=1}^{N_P} p_n n L^{n-1} = 0 \quad (4.80)$$

Combining Eqs. (4.79) and (4.80), we get,

$$P(\xi) = \sum_{n=2}^{N_P} p_n \left\{ \xi^n - n L^{n-1} \xi \right\} \quad (4.81)$$

Applying the Least-Square-Method (LSM) to Eq. (4.81), for a set of  $N_{sl}$  points  $(\xi_i, f(\xi_i))$  on  $\Gamma_{sl}$ , we get a linear system of equations for the polynomial coefficients,  $p_n; n = 1, \dots, N_P$ ,

$$\sum_{l=1}^{N_P} A_{ln} p_l = B_n \quad (4.82)$$

with, for  $l, n = 2, \dots, N_P$ ,

$$A_{ln} = \sum_{i=1}^{N_{sl}} \left\{ \xi_i^n - n L^{n-1} \xi_i \right\} \left\{ \xi_i^l - l L^{l-1} \xi_i \right\} \quad (4.83)$$

and

$$B_n = \sum_{i=1}^{N_{sl}} f_i \left\{ \xi_i^n - n L^{n-1} \xi_i \right\} \quad (4.84)$$

where subscripts  $i$  indicate a value taken for  $\xi = \xi_i$ , and,

$$A_{1n} = N_P N_{sl} L^{n-1} \quad , \quad B(1) = 0 \quad (4.85)$$

After solving Eq. (4.82), with (4.83)-(4.85), the quality of the curve fitting is quantified by calculating,

$$R^2 = 1 - \frac{\sum_{i=1}^{N_{sl}} \{f_i - \bar{f}\}^2}{\sum_{i=1}^{N_{sl}} \{f_i - P_i\}^2} \quad (4.86)$$

where,

$$\bar{f} = \frac{1}{N_{sl}} \sum_{i=1}^{N_{sl}} f_i \quad (4.87)$$

is the average value of  $f(\xi_i)$ .

The slick volume is calculated, in between the fitted curves for  $m$  and  $\eta$ ,  $P_m$  and  $P_\eta$ , as,

$$\begin{aligned} V &= \int_0^L \{P_m(\xi) + P_\eta(\xi)\} d\xi \\ &= \sum_{l=1}^{N_{P_m}} \frac{1}{l+1} M_l L^{l+1} + \sum_{n=1}^{N_{P_\eta}} \frac{n}{n+1} E_n L^{n+1} \end{aligned} \quad (4.88)$$

where  $M_l$  ( $l = 1, \dots, N_{P_m}$ ) and  $E_n$  ( $n = 1, \dots, N_{P_\eta}$ ) denote the coefficients  $p$  found for polynomials  $P_m$  and  $P_\eta$ , respectively. A volume error  $\Delta V = V - V_o$  is thus found, and a correction applied to the back of the slick, by either extending or reducing the slick at the boom skirt by a value,

$$\Delta L = -\frac{1}{2} \frac{\Delta V}{D(1 + \chi)} \quad (4.89)$$

while maintaining the slick depth at the boom constant to  $D = \eta(L)$ . [Note, only half the error is corrected at each single iteration to ensure faster convergence.]

After the volume correction is applied, BEM nodes are regridded to equal  $\Delta\xi$  intervals on  $\Gamma_{sl}$ , and the FCF  $C_f$  is recalculated using Eq. (4.63). To asses whether the geometric shape of the oil slick is converging with the iterations, the following RMS error is calculated for  $\eta$ ,

$$\text{RMS}_\eta = \frac{1}{D} \left\{ \frac{1}{N_{sl}} \sum_{i=1}^{N_{sl}} \{P_\eta^{k+1}(\xi_i) - \eta_i^k\}^2 \right\} \quad (4.90)$$

Finally, a correction is applied to  $C_{fo}$  to achieve the specified value of the average friction  $C_{fm}$  or  $C'_{fm}$ ,

$$C_{fo}^{k+1} = C_{fo}^k \frac{(C_{fm}, C'_{fm})}{(\overline{C_f^k}, \overline{C_f^k u_s'^{2k}})} \quad (4.91)$$

where the overlines denote average values calculated over the water-oil slick interface.

## 4.2.7 Results and discussion

Results of Stage 2 model are illustrated by calculating the stable static shape of a slick with physical parameters identical to those used in the examples for Stage 1, i.e.,  $Y = 1/3$ ,  $\varphi = 0.927$ , and  $V_o = 0.0235 \text{ m}^3/\text{m}$ , for  $U = 0.1$  or  $0.3 \text{ m/s}$  assuming  $C_{fm} = 0.1$  and  $\lambda = 3$ . These actually correspond to cases a and c in Fig. 4.9. The boom draft is set to  $0.2 \text{ m}$  with width  $0.05 \text{ m}$ ; the water depth is set to  $1 \text{ m}$  (i.e., 5 boom drafts). The domain is  $4.82 \text{ m}$  long (A-F on Fig. 4.10) with  $2.41 \text{ m}$  in front of the boom.

Stage 2 model was run for 10 iterations. The BEM discretization had 61 nodes on the free surface and slick interface in front of the boom (A-B in Fig. 4.10), 15 nodes on the boom, 25 nodes on the free surface behind the boom (E-F), 9 nodes on each lateral boundary and 26 nodes on the bottom.

Values of residual errors,  $\text{RMS}_e$  (Eq. (4.78)) and  $\text{RMS}_\eta$  (Eq. (4.90)) for the last iteration were 7.9% and 0.34%, respectively. Typically, for a given BEM discretization, it is observed that the former error quickly reaches a minimum value for which the free surface shape then converges with increasing iterations  $k$ , leading to a small value for the latter error. To reduce the  $\text{RMS}_e$  error, it would be necessary to further refine the initial BEM discretization.

Fig. 4.13 gives plots of the convergence of oil slick parameters, as a function of the number of iterations  $k$ , for the two selected cases. Note, parameters without  $k$  indices represent converged values, i.e.,  $L = \text{a: } 1.055 \text{ m, c: } 0.613 \text{ m; } D = \text{a: } 0.024 \text{ m, c: } 0.040 \text{ m; } \chi = \text{a: } 0.0926, \text{ c: } 0.1460; \text{ and } S_h = \text{a: } 0.869, \text{ c: } 0.846$ . The figure shows a good rate of convergence for all of these parameters.

Fig. 4.14 gives the calculated shapes for the oil slick ( $m(\xi)$  and  $\eta(\xi)$ ), for the two cases at iterations 1, 5, and 10. Fig. 4.15 gives corresponding tangential velocities  $u_s(\xi)$  calculated in the model on the water-oil interface boundary  $\Gamma_{sl}$ . Convergence of the calculations is quite clear on the figures. As expected, velocities drop in front of the slick to a value below the current velocity  $U$  and then increase under the slick headwave to a value larger than  $U$ . For the lower velocity  $U$ ,  $u_s(x)$  stabilizes in the back of the headwave and then gradually drops to reach zero at the boom. For the larger velocity, no real stabilization of  $u_s$  is observed, but just a continuous drop to zero at the boom. The interface shape in this case also shows large scale oscillations (Fig. 4.14). In both cases, the region where velocity is larger than  $U$ , which can be identified as the headwave, covers about a third of the slick length. This *a posteriori*

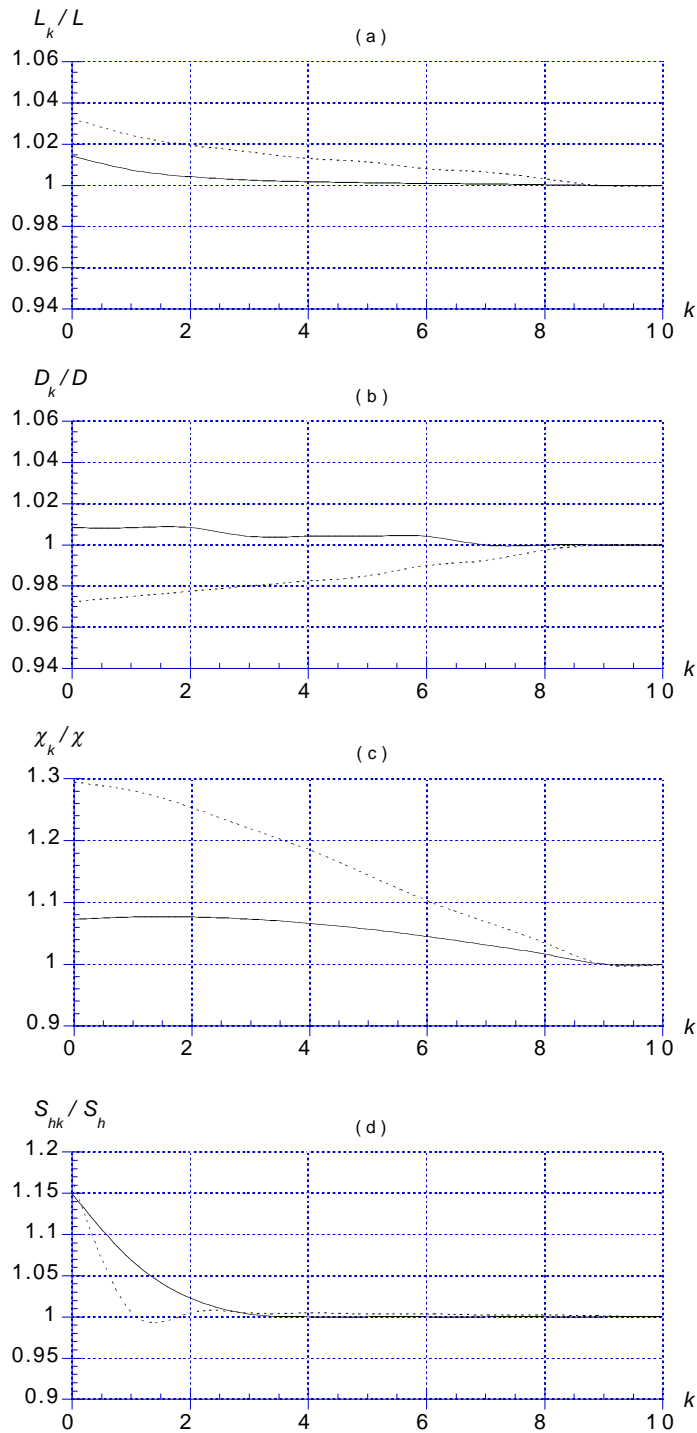


Figure 4.13: Convergence of oil slick parameters at Stage 2, as a function of number of iterations  $k$ , for cases a and c of Fig. 4.9, with  $Y = 1/3$ ,  $\varphi = 0.927$ ,  $V_o = 0.0235$  m<sup>3</sup>/m,  $C_{fm} = 0.1$  and  $U = : 0.1$  (—),  $0.3$  (- - - -) m/s. Note, parameters without  $k$  indices represent converged values.

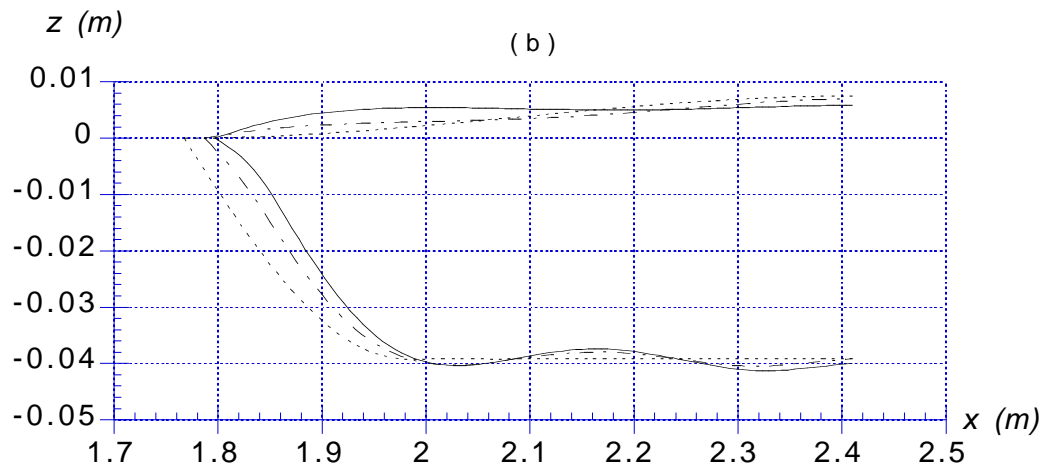
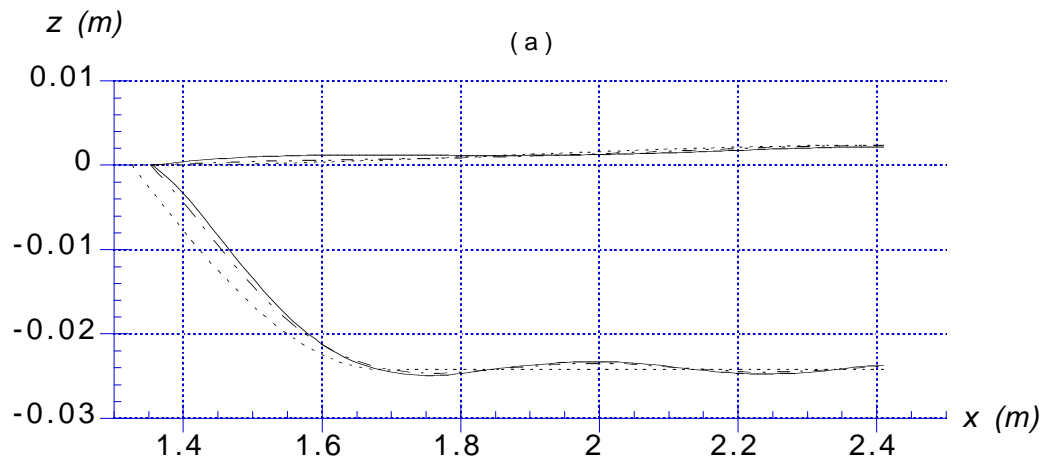


Figure 4.14: Convergence of oil slick shape at Stage 2, as a function of number of iterations  $k = 1$  (-----),  $5$  (----),  $10$  (—), for  $Y = 1/3$ ,  $\varphi = 0.927$ ,  $V_o = 0.0235$   $\text{m}^3/\text{m}$ ,  $C_{fm} = 0.1$  and  $U = : 0.1$  (a),  $0.3$  (b)  $\text{m/s}$ .

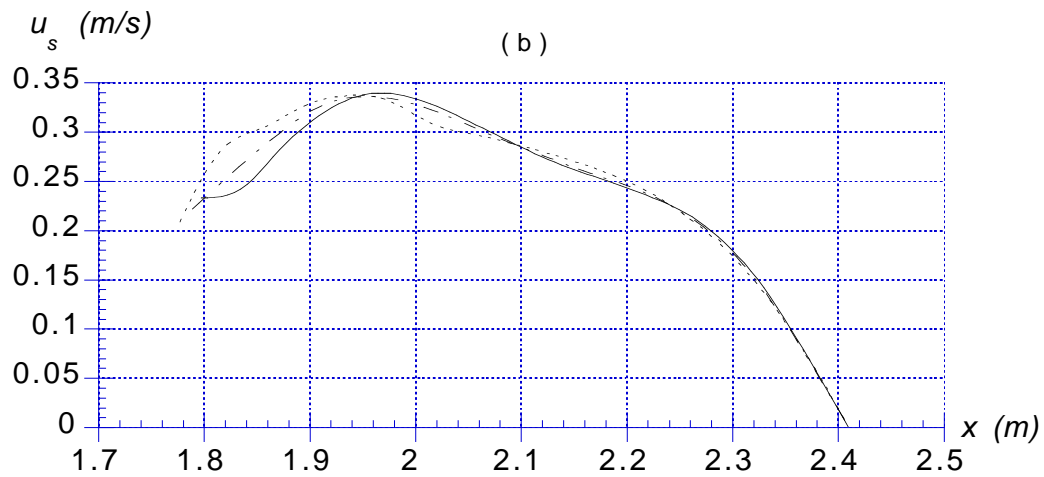
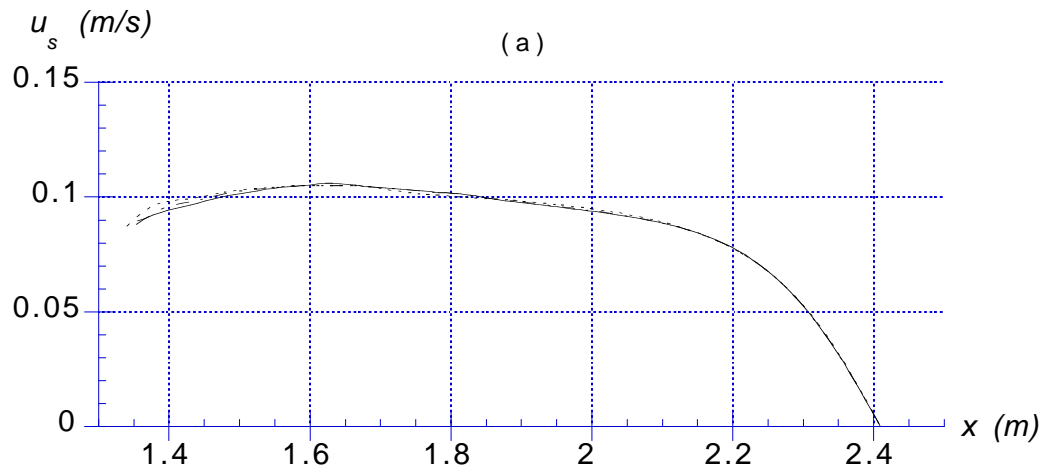


Figure 4.15: Convergence of tangential velocity at water-oil interface at Stage 2, as a function of number of iterations  $k = 1$  ( - - - - ), 5 ( - - - ), 10 ( ——— ), for  $Y = 1/3$ ,  $\varphi = 0.927$ ,  $V_o = 0.0235 \text{ m}^3/\text{m}$ ,  $C_{fm} = 0.1$  and  $U = : 0.1$  (a), 0.3 (b) m/s.

justifies the value  $Y = 1/3$  typically used in the Stage 1 Model.

### 4.3 Time Updating of Oil Slick : Stage 3 Model

In the Stage 3 model, the oil slick geometry and water-air, water-oil, and oil-air interfaces are allowed to dynamically evolve as a function of time, in order to calculate whether, for the specified input parameters (essentially,  $V_o, \varphi, U$ ), and for the specified boom skirt geometry and water depth, the slick reaches an equilibrium shape or exhibits the unstable shortening characteristic of *critical accumulation*.

As in Stage 2 model, the oil is assumed to be in pseudo-hydrostatic equilibrium on top of an ideal water flow (Section 4.3.5). Here, however, the water flow and interface geometries are treated as being unsteady. Thus, both kinematic and dynamic boundary conditions are specified over the water-air and water-oil interfaces (instead of just dynamic conditions) (Section 4.3.1). The former condition expresses that fluid particles on an interface stay on that interface while it deforms and moves. The latter condition expresses a total pressure balance across the interface. In this balance, for the water-oil interface, unlike in previous stages, we include : (i) *interfacial tension* effects in the form of a pressure jump proportional to the interface curvature and to  $\sigma_{wo}$  or  $\sigma_{wa}$ ; (ii) a pressure  $p_i$  corresponding to the *inertia of the oil* slick that the water must move (Section 4.3.7); and (iii) a *damping* pressure  $p_d$  corresponding to the energy (head) loss due to interfacial friction and slow viscous circulation within the slick (Section 4.3.6). [Note that, as for Stage 2, the use of a pressure results from the assumption of an ideal flow for the water, i.e., no shear can be transmitted to the (inviscid) flow as boundary condition, but only a pressure.]

Calculations with the Stage 3 model are initialized for time  $t = 0$ , based on stabilized static results calculated with the Stage 2 model. Fully nonlinear kinematic and dynamic boundary conditions on the water-air and water-oil interfaces are integrated using a time stepping method based on two second-order explicit Taylor series expansions of the interface shape and potential (Section 4.3.2). Coefficients in these series depend on geometry and flow velocity and acceleration on the water boundary. Flow fields are calculated by solving Laplace's equations for both the potential and its time derivatives over the water domain. This is done using a higher-order BEM method similar to that used in Stage 2 (Section 4.3.4). Results are thus calculated at time  $t + \Delta t$ , first in the water and on the boundary of the water domain; then, the corresponding oil-air interface shape ( $m(\xi)$ ) is calculated by integrating the pseudo-hydrostatic equilibrium equations, as done in Stage 2 (Section 4.3.9). At each time step, oil volume conservation is verified and, if needed, corrections of slick shape are applied various ways. Smoothing and curve fitting of interfaces geometry and field variables are also performed after each time step in order to filter out small oscillations, resulting from under-resolved small scale interfacial instabilities or numerical errors (Section 4.3.10).

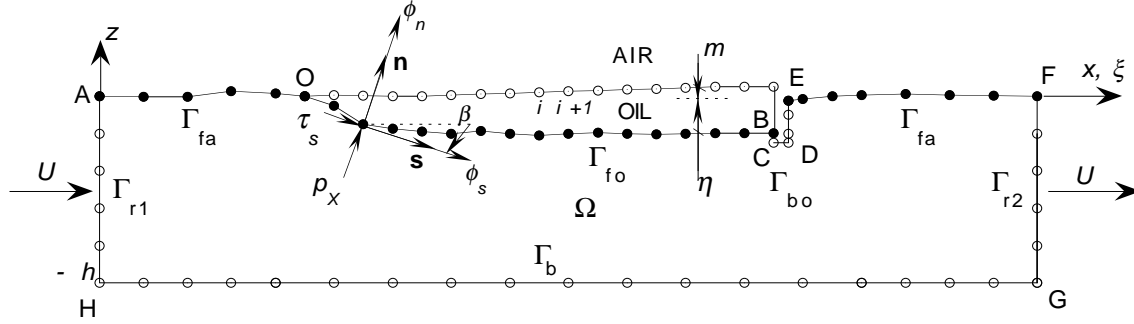


Figure 4.16: Sketch of computational domain  $\Omega$  with boundaries :  $\Gamma_{fa}$  (A-O and E-F),  $\Gamma_{fo}$  (O-B),  $\Gamma_{r1}$ ,  $\Gamma_{r2}$ ,  $\Gamma_b$  and  $\Gamma_{bo}$  (B-E), for potential flow computations with Stage 3 BEM mode (nodes (o) and (●)). Boundaries  $\Gamma_b$  and  $\Gamma_{bo}$  are rigid no-flow boundaries and a uniform flow  $U$  is specified on boundaries  $\Gamma_{r1}$  and  $\Gamma_{r2}$ . Water-air and water-oil interfaces ( $\Gamma_{fa}$ ,  $\Gamma_{fo}$ ; (●)) are time updated to  $t + \Delta t$ . Locations of nodes (⊙) on the slick oil-air interface are calculated at each time step to satisfy pseudo-hydrostatic equilibrium equations in the slick. Nodes marked as  $i, i + 1$ , illustrate the integration method used.

As in the earlier stages, proper modeling and calibration of the interfacial *friction* and (here) of *viscous dissipation* within the slick, and of the resulting energy dissipation at the water-oil interface is the key component which will enable the model to correctly compute slick shape evolution, and assess whether equilibrium will be reached for the specified input parameters. According to Delvigne's [9] analysis, critical accumulation is initiated when these dissipative mechanisms become unable to balance the energy input from the water flow. A more active interfacial dissipation may first result from small scale interfacial waves (Kelvin-Helmholtz waves) which increase friction but, at the end, an unstable shortening of the slick occurs. Hence, the proper representation and calibration of dissipative mechanisms in the model are of prime importance for the model's predictive ability. The friction coefficient function model equation introduced in Stage 2 is re-used in Stage 3. However, in order to account for the effect of unresolved small scale *Kelvin-Helmholtz instabilities* occurring at the water-oil interface as the water velocity increases, additional flow-dependent parameters are included in  $C_f$  (Section 4.3.8). Similarly, a new *equivalence of mechanical work* equation is developed for Stage 3, in order to derive the expression of the *damping pressure* and thus specify energy dissipation for the underlying potential flow, corresponding to the energy loss due to interfacial friction and viscous circulation in the slick (Section 4.3.6). Finally, the inertia resulting from increased small-scale interfacial motion is modeled as an *inertia pressure* term (Section 4.3.7).

### 4.3.1 Governing equations, boundary and initial conditions for the water flow

The two-dimensional water flow in the vertical plane  $(x, z)$  is assumed to be ideal, i.e., incompressible, inviscid, and irrotational. A velocity potential  $\phi(\mathbf{x}, t)$  is introduced, based on which the velocity field is defined as,  $\mathbf{u} = \nabla\phi = (u, w)$ . Mass conservation in the fluid domain  $\Omega(t)$ , with boundary  $\Gamma(t)$ , is governed by a Laplace's equation for  $\phi$  (Fig. 4.16),

$$\nabla^2\phi = 0 \quad \text{in } \Omega(t) \quad (4.92)$$

Introducing the free space Green's function  $G(\mathbf{x}, \mathbf{x}_l) = -\frac{1}{2\pi} \log |\mathbf{x} - \mathbf{x}_l|$ , Eq. (4.92) transforms into a boundary integral equation (BIE),

$$\alpha(\mathbf{x}_l)\phi(\mathbf{x}_l) = \int_{\Gamma(\mathbf{x})} \left\{ \frac{\partial\phi}{\partial n}(\mathbf{x}) G(\mathbf{x}, \mathbf{x}_l) - \phi(\mathbf{x}) \frac{\partial G(\mathbf{x}, \mathbf{x}_l)}{\partial n} \right\} d\Gamma(\mathbf{x}) \quad (4.93)$$

where  $\mathbf{x} = (x, z)$  and  $\mathbf{x}_l = (x_l, z_l)$  denote position vectors for points on the boundary,  $\mathbf{n}$  is the unit outward normal vector. and  $\alpha(\mathbf{x}_l)$  is a geometric coefficient.

The dynamic boundary condition on the water-air  $\Gamma_{fa}(t)$  and water-oil  $\Gamma_{fo}(t)$  interfaces (with  $\Gamma_f = \Gamma_{fo} \cup \Gamma_{fa}$ ) is obtained from the generalized Bernoulli equation. Hence, as in Eq. (4.13), assuming a pseudo-hydrostatic pressure in the slick (with a zero atmospheric pressure) for any point  $X$  on the water-oil interface  $\Gamma_{fo}(t)$ , we find (Fig. 4.16; note  $\phi_s = \partial\phi/\partial s$  and  $\phi_n = \partial\phi/\partial n$ ),

$$p_X = -\rho_w \left\{ \frac{\partial\phi}{\partial t} + gz + \frac{1}{2} |\nabla\phi|^2 \right\} = \rho_o g q - \sigma_{wo} \beta_s + p_d + p_i \quad (4.94)$$

where  $p_d$  and  $p_i$  denote damping and "inertia" pressures, respectively,  $\beta_s$  is the interface curvature,  $z = -\eta$ , and  $|\nabla\phi|^2 = \phi_s^2 + \phi_n^2$ . With the definition of the hydrostatic pressure, we also have,  $p_D = p_X - \rho_w g \eta$ , which is the dynamic pressure to use in the first Eq. (4.55) to calculate slick shape in Stage 3 model. Moving the time derivative in Eq. (4.94) to the left-hand-side and using the definition of the material derivative (i.e., a time derivative while moving with the flow),

$$\frac{D}{Dt} \equiv \frac{\partial}{\partial t} + \mathbf{u} \cdot \nabla \quad (4.95)$$

we obtain the dynamic boundary condition on the water-oil interface,

$$\frac{D\phi}{Dt} = \frac{1}{2} |\nabla\phi|^2 - g \{ \varphi q - \eta \} + \frac{\sigma_{wo}}{\rho_w} \beta_s - \frac{p_d + p_i}{\rho_w} \quad \text{on } \Gamma_{fo}(t) \quad (4.96)$$

On the water-air interface, we similarly obtain,

$$\frac{D\phi}{Dt} = \frac{1}{2} |\nabla\phi|^2 - g z + \frac{\sigma_{wa}}{\rho_w} \beta_s \quad \text{on } \Gamma_{fa}(t) \quad (4.97)$$

in which  $\sigma_{wa}$  denotes the water-air interfacial tension.

The kinematic boundary condition on the whole water-air plus water-oil interface  $\Gamma_f(t)$  expresses that points on the interface stay on the interface while it moves and deforms under the action of the flow. Thus, defining the interface position by vector  $\mathbf{r}(t)$ , we simply have,

$$\frac{D\mathbf{r}}{Dt} = \mathbf{u} = \nabla\phi \quad \text{on } \Gamma_f(t) \quad (4.98)$$

Lateral boundaries  $\Gamma_{r1}$  and  $\Gamma_{r2}$  are located far enough upstream and downstream, respectively, of the slick/boom for the flow velocity to be reasonably close to the uniform current velocity specified as,  $u(z) = U$  (for  $z = [-h, z_f]$ ), where  $h$  is the undisturbed water depth and  $z_f$  is the local water-air interface elevation at the lateral boundary. Thus, lateral boundary conditions can be expressed as,

$$\overline{\frac{\partial\phi}{\partial n}} = \mp U \quad \text{on } \Gamma_{r1} \text{ and } \Gamma_{r2} \quad (4.99)$$

where the overline denotes specified values.

Along the stationary bottom  $\Gamma_b$  and the boom boundary  $\Gamma_{bo}$  we have the no-flow condition,

$$\overline{\frac{\partial\phi}{\partial n}} = 0 \quad \text{on } \Gamma_b \text{ and } \Gamma_{bo} \quad (4.100)$$

Initial conditions for the water-air and water-oil interfaces, are specified at Stage 3, using results of the last iteration of Stage 2. For the geometry, we simply have,  $z = 0$  on  $\Gamma_{fa}(0)$  and  $z = -\eta_o$  on  $\Gamma_{fo}(0)$  (where  $\eta_o(x)$  denotes the geometry of the water-oil interface calculated at Stage 2). The geometry of the other boundaries is straightforward. In the BIE formulation (4.93), either the potential or its normal derivative must be specified as boundary conditions on the whole boundary  $\Gamma(0)$ . As discussed above, such conditions are straightforward on  $\Gamma_{r1}$ ,  $\Gamma_{r2}$ ,  $\Gamma_b$  and  $\Gamma_{bo}$  for  $t = 0$  (Eqs. (4.99), (4.100)). On the interface boundary  $\Gamma_f(0)$ , however, a no-flow condition was specified at Stage 2, due to the static calculation. In Stage 3, this boundary is free to move and we must therefore specify the potential as a boundary condition. The initial boundary values of the potential are found by integrating the tangential velocity obtained at the last iteration of Stage 2 as,

$$\overline{\phi}(\mathbf{r}(s_o), 0) = \int_0^{s_o} \frac{\partial\phi}{\partial s}(s) ds \quad (4.101)$$

where  $s$  and  $s_o$  denote curvilinear abscissa measured, from the leftward extremity (point A in Fig. 4.16), on the whole upward boundary of domain  $\Omega$ , i.e.,  $\Gamma_f(0) \cup \Gamma_{bo}$  (denoted by  $\Gamma_f$  or A-F in Fig. 4.10), and,

$$\frac{\partial\phi}{\partial s} = u_s = -\frac{\partial\psi_o}{\partial n} \quad (4.102)$$

where  $\psi_o$  denotes the streamfunction calculated on boundary  $\Gamma_f$  in Fig. 4.10, at the last iteration of Stage 2. The integral in Eq. (4.101) is easily calculated within each boundary element of the  $\Gamma_f$  boundary BEM discretization of Stage 2.

### 4.3.2 Time stepping

In the Stage 3 model, free surface boundary conditions (4.96),(4.97) and (4.98) are integrated at time  $t$ , to calculate both the new geometry,  $\mathbf{r}(t + \Delta t)$ , and potential,  $\phi(\mathbf{r}(t + \Delta t))$ , on the free surface at a next time level  $t + \Delta t$  (with  $\Delta t$  the time step). This is done using second-order Taylor series expansions,

$$\begin{aligned}\bar{\mathbf{r}}(t + \Delta t) &= \mathbf{r}(t) + \Delta t \frac{D \mathbf{r}}{Dt}(t) + \frac{(\Delta t)^2}{2} \frac{D^2 \mathbf{r}}{Dt^2}(t) + \mathcal{O}[(\Delta t)^3] \\ \bar{\phi}(t + \Delta t) &= \phi(t) + \Delta t \frac{D \phi}{Dt}(t) + \frac{(\Delta t)^2}{2} \frac{D^2 \phi}{Dt^2}(t) + \mathcal{O}[(\Delta t)^3]\end{aligned}\quad (4.103)$$

First-order coefficients in the series are given by Eqs. (4.96),(4.97) and (4.98), as a function of geometry, and  $\phi$  and  $\partial\phi/\partial n$ , calculated at time  $t$ . Second-order coefficients require also knowing values of the time derivatives of both of these. The principle of time updating in the model is thus as follows : assuming the potential is known on the free surface at time  $t$  (the potential is calculated at  $t = 0$  by Eqs. (4.101), (4.102)), continuity equation is solved in its BIE form (4.93), using Eqs. (4.99) and (4.100) on the lateral and bottom/boom boundaries, and the potential on the free surface, as boundary conditions. Based on this solution,  $\partial\phi/\partial t$  is calculated on the free surface using (Bernoulli) Eqs. (4.96) and (4.97). A second BIE equation is then solved, which is the time derivative of Eq. (4.93). To do so, specified values of  $\partial\phi/\partial t$  are used as boundary conditions on the free surface, together with prescribed values of  $\partial^2\phi/\partial t\partial n$  on the other boundaries. [Note that BIEs for  $\phi$  and  $\partial\phi/\partial t$  correspond to the same boundary geometry and, hence, have the same BEM discretized form. Therefore, the solution of the second BIE only takes a small fraction of the time needed to solve the first BIE.]

For the additional boundary conditions on the water-oil interface boundary, we simply have from Eq. (4.96),

$$\frac{\partial\bar{\phi}}{\partial t} = -\frac{1}{2} |\nabla\phi|^2 - g \{\varphi q - \eta\} + \frac{\sigma_{wo}}{\rho_w} \beta_s - \frac{p_d + p_i}{\rho_w} \quad \text{on } \Gamma_{fo}(t) \quad (4.104)$$

with  $q = m + \eta$ , and on the water-air interface, we similarly get, from Eq. (4.97),

$$\frac{\partial\bar{\phi}}{\partial t} = -\frac{1}{2} |\nabla\phi|^2 - g z + \frac{\sigma_{wa}}{\rho_w} \beta_s \quad \text{on } \Gamma_{fa}(t) \quad (4.105)$$

For the additional boundary conditions on lateral boundaries, we simply have from Eq. (4.99),

$$\frac{\partial^2\bar{\phi}}{\partial t\partial n} = \mp \frac{\partial U}{\partial t} \quad \text{on } \Gamma_{r1} \text{ and } \Gamma_{r2} \quad (4.106)$$

For the additional boundary conditions on the bottom and boom boundaries, we simply have from Eq. (4.100),

$$\frac{\partial^2\bar{\phi}}{\partial t\partial n} = 0 \quad \text{on } \Gamma_b \text{ and } \Gamma_{bo} \quad (4.107)$$

Applying the material derivative operator (4.95) to Eqs. (4.96), (4.97), and (4.98), second-order terms in the Taylor series Eqs. (4.103) are finally obtained, after some derivations (see, Grilli *et al.* [22, 24]), as,

$$\frac{D^2\phi}{Dt^2} = \nabla\phi \cdot \frac{Du}{Dt} - g(1-\varphi)w - g\varphi \frac{Dm}{Dt} + \frac{\sigma_{wo}}{\rho_w} \frac{\partial\phi}{\partial s} \frac{\partial^2\beta}{\partial s^2} - \frac{1}{\rho_w} \frac{D(p_d + p_i)}{Dt} \quad \text{on } \Gamma_{fo}(t) \quad (4.108)$$

in which  $Dm/Dt$  and  $D(p_d + p_i)/Dt$  will be detailed later, and,

$$\frac{D^2\phi}{Dt^2} = \nabla\phi \cdot \frac{Du}{Dt} - gw + \frac{\sigma_{wa}}{\rho_w} \frac{\partial\phi}{\partial s} \frac{\partial^2\beta}{\partial s^2} \quad \text{on } \Gamma_{fa}(t) \quad (4.109)$$

with,

$$\begin{aligned} \frac{D^2\mathbf{r}}{Dt^2} = \frac{Du}{Dt} &= \left\{ \frac{\partial^2\phi}{\partial t\partial s} + \frac{\partial\phi}{\partial s} \frac{\partial^2\phi}{\partial s^2} + \frac{\partial\phi}{\partial n} \frac{\partial^2\phi}{\partial n\partial s} \right\} \mathbf{s} + \left\{ \frac{\partial^2\phi}{\partial t\partial n} - \frac{\partial\phi}{\partial n} \frac{\partial^2\phi}{\partial s^2} \right. \\ &\quad \left. + \frac{\partial\phi}{\partial s} \frac{\partial^2\phi}{\partial n\partial s} + \frac{\partial\beta}{\partial s} |\nabla\phi|^2 \right\} \mathbf{n} \quad \text{on } \Gamma_f(t) \end{aligned} \quad (4.110)$$

In deriving Eqs. (4.108) to (4.110), the following relationships have been used,

$$\mathbf{s} = \{\cos\beta, \sin\beta\} \quad \text{and} \quad \mathbf{n} = \{-\sin\beta, \cos\beta\} \quad (4.111)$$

$$\nabla \equiv \frac{\partial}{\partial s} \mathbf{s} + \frac{\partial}{\partial n} \mathbf{n} \quad (4.112)$$

with,  $\cos\beta = \frac{\partial x}{\partial s}$ ,  $\sin\beta = \frac{\partial z}{\partial s}$ , and  $\frac{\partial\beta}{\partial n} = \frac{\partial\beta}{\partial t} = 0$ , which express the definition of a curvilinear coordinate system on the water domain boundary  $\Gamma$ , and,

$$\frac{\partial^2\phi}{\partial n^2} = -\frac{\partial^2\phi}{\partial s^2} + \frac{\partial\phi}{\partial n} \frac{\partial\beta}{\partial s} \quad \text{and} \quad \frac{\partial^2\phi}{\partial s\partial n} = \frac{\partial^2\phi}{\partial n\partial s} \quad (4.113)$$

which express continuity equation (4.92) and the irrotationality of the flow, respectively.

The accuracy of Taylor series Eqs. (4.103) is function of the size of time step  $\Delta t$ , with truncation errors of  $\mathcal{O}[(\Delta t)^3]$ . This error behavior, however, can only be achieved provided the spatial BEM discretization is selected to resolve sufficiently small features of the flow such as to produce accurate enough values for the Taylor series coefficients. Hence, time step size and spatial discretization are related. Grilli *et al.* [25, 24] introduced an adaptive time stepping method in their 2D wave propagation model. By computing the propagation of fully nonlinear solitary waves over constant depth in the model, for many spatio-temporal discretizations, they showed that an optimal mesh Courant number  $\mathcal{C}_o$  exists for which numerical errors on mass and energy conservation reach a minimum. Therefore, at all times, they adaptively selected the time step as,

$$\Delta t = \mathcal{C}_o \frac{\Delta |\mathbf{r}|^{min}}{\sqrt{gh}} \quad (4.114)$$

where  $\Delta | \mathbf{r} |^{min}$  denotes the instantaneous minimum distance between nodes on the free surface, and  $h$  is a characteristic depth. For cubic BEM elements with continuous slope, such as those used on free surfaces and interfaces here, Grilli and Subramanya [24] showed that  $\mathcal{C}_o \simeq 0.45$ .

The denominator of Eq. (4.114) represents the maximum speed of propagation of shallow water waves, i.e., perturbations in the solution. In the present case, however, such speed is dictated by the flow velocity  $U$ . After various numerical tests, it was found that Stage 3 model solution was most accurate when a velocity quite larger than  $U$  was selected or, using  $U$ , when  $\mathcal{C}_o \simeq 0.15$ . In Stage 3 model, the time step size at time  $t$  was thus calculated as,

$$\Delta t = \mathcal{C}_o \frac{\Delta | \mathbf{r} |^{min}}{U} \quad (4.115)$$

using the above value of  $\mathcal{C}_o$ .

### 4.3.3 Analogy with Vortex Sheet method

In Phase I and II models, *Vortex Sheet* dynamics was used to express the rate of change of vorticity (i.e., vortex sheet strength)  $\gamma$  at the interface between two fluids, due to inertia, gravity, surface tension, and friction effects (e.g. Section 2.3 in Phase I report, Grilli *et al.* [17], or Eq. 2.7 in Phase II report, Grilli *et al.* [19]). As explained before, however, although this methodology worked well for periodic or semi-infinite problems without solid boundaries (other than a flat bottom), it was found that Biot-Savart equations, which were used to relate velocity and vorticity fields were improperly posed on solid boundaries. This led model results based on these equations to gradually deteriorate as a function of time, as no-flow conditions on solid boundaries were increasingly violated. Due to this unforeseen problem, the potential flow formalism coupled to the BIE representation of mass conservation equation was adopted for Phased III models. In the new formalism, no-flow conditions on solid boundaries can directly be included as boundary conditions.

Now, it is of interest to verify that the time evolution equation (4.96) or (4.104), expressed for the potential at the water-oil interface, is similar in form to the evolution equation derived for the continuous vortex sheet strength in Phase II model. This is done by recalling that, for oil (o) and water (w), we have,

$$\gamma = u_s^o - u_s^w \simeq -u_s^w \quad (4.116)$$

since, here, we neglect the fluid motion in the oil, due to the pseudo-hydrostatic hypothesis, and, following the vortex sheet motion, we have,

$$\frac{d\gamma}{dt} = \frac{\partial\gamma}{\partial t} + \frac{1}{2} (\mathbf{u}^w + \mathbf{u}^o) \cdot \nabla\gamma \simeq \frac{\partial\gamma}{\partial t} + \frac{1}{2} \mathbf{u}^w \cdot \nabla \quad (4.117)$$

Now, taking the tangential derivative of Eq. (4.104) along the interface, and noting  $\mathbf{u}^w = \mathbf{u} = \nabla\phi$ , and, with Eq. (4.116),  $u_s^w = u_s = \partial\phi/\partial s = -\gamma$ , we find,

$$-\frac{\partial\gamma}{\partial t} = \left\{ \frac{\partial\phi}{\partial s} \frac{\partial\gamma}{\partial s} + \frac{\partial\phi}{\partial n} \frac{\partial\gamma}{\partial n} \right\} - g\varphi \frac{\partial m}{\partial s} - g(1-\varphi) \frac{\partial z}{\partial s} + \frac{\sigma_{wo}}{\rho_w} \frac{\partial^2\beta}{\partial s^2} - \frac{1}{\rho_w} \frac{\partial(p_d + p_i)}{\partial s} \quad \text{on } \Gamma_{fo}(t) \quad (4.118)$$

or, noting that by definition of vortex sheets,  $\frac{\partial\gamma}{\partial n} = 0$  and using Eq. (4.95), we finally get,

$$\frac{d\gamma}{dt} = \frac{1}{2}\gamma \frac{\partial\gamma}{\partial s} + g\varphi \frac{\partial m}{\partial s} + g(1-\varphi) \sin\beta - \frac{\sigma_{wo}}{\rho_w} \frac{\partial^2\beta}{\partial s^2} + \frac{1}{\rho_w} \frac{\partial(p_d + p_i)}{\partial s} \quad \text{on } \Gamma_{fo}(t) \quad (4.119)$$

which expresses the rate of change of the vortex sheet strength at the water-oil interface, when following the vortex sheet with its own velocity  $\mathbf{u}/2$ , assuming that the oil is in pseudo-hydrostatic state. Eq. (4.119) is clearly similar to equations derived for two semi-infinite fluid layers problems, in Phases I and II.

#### 4.3.4 External flow calculation

At each time step, the flow in water domain  $\Omega(t)$  is calculated, similar to Stage 2, using the Boundary Element Method (BEM). The BIE (4.93) for the potential  $\phi$ , and a similar equation for  $\partial\phi/\partial t$  are solved by discretizing the whole boundary  $\Gamma(t) = \Gamma_{r1} \cup \Gamma_f \cup \Gamma_{bo} \cup \Gamma_b$  using nodes and higher-order elements to interpolate in between nodes (Fig. 4.16). Because they are expressed for the same boundary geometry, both discretized BIEs lead to the same algebraic system matrix. Only the system right-hand-side differs for  $\phi$  or  $\partial\phi/\partial t$ .

At each time step  $t$ , boundary conditions for  $\overline{\phi}$  (Eq. (4.103)) or  $\overline{\partial\phi/\partial t}$  (Eqs. (4.104),(4.105)) are specified on  $\Gamma_f$  and boundary conditions for  $\overline{\partial\phi/\partial n}$  (Eqs. (4.99), (4.100)) or  $\overline{\partial^2\phi/\partial t\partial n}$  (Eqs. (4.106), (4.107)) are specified on the other boundaries. The BEM solution of the two BIEs (based on these boundary conditions) provides boundary values of :  $\phi, \partial\phi/\partial n, \partial\phi/\partial t, \partial^2\phi/\partial t\partial n$ . Tangential  $s$ -derivatives of these are then calculated using higher-order (4th-order) sliding polynomials on the boundary (Grilli and Subramanya [24]).

Based on these fields and their tangential derivatives, both the geometry and the potential on  $\Gamma_f$  are updated to time  $t + \Delta t$  using Taylor series Eqs. (4.103) with expressions of the coefficients (4.96) to (4.98), (4.108) to (4.111).

#### 4.3.5 Pseudo-hydrostatic equilibrium in the slick

These equations are derived, as in Stages 1 and 2, assuming that the oil slick is in hydrostatic equilibrium on top of an ideal fluid flow. This flow imposes both a dynamic pressure  $p_D$  and a shear stress  $\tau_s$  at the water-oil interface boundary  $\Gamma_{fo}$  (Fig. 4.16).

The pressure equilibrium at the water-oil interface is defined by Eq. (4.94) and represents the vertical equilibrium equation used for the slick at Stage 3. Hence, by analogy with Stages 1 and 2, using Eq. (4.9), we have,

$$p_D = -\rho_w \left\{ \frac{\partial \phi}{\partial t} + \frac{1}{2} |\nabla \phi|^2 \right\} = \rho_w g \{ \varphi q - \eta \} - \sigma_{wo} \beta_s + p_d + p_i \quad (4.120)$$

or, using the non-dimensional variables introduced in Stage 2 (Eqs. (4.50),(4.51)), we get,

$$q' = \frac{1}{\varphi} \{ p'_D + \eta' + \sigma'_{wo} \beta_{s'} - p'_d - p'_i \} \quad (4.121)$$

with  $\sigma'_{wo} = \sigma_{wo}/\rho_w$  and  $\beta_{s'} = \frac{\partial \beta}{\partial s'}$ , in which  $p_D$  denotes the hydrodynamic pressure calculated at time  $t$  for the potential flow at the water-oil interface boundary, defined in the first equality of Eq. (4.120).

The first-order horizontal equilibrium equation for the slick is the same as for Stages 1 and 2, i.e., Eq. (4.20). Using Eqs. (4.9) and (4.121), and the nondimensional variables, we get,

$$\frac{dm'}{d\xi'} = \frac{C'_f}{2\varphi q'} + \frac{1}{\varphi q'} \{ p'_d + p'_i - \sigma'_{wo} \beta_{s'} \} \frac{d\eta'}{d\xi'} \quad (4.122)$$

Comparing the orders of magnitude of the two terms on the right-hand-side of this equation, one can see that the second term is negligible. Hence, the horizontal equilibrium equation used in the slick for Stage 3 is,

$$\frac{dm'}{d\xi'} \simeq \frac{C'_f}{2\varphi q'} \quad (4.123)$$

which is the same equation as used in Stage 2, with  $q'$  given by Eq. (4.121), whose terms in the right-hand-side are calculated in the potential flow solution for time  $t$ . The shape of the oil-air interface will again be found by integrating Eq. (4.122) at each time step (see below).

### 4.3.6 Mechanical work and expression of pressure damping

As in the previous two stages, head loss coefficients  $C_h$  or  $S_h$  are re-calculated at Stage 3 for each time step calculation of the slick shape  $\eta(s, t)$  and underlying flow interfacial velocity  $\mathbf{u}(s, t)$  (where  $s$  denotes the curvilinear abscissa measured from point O in Fig. 4.16). As in Stages 1 and 2, this is done by expressing that the work of the frictional shear stress along the water-oil interface (denoted as boundary  $\Gamma_{fo}$  between O and B on Fig. 4.16), and of the additional shear stress caused by viscous circulation within the slick, is equivalent to the work of an interfacial damping pressure (similar to a head loss) defined as  $p_d(s, t)$  (see Eq. (4.94)). Here, however, the damping pressure directly affects the underlying potential flow calculation, through its effect

in the dynamic free surface boundary condition (4.96). This in fact is similar to a so-called “absorbing beach” used in nonlinear surface wave computations to absorb surface wave energy at the boundary of a potential flow computational domain, where otherwise no dissipation can be included (Grilli and Horrillo [16]).

Equations for the work of the total interfacial shear stress  $\tau_s$  are the same as those used in Stages 1 and 2, i.e., Eqs. (4.37) to (4.40) for  $\mathcal{P}_\tau$ ,  $\tilde{C}'_f$ ,  $T_t$ , and  $\mathcal{W}_\tau$ , with  $u_s = |\partial\phi/\partial s(s, t)|$  (where the modulus is specified to account for the possibility of a reversing flow, due to Kelvin-Helmholtz interfacial waves). Integrals in the equations are numerically calculated using the BEM discretization, assuming that  $\Gamma_{sl} \equiv \Gamma_{fo}$ .

For the work of the damping pressure  $p_d$ , due to interfacial motion, it is assumed that this pressure acts to damp such motions and hence is applied parallel to the normal direction  $\mathbf{n}$ , to the water-oil interface, and in direction opposite to the motion velocity  $\partial\phi/\partial n$ . By analogy with “absorbing beaches”, and according to the analytic form of the interfacial shear stress (4.21), this pressure is defined as,

$$p_d = \nu(x) \operatorname{sign}\left(\frac{\partial\phi}{\partial n}\right) \left\{\frac{\partial\phi}{\partial s}\right\}^2 \quad (4.124)$$

with  $\nu = \nu_f(x)\nu_v$  a damping function (with  $\nu_f$  and  $\nu_v$  the friction and circulation effects, respectively) and,

$$\operatorname{sign}\left(\frac{\partial\phi}{\partial n}\right) = \frac{\frac{\partial\phi}{\partial n}}{\left|\frac{\partial\phi}{\partial n}\right|} \quad (4.125)$$

Applying the material derivative (4.95) to Eq. (4.124), with definition (4.112), and assuming  $\nu$  is only a function of  $x$ , we also find,

$$\frac{D p_d}{D t} = \frac{2 p_d}{\frac{\partial\phi}{\partial s}} \left\{ \frac{\partial^2\phi}{\partial t\partial s} + \frac{\partial\phi}{\partial n} \frac{\partial^2\phi}{\partial n\partial s} + \frac{\partial\phi}{\partial s} \frac{\partial^2\phi}{\partial s^2} + \frac{u}{2\nu} \frac{\partial\phi}{\partial s} \frac{\partial\nu}{\partial x} \right\} \quad (4.126)$$

which is needed for Eq. (4.108).

### Effect of friction

The part of the damping function due to interfacial friction is simply assumed to be proportional to the friction coefficient function,

$$\nu_f(x) = K C_f(x) \quad \text{and,} \quad \frac{\partial\nu_f}{\partial x} = K \frac{\partial C_f}{\partial x} \quad (4.127)$$

where  $\nu_f$  denotes the damping function due to interfacial friction.

The power dissipated by the damping pressure now reads,

$$\mathcal{P}_p = \int_{\Gamma_{fo}} p_{df} \frac{\partial\phi}{\partial n} ds = K U^3 L C_f^* \quad (4.128)$$

where  $p_{df}$  denotes the fraction of the damping pressure due to interfacial friction, and,

$$C_f'^* = \frac{1}{U L} \int_{\Gamma_{fo}} C_f' \left| \frac{\partial \phi}{\partial n} \right| ds = \frac{1}{U^3 L} \int_{\Gamma_{fo}} C_f' \left| \frac{\partial \phi}{\partial n} \right| \left\{ \frac{\partial \phi}{\partial s} \right\}^2 ds \quad (4.129)$$

Similarly, with the simplified definition of  $T_t$  used in Stage 1, the work of  $p_d$  is,

$$\mathcal{W}_p \simeq T_t \mathcal{P}_p \simeq K U^2 L^2 C_f'^* \quad (4.130)$$

It is now assumed that, for any time  $t$ ,  $\mathcal{W}_p \equiv \mathcal{W}_\tau$  and, from Eqs. (4.37) to (4.40), and (4.124) to (4.130), we find,

$$K = \frac{1}{2} \rho_w \frac{\tilde{C}_f'}{C_f'^*} \quad (4.131)$$

The equivalent head loss coefficient for interfacial friction,  $C_h$  can now be calculated by making the work of the damping pressure equivalent to that of the head loss pressure drop  $\Delta p_X$  used in Stages 1 and 2, expressed by Eqs. (4.41) to (4.43), with  $u_s = |\partial \phi / \partial s(s, t)|$ . As in Stage 2, we find, using Eqs. (4.130),(4.131),

$$C_h = \frac{\tilde{C}_f' D}{\tilde{\eta}} \quad (4.132)$$

[Using Eq. (4.12), we similarly get  $S_h$ .] with,

$$\tilde{C}_f' = \frac{1}{U^3 L} \int_{\Gamma_{fo}} C_f' \left| \frac{\partial \phi}{\partial s} \right|^3 ds \quad (4.133)$$

and,

$$\tilde{\eta} = \frac{1}{U L} \int_{\Gamma_{fo}} \eta \left| \frac{\partial \phi}{\partial s} \right| ds \quad (4.134)$$

where all quantities are calculated at time  $t$ .

### Effect of slick viscous circulation

Delvigne [9] described the mechanism of *critical accumulation* as the result of the inadequacy of viscous circulation in the slick to absorb the energy of the water flow conveyed to the oil-water interface, through the build-up of interfacial KH waves.

This important dissipative effect is modeled in SlickMap by assuming that the tangential velocity jump at the oil-water interface drives a slow circulation in the slick. This slow circulation, in turn, induces viscous dissipation effects.

In Stage 3 model, the oil slick is assumed to be in quasi-static equilibrium. For calculating the viscous dissipation, however, we assume that a fraction  $\alpha_v \in [0, 1]$  of the tangential velocity in the water  $u_s$  is applied to the bottom of the oil slick. We

further assume that this velocity varies linearly over the slick thickness  $q$ , to reach an opposite maximum value on the slick oil-air interface. Thus,

$$u_o(\xi, \zeta) = \alpha_v u_s(\xi) \left\{ 1 - 2 \frac{\zeta}{q(\xi)} \right\} \quad (4.135)$$

where  $\zeta = z + \eta(\xi)$ ,  $u_o$  denotes the horizontal velocity in the oil slick, and  $u_s = \partial\phi/\partial s$  (see Fig. 4.16).

Now, for an incompressible Newtonian fluid of dynamic viscosity  $\mu_o$ , moving at low Reynolds number, the viscous power dissipation per unit volume is expressed, assuming a two-dimensional flow in the vertical plane, as (Batchelor [4]),

$$\Phi = \mu_o \left\{ 2 \left( \frac{\partial u_o}{\partial x} \right)^2 + \left( \frac{\partial u_o}{\partial z} \right)^2 \right\} \quad (4.136)$$

Hence, the total viscous energy dissipation over time  $\Delta t$  per unit area in the slick is, using Eqs. (4.135) and (4.136),

$$\begin{aligned} \mathcal{D} &= \Delta t \int_0^q \Phi(\xi, \zeta) d\zeta \\ &= 2 \Delta t \alpha_v^2 \mu_o \left\{ \frac{q}{3} \left( \frac{du_s}{d\xi} \right)^2 + \frac{2}{q} u_s^2 \right\} \end{aligned} \quad (4.137)$$

Now, to model this energy dissipation in SlickMap, we again use the average work of a damping pressure applied to the oil-water interface, defined by Eq. (4.124). We thus define  $\nu_v$  the damping function due to viscous dissipation, in such a way that,

$$\frac{1}{L} \int_0^L \mathcal{D} d\xi = \frac{\Delta t}{L} \int_0^L p_{dv} \frac{\partial\phi}{\partial n} d\xi \quad (4.138)$$

where  $p_{dv}$  denotes the fraction of the damping pressure due to viscous circulation, and combining Eqs. (4.137) to (4.138), we obtain the damping function due to viscous circulation as,

$$\nu_v = \frac{2 \mu_o \alpha_v^2}{\int_0^L |\phi_n| \phi_s^2 d\xi} \int_0^L \left\{ \frac{q \phi_{ss}^2}{3} + \frac{2 \phi_s^2 \cos^2 \beta}{q} \right\} d\xi \quad (4.139)$$

where  $\phi_n = \partial\phi/\partial n$ ,  $\phi_s = u_s$  and  $\phi_{ss} = \frac{\partial u_s}{\partial s}$ . In Stage 3 model, the constant  $\nu_v$  is calculated at each time step and added to  $\nu_f(x)$ , to constitute  $\nu$  in the expression of the damping interfacial pressure, Eq. (4.124). Typical values of  $\alpha$  for high viscosity oils are 0.1 to 0.2. Calibration of coefficient  $\alpha$  is discussed later.

### 4.3.7 Expression of slick inertial damping

When the water-oil interface  $\Gamma_{fo}$  moves under the action of the water flow, this motion has to counteract the inertia of the oil slick. This results in an additional (equivalent) pressure applied to the interface of the water domain,  $p_i$  referred to as *inertial pressure*.

Assuming the oil slick only undertakes vertical motion, the inertial pressure externally applied to the water-oil interface can be estimated by,

$$p_i = \rho_o q \frac{D w}{D t} \quad (4.140)$$

in which the last term represents the vertical acceleration of the interface, given by the second component of Eq. (4.110), which is supposed to be transmitted as a whole to the overlying slick.

The inertial pressure represents another damping term applied to the dynamic free surface condition Eq. (4.96) as a result of the slick motion. At a given time  $t$ , all the terms needed to calculate  $p_i$  are available, based on solutions of both Laplace's equations for  $\phi$  and  $\partial\phi/\partial t$  and calculation of  $s$ -derivatives. Due to the second-order Taylor series expansions, the material derivative of  $p_i$  is also needed (see Eq. (4.108)),

$$\frac{D p_i}{D t} = \rho_o \left\{ \frac{D q}{D t} \frac{D w}{D t} + q \frac{D a_z}{D t} \right\} \quad (4.141)$$

where  $a_z = Dw/Dt$  is the vertical acceleration, and  $Dq/Dt = Dm/Dt - w$ . The value of  $Dm/Dt$  is calculated as part of the oil slick updating (see a following section) but the material derivative of the acceleration is not known at time  $t$ . This term is estimated in the model by a finite difference as,

$$\frac{D a_z}{D t}(\mathbf{x}, t) \simeq \frac{1}{\Delta t} \{a_z(\mathbf{x}, t) - a_z(\mathbf{x}, t - \Delta t)\} \quad (4.142)$$

Note, due to node regridding on the interface, only a first-order backward finite difference is used, relative to the vertical acceleration of the same node/water-particle calculated at two different time steps.

### 4.3.8 Expression of friction coefficient function

In the Stage 3 model, the parameterization of the Friction Coefficient Function  $C_f$  used in Stage 2 (Eq. (4.63)) is modified to account for changes due to small scale interfacial waves, referred to as *Kelvin-Helmholtz* (KH) waves. These waves increase the roughness of the water-oil interface and hence, enhance friction. KH waves correspond to unresolved sub-grid scales in the BEM model. When they occur, however, the modeled water-oil interface experiences more motions in its normal direction, which translate into normal accelerations.

To account for KH waves, the following model of friction is used at Stage 3,

$$C_f = C_{fo} \left( 1 + \mathcal{K} \Delta t \left| \frac{\phi_{tn}}{\phi_n} \right| \right) \left\{ 1 - e^{-\mu \xi'} + \alpha \chi e^{-\beta \chi} \right\} \quad \text{with,} \quad \chi = \left( \frac{\xi'}{\xi_p} \right)^\gamma \quad (4.143)$$

where  $\mu$ ,  $\alpha$ ,  $\beta$ , and  $\gamma$ , are nondimensional coefficients,  $C_{fo}$  and  $\xi'_p$  are partly estimated based on experiments,  $\phi_n = \partial\phi/\partial n$ ,  $\phi_{tn} = \partial^2\phi/\partial t\partial n$ , and  $\mathcal{K}(\xi') \geq 0$  is a weighting

function expressing the effects of KH waves on friction. This function is also calibrated using experimental results.

When  $\mathcal{K} = 0$ , the FCF is identical to the function used in Stage 2 (Eq. (4.63)). Hence, the computation and discussion of values of parameters  $\mu$ ,  $\alpha$ , and  $\beta$ , as a function of  $\epsilon$ ,  $Y$ ,  $\gamma$ ,  $\lambda$ , and  $\delta$ , and of their effect on  $C_f$  made earlier are applicable to Stage 3 (Eqs. (4.64) to (4.66)). As in Stage 2, the following values will be used for these parameters,  $\epsilon = 0.01$ ,  $Y = 1/3$ ,  $\gamma = 2$ , and  $\delta = 0.5$ , and  $\lambda$  will be made problem dependent (i.e., used as calibration factor).

Unlike in Stage 2, the average value of the friction coefficient  $C_{fm}$  will be left free to change, as KH waves develop on the interface. The value of  $C_{fo}$  used for the last iteration in Stage 2 (obtained as a function of user-supplied  $C_{fm}$  or  $C'_{fm}$  values; see Eq. (4.67)) will be used and kept constant in Stage 3, and the average friction will thus change as a function of time, for specified values of  $\lambda$  and  $\mathcal{K}$ , assuming that the other parameters have the values given above. Thus,

$$C_{fm}(t) = \frac{1}{L(t)} \int_0^{L(t)} C_f\{\xi, \lambda, \mathcal{K}, \phi_n(t), \phi_{tn}(t)\} d\xi \quad (4.144)$$

Both  $C_f$  and its derivative with respect to  $x$  (i.e.,  $\xi$ ; e.g. Eq. (4.127)) are needed to update the water-oil interface, using the second-order time stepping procedure. From Eq. (4.143),

$$\begin{aligned} \frac{\partial C_f}{\partial x} &= \frac{g C_{fo}}{U^2} \left\{ \left( 1 + \mathcal{K} \Delta t \left| \frac{\phi_{tn}}{\phi_n} \right| \right) \left\{ \mu e^{-\mu\xi'} + \frac{\alpha\gamma\chi}{\xi'} e^{-\beta\chi} (1 - \beta\chi) \right\} \right. \\ &+ \left. \Delta t \left( \mathcal{K} \left| \frac{\phi_{tn}}{\phi_n} \right|_{\xi'} + \frac{d\mathcal{K}}{d\xi'} \left| \frac{\phi_{tn}}{\phi_n} \right| \right) \left\{ 1 - e^{-\mu\xi'} + \alpha\chi e^{-\beta\chi} \right\} \right\} \end{aligned} \quad (4.145)$$

with,

$$\left| \frac{\phi_{tn}}{\phi_n} \right|_{\xi'} = \frac{U^2}{g \cos \beta} \left| \frac{\phi_n \phi_{tns} - \phi_{tn} \phi_{ns}}{\phi_n^2} \right| \quad (4.146)$$

with the subscripts  $s$  indicating the tangential  $s$ -derivative.

### 4.3.9 Time updating of slick geometry

An initial BEM discretization is defined for the water domain at  $t = 0$ , such as sketched in Fig. 4.16, using the slick shape calculated in Stage 2 [ $\eta^o(\xi)$ ,  $m^o(\xi)$ ]. The initial potential for the water flow velocity  $\overline{\phi}_o$  (calculated with Eqs. (4.101),(4.102)) is specified along the water-air and water-oil interface boundaries ( $\Gamma_{fa}$  and  $\Gamma_{fo}$  in the figure), along with other boundary conditions. Using SlickMap's interface, as in Stage 2, the user can easily define parameters for both the BEM discretization and time stepping procedures. These are the size of the BEM domain in front and behind the boom, node and element densities on each boundary segment of the BEM domain (Fig. 4.16), and the initial time step. Default values for the BEM parameters are

first proposed, that the user is then free to modify at will (see details in Chapter 5). The initial time step is calculated, based on selected node densities using the optimal Courant number criterion Eq. (4.115). This value is then automatically updated as a function of time, as grid resolution varies on the water-air and water-oil interfaces.

The time stepping method, described before, is used to calculate the change in shape of boundary  $\Gamma_f$  as a function of time, together with the water flow characteristics. For each new time  $t + \Delta t$ , pseudo-hydrostatic Eqs. (4.120)-(4.123) are integrated node by node along  $\Gamma_{fo}$ , with respect to  $\xi'$ , to calculate the updated slick geometry  $m(\xi, t + \Delta t)$ . For each time step, the geometry is smoothed and conservation of oil volume is specified.

More specifically, for each new time (step)  $t + \Delta t$ , the water upper boundary geometry and potential are first updated using Taylor series Eqs. (4.103). A 10th-order polynomial fit,  $P_\eta(\xi)$ , similar to those used in Stage 2 (see Eq. (4.79)), is applied to  $\eta$  between points A and B on Fig. 4.16, with zero slope in B, in order to remove small scale under-resolved geometric irregularities. A 4th-order polynomial fit, with initial tangent in A equal to  $U$ , is similarly applied to  $\phi$  between A and O and used to smooth results for the first few nodes on  $\Gamma_{fa}$ , next to point A, where small instabilities could otherwise occur, due to the strong incoming shear flow specified over the lateral boundary  $\Gamma_{r1}$ . New potential flow fields at  $t + \Delta t$ ,  $[\phi, \partial\phi/\partial n, \partial\phi/\partial t, \partial^2\phi/\partial t\partial n]$  and their  $s$ -derivatives are calculated next on  $\Gamma_f$ , using the BEM method; these are also smoothed, using a 2nd-order 7-point Savitzky-Golay filter, to remove under-resolved oscillations on the interfaces. The friction function  $C_f$  and its  $x$ -derivative are then calculated on  $\Gamma_{fo}$  for time  $t + \Delta t$ .

Integrating Eq. (4.123) for points  $i = 1, \dots, N_{sl} - 1$  on  $\Gamma_{fo}$  (from O to B), at  $t + \Delta t$ , we define,

$$\Delta m'_i = \int_i^{i+1} \frac{C'_f(\xi')}{2\varphi q'(s'(\xi'))} \cos\beta ds' \quad (4.147)$$

with the value of  $q'$  calculated with Eq. (4.121), and  $d\xi' = \cos\beta ds'$ , with  $s'$  the nondimensional curvilinear abscissa along the water-oil interface  $\Gamma_{fo}$ , discretized by  $N_{sl}$  points. These integrals are calculated by numerical integration (Gauss quadrature) within each BEM element of  $\Gamma_{fo}$ . Based on the oil-air interface geometry and Eq. (4.123), we define the residual function,

$$\mathcal{R} = \frac{1}{\cos\beta} \frac{\partial m}{\partial s} - \frac{C'_f}{2\varphi q'} \quad (4.148)$$

which tends to zero when pseudo-hydrostatic equilibrium equations are fully satisfied in the slick.

The slick updating to time  $t + \Delta t$  is performed as follows. The new value of the slick elevation at the boom skirt,  $m'(L', t + \Delta t)$  is first calculated using the vertical equilibrium Eq. (4.121) as,

$$\tilde{m}'_{N_{sl}} = \left(\frac{1}{\varphi} - 1\right) \eta'_{N_{sl}} + \frac{1}{\varphi} \{p'_D - p'_d - p'_i\}_{N_{sl}} \quad (4.149)$$

where the right-hand-side is calculated for  $\xi' = L'$  and surface tension effect is zero due to the horizontal tangent at the boom. We also have,

$$m'(L', t + \Delta t) = m'(L', t) + (1 - \rho) \{ \tilde{m}'_{N_{sl}} - m'(L', t) \} \quad (4.150)$$

where  $\rho$  indicates a relaxation coefficient (selected to 0.5 in SlickMap) aimed at stabilizing changes over one time step by partly using results from the previous time step. Finally, for  $i = N_{sl} - 1, \dots, 1$ , on  $\Gamma_{fo}$  we then have,

$$\begin{aligned} \tilde{m}'_i &= m'_{i+1} - \Delta m'_i \\ m'^c_i &= \left( \frac{1}{\varphi} - 1 \right) \eta'_i + \frac{1}{\varphi} \{ p'_D + \sigma'_{wo} \beta_{s'} - p'_d - p'_i \}_i \\ m'_i(t + \Delta t) &= m'_i(t) + (1 - \rho) \left\{ \frac{1}{2} \{ \tilde{m}'_i + m'^c_i \} - m'_i(t) \right\} \end{aligned} \quad (4.151)$$

where, again,  $\rho$  indicates the relaxation coefficient (selected to 0.5 in SlickMap), and the average  $m$  calculated with the vertical and horizontal pseudo-hydrostatic equilibrium equations (4.121) and (4.123) has been used.

At each time step, a residual root-mean-square error is calculated, using Eq. (4.148), for the equilibrium equations applied along the slick interface, as,

$$\text{RMS}_e = \left\{ \frac{1}{N_{sl}} \sum_{i=1}^{N_{sl}} (\mathcal{R}_i)^2 \right\}^{1/2} \quad (4.152)$$

### 4.3.10 Smoothing and oil volume conservation

A 5th-order polynomial fit  $P_m(\xi)$ , with zero extremity slope, similar to the one used at Stage 2 (see Eq. (4.79)), is first applied to the values of the oil-air interface,  $m_i(t + \Delta t)$  (for  $i = 1, \dots, N_{sl}$ ), newly calculated with Eq. (4.151) for time  $t + \Delta t$ . As in Stage 2, the new slick volume is given by,

$$V(t + \Delta t) = \sum_{l=1}^{N_{Pm}} \frac{1}{l+1} M_l L^{l+1} + \sum_{n=1}^{N_{P\eta}} \frac{n}{n+1} E_n L^{n+1} \quad (4.153)$$

where  $M_l$  ( $l = 1, \dots, N_{Pm} = 5$ ) and  $E_n$  ( $n = 1, \dots, N_{P\eta} = 10$ ) denote the coefficients of polynomials  $P_m$  and  $P_\eta$ , respectively. A volume error  $\Delta V(t + \Delta t) = V - V_o$  is thus found. Volume corrections are applied to the slick when  $|\Delta V/V| > \epsilon_v$  (with typically  $\epsilon_v = 1\%$ ).

When  $\Delta V > 0$ , the slick volume must be reduced and this is done as follows. The total volume error is divided into two parts :  $\Delta V_1 = \mu \Delta V$  and  $\Delta V_2 = (1 - \mu) \Delta V$ , with  $\mu \in [0, 1/2]$  (and typically  $\mu = 0.33$ ). The correction  $\Delta V_1$  is applied as a small triangular reduction in slick volume, right at the slick leading edge. The following

equation based on the polynomial curve fits for  $m$  and  $\eta$ , is solved for  $\xi^*$  by Newton iterations,

$$-\Delta V_1 = \sum_{l=1}^{N_{Pm}} \frac{1}{l+1} M_l (\xi^*)^{l+1} + \sum_{n=1}^{N_{P\eta}} \frac{n}{n+1} E_n (\xi^*)^{n+1} \quad (4.154)$$

which means that a new intersection point  $\xi = \xi^*$ , defining the new location of the slick leading edge, is found such that the volume from  $\xi = 0$  to that point is equal to  $\Delta V_1$ . Two cases are then considered :

- If  $\xi^* < 0$  : then no change in leading edge location should occur and the whole volume correction  $\Delta V$  is applied as a “triangular” correction with a reduction of slick elevation at the boom,

$$\Delta m = \frac{-2\Delta V}{L} \quad (4.155)$$

and a reduction of  $m$  from zero to  $\Delta m$ , proportionally to  $\xi$ , by adjusting one of the polynomial coefficients for  $m$  as follows :  $M'_1 = M_1 - \Delta m$  and  $M'_2 = M_2 + \Delta m/L$ .

- If  $\xi^* \geq 0$  : there is a change in leading edge location (note, we limit this change to a maximum horizontal change in slick length of  $L/20$  at any given time step). For the  $\Delta V_2$  correction, we calculate  $q^* = m(\xi^*) + \eta(\xi^*)$  and check whether the volume correction,  $\Delta \tilde{V} = q^*(L - \xi^*)/2$ , is greater than  $\Delta V_2$ . Then,

- If  $\Delta \tilde{V} > \Delta V_2$  : we apply a vertical correction,

$$\Delta m = \frac{-2\Delta V_2}{L - \xi^*} \quad (4.156)$$

at  $\xi = \xi^*$  and a reduction of  $m$  from zero at the boom, to  $\Delta m$  at the new leading edge, proportionally to  $L - \xi$ , by adjusting the polynomial coefficients for  $m$  as follows :  $M'_1 = M_1 + \Delta m L/(L - \xi^*)$  and  $M'_2 = M_2 - \Delta m/(L - \xi^*)$ .

- If  $\Delta \tilde{V} \leq \Delta V_2$  : we apply a trapezoidal correction to the slick, with vertical corrections,  $\Delta m_1 = q^*$  at  $\xi = \xi^*$ , and,

$$\Delta m_2 = \frac{2\Delta V_2}{L - \xi^*} - q^* \quad (4.157)$$

at  $\xi = L$  and a reduction of  $m$  from  $\Delta m_2$  to  $\Delta m_1$  from the boom to the new leading edge, proportionally to  $L - \xi$ , by adjusting the polynomial coefficients for  $m$  as follows :  $M'_1 = M_1 + (\Delta m_2 \xi^* - q^* L)/(L - \xi^*)$  and  $M'_2 = M_2 + (q^* - \Delta m_2)/(L - \xi^*)$ .

When  $\Delta V < 0$ , then the slick volume must be increased and this is done as follows. The total volume error is divided into two parts :  $\Delta V_1 = (1 - \mu) \Delta V$  and  $\Delta V_2 = \mu \Delta V$ , with  $\mu \in [0, 1/2]$  (and typically  $\mu = 0.33$ ). The correction  $-\Delta V_1$  is applied as a “triangular” increase in slick height, from the slick leading edge to the boom. We define,

$$\Delta m = \frac{-2\Delta V_1}{L} \quad (4.158)$$

and we specify an increase of  $m$  from  $\Delta m$  at the leading edge to 0 at the boom, proportionally to  $\xi$ , by adjusting the polynomial coefficients for  $m$  as follows :  $M'_1 = M_1 + \Delta m$  and  $M'_2 = M_2 - \Delta m/L$ . The correction  $\Delta V_2$  is applied as a small triangular volume at the leading edge. The following equation for  $\xi^*$  is first solved by Newton iterations,

$$-\Delta V_2 = \sum_{l=1}^{N_{Pm}} \frac{1}{l+1} M'_l (\xi^*)^{l+1} + \sum_{l=1}^{N_{P\eta}} \frac{n}{n+1} E_n (\xi^*)^{n+1} \quad (4.159)$$

where new polynomial coefficients  $M'_l$  are used for  $m$ , based on a second-order curve fit of the first eight corrected points of the slick oil-air interface, from the old leading edge. [This is to have a more stable way of extrapolating the slick position.] The new intersection point  $\xi = \xi^*$  thus defines a new location of the slick leading edge, such that the volume from  $\xi = 0$  to that point is equal to  $-\Delta V_2$ . Two cases are then considered :

- If  $\xi^* > 0$  : then no change in leading edge location should occur and the volume correction  $-\Delta V_2$  is applied as a “triangular” correction, with an increase of slick elevation at the boom,

$$\Delta m = \frac{-2\Delta V_2}{L} \quad (4.160)$$

and an increase of  $m$  from zero to  $\Delta m$ , proportionally to  $\xi$ , by adjusting one of the polynomial coefficients for  $m$  as follows :  $M'_1 = M_1 - \Delta m$  and  $M'_2 = M_2 + \Delta m/L$ .

- If  $\xi^* \leq 0$  : there is a change in leading edge location (note, we limit this change to a maximum horizontal change in slick length of  $L/10$  at any given time step). The 5th-order curve fit for  $m$  is re-calculated, for the whole slick, after new slick points have been added at the front of the old leading edge, using the 2nd-order local fit.

After slick volume corrections have been made, the total slick volume is re-calculated using Eq. (4.153), for the new polynomial curve fits that were corrected or re-applied to  $m$ . A final volume error  $|\Delta V/V|$  is then calculated and used in SlickMap as one of the measures of accuracy of calculations with the Stage 3 model. If  $\xi^* \neq 0$  then regridding of the BEM discretization is performed for the water-oil interface and the FCF  $C_f$  and its  $x$ -derivative are recalculated.

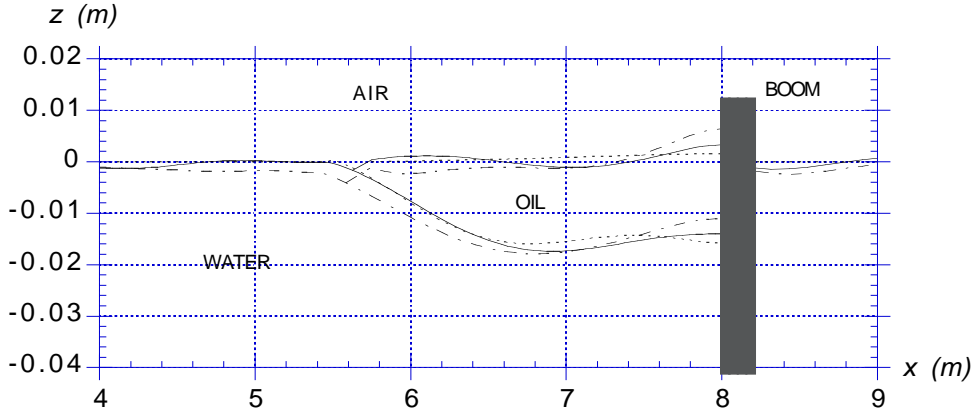


Figure 4.17: Results of computations with Stage 3 model for  $U = 0.1$  m/s,  $\varphi = 0.938$ ,  $\mu_o = 9.2$  Kg/m.s,  $\sigma_{ow} = 0.0379$  N/m,  $V_o = 0.03183$  m<sup>3</sup>/m,  $C_{fm} = 0.0185$ . Model parameters have the standard values ( $Y = 0.333$ ,  $\epsilon = 0.01$ ,  $\delta = 0.5$ ,  $\gamma = 2$ ,  $\lambda = 3$ ,  $\alpha_v = 0.05$ ,  $\mathcal{K} = 0.05$ ). Oil slick shape and free surface at  $t = (- \text{---} - \text{---})$  0; ( $- \text{---} - \text{---}$ ) 4.20; ( $\text{---}$ ) 8.64 s.

### 4.3.11 Results and discussion

Results of the Stage 3 model are illustrated by calculating the shape of a slick with physical parameters corresponding to Sundex oil spilled at sea :  $\varphi = 0.938$  (for  $\rho_w = 1,025$  kg/m<sup>3</sup>),  $\mu_o = 9.2$  Kg/m.s,  $\sigma_{ow} = 0.0379$  N/m. The slick linear volume is set to  $V_o = 0.0316$  m<sup>3</sup>/m and the initial average friction coefficient to  $C_{fm} = 0.0185$ , which corresponds to experimental results obtained at OHMSETT for  $U = 0.1$  m/s (Fig. 2.20). The boom skirt draft is set to 0.2 m, with skirt thickness 0.2 m in the current direction (note, due to vertical and horizontal scales distortion, the boom skirt does not appear with the right shape in the figures); the water depth is set to 1 m (i.e., 5 boom drafts). The domain is 13 m long (A-F on Fig. 4.16) with 8 m upstream of the boom. Stage 1 model was used to initialize computations, Stage 2 model was run for 10 iterations, and then the Stage 3 model was launched. The BEM discretization for Stage 2 and 3 models had 193 nodes on the free surface and slick interface upstream of the boom (A-B in Fig. 4.16), 23 nodes on the boom, 42 nodes on the free surface downstream of the boom (E-F), 9 nodes on each lateral boundary and 26 nodes on the bottom. Friction parameters have the standard values :  $Y = 0.333$ ,  $\epsilon = 0.01$ ,  $\delta = 0.5$ ,  $\gamma = 2$ ,  $\lambda = 3$ ,  $\alpha_v = 0.05$ ,  $\mathcal{K} = 0.05$ .

Two cases were successively solved, for  $U = 0.1$  and 0.3 m/s. In Fig. 4.17, for  $U = 0.1$  m/s, results are plotted for the initial slick shape, imported from the last iteration of the Stage 2 model for this case ( $t = 0$ ), and after 80 and 160 time steps, or  $t = 4.20$  and 8.64 s, respectively. The oil slick initially oscillates as Stage 3 model computations are started. Only small changes in slick shape (length and thickness), however, are observed as oscillations gradually damp out. Slick length  $L$  stabilizes

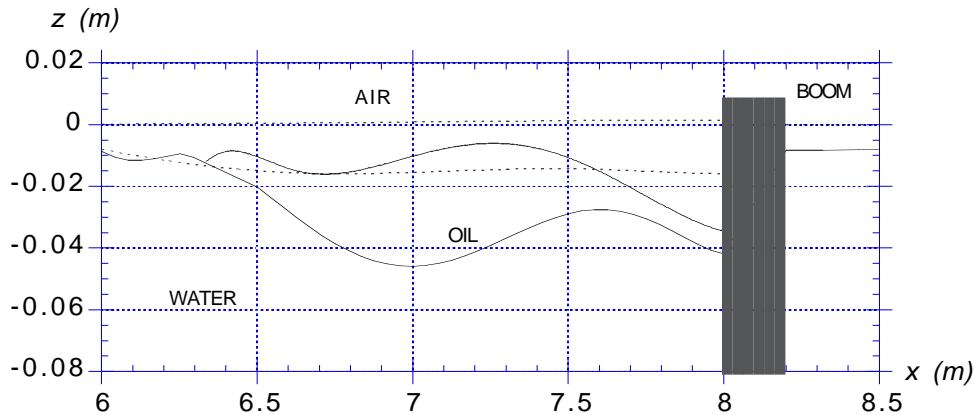


Figure 4.18: Same case as Fig. 4.17 for  $U = 0.3$  m/s. Oil slick shape and free surface at  $t = (- - - -) 0$ ; ( $—$ ) 5.46 s.

at about 2.4 m and the average slick thickness at about 0.013 m. For  $U = 0.3$  m/s, computations were first run with  $U = 0.1$  m/s for Stages 1 and 2, and for Stage 3 up to  $t = 1.05$  s. The current speed was then gradually increased to 0.3 m/s (over a 2 s period following a tanh law). With increasing speed, the oil slick shortened and thickened, and a large headwave developed, including oscillations of the slick in front of the boom. Fig. 4.18 shows results obtained after 100 time steps, or  $t = 5.46$  s. Slick length  $L$  has been reduced to about 1.6 m and average slick thickness increases to about 0.020 m. Slick shape, however, does not stabilize and many oscillations of the oil-water and oil-air interfaces occur. Computations for  $U > 0.3$  m/s quickly led to unstable shortening of the slick, identified as critical accumulation, and to eventual thickening of the slick at the boom up to reach the boom draft. BEM computations failed beyond that stage.

## 4.4 Conclusions and future developments

This Chapter described both the background for and the numerical models composing SlickMap, a user-friendly interactive software developed for the numerical modeling of oil containment by booms. SlickMap employs a graphical user interface (GUI) developed in the *Visual Basic*<sup>TM</sup> environment, for PC computer platforms.

SlickMap is divided into three stages of increasingly accurate modeling, first simulating static then real-time dynamic oil spill behavior, in a vertical plane through the boom apex. Stage 1 and 2 models predict the stable static shape of an oil slick, for low relative velocities. The Stage 3 model simulates the time dependent dynamic behavior of the slick-boom system. A data base of oil-boom experiments conducted at OHMSETT and UNH is available to assist users in setting up model parameters (essentially interfacial friction and dissipation terms). Model results are calibrated using

data collected in a carefully designed set of experiments performed at the OHMSETT facility. All models are linked to and run by SlickMap's GUI, which automatically sets-up data and grids for the models, using only a few simple user-supplied parameters. Graphical techniques are used to visualize model results.

SlickMap is not meant to be a closed system, and we anticipate further improvements in the underlying models and data bases. Other models could be easily accessed and run with minimum changes in SlickMap's GUI. Stage 1 and 2 models, for instance, are useful as stand-alone models, and can quickly provide shapes of contained oil slicks for various oil types and boom characteristics. It would thus be fairly easy, based on results of these models, and on OHMSETT's and UNH's experiments, to develop specific design tools in SlickMap, for use by spill response teams, providing maximum volumes of oil contained by a boom of given draft and shape (i.e., straight, catenary, . . . ), for specified oil types and relative current speed. SlickMap already has a tool that allows the user to estimate the standard linear volume of oil  $V_o$  ( $\text{m}^3/\text{m}$  of boom), based on the total oil volume  $v_o$  ( $\text{m}^3$ ) contained by a catenary-shaped boom. This tool could be modified to instead provide  $v_o$ , based on  $V_o$  calculated by Stage 1 and 2 models for conditions close to drainage failure.

SlickMap is to our knowledge the first experimentally validated comprehensive model of oil containment by booms that was developed in a user-friendly graphical environment, making it potentially accessible to a wide range of users, from modelers to (educated) field response team members. The ideal flow modeling approach used in SlickMap is simplified, compared to other proposed models based on full Navier-Stokes equations. The model, however, contains all the relevant physics for accurately simulating oil containment by booms. In particular, fully nonlinear kinematic and dynamic boundary conditions are included in the Stage 3 model, to accurately simulate changes in both free surface position, due to interaction of the boom with the water flow, and the various interfacial waves that develop during containment failure. Physical phenomena not specifically included in the model equations, such as interfacial friction, are modeled using semi-empirical equations and calibrated based on experimental results. All model parameters, both physical and numerical, can be accessed and modified by users. SlickMap's models are efficiently implemented, using accurate state-of-the-art numerical methods such as the BEM. Hence, SlickMap can be set-up and run in a matter of minutes on a high end PC platform (typical recommended minimum configuration is P5-200MHz with 64Mb of RAM).

As discussed earlier, we anticipate further developments of SlickMap in several directions. In its present stage of development, however, SlickMap can provide both significant insight and useful quantitative results regarding oil slick containment by booms. Finally, it should be pointed out that SlickMap is not a turn-key system that can be run as a black box, despite its friendly GUI. The system still requires the user to fully understand both the physics modeled (or not modeled) and the various underlying hypotheses used in SlickMap models.

# Chapter 5

## SlickMap user manual

### 5.1 Introduction

A user's manual describing how to set-up and use SlickMap software on a PC computer platform is presented in the following. SlickMap is an interactive software product designed at the University of Rhode Island to simulate oil spill containment by a straight boom with a vertical skirt (Chapter 4).

SlickMap was designed to model slicks spilled upstream of straight boom placed in a water flow, i.e., booms for which no or little change occurs along the boom axial direction. For such booms, it is accurate to study oil containment in a two-dimensional vertical cross-section going through the boom middle section (apex). However, experimental studies conducted at OHMSETT as part of this project (Chapter 2) showed that, assuming proper scaling, results of experiments with a towed boom having a catenary shape can be transformed into results applicable to an equivalent straight boom. In such a case, the scaled variation of slick length measured in front of the boom apex as a function of tow speed, quite well agrees with that measured for the same boom having a straight shape. In SlickMap, a pre-design tool is thus provided to help the user transform the oil slick volume  $v_o$  (given in  $\text{m}^3$ ), corresponding to a boom with catenary shape of specified characteristics, to an equivalent linear volume  $V_o$  (in  $\text{m}^3/\text{m}$ ), to be used in SlickMap for running simulations with a straight boom. In addition, the user must provide oil parameters (density, viscosity, surface tension) boom geometry (skirt draft and width) and water density and flow velocity.

Models implemented in SlickMap rely on a number of simplifying assumptions, such as an inviscid water flow and a quasi-static equilibrium within the slick (Chapter 4). Dissipative mechanisms, such as interfacial friction variation at the water-oil interface and slow viscous circulation within the slick are represented in the models by semi-empirical equations. Experiments carried out at OHMSETT (Chapter 2) and at the University of New Hampshire (Chapter 3) were used to calibrate parameters in these semi-empirical representations. SlickMap model results therefore only have predictive ability within the range of experimental parameter variations for which

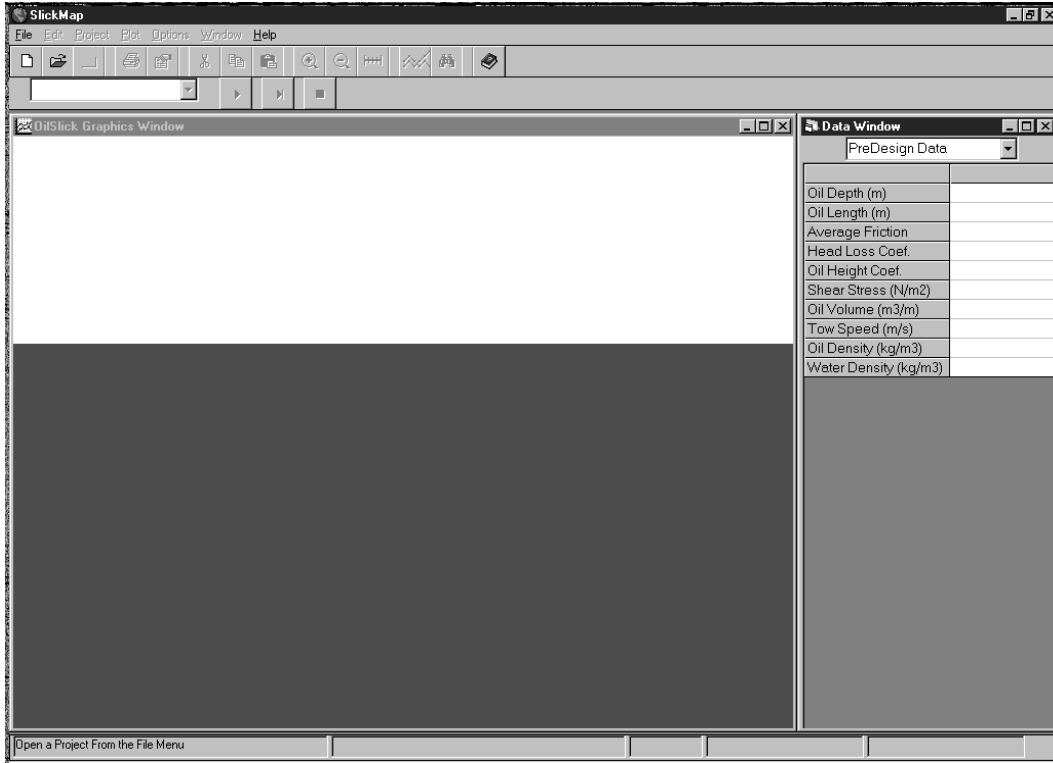


Figure 5.1: Typical SlickMap interface screen

dissipation in the models was calibrated : i.e., a boom draft  $d = 0.064$  to  $0.483$  m (2.5 to 19 in.), Sundex or Hydrocal oil, and a tow speed  $U = 0.1$  to  $0.45$  m/s (0.2 to 0.9 Kn). For intermediate values of draft or tow speed, SlickMap linearly interpolates experimental data in order to calibrate interfacial friction parameters.

SlickMap is implemented as an interactive Graphical User Interface (GUI), programmed in *Visual Basic*<sup>TM</sup> (Fig. 5.1). SlickMap's models are programmed in FORTRAN. The GUI is specifically designed to be user-friendly and work efficiently with the FORTRAN codes of the models. These models represent the implementation of various Computational Fluid Dynamics (CFD) tools developed to simulate oil slick containment by straight booms, with vertical skirts, placed transversally in a water flow (Chapter 4). These models assume ideal flows (incompressible, inviscid, and irrotational), for which a velocity potential can be defined. The governing equation is thus a Laplace's equation for the potential, which expresses mass conservation. Boundary conditions are specified to describe the solution behavior on the lateral boundaries (inflow and outflow), on the free surfaces (before and beyond the boom) and on the boom and bottom (no-flow).

The key computational models in SlickMap are based on a Boundary Element Method (BEM). The BEM is a numerical method used for the efficient and accurate numerical solution of partial differential equations (such as Laplace's equation), over

domains of complex shape. It is based on a Boundary Integral representation of the governing differential operator. Hence, the BEM uses no interior discretization but only a boundary discretization. Collocation nodes are placed on the boundary of the domain and elements, i.e., small pieces of the boundary are used to define a certain level of interpolation of both the geometry and the field variables in between the nodes. SlickMap enables the user to control the node and element generation on the boundary, for use in the BEM models. The computational domain and boom geometry must first be specified and then the boundary discretization (grid) is generated. SlickMap suggests default values for both the geometry and grid on various parts of the boundary. These can be modified at will by the user before further analyses are performed.

SlickMap's solution of a slick containment problem is run in three stages. The first stage is used to find the initial (static) shape of an oil slick, of specified characteristics, when a boom is deployed to contain the slick, and an initial flow velocity is also specified; no water flow computation is performed at this stage which just uses static equilibrium and energy conservation equations to estimate slick shape. The second stage is used to refine the first stage estimate and find the steady state solution of the oil slick shape; the ideal water flow is solved at this stage, while slick shape is being iteratively refined again using static equilibrium and energy conservation equations. The third stage uses results of the second stage as initial conditions to simulate the dynamic behavior of the contained slick as a function of time. The ideal flow solution is still performed in the water, for each time level (or step) in the simulation, but various interfaces (oil-water, oil-air and water-air) are treated as dynamic free surfaces, as opposed to the rigid (no-flow) boundaries used for stages 1 and 2. SlickMap's GUI allows the user to control all the parameters of the analyses performed at stages 1 to 3, both physical (as mentioned above) and numerical (grid generation, number of iterations for convergence of slick shape, ...). The entire purpose behind SlickMap's GUI is to provide easy to understand results of the model solutions.

Details of the Stage 1, 2, and 3 models equations and implementations can be found in Chapter 4. A complete user's manual for SlickMap's GUI is given in the following.

## 5.2 Installation and setup

For SlickMap to run properly the following minimum requirements for the PC platform are suggested.

- Operating System - Win9x
- Processor Speed - 75 MHz or greater
- Random Access Memory - 32M or greater

To install and setup SlickMap onto a PC, insert the SlickMap installation CD into the CD-ROM drive. If the setup program doesn't automatically execute simply run setup.exe off the CD-ROM drive to initialize the setup procedure. Once setup.exe is executed, installation files will be generated before the SlickMap setup window is opened. From the SlickMap setup window choose *OK* to continue the setup procedure. Next, the directory where SlickMap will be installed is displayed, given the option to change this directory (it is recommended to use the default directory location to reduce run time errors with SlickMap). Clicking on the provided button on the SlickMap setup window will now install SlickMap into the specified directory. Once the setup application is finished SlickMap is ready for execution.

## 5.3 Getting started

### 5.3.1 Opening SlickMap

Installing SlickMap will create a shortcut available in the start menu program options and on the windows desktop. This shortcut is titled SlickMap and will open the software (SlickMap.exe) when selected. SlickMap may also be opened from the directory where it was installed. This directory (if not chosen otherwise) is the default directory (C:\SlickMap\Bin\) provided in the setup process (see Section 5.2). Opening SlickMap will produce a graphical window such as displayed in Fig. 5.1. The software is now ready for executing a project.

### 5.3.2 SlickMap project philosophy

Under SlickMap's design philosophy, certain steps are required to properly setup a project for execution and analysis. Three basic preliminary steps, with the second step being optional, are necessary to properly setup a project. Once these three preliminary steps are complete, the project is ready for execution. After execution of the project is finished, analysis and post-processing of SlickMap's project results can be done using various tools, provided in SlickMap's GUI, or with any other software package that is useful to analyze the data output from the source code. The following outline is the basic SlickMap project philosophy, or necessary steps taken to build, solve, and analyze a project :

1. **Opening Project** (Section 5.4 : *Starting a new project*)
2. **Creating Database** (Section 5.5 : *Building a database*)
3. **Predesign Project** (*Optional* Section 5.6 : *Predesign toolbox*)
4. **Execute Project** (Section 5.7 : *Executing a project*)
5. **Analyze Results** (Section 5.8 : *Analysis options*)

Details of each step are given in the following sections.

## 5.4 Starting a new project

To start a new project, the user first opens the program by clicking on the SlickMap.exe icon. Then, one either selects *New Project* from the *file* option on the menu, or clicks on the “open new project” button on the toolbar (see below).



The window shown in Fig. 5.2 will next appear on the screen. This window provides the user with the ability to create a “Project Folder”. SlickMap does not run off an individual file but off several files that are created and used at various stages of the simulation. Consequently, when creating a new project, a “Project Folder” should be created where all the information for that project will be stored and accessed by various modules in SlickMap. Typically, all “Project Folders” should be created as a sub-folder in the *Projects* folder, but the user can also elect to create a folder anywhere on the hard drive.

To create a “Project Folder”, simply select which directory the folder will be located in and then click on the “Create Folder” button. This will open a window, which will ask for the name of the “Project Folder” to be entered. After selecting a name for the “Project Folder”, the program will request that a name be given to the Project. If no name is entered, then the name given to the “Project Folder” will be used by default as the project name.

If no “Project Folder” name is entered, then no “Project Folder” will be created and a project name should not be entered. If this happens, select cancel when asked to enter a project name and start over.

Once a Project Folder is created, the window shown in Fig. 5.2 will display that SlickMap is now currently working under the created Project Folder. Select OK to begin working on the newly created project. The next step to take when setting up a project in SlickMap is to build a database.

## 5.5 Building a database

Once a “Project Folder” has been created, building a database for the current project is the next procedure required. The database will control all physical and numerical parameters of the oil slick containment simulation. These parameters range from physical properties of oil and water, boom and domain geometry, to grid generation parameters of the model. Building a database is essential to run a simulation. Without

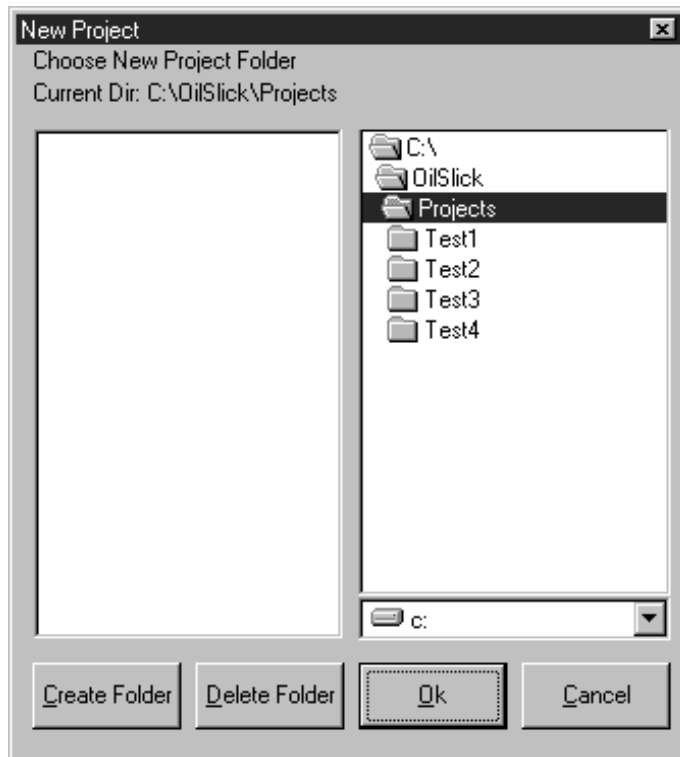


Figure 5.2: SlickMap open project window

a database, the source code has no parameters to use for the analysis.

To build a database, select the option “Build Database”, from the “Project” menu. This will open the database building tools window (Figure 5.3). This window has three main sections, which control different parameters of the simulation, denoted by three different tabs. The first section handles the geometric and physical data in the problem, the second section defines the generic numerical data used for the BEM models in stages 2 and 3, and the third section is nodal data which will ultimately define the BEM grid used to solve the problem. There are three different ways to build a database from scratch : (1) use user defined values; (2) use default data provided by the software; or (3) *Pre-design* the problem using data collected during experimental tests at OHMSETT. The latter two options will be discussed later. The next section will concentrate on defining all the values for the parameters (option (1)), and how these affect the final solution of the problem.

How to wisely choose the proper values for all parameters while building a database will be discussed later.

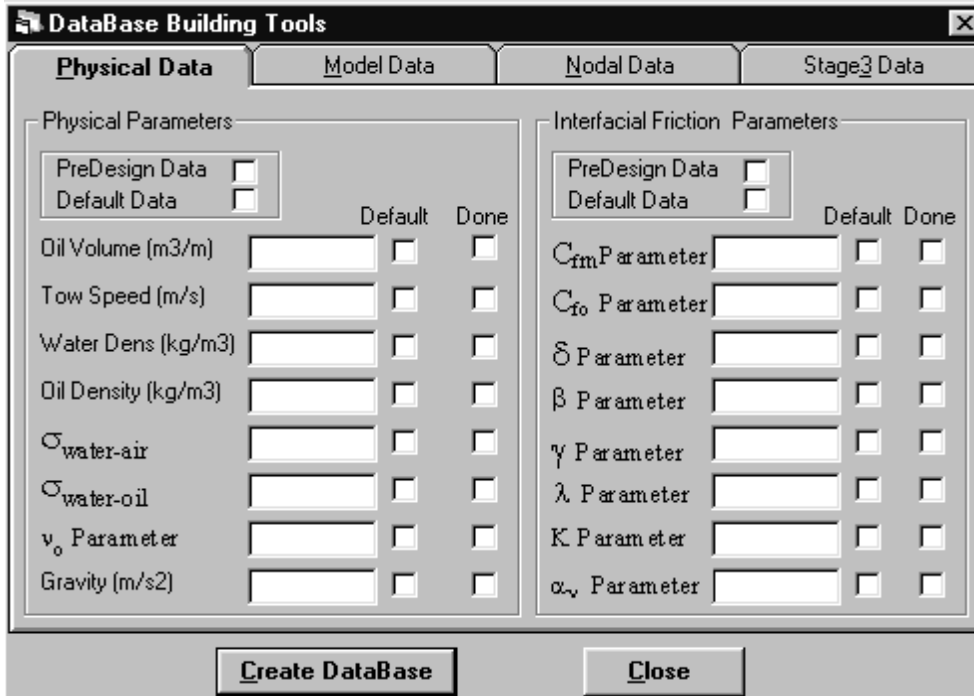


Figure 5.3: Database Building Tools Window

### 5.5.1 Defining parameters of database and building tools window

There are three sections contained within the database building tools window.

The *first section* deals with the physical data of the problem. Two subsections are defined under this section : (i) physical parameters; and (ii) interfacial friction parameters. The first subsection requires the user to specify the physical parameters of the solution, labeled and defined below :

- Linear oil volume ( $V_o$ ) : the oil volume is defined for this problem as the volume of oil per unit width of boom, expressed in cubic meters per meter ( $m^3/m$ ). [Note that a special tool is available to transform the volume of the slick in a catenary shaped boom ( $v_o$  in  $m^3$ ) into a linear volume for an equivalent straight boom. See predesign section]
- Initial tow speed ( $U_o$ ) : This is the relative flow speed between the boom and the water, expressed in meters per second ( $m/s$ ). This speed is used to calculate an initial (static) slick shape, implicitly assumed to be stable. Thus the initial speed should be low enough (typically around 0.1  $m/s$ ). [Note, a gradual speed increase from  $U_o$  to a larger value can be specified in SlickMap by choosing to build a database with a velocity ramp (See Section : *Building a database with a velocity ramp*).]

- Water density ( $\rho_w$ ) : the density of water over which the oil is located, expressed in kilogram per cubic meter ( $\text{kg}/\text{m}^3$ ).
- Oil density ( $\rho_o$ ) : the density of oil in the slick, expressed in kilogram per cubic meter ( $\text{kg}/\text{m}^3$ ).
- Water-air interfacial tension ( $\sigma_{wa}$ ) : expressed in Newton per meter ( $\text{N}/\text{m}$ ).
- Water-oil interfacial Tension ( $\sigma_{wo}$ ) expressed in Newton per meter ( $\text{N}/\text{m}$ ).
- Oil kinematic viscosity ( $\nu_o$ ) expressed in Stokes ( $\text{cm}^2/\text{s}$ ).
- Gravitational acceleration ( $g$ ) : the acceleration due to the force of gravity expressed in meters per second squared ( $\text{m}/\text{s}^2$ ; typically  $9.81 \text{ m}/\text{s}^2$ ).

The second subsection under the physical data section handles the water-oil interfacial friction parameters defined below :

- Average friction coefficient ( $C_{fm}$ ) : this parameter defines the initial value of average friction used to calculate the oil-water interface shape for a flow speed  $U_o$ .
- Friction function parameters (see Chapter 4) : These are the nondimensional parameters used to define the functional form of the interfacial coefficient function in Stage 2 and 3 models, i.e. :
  - $C_{fo}$  : friction coefficient function value in the back of the slick.
  - $\lambda \geq 1$  : coefficient defining the maximum value of the friction function in the slick headwave, in terms of multiples of  $C_{fo}$  (increases with  $\lambda \geq 1$ ).
  - $\gamma$  : coefficient defining the peakedness of the friction function in the slick headwave (increases with  $\gamma$ ).
  - $\delta$  : coefficient which specifies where the maximum value of the friction function occurs in the slick headwave (varies from 0 to 1 from front to back of headwave).
  - $\mathcal{K}$  : coefficient which specifies the intensification of friction due to KH waves for Stage 3.
- viscous slick circulation :  $\alpha_v$  coefficient which specifies which part of the tangential velocity in the water along the oil-water interface is transmitted to the slick to induce a slow viscous circulation.

The *second section* in the database building tools window deals with model data. Two subsections in this section are defined for : (i) grid parameters; and (ii) Stage 2 iterations and time stepping data. The grid and iterations parameter subsection defines the geometry of the boom being used in the simulations and requests information

about the desired grid for the BEM. The size of the grid directly affects the accuracy of results; an increased resolution, beyond the required minimum, usually leads to more accurate results but requires longer computational times. These parameters are as follows :

- $d$  : draft of boom skirt used for the oil containment simulations (in meters).
- $W$  : width of boom skirt used for the oil containment simulations (in meters).
- Modeled distance upstream of boom : horizontal distance from the boom to the front of the BEM grid (in meters).
- Length of BEM grid : total horizontal length of BEM grid from front to back (in meters).
- $h$  : water depth : vertical distance from mean free surface to bottom (i.e. grid height in meters).

The iteration data subsection defines information about the maximum number of iterations allowed to calculate the convergence to steady state in Stage 2 model, and which minimum residual error between iterations is acceptable before steady state is reached. Thus, Stage 2 model calculations will be stopped whenever the maximum number of iterations or the minimum residual error are reached.

The *third section* in the database building tools window is grid nodal data. This section defines the way the boundary element grid is constructed and thus controls the resolution and accuracy of the BEM computations in SlickMap models for Stages 2 and 3. Two subsections are also defined within this section : (i) node spacing data; and (ii) node data. Parameters are as follows :

- Spacing upstream of boom : Initial node spacing on the free surface of the boundary element grid, from the leftward side up to the location of the boom.
- Spacing downstream of boom : Node spacing between each node on the free surface of the boundary element grid, from the boom to the rightward side.
- Spacing on bottom : Node spacing between each node on the bottom of the boundary element grid from the leftward to the rightward sides.
- Nodes on boom : Number of nodes located on the grid representing the boom boundary; these nodes will be equally spaced.

The boom is made of linear straight segments separated by quarter of circles of radius  $W/10$ , representing the two bottom corners of the skirt.

- Nodes on Vertical Boundaries : The number of nodes on the vertical side boundaries of the BEM grid (in- and out-flow boundaries).

The *fourth section* is labeled Stage 3 Data. This section contains one subsection titled *Simulation time data*. When selecting to build a database with a velocity ramp, an additional subsection (titled *Velocity time stepping data*) is provided to allow the user to define the desired velocity stepping information. This option is discussed in Section *Building a database with a velocity ramp*. Within this subsection, one may define parameters controlling the temporal simulations of Stage 3, which are labeled and defined as follows :

- Simulation Time : Amount of time (in seconds) requested to run Stage 3 model solution.
- Maximum Time Step : The maximum duration of time steps (in seconds) used in Stage 3 model computations.
- Release Time : The amount of time requested to allow the water to stabilize, when starting Stage 3 computations based on Stage 2 results, before releasing the entire system into the dynamic Stage 3 state (Note, during this stabilization time, the oil slick geometry is not updated, but just vertically moved to follow the water motion, while the water-oil interface is being updated as a function of time).

### 5.5.2 Working with the database building tools parameters

To wisely build a database that will enable the source code to accurately produce results, knowledge of how the parameters in the database will affect the final solution is key. This section explains how to wisely build a database.

#### Physical parameters

The linear oil volume  $V_o$  is crucial to the problem's solution. SlickMap assumes straight booms and uses a value of volume per unit length, i.e., the linear oil volume. In general, this measurement is the total volume of oil being contained divided by the width of the containment area. For example, if the boom skirt has a horizontal width of  $w = 10$  ft and  $v_o = 200$  gallons of oil are being contained, then the amount of oil used for this problem would be  $V_o = v_o/w = 20$  gal/ft. Since this program is designed to work in the metric system (SI; International system), this value needs to be converted, i.e., using  $3.81 \cdot 10^{-3}$  m<sup>3</sup>/gal and 0.3048 m/ft, respectively. Applying these conversion factors the final value of  $V_o$  used in this problem is 0.250 m<sup>3</sup>/m.

Whereas stationary booms installed across flowing rivers may be fairly linear and straight in shape, most towed booms often take a catenary shape. As mentioned above, SlickMap provides a tool to users, to calculate the equivalent linear volume  $V_o$  for a straight boom, when given the *gap-to-boom-length* value  $g_o/\ell$ , and the number of boom segments, based on the equations detailed in Chapter 2.

Initial tow speed should be around  $U_o = 0.2$  knot (0.1 m/s). Tow speed variation should be specified in between that value and a maximum of about  $U \simeq 1$  knot (0.5 m/s). Experiments have proven that most conventional booms fail at a critical speed of 1 knot or less (e.g., Chapter 2). With this in mind the program has been designed to work best within the above specified tow speed range. Although any tow speed can be used in a simulation the results may sometimes become unrealistic.

Water density and oil density are self-explanatory. These parameters are simply the densities of the fluids, oil and water, in the simulation. Water-air and water-oil interfacial tension values may be harder to identify, as well as oil viscosity. Usually, however, when not directly known, oil density, viscosity, and interfacial tensions can be found in tables, for standard oils, as a function of the operating temperature. Gravitational acceleration also, for all practical purposes, can be assumed constant to,  $g = 9.81$  m/s<sup>2</sup>.

### **Interfacial friction parameters**

These parameters are very crucial to the results of the model simulation. Unless the user has knowledge of friction coefficients for the given fluids in the problem, the best option is to use the default values provided by the SlickMap. Using default values will be discussed in a later section.

Defining  $C_{fm}$  will provide an initial value of the average friction coefficient, for the numerical model to use while initializing a static oil slick shape (Stage 1 model). By defining the remaining terms in this database section the user is allowed to control the way friction varies along the oil-water interface, i.e., the “Friction Coefficient Function” (FCF) (Chapter 4).

### **Grid length parameters**

All values used in this section will directly control the size and geometry of the BEM grid. Here the draft of the boom and width of the boom should be the exact dimensions of the boom desired to be modeled. The distance specified upstream of the boom is a crucial dimension which ultimately affects the uniform flow velocity specified, upstream of the slick, within the water column. The total length of grid will not play as crucial a role as the distance upstream of the boom but should be no less than twice that distance. Water depth is a key dimension, which also effects the uniform flow velocity within the water column. If this parameter is not specified properly the water velocity profile will not be accurately represented by the source code.

SlickMap’s GUI verifies upper and lower bounds on some of the parameters so a user will not be able to enter a value that is unreasonable for the problem. These bounds on the parameters are discussed in Section 5.5.4.

## **Iteration and time stepping data**

Stage 2 and 3 parameters are both defined within this database building tools section. It is here that the user will define iteration and time stepping data that will allow the source code to properly simulate the shape of the oil slick for a given tow speed. The first parameters defined in this section are the number of iterations required for the quasi-static oil slick shape to converge, and the maximum allowable Root-Mean-Square (RMS) error (measured in percentage) between slick shapes calculated for successive iterations with Stage 2 model, and for the verification of quasi-hydrostatic equilibrium equations.

Time stepping information is defined for Stage 3 model. The key parameters here are the maximum number of time steps and/or maximum time of stepping. Stage 3 model solves the oil slick equilibrium shape as it evolves in time, such that after a certain time period the slick will either have stabilized for a given tow speed or will have entered an unstable shortening mode. Thus, it is important that an adequate time duration be used in order for the slick to properly reach stabilization, when that occurs.

## **Node spacing data**

Since the solution of the oil slick shape is the critical aspect of this software the boundary element grid may have nodes spaced differently according to their location. The node spacing from the front of the grid to the boom is the most important discretization area to provide accuracy along the oil-water and oil-air interfaces. These nodes are spaced closer together than nodes located on the bottom of the grid and from the boom to the back of the grid.

Again, these values are bounded to assure that the user doesn't enter unrealistic values (see Section 5.5.4).

## **Node data**

These values are defined to suit the values entered for the node spacing data. Typically a user will specify the node spacing for the boundary element grid. This, in turn, will define the number of nodes on each surface, depending on the specified lengths of the grid. To improve accuracy of results, the user may increase the number of nodes for these parameters. This will help avoid reduce numerical errors in the source code and will improve resolution along these interfaces. Computational time, however, will be increased accordingly, typically, proportionally to the square of the total number of BEM nodes.

### 5.5.3 Using the default Database values

The default values provided by SlickMap were chosen based on the experimental results from tests conducted at UNH and OHMSETT. SlickMap default values are calibrated according to these experimental results. First the default values will be detailed then explained why they should be used when necessary. Default parameters, which are dependent upon other parameters and bounds placed on particular database parameters are discussed in Section *Controlled and dependent default database parameters*. The following are tables for the default values used in each section while building a database in SlickMap.

Parameter	Default Value
Oil linear volume $V_o$ ( $\text{m}^3/\text{m}$ )	0.0253
Tow speed $U$ (m/s)	0.1
Water density $\rho_w$ ( $\text{Kg}/\text{m}^3$ )	1,025
Oil density $\rho_o$ ( $\text{Kg}/\text{m}^3$ )	950
Oil viscosity $\nu_o$ (cSt or $\text{mm}^2/\text{s}$ )	10,000
Interf. tension $\sigma_{wa}$ (N/m)	0.0744
Interf. tension $\sigma_{wo}$ (N/m)	0.0379
Gravity Constant $g$ ( $\text{m}/\text{s}^2$ )	9.81
Friction parameter $C_{fm}$	0.05
Friction parameter $C_{fo}$	0.025
Friction parameter $\delta$	0.5
Friction parameter $\beta$	0
Friction parameter $\gamma$	2
Friction parameter $\lambda$	3
Friction parameter $\mathcal{K}$	0.05
Circulation parameter $\alpha_v$	0.05

Table 5.1: Default physical data values in SlickMap. Note oil data corresponds to Sundex oil.

In Table 5.1 the physical parameter default values are taken from some of the experiments conducted at OHMSETT (Chapter 2). The oil volume, which is the linear oil volume, is taken from experiments conducted during May 1997. The densities chosen are nominal values for sea water and Sundex oil, both used during the experiments. The surface tension values are from the fluid physical properties data reported to URI from OHMSETT, after fluid properties were analyzed at the OHMSETT facilities. All default interfacial friction parameters were developed to properly calibrate friction along the oil-water interface and produce results measured during field experiments at OHMSETT.

Parameter	Default Value
Draft of boom (m)	0.2
Width of boom (m)	0.2
Distance upstream of boom (m)	8.00
Length of grid (m)	13.00
Water depth (m)	1
Number of Stage 2 iterations	10
RMS error for Stage 2 (%)	0.5
Max. nb. of Stage 3 time steps	150
Max. time of Stage 3 stepping (s)	300

Table 5.2: Default Stage 2 and 3 model data values : geometry of computational BEM domain and numerical parameters.

The default grid length data values in Table 5.2 are partly dependent on the physical parameters. The draft and width default values are chosen arbitrarily. The distance in front of the boom is defined here as forty times the boom draft. Length of the grid is by default here the distance in front of the boom plus 60%, plus boom width. Water depth is selected to five times the boom draft. The number of iterations and time steps are chosen based on observations made for how many iterations the source code typically requires to solve a quasi-static equilibrium shape at Stage 2, and how many time steps are typically needed to achieve a stabilized slick shape at Stage 3 for one velocity value. Residual Iteration Error is by default one fifth of a percent. This is the RMS error in percentage of the slick shape change between 2 iterations and for the verification of equilibrium equations, that would cause the source code to find a quasi-static equilibrium shape before the specified number of iterations have been reached. Maximum time is arbitrarily chosen as 300 seconds.

Parameter	Default Value
Spacing upstream of boom (m)	0.04
Spacing downstream of boom (m)	0.10
Spacing on bottom (m)	0.50
Nb. of nodes on boom	23
Nb. of nodes up to boom	201
Nodes on free surface	250
Nodes on vert. boundaries	9

Table 5.3: Default Stage 2 and 3 model data values : node spacing and numbers.

The node spacing parameters in Table 5.3 are dependent more on previous defined data than any other set of data. Node spacing upstream of the boom is set by SlickMap as boom draft divided by five. Node spacing after the boom is set to equal half the draft of the boom. Node spacing on the bottom of the BEM grid is defined as the minimum value of the grid length divided by twenty five or half the water depth. The number of nodes on the boom is set as twenty three. The amount of nodes the user can specify on the boom is controlled by SlickMap and can only be increased by multiples of 4 nodes (i.e., 23, 27, 31, . . .). Number of nodes up to the boom is by default the distance in front of the boom divided by the node spacing prior to the boom plus one. The number of nodes on the free surface is set as the length of grid, minus the distance upstream of the boom, and the width of the boom, divided by the spacing downstream of the boom, plus the number of nodes up to the boom, plus one. Number of nodes on the vertical boundaries is set as nine and is also controlled by SlickMap and can only be increased by multiples of 2 nodes (i.e., 9, 11, 13, . . .).

#### 5.5.4 Controlled and dependent default database parameters

This section defines database parameters used for the Stage 2 and 3 models, which are dependent on other parameters or have bounds attached to them and verified by SlickMap. First, we will define the dependent parameters as well as the parameters used to define these values.

- Draft of Boom ( $d$ )
- Width of Boom ( $W$ )
- Length of Grid ( $L_g$ )
- Length of Oil Slick ( $L$ ) (estimated at Stage 1)
- Water Depth ( $h$ )
- Distance upstream of boom ( $D_1$ )
- Node spacing upstream of the boom ( $S_1$ )
- Node spacing downstream of the boom ( $S_2$ )
- Node spacing on the bottom ( $S_3$ )
- Nodes nb. on boom ( $N_1$ )
- Nodes nb. up to boom ( $N_2$ )
- Nodes nb. on free surface ( $N_3$ )

- Nodes nb. on vertical boundaries ( $N_4$ )

Now the dependent default parameters are expressed as a function of the other database parameters.

$$C_{fo} = \frac{C_{fm}}{2} \quad (5.1)$$

$$h = 5d \quad (5.2)$$

$$L_g = 75d \text{ or } 55d + L \quad (5.3)$$

$$D_1 = L + 30d \text{ or } 40d \quad (5.4)$$

$$S_1 = \frac{L}{30} \text{ or } \frac{d}{5} \quad (5.5)$$

$$S_2 = \frac{d}{2} \quad (5.6)$$

$$S_3 = \frac{L_g}{25} \text{ or } \frac{h}{2} \quad (5.7)$$

$$N_2 = \frac{D_1}{S_1} + 1 \quad (5.8)$$

$$N_3 = \frac{L_g - D_1 - W}{S_2} + N_2 + 1 \quad (5.9)$$

In Eqs. 5.4, 5.5, and 5.7, the dependent parameter is equal to the minimum value of the functions defined. To ensure that the user does not enter an unreasonable value that would cause the source code to crash, controls have been placed on two of the database parameters. These parameters are the number of nodes on the boom ( $N_1$ ) and the vertical boundaries ( $N_4$ ). Both of these parameters are controlled in a similar manner. Each has minimum and maximum values, and if they are between these minimum and maximum values, their values must also be a specific integer value, which is defined as a certain multiple times a constant. These controls are detailed in Tables 5.4 and 5.5.

User Input	Controlled Value
$N_1 < 23$	$N_1 = 23$
$N_1 > 55$	$N_1 = 55$
$23 \leq N_1 \leq 55$	$N_1 = 23 + (4I)$

Table 5.4: Controls on  $N_1$ .

In Table 5.4, the value  $I$  is an integer value between zero and nine. The value of  $I$  used is found by determining the user input value of  $N_1$  that is larger than  $23 + (4I)$ , but is less than  $23 + (4(I + 1))$ . In Table 5.5, the value  $I$  is also an integer value between zero and nine, which value is found by determining the user input value of  $N_4$  that is larger than  $9 + (2I)$ , but is less than  $9 + (2(I + 1))$ .

User Input	Controlled Value
$N_4 < 9$	$N_4 = 9$
$N_4 > 29$	$N_4 = 29$
$9 \leq N_4 \leq 29$	$N_4 = 9 + (2I)$

Table 5.5: Controls on  $N_4$ .

### 5.5.5 Building a database with a velocity ramp

To build a database with a velocity ramp, the same procedures as discussed earlier should be used, except that, when selecting an item under *Build Database* from the *Project Menu*, instead of choosing to build a database *Without Velocity Ramp*, choose to build a database *With Velocity Ramp*. This sequence will open Figure 5.4). The only difference when building a database with a velocity ramp is that an additional subsection in the DataBase Building Tool, titled *Velocity Time Stepping Data*, is provided. Within this subsection information about the desired kind of velocity steps to occur during Stage 3 analysis is enter. This information is labeled and defined below :

- Maximum Velocity : The maximum tow/flow velocity attained during the Stage 3 solution, measured in meters per second.
- Number of Steps : The number of times the tow/flow velocity is increased during a Stage 3 solution.
- Stepping Time : Amount of time in seconds between each velocity increment.

## 5.6 Predesign toolbox

An additional option provided by SlickMap to help building a database is the Pre-design ToolBox (Figure 5.5). This feature is designed to allow a user to interactively design the physical parameters of a database, three different ways. The three options provided to predesign a database are titled as follows :

- User defined data
- Experimental data
- Catenary boom data

If a user has already predesigned a project and wishes to create a new database for the same project, after already creating one, using the same predesign data, selecting *Predesign Values* from the *Database Building Tools* window will access these values.

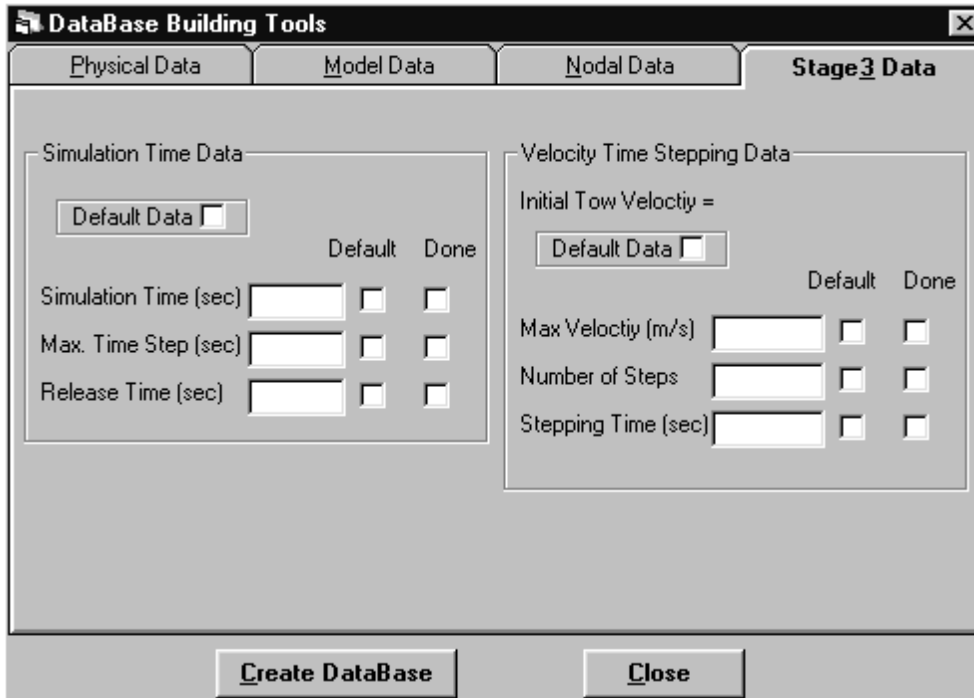


Figure 5.4: Velocity ramp option for DataBase building

### 5.6.1 User defined data

Using the *User Defined Data* option of the *PreDesign ToolBox* enables the user to define physical parameters such as oil and water density, tow speed and linear oil volume. Two options are available : *Option 1* requires the user to specify slick length; then the Stage 1 model will solve for the required average friction along the oil water interface to produce the user defined slick length. *Option 2* requests that friction is defined; then again the Stage 1 model will solve for the slick length that will exist for the specified physical parameters and average friction value.

The user can then, for both cases, visualize what this slick shape will look like by using the plotting option provided. If the results are not satisfactory one can clear the defined data and start over. Otherwise, the user can select to now build a database using the predesign values established under the *User Defined Data* section of the *PreDesign ToolBox*. By choosing the build database button, which is enabled after the user has checked off each predesign value, the *Database Building Tools* window will open with the predesigned values entered into their respective boxes.

### 5.6.2 Experimental data

The Experimental Data predesign option (see Figure 5.6) interactively uses information collected during experiments at UNH and OHMSETT, to help guide the user to

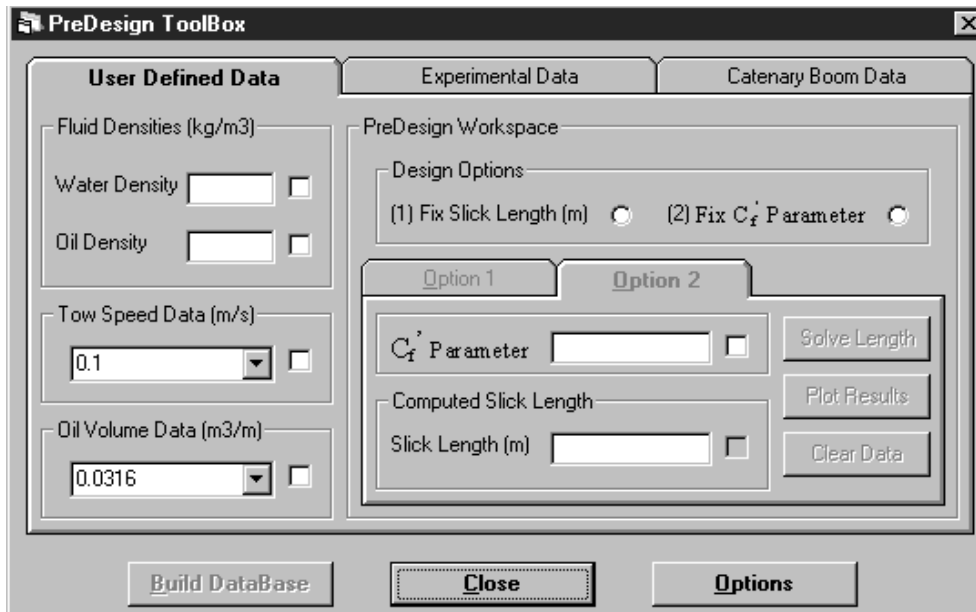


Figure 5.5: Predesign toolbox user defined data tab

design a project based upon previous experiments. Depending on the selected boom draft  $d$ , various choices of oil densities are available. These combinations of boom draft choice and oil densities correspond to separate databases of experimental data which will solve for the correct slick length and average friction for the select set of oil volume and tow speed. After slick length and average friction has been solved for, options for viewing the curve fits from which the data was produced can be viewed along with the solved data. These option buttons will open the *Experimental Curve Fits* window and will display the used curve fit for the chosen problem. Once the user is satisfied with the results, a database can now be created by choosing the *Build DataBase* button, which will open the *Database Building Tools* window.

### 5.6.3 Catenary boom data

Typically, oil containment procedures are performed with a boom being towed behind a vessel or place in a body of water. The shape, the boom assumes in each of these cases, is a catenary shape. Since SlickMap was developed for straight booms, this section of the *Predesign ToolBox* (see Figure 5.7) was created to allow a user to specify a particular catenary-shaped boom, with a defined length to gap ratio, to be used in a clean up procedure. SlickMap Stage 1 model will solve for the slick length from the apex of the boom to the leading edge of the oil slick, given the volume of oil and tow speed for the problem. This is done by using a database of experimental data collected for catenary boom shapes. Then, SlickMap will convert this catenary boom data into the equivalent 2-D slick length contained by a straight boom, for the

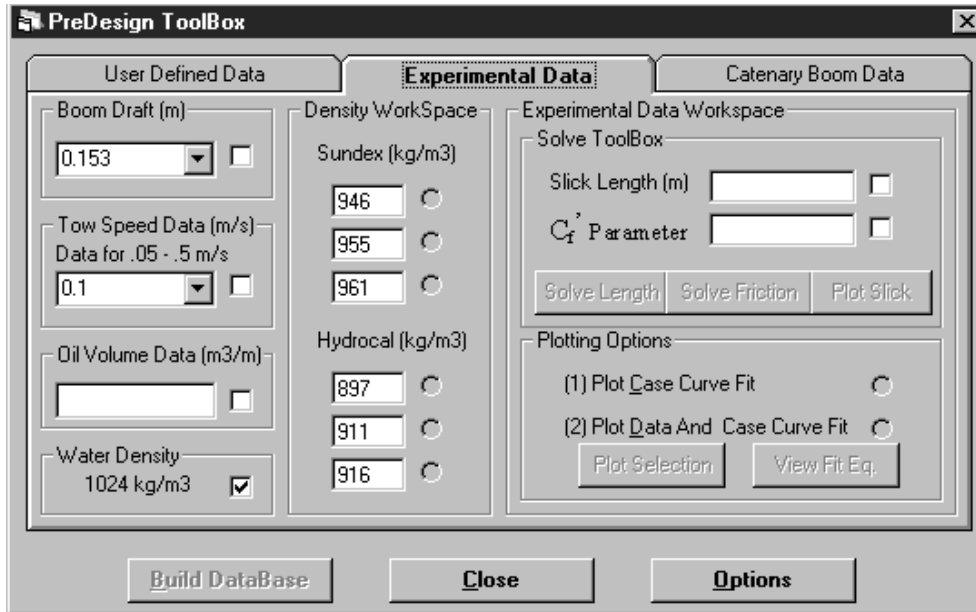


Figure 5.6: Predesign toolbox experimental data tab

same problem, in order to run simulations. This will then enabled the source code to solve for the average friction required along the oil-water interface to produce this slick length.

Various plotting options are provided for the user to view curve fits used and what the predesign slick shape looks like for this particular case. Once the user is satisfied with the results a database can now be created by choosing the *Build DataBase* button, which will open the *Database Building Tools* window.

## 5.7 Executing a project

A project can only be executed if a database specifying physical and numerical data has been created. To create a database, see Section 5.5).

SlickMap provides two options for executing a project. Simply choose *Project* from the Toolbar then select *Execute Project* or select the first button on the third toolbar (see Figure 5.8).

Selecting either of these options will provide the same result. Once a Project is executed, SlickMap will interact with the Stage 1, 2, and 3 models, to calculate results and provide data for visualization of slick shape in the GUI, and allow the user to interact with the source code.

The first procedure launched by SlickMap is to run an executable which contains the source code. Once the source code has been executed by SlickMap, Stage 1 solution will immediately be solved for. Upon completion of Stage 1 solution, SlickMap

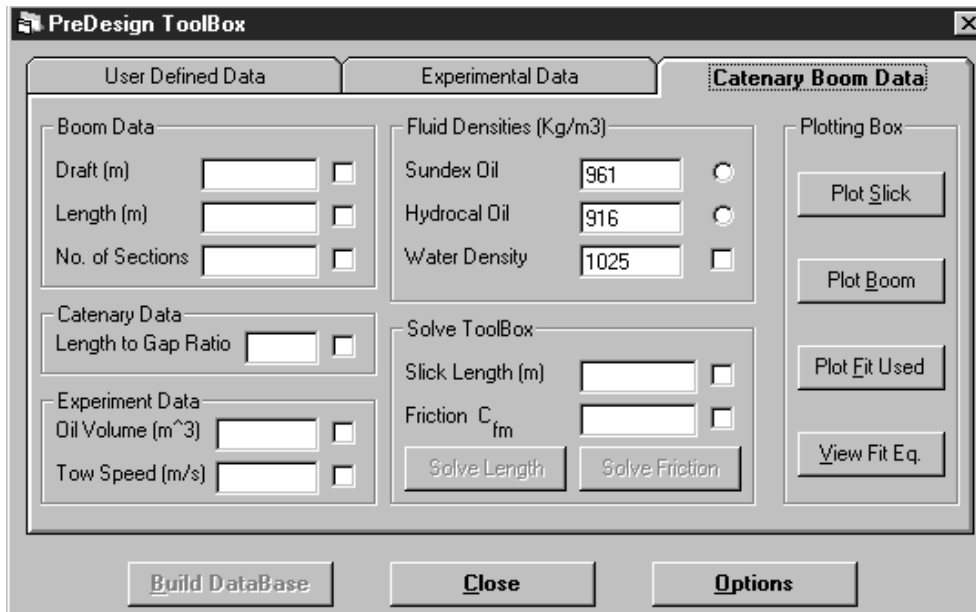
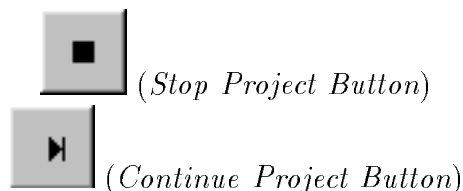


Figure 5.7: Predesign toolbox catenary boom data tab

will prompt the user that the solution is complete and the solution process may be paused in order to review the results of Stage 1. If the user chooses to pause to review the results, two options become available to the user. If the results are not satisfactory and project parameters must be changed, or if the user wishes to stop the solution, by choosing *Project* from the menu and selecting *Stop Project*, or by clicking on the stop button (see below) on the toolbar, the project simulation will stop. If the user wishes to continue onto Stage 2, after pausing to review Stage 1 results, one should either choose the *Project* option from the menu, then select *Continue Project* or choose the *Continue Project* button (see below) on the toolbar. Otherwise the project can be selected to continue solving the solution and not pause, which will advance the solution state to Stage 2.



During the solution of Stage 2, SlickMap will update the user on the status of the solution by displaying on the bottom of the window the percentage of completion, as well as a status bar also representing the percentage of completion. Similar to Stage 1, when Stage 2 is complete, SlickMap will prompt that Stage 2 solution is complete,

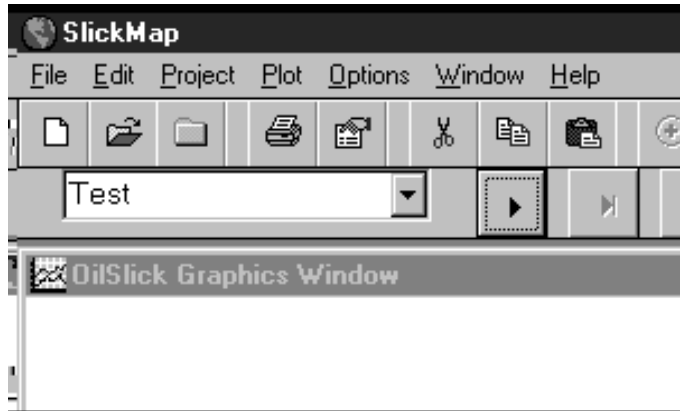


Figure 5.8: Execution button location on toolbar

giving the same options to the user as when Stage 1 solution is complete. If the solution is chosen to be continued at this point, the solution state will now advance to Stage 3. Stage 3 solution status will also be updated by SlickMap on the bottom of the window. Upon completion of Stage 3, SlickMap will prompt that the solution is finished. SlickMap will then enable analysis tools and various options to aid the user in investigating the results (see Section 5.8).

### 5.7.1 OilSlick graphics window

During the solution state in SlickMap, the *OilSlick Graphics Window* (e.g., Fig. 5.9) will display the oilslick geometry. For Stage 1 solution, since the problem is assumed static at this point, the results are displayed after the solution is finished. Stage 2 and Stage 3 results are displayed and updated realtime as the solution is being solved for.

### 5.7.2 Data window

The Data Window, located to the right of the SlickMap Window (see Fig. 5.1), details various values relative to the solution state of the oilslick. There are four separate value cases according to the solution state, i.e. PreDesign, Stage 1, Stage 2, or Stage 3. Table 5.6 gives a description of each available set of information for all solution Stages.

### 5.7.3 Project execution options

#### Solution step viewing options

A tool is provided by SlickMap to allow only Stage 3 results to be viewed as the solution is taking place. Stage 1 and Stage 2 will be solved independently and, upon completion, Stage 3 will be launched. The only difference is that the user will not be

<b>PreDesign Data</b>	<b>Stage 1 Data</b>
Oil depth $D$	Oil depth $D$
Oil length $L$	Oil length $L$
Average friction $C_{fm}$	Distance to head $x_h$
Head loss coefficient $C_h$	Head loss
Oil height coefficient $\chi$	Head loss coefficient $C_h$
Shear stress $\tau_s$	Shear stress $\tau_s$
Linear oil volume $V_o$	Linear oil volume $V_o$
Tow speed $U$	Tow speed $U$
Oil density $\rho_o$	Oil density $\rho_o$
Water density $\rho_w$	Water density $\rho_w$
<b>Stage 2 Data</b>	<b>Stage 3 Data</b>
Oil depth $D$	Oil depth $D$
Oil length $L$	Oil length $L$
Distance to head $x_h$	Distance to head $x_h$
Average friction $C_{fm}$	Average friction $C_{fm}$
Average Friction Coefficient	Initial Friction
Oil-air curve fit error $R^2$	RMS residual Error on M&VH Eqs.
Oil-water curve fit error $R^2$	Oil-water curve fit error $R^2$
Linear oil volume $V_o$	Oil-air curve fit error $R^2$
Tow speed $U$	Equivalence of Work
Oil density $\rho_o$	Linear oil volume $V_o$
Water density $\rho_w$	Tow speed $U$
	Oil density $\rho_o$
	Water density $\rho_w$
	Elapsed time $t$

Table 5.6: Data window display options.

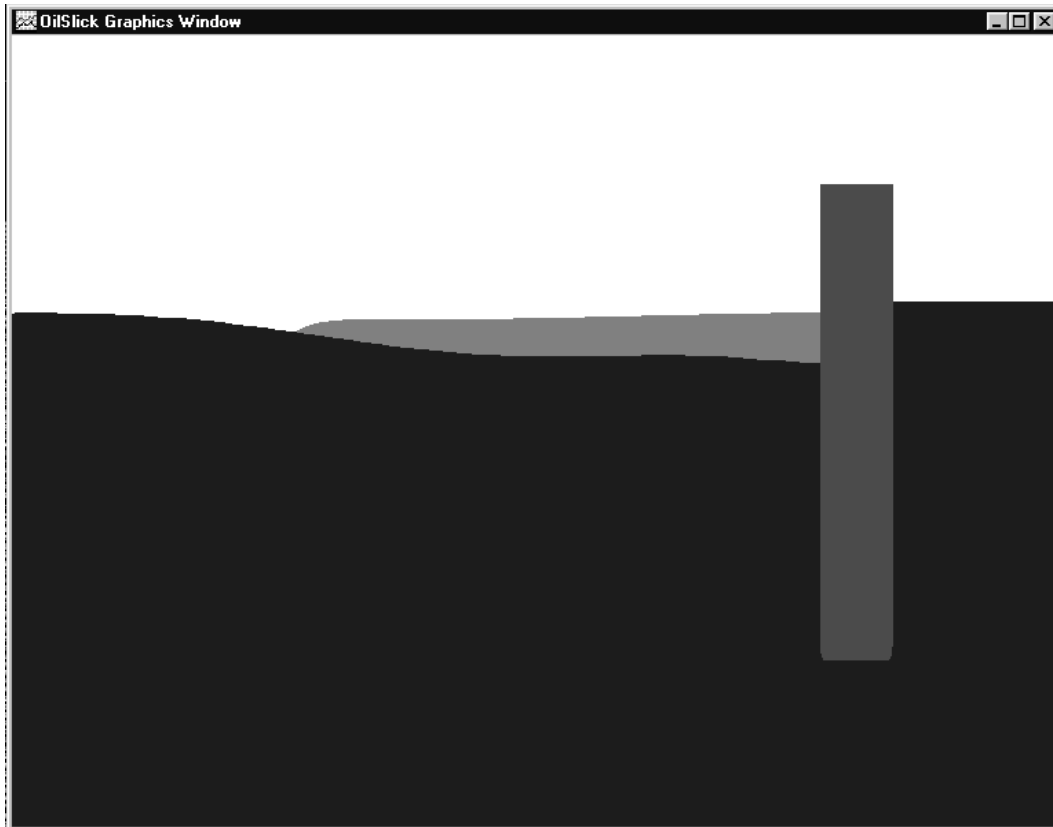


Figure 5.9: SlickMap graphics window

able to pause between stages of the solution and view results. This will allow only results from Stage 3 to be viewed during the solution state. After Stage 3 is complete, results from Stages 1 and 2 are available for viewing. To enable this option select *Options* from the Toolbar and choose *Only View Time Updating Steps*. To disable this option simply choose *Options* from the Toolbar then select *View Intermediate Steps*.

### **Time updating friction stack plot**

An additional option available only during Stage 3 solution is a time updating friction and oilslick stack plot window (see Fig. 5.10). To enable this option for Stage 3, select *Options* from the toolbar then choose *Time Updating Friction Stack Plot*. This will tell SlickMap to open this window during the solution of Stage 3 to give users a better understanding and control of the correlation between friction and the oil-water interface geometry.

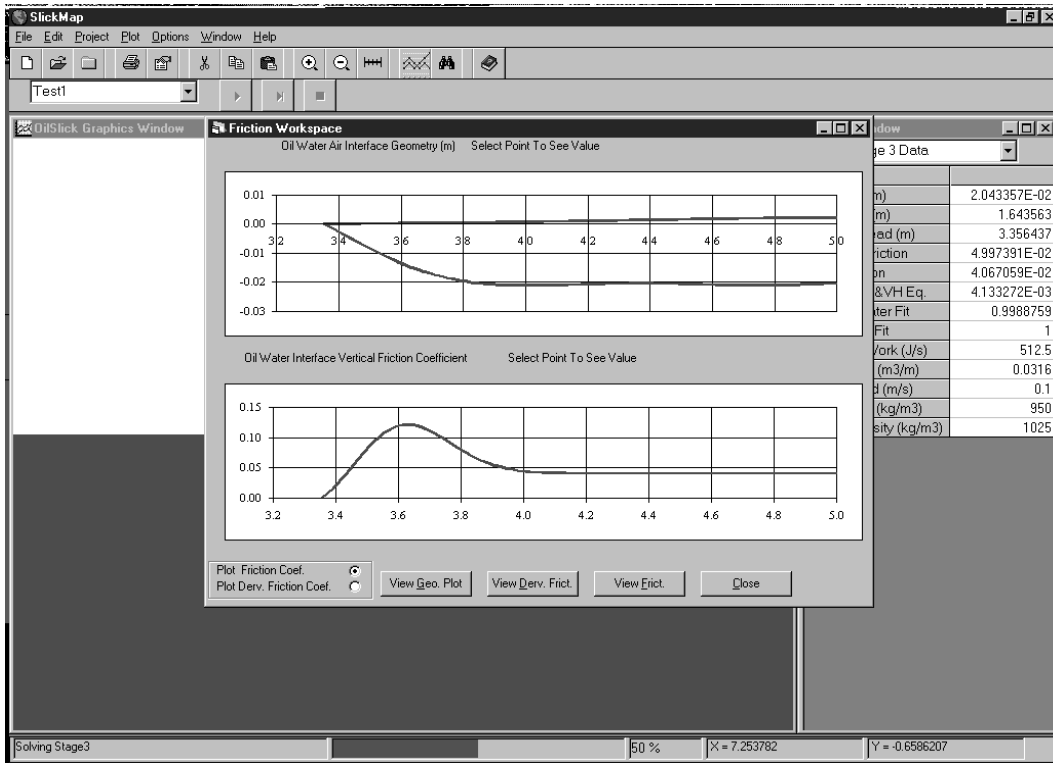


Figure 5.10: Time updating friction stack plot

### OilSlick graphics window axis

A useful tool provided by SlickMap is turning a axis grid on in the OilSlick Graphics Window (see Fig. 5.11). This will allow distances and scales of results to be easily visualized. Although coordinates of the Graphics Window are also displayed in the lower toolbar, using the axis in SlickMap is a quick way to analyze results.

## 5.8 Analysis options

SlickMap provides various options to analyze the data output produced by the source code, while simulating the use specified test case. All output data is stored in the Project Folder which was defined when creating a project in SlickMap. This data is available to be accessed and analyzed using tools provided by SlickMap, as well as any additional analysis tools the user desires to utilize. The various tools provided by SlickMap are discussed within this section.

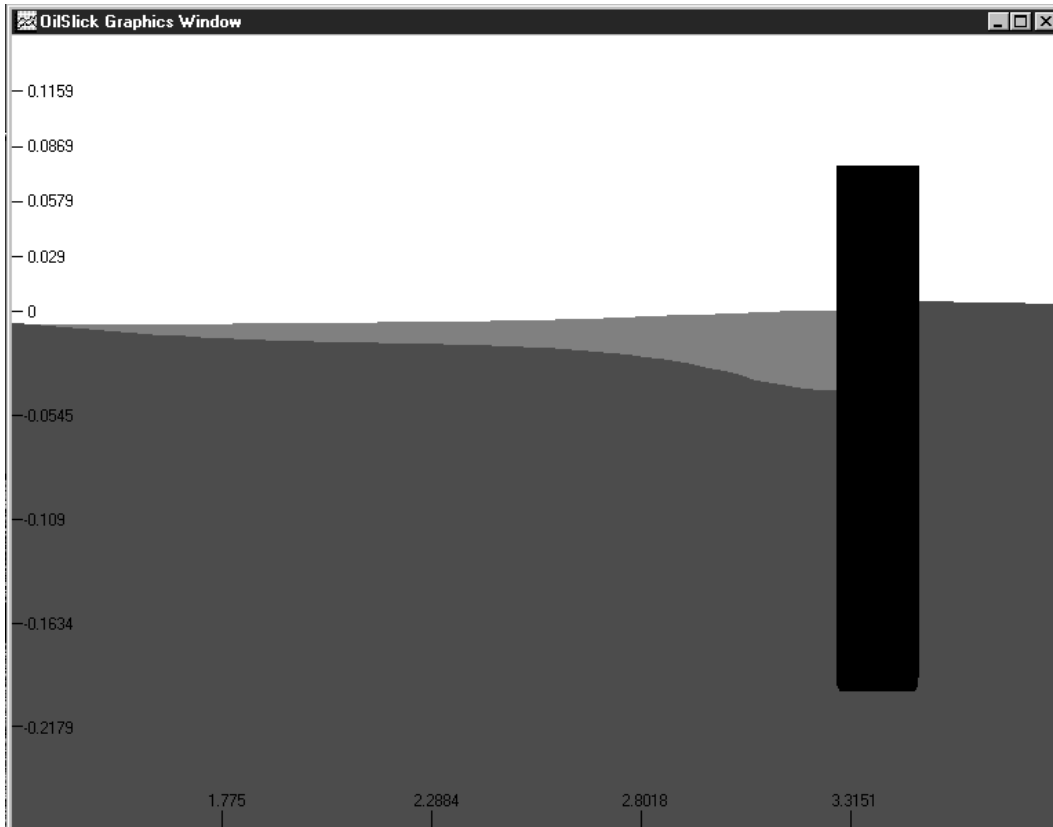


Figure 5.11: SlickMap Graphics Window Axis

### 5.8.1 SlickMap plotting options

As various stages of analysis, for a user specified project, are completed, plotting options available in SlickMap are enabled for the users to use. These options are made available to the users two different ways. All the plotting options are accessible from the plot menu, as well as from the *Plot Options* detailed below.



#### Plotting various analysis stages

During the various stages of running a project the user may view previous and current results when pausing the analysis. For instance, if a predesign of the specified problem was chosen, after the completion of Stage 1, the analysis may be paused and the predesign results are available for plotting. This will allow a closer comparison of the results for the predesign and Stage 1 phases, which will hopefully help the user better

understand the results and decide whether to stop or continue the analysis. Likewise, this can be done at the completion of Stage 2 and, obviously, Stage 3.

## BEM grid

The boundary element grid, which is setup by defining parameters with the database building tools, is used in the analysis of the existing project. It is sometimes hard to visualize at the scale of node spacing and actual geometry of the grid. SlickMap provides an easy way to plot the BEM grid with or without graphics. No BEM grid is available for the predesign phase and Stage 1, which do not use a BEM analysis to solve for the initial slick shape. Only Stages 2 and 3 BEM grids are available to plot. Figure 5.12 is an example of what a BEM grid for Stage 2 might look like when using SlickMap to plot the grid data.

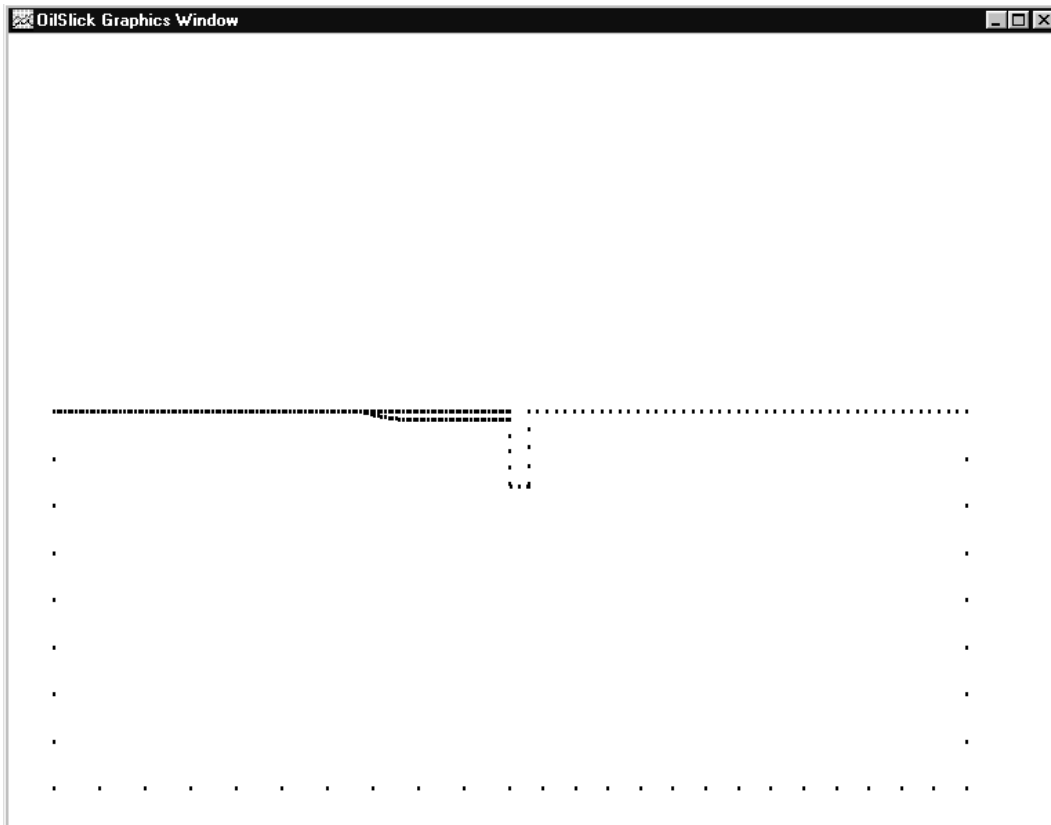


Figure 5.12: Example of BEM Grid Data for Stage 2

The BEM grid data may also be plotted over the graphics for each stage. This is done by enabling the option to *Plot BEM Grid With Graphics* from the *Options* menu. The default option for plotting the BEM grid is without graphics and should have a check mark next to it in the options menu. By clicking on the option to plot

the BEM grid with graphics will put a check next to it making it the current default plot option for this function.

### **Experimental curve fits**

The predesign phase of SlickMap is a tool provided to help design a project by utilizing experimental results which are embedded within SlickMap. When the project's specified design parameters, such as tow speed and boom draft, do not match the available experimental parameters, curve fits are applied (see Section 2.4) which describe the behavior of particular oil types for various tow speeds and boom drafts. These curve fits can be used to interpolate necessary data for a predesign case. For example, if a project is being predesigned and the predesign method is to use the experimental data, the user has various boom drafts and tow speeds to choose from. If the tow speed and/or boom draft chosen are different from the provided options, the predeveloped curve fits are used to interpolate what the corresponding oil slick length would be. Otherwise, these curve fits are used directly to solve for the oil slick length corresponding to the specified parameters (note that only two oil types are provided when using the experimental data to predesign a project : Sundex and Hydrocal). The curve fits being used in this predesign phase are available to be plotted with the predesign results. This is done with the *Predesign Toolbox* in the *experimental data* tab, using the plotting options. These experimental curve fits can also be plotted individually and separately for all boom drafts and oil types. The raw data used to create these curve fits are also available, for plotting and viewing, from the Experimental Curve Fit Plotting Window (See Fig. 5.13).

### **Friction coefficient**

The value of the friction coefficient calculated by the friction coefficient function (FCF), as described in Chapter 4, is stored as output data available for plotting and analysis. By selecting to plot *Friction Coefficient* from the *plot* menu options on the toolbar, the Friction Coefficient window is opened (see Fig. 5.14), which plots the friction function along the oil-water interface. Data used to generate this graph is available to view, and the graph maybe exported as a picture file or copied for use with other software. The default data used to generate the friction coefficient graph is that from the last time step in Stage 3. Previous values of the friction coefficient from earlier time steps are also available for plotting in this window.

### **Derivative friction coefficient**

Chapter 4 discusses the derivative of the friction coefficient function and its use in the analysis of the oil slick geometry as it evolves in time. Therefore, it is important to be able to visualize this value similarly to viewing the friction coefficient. SlickMap provides a tool, identical to the tool used for plotting and analyzing the

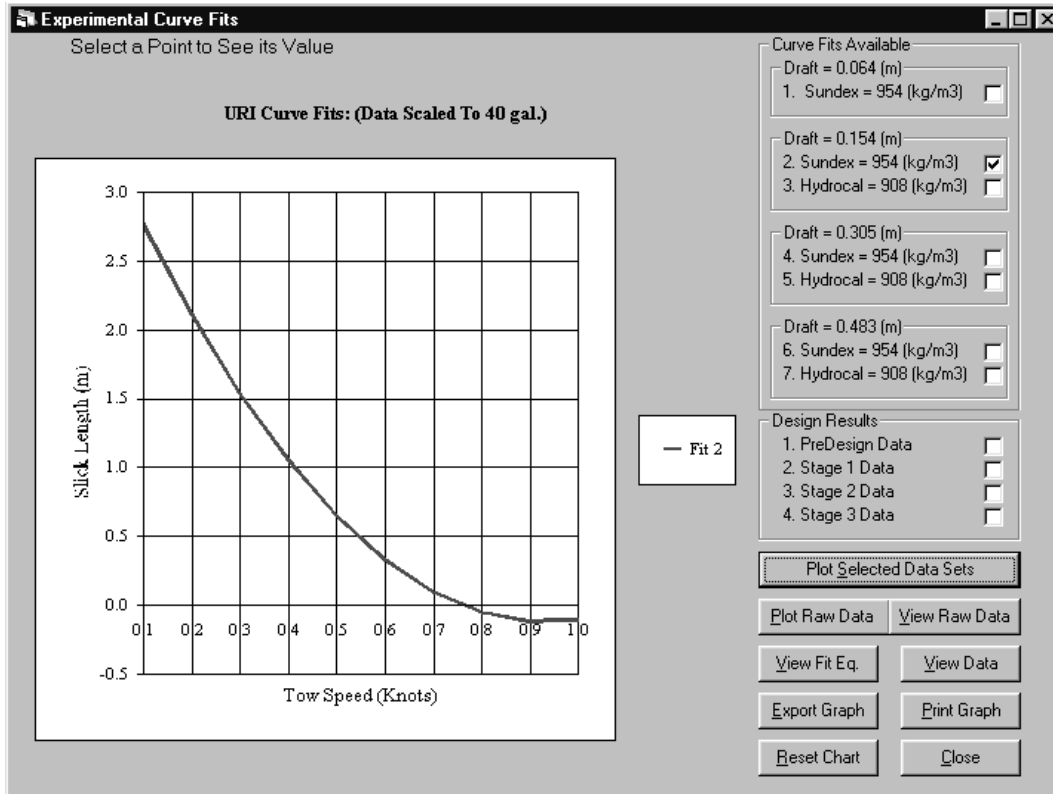


Figure 5.13: Experimental Curve Fit Plotting Window

friction coefficient (See Figure 5.14), to plot and analyze the derivative of the friction coefficient. By choosing to plot the *Derivative Friction Coefficient* from the *plot* menu the Derivative Friction Coefficient window is opened. As with the friction coefficient, the default graph of the derivative is generated from the data produced at the last time step of Stage 3, and likewise previous values from earlier time steps are also available. Copying and exporting the graph is enabled and viewing the data used to generate the graph is possible, from this window.

### Time updated oil slick shapes

SlickMap developers thought a useful device to analyzing the results of Stage 3 would be to allow the slick shapes calculated at each time step to be superimposed on each other. This would create a time series of slick shapes as a function of time for all time steps, to be viewed simultaneously. By creating this ability in SlickMap, the analysis of the slick shape evolution for various input parameters can easily be made.

To access this tool (see Fig. 5.15) select *Time Updating Oil Slick Shapes* from the *plot* menu options. Additional functions such as exporting and copying the graph, as well as viewing the data sets used, are made readily available with this SlickMap tool.

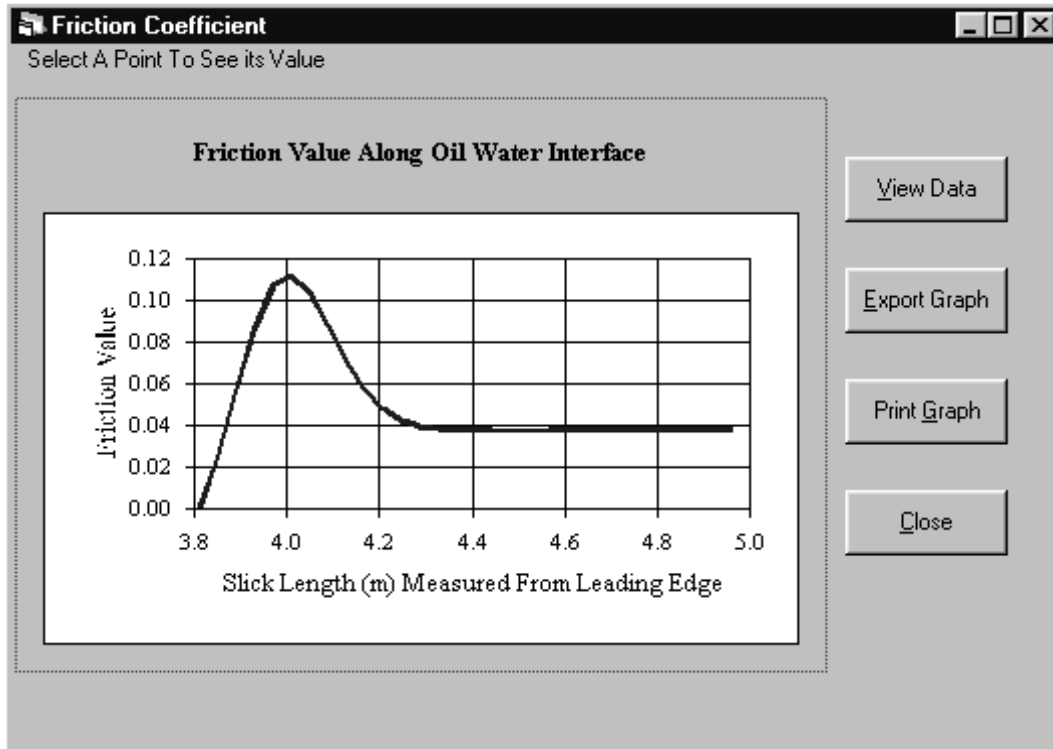


Figure 5.14: Friction Coefficient Plot Window

### Friction oil slick stack plot

A useful way to analyze the effect friction has on the oil slick geometry is to view a graph containing both data sets on the same horizontal scale. That is to say, being able to view the friction coefficient along the oil-water interface along with the geometry of the oil slick. SlickMap provides a useful tool which plots that data. By choosing to plot the friction oil slick stack plot, a representation of both the oil slick geometry and the friction coefficient along the oil-water interface, is graphed (see Fig. 5.10).

The graph initially plotted contains values for the last time step of Stage 3 calculations. Previous time step information is made available through the *Friction Workspace* window. The ability to view the derivative of the FCF in place of the FCF is made possible by selecting to plot the derivative of friction coefficient. Each data set (Friction Coefficient, Derivative of Friction Coefficient, and Oil Slick Geometry) may be viewed as a separate plot, in a new window, by selecting the proper option from the *Friction Workspace* window. The friction oil slick stack plot is also available during Stage 3 analysis, which is discussed in Section *Time Updating Friction Stack Plot*.

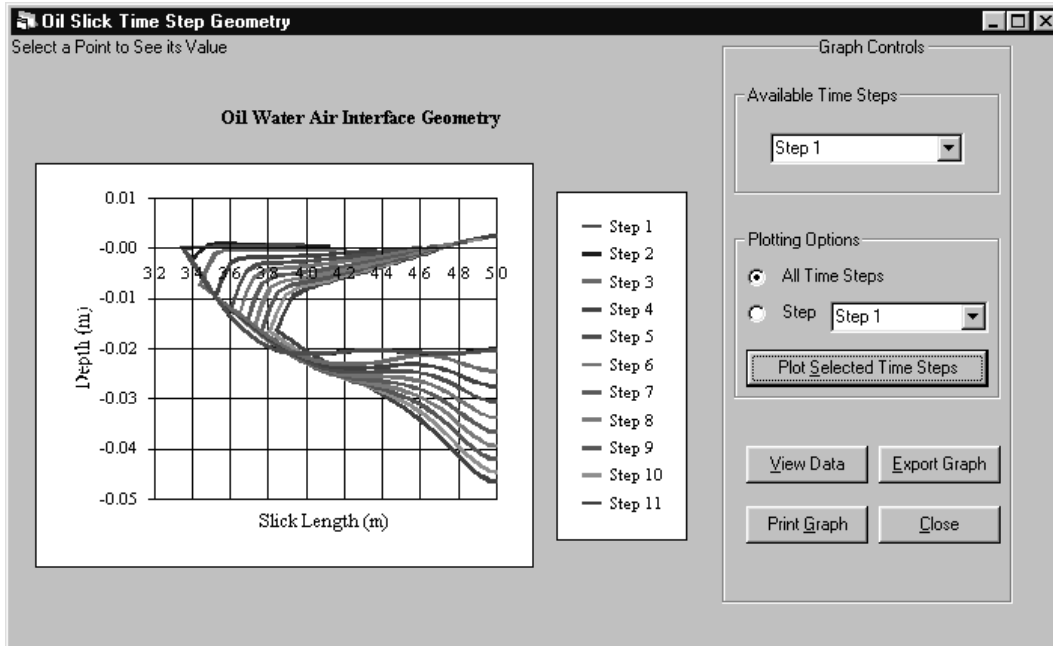


Figure 5.15: Time Updated Oil Slick Shapes Window

### 5.8.2 Zooming in graphics window

Zooming options in SlickMap allow the display in the *Graphics Window* to be re-scale for viewing purposes. Zooming is done by selecting the zoom in or out button (displayed below respectively) or by selecting *zoom in* or *zoom out* under the *options* menu.



To zoom in, a zoom window must be properly created in the *Graphics Window* for the desired region. A properly created zoom window is started at the upper left hand corner of the desired zoom region and sized accordingly from that point to the lower right hand corner of the zoom window. This is done by choosing zoom option, then using the mouse left click, holding at the location of the upper left hand corner of the desired zoom region, and moving the mouse to the lower right corner, thus sizing the zoom window to the desired size. Letting up on the left button will then fill the *Graphics Window* with the chosen zoom region. If this process is not correctly done, the desired zoom region may not be properly displayed. When zooming out, SlickMap restores the original plot size in the *Graphics Window*. By selecting the

zoom out option, this will automatically be executed.

### 5.8.3 Measuring distances

The ability to resolve various measures of distances from the results may come in handy. The vertical and horizontal locations of the mouse pointer are displayed in SlickMap, which makes getting distances between two points a trivial, but time consuming, task. To speed-up this process, SlickMap has provided a tool (see Fig. 5.16) that automatically measures distances between two user defined points, at any location in the *Graphics Window*. This tool is accessible through the *get distance* option under the options menu and from the *get distance* button on the toolbar (see below).

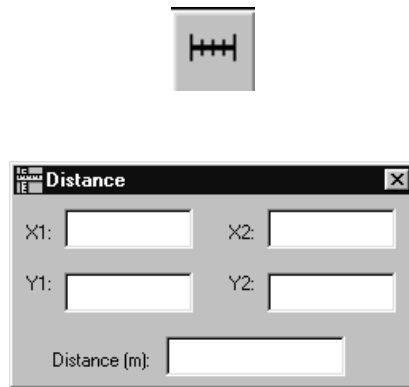


Figure 5.16: Measuring Tool Window.

Using this tool is simple and straightforward. Measuring a distance with this tool only requires the user to select two points. These selection points are defined as small circles and the distance between the two points is represented as a solid line. To select points, use the mouse to click on the starting point of measurement then click on the ending point of measurement. This will input the required data needed by the distance measuring tool to calculate the distance between the two selected points. After selecting the second point, the distance between these points will automatically be displayed. Fig. 5.17 shows an example of how the measuring tool device works. When closing the measuring tool window, the points and lines generated by the device will be cleared from the *Graphics Window*.

## 5.9 Project options

Multiple functionalities are programmed into SlickMap to open old projects, access previously created databases, editing default parameters provided by SlickMap, and various additional functions. These options are additional tools to help the user when creating a project or modifying an existing project. None of these are necessary

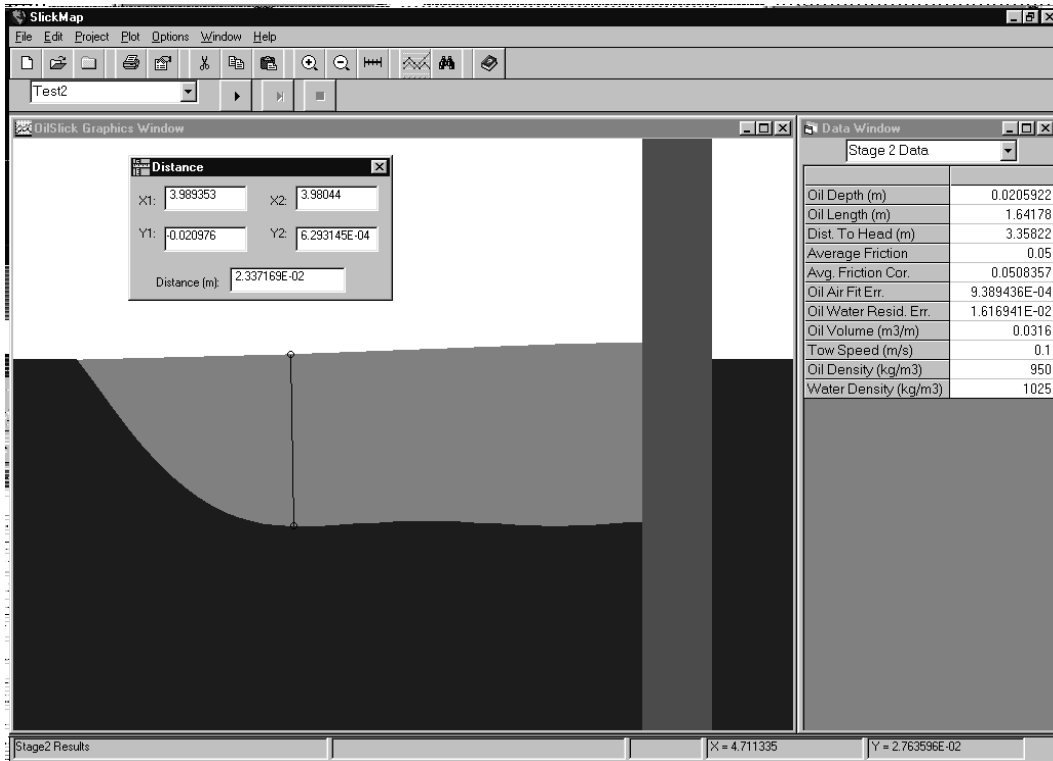


Figure 5.17: Measuring Tool Example.

functions to create and execute a project; they only provide additional help for specific functions. These options are discussed in detail within the following sections.

### 5.9.1 Opening old projects

Once a project has been created, it may always be reopened at a later time for analysis or to continue a simulation. Projects are saved as multiple files in a directory specified when opening a new project. To access these projects, SlickMap must already be activated. Selecting the *New Project* option from the file menu or clicking on the open new file button (see below) on the toolbar, will open a window similar to the open project window displayed in Fig.5.2.



From within this window, select the directory where the desired project to open is located. After selecting the appropriate directory, the files included in the old project are displayed on the left file window. If this selected directory contains the desired project and associated files, select *OK* to open the old project. Once a project

opened, all analysis options are enabled. The reopened project may also be restarted to continue time stepping in Stage 3. This option is discussed in section *Restarting a project*.

### 5.9.2 Opening multiple projects

SlickMap allows the user to have multiple projects opened at the same time. Only one project, however, may be executed at a time to ensure proper file input/output continuity. To open multiple projects, just repeat the procedure to open an old project, as discussed in section *Opening old projects*. SlickMap will open and maintain up to six opened projects. Once a multiple project is opened, it is made the current active project available to work on through the SlickMap interface. To switch to an earlier, or any other project that is opened, use the *Project Name Display Device* (see Fig. 5.18) to select which project is active.



Figure 5.18: Project Name Display Device.

### 5.9.3 Closing projects

Closing a project may be desired when multiple projects are opened or a new project is started. This is done by either selecting *Close Project* from the file menu or by clicking on the close project button (see below) on the toolbar. Closing a project does not erase any project information. All data particular to a project is automatically stored and saved in the directory the project is working out of. Thus, there is no need to fear that information will be accidentally lost by closing a project.



### 5.9.4 Use default database

Selecting to use the default database will open the *Database Building Tools Window* (see Fig. 5.3) with all parameters assigned the default values provided by SlickMap (see Section *Building a database*). This option will not automatically create a database using the default values, but pause and allow the user to view the values, and decide whether to change or keep them. Then, after reviewing these values, since all necessary transactions and data verification have already been automatically made by SlickMap (i.e. all checked boxes have been selected as done), just select to create a database.

### 5.9.5 Edit existing database

After creating a new project or opening an old project, one may desire to use a database, previously created for a different project, for the current project opened in SlickMap. A previously created database can easily be used for the database of a new project or be used to rerun an old project. To open an existing project, select *Edit Existing Database* from the *project* menu. This will open a window similar to the one displayed in Fig. 5.2. From here, select the directory where the desired database to open exists, and select *OK*.

Opening an existing database will open the *Database Building Tools Window* (see Fig. 5.3). The parameters within this window will be assigned the values of the previously defined database. At this time, these values can be edited to change the projects description (i.e. oil density value). Once the values for each parameter in this window are satisfactory, the database can be created. For a new project, this will enable the project's execution options, and for an old project, this will simply create a new database. Executing the project problem for both scenarii is identical and described in Section *Executing a project*.

### 5.9.6 Editing default database

SlickMap has provided default values for all the parameters in the building tools window (see Section *Database building tools*). These default values can be used or can be chosen not to be used. A combination of user specified values for these parameters and default values can also be used to create a database. A quick way to edit the default values provided by SlickMap is to choose the *Edit Default Database* option under the *Project* menu. This will open the *Database Building Tools Window* (see Fig. 5.3) with all the default values provided by SlickMap entered as values for all available parameters. This option can be used when creating a database for a new project or an old project. Once the parameter values are all satisfactory, a database can be created.

### 5.9.7 Reasserting a project

After Stage 3 solution is complete, SlickMap generates a restart file that can be used to continue a project. Restarting a project will start executing an existing project from the solution results obtained at the last time step of Stage 3.

To restart a project, open an existing project that has completed a solution for Stage 3, then select *Restart Project* option from the *Project* menu. This will open the *Restart Options Window*. From this window, SlickMap prompts the current number of time steps chosen and the time of each time step. Selecting to use these values will cause SlickMap to execute the opened project, starting from the last time step solved for in Stage 3. Selecting not to use these values will open the *Project Restart Data Window* (See Fig. 5.19). In this window enter the desired length of simulation time

and value in seconds of each time step. Select *OK* to restart the project with these time stepping values from the last time step solved for during Stage 3.



Figure 5.19: Project Restart Data.

## 5.10 SlickMap accessories

SlickMap developers have tried to provide most commonly found accessories in MS Windows applications. The main accessories provided by SlickMap are printing options, open, and editing data files, exporting graphics as picture files, and getting help.

### 5.10.1 Printing

Two print options are available to the user through SlickMap, printing the graphics window and printing opened files. Choosing to *Print Graphics Window* option from either the *File* menu or from the print button provided on the toolbar (see below) is only available when the graphics window is the active window.



Selecting the *Print* option from the *File* menu or from the print button (see below) on the toolbar or by selecting to *Print Graphics Window* the *Print Window* will open.



From this window, print options will be available, such as which printer is desired to print to, landscape and portrait printing, printing to a file, etc... If the user is

familiar with MS Windows printing this should be old news. To seek help on printing, see MS Windows printing documentation.

Printing options are also available in various plotting windows. These printing options will print the current plot to the specified printer device.

### 5.10.2 Opening data files

All files generated by SlickMap are available to view in ascii form, if desired. It is not recommended to edit these files within the project directory, although the data may be exported for additional analysis with other software. To open the files in a project directory, select *Open Data File* from the *Options* menu or click on the open file button (see below) on the toolbar.



Choosing one of the above mentioned options will open a standard windows file menu opening device. From this window select which file to open and select *OK*. See section *Data I/O structure* to learn which files contain data of interest.

### 5.10.3 Editing options

Standard editing options such as *cut*, *copy*, and *paste* are available for use with ascii characters as well as with certain graphics. Opened data files in SlickMap may also be edited using the editing functions (it is not recommended to edit the files contained within a project folder).

Generated plots enable the *copy* command. For instance, if the *Friction Coefficient* is plotted, a notepad can be opened and if paste is selected within the notepad the data from the plot will be inserted. The graphics may also be saved as a picture file; this option is discussed in section *Exporting graphics*.

### 5.10.4 Exporting graphics

Graphics and plots displayed in SlickMap can be exported as a bitmap (\*.bmp) file. For most plots, this option is represented as a button titled *Export Graphics*. This option will prompt where to save and what name to save the plot under. The *Graphics Window* may also be saved as a bitmap file. When this window is active the *Export Graphics Window* option is available under the *File* menu. This option will similarly prompt where to save and what name to save the graphics window.

### 5.10.5 Color options

Default colors used to represent the oil slick, boom, and water are preset in SlickMap. At runtime, the user has full control over these colors. These colors can be changed from the color option under the *Options* menu. The color option allows each color characteristic (water, oil, and boom) in the graphics window to be changed independently. The default colors preset in SlickMap may always be restored using the color option and selecting *Default Colors*.

### 5.10.6 Getting help

This documentation is available online at <http://www.oce.uri.edu/~fake>. It can also be viewed in PDF format from SlickMap. To access this manual from SlickMap, select *SlickMap Help Topics* from the *Help* menu or click on the help button (see below).



## 5.11 Data I/O structure

There are various files generated by the source code and SlickMap. Some of which serve as an interaction medium between the two and some of which provide critical information for each other. This section will define the files which provide critical information during and after runtime.

The general data flow is described in Fig. 5.20. This shows the data exchange process between the source code and SlickMap. SlickMap initially generates two critical files that provide all necessary data for the source code to begin an execution. These generated files are created when building a database and are named *ancilar.dat* and *general.dat*. Pre-design information is stored in *Inshap.txt* and *preout.txt*. These files contain geometry and physical data, respectively for the pre-design oil slick shape. All data pertaining to Stage 1, Stage 2, and Stage 3 are stored respectively in *stage1.dat*, *stage2.dat*, and *stage3.dat*. Slick shapes calculated at each time step during Stage 3 are stored in files *OILSHAPE\*.dat*. Likewise, friction coefficient values calculated during Stage 3 are stored in files *CFSAVE\*.dat*. Editing or moving these files from their project folder is not recommended.

The general output file generated by the source code titled *listing.dat* contains all information about the project problem and analysis output for all stages. The restart option utilizes file *restart.lis* which is an output file from the source code containing the information from the last time step solved for during Stage 3. Multiple files have not been discussed within this section because they are not relevant to the user, and should not be edited. Doing so may cause SlickMap to crash.

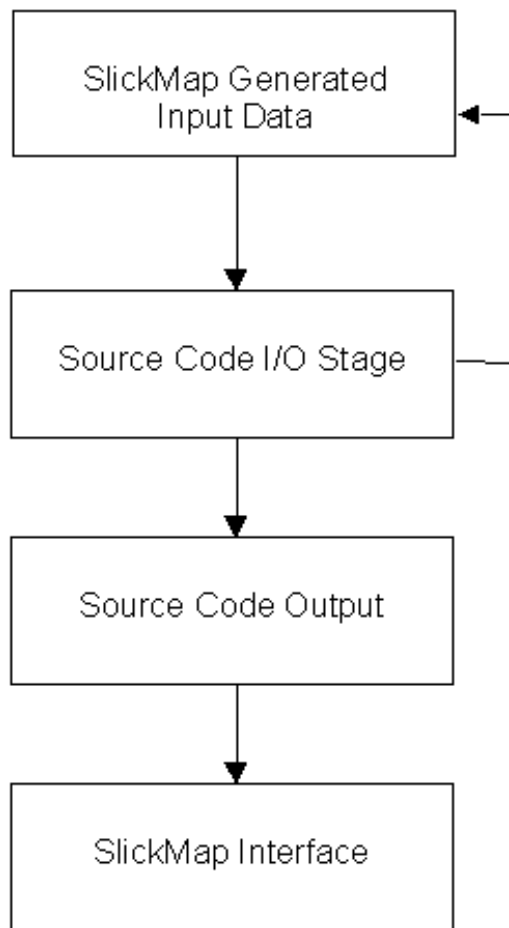


Figure 5.20: SlickMap Source Code Data Flow Chart.



# Bibliography

- [1] Agrawal, R.K. and Hale, L.A. 'A new criteria for predicting head wave instability of an oil slick by a barrier', *Proc. Offshore Tech. Conf.*, Dallas, Texas, pps. 461-466, 1974.
- [2] Bai, K.J. and Kim, J.W. 'A computational model for flow around an oil boom', *Proc. Workshop on Tidal and Oil Spill Modeling*, 5-17, 1993.
- [3] Baker, G.R. and M.J., Shelley 'On the connection between thin vortex layers and vortex sheets.' *J. Fluid Mech.*, **215**, 161-194, 1990.
- [4] Batchelor, G. K., *An introduction to fluid dynamics* Cambridge University Press, 1967.
- [5] Benjamin, T.B. 'Gravity currents and related phenomena', *J. Fluid Mech.*, **31** (2), 209-248, 1968.
- [6] Brebbia, C.A., *The Boundary Elements for Engineers* John Wiley and Sons, 1978.
- [7] Clavelle, E.J. and Rowe, R.D. 'Numerical simulation of oil-boom failure by critical accumulation', *Arctic Marine Oil Spill Prog. Tech. Seminar*, 409-418, 1993.
- [8] Cross, R.H. and Hoult, D.P. 'Oil booms in tidal currents', *J. Waterways, Port. Coastal Ocean Engng.*, **98**, 1745-1758, 1972.
- [9] Delvigne, G.A.L. 'Barrier failure by critical accumulation of viscous oil', *Proc. Oil Spill Conf.*, USEPA, USCG, and Amer. Petrol. Inst., pps. 143-148, 1989.
- [10] Di Pietro, N. D. and Cox, R. G. 'The containment of an oil slick by a boom placed across a uniform stream', *J. Fluid Mech.*, **96**, 613-640, 1980.
- [11] Drazin, P.G. 'Kelvin-Helmholtz instability of finite amplitude', *J. Fluid Mech.*, **42**, 321-335, 1970.
- [12] Drazin, P.G. and Howard, L.N. 'Hydrodynamic stability of parallel flow of inviscid fluid', *Advanc. Applied Mech.*, **9**, 1, 1966.
- [13] Ertekin, R.C. and Sundararaghavan, H. 'The calculation of the instability criterion for a uniform viscous flow past a boom', *J. Offshore Mech. Artic Engng.*, **117**, 24-29, 1995.
- [14] Fink, P.T. and Soh, W.K. 'Calculation of vortex sheets in unsteady flow and application in ship hydrodynamics', *Proc. 10th Symp. on Naval Hydrodynamics*, Office of Naval Res., Washington, D.C., 463-491, 1974.
- [15] Guiggiani, M., Krishnasamy, G., Rudolph, T.J., and F.J. Rizzo 'A general algorithm for the numerical solution of hypersingular boundary integral equations.' *Trans. ASME*, **59**, 604-614, 1992.
- [16] Grilli, S.T. and Horrillo, J. 'Numerical Generation and Absorption of Fully Nonlinear Periodic Waves' *J. Engineering Mechanics*, **123**(10), 1060-1069, 1997.

- [17] Grilli, S.T., Hu, Z., and Spaulding, M.L. 'A hydrodynamic model of oil containment by a boom : Phase I', *Final Technical Report for DOT Grant No. DTRS57-94-G-00076*, Dept. Ocean Engng., Univ. of Rhode Island, 70pps, 1996.
- [18] Grilli, S.T., Hu, Z., and Spaulding, M.L. 'Numerical modeling of oil containment by a boom', *Proc. 19th Arctic and Marine Oilspill Program Technical Seminar (AMOP)*, 6/96, Calgary, Alberta, Canada, pps. 343-376. Environment Canada, 1996.
- [19] Grilli, S.T., Hu, Z., and Spaulding, M.L. 'Numerical Modeling of Oil Containment by a Boom /Barrier System : Phase II', *Final Technical Report for DOT Grant No. DTRS57-95-G-00065*, Dept. Ocean Engng., Univ. of Rhode Island, 83pps, 1997.
- [20] Grilli, S.T. and Hu, Z. 'Computation of Periodic Instability of Stratified Fluid Using Continuous Vortex Sheet Dynamics.' In *Proc. 19th Intl. Conf. on Boundary Elements in Engineering (BEM19, Rome, Italy, September 1997)* (eds. M. Marchetti, C.A. Brebbia, & M.H. Aliabadi), pps. 543-552. Computational Mechanics Publications, Boston. (invited paper), 1997.
- [21] Grilli, S.T. and Hu, Z. 'A Higher-order Hypersingular Boundary Element Method for the Modeling of Vortex Sheet Dynamics.' *Engineering Analysis with Boundary Elements*, **21**(2), 117-129, 1998.
- [22] Grilli, S.T. and Subramanya, R. 'Recent advances in the BEM modelling of nonlinear water waves'. Chapter 4 in *Boundary Element Applications in Fluid Mechanics* (ed. H. Power), pps. 91-122. Advances in Fluid Mechanics Series. Computational Mechanics Publication, Southampton, UK, 1995.
- [23] Grilli, S.T. and Subramanya, R. 'Quasi-singular Integrations in the Modelling of Non-linear Water Waves.' *Engng. Analys. with Boundary Elements*, **13**(2), 181-191, 1994.
- [24] Grilli, S.T. and Subramanya, R. 'Numerical modeling of wave breaking induced by fixed or moving boundaries.' *Computational Mechanics*, **17**(6), 374-391, 1996.
- [25] Grilli, S.T. and I.A., Svendsen 'Corner Problems and Global Accuracy in the Boundary Element Solution of Nonlinear Wave Flows.' *Engng. Analys. with Boundary Elements*, **7**(4), 178-195, 1990.
- [26] Hu, Z. and Grilli, S.T. 'Computation of Periodic Instability of Stratified Fluid Using Continuous Vortex Sheet Dynamics.' In *Proc. 1997 ASME Fluids Engineering Summer Meeting*, paper No. FEDSM97-3502, 12pps, 1997.
- [27] Johnston, A.J., Fitzmaurice, M.R. and Watt, R.G. 'Oil spill containment : viscous oils', *Proc. Oil Spill Conf. (USEPA, USCG)*, Amer. Petrol. Inst., pps. 89-94, 1993.
- [28] Jones, W. T. 'Instability at an interface between oil and flowing water', *J. of Basic Engng.*, **94**, 874-878, 1972.
- [29] Krasny, R. 'A study of singularity formation in a vortex sheet by the point-vortex approximation.' *J. Fluid Mech.*, **167**, 65-93, 1986.
- [30] Kelvin, Lord *Mathematical and Physical Papers* 4 76-100, Cambridge University Press, 6th edition, 1910.
- [31] Lamb, H. *Hydrodynamics*. Cambridge University Press, 6th edition, 1932.
- [32] Lau, Y.L. and Kirchifer, S.A. 'A review of the dynamics of contained oil slicks in flowing water', *J. Hydraulics Div.*, 1974.

- [33] Leibovich, S. 'Oil slick instability and the entrainment failure of oil containment booms', *J. Fluids Engng.*, **98**, 98-105, 1976.
- [34] Milgram, J.H. and Van Houten, R.J. 'Mechanics of a restrained layer of floating oil above a water current', *J. Hydronautics*, **12** (3), 93-108, 1978.
- [35] Meiron, D.I., Baker, G.R., and S.A. Orszag 'Analytic structure of vortex sheet dynamics. Part 1. Kelvin-Helmholtz Instability.' *J. Fluid Mech.*, **114**, 283-298, 1982.
- [36] Moore, D.W. 'A numerical study of the roll-up of a finite vortex sheet.' *J. Fluid Mech.*, **63**(2), 225-235, 1974.
- [37] Moore, D.W. 'The spontaneous appearance of a singularity in the shape of an evolving vortex sheet.' *Proc. Roy. Soc. London*, **A365**, 105, 1979.
- [38] Rangel, R.H. and Sirignano, W.A. 'Nonlinear growth of Kelvin-Helmholtz instability : Effect of surface tension and density ratio', *Phys. of Fluids*, **31** (7), 1845-1855, 1988.
- [39] Rangel, R.H. and Sirignano, W.A. 'The linear and nonlinear shear instability of a fluid sheet', *Phys. of Fluids*. **A3** (10), 2392-2400, 1991.
- [40] Rosenhead, L. 'The formation of vortices from a surface of discontinuity.' *Proc. Roy. Soc. London*, **A134**, 170-192, 1931.
- [41] Rottman, J. W. and Olfe, D.B. 'Comment on "discretized simulation of vortex sheet evolution with buoyancy and surface tension effects" ', *J. AIAA* **15**, 1214-1215, 1977.
- [42] Van de Vooren, A.I. 'Numerical investigation of the rolling-up of vortex sheets', *Proc. R. Soc. Lond.*, **A 373**, 67-91, 1980.
- [43] Von Karman T., 'The engineer grapples in the nonlinear problems', *Bull. Am. Math. Soc.* **46**, 615-586, 1940.
- [44] Wicks, M. 'Fluid dynamics of floating oil containment by mechanical barriers in the presence of water currents', *Proc. API-FWPCA Joint Conf. on Prevention and Control of Oil Spills*, New York, Dec 15-17, Amer. Petrol. Inst., pps. 55-106, 1969.
- [45] Wilkinson, D. L. 'Dynamics of contained oil slicks', *J. Hydraulics Div.*, **98**, 1013-1031, 1972.
- [46] Wilkinson, D. L. 'Limitations to length of contained oil slicks', *J. Hydraulic Div.*, **99**, 701-713, 1973.
- [47] Zalosh, R.G. 'A numerical model of droplet entrainment from a contained oil slick', *Report No. CG-D-65-75*, DOT/USCG, 1974.
- [48] Zalosh, R.G. 'Discretized simulation of vortex sheet evolution with buoyancy and surface tension effects', *J. AIAA*, **14**, 1517-1523, 1976.
- [49] Zalosh, R.G. and Jensen, D.S. 'A numerical model of droplet entrainment from a contained oil slick', *Proc. Fluid Mech. in Petrol. Indus.*, ASME, 17-27, 1975.
- [50] Zaroodny, S.J. and Greenberg, M.D. 'On a vortex sheet approach to the numerical calculation of water waves', *J. Comp. Phys.*, **11**, 440-446, 1973.